TROPISM, MAPPING, MODELING, OR THERAPY USING CANINE ADENOVIRUS TYPE 2 (CAV-2) VECTORS IN THE CNS

EDITED BY: Eric J. Kremer, Melissa R. Andrews, Iria Gonzalez Dopeso-Reyes and Mathieu Wolff

PUBLISHED IN: Frontiers in Molecular Neuroscience and Frontiers in Neuroanatomy

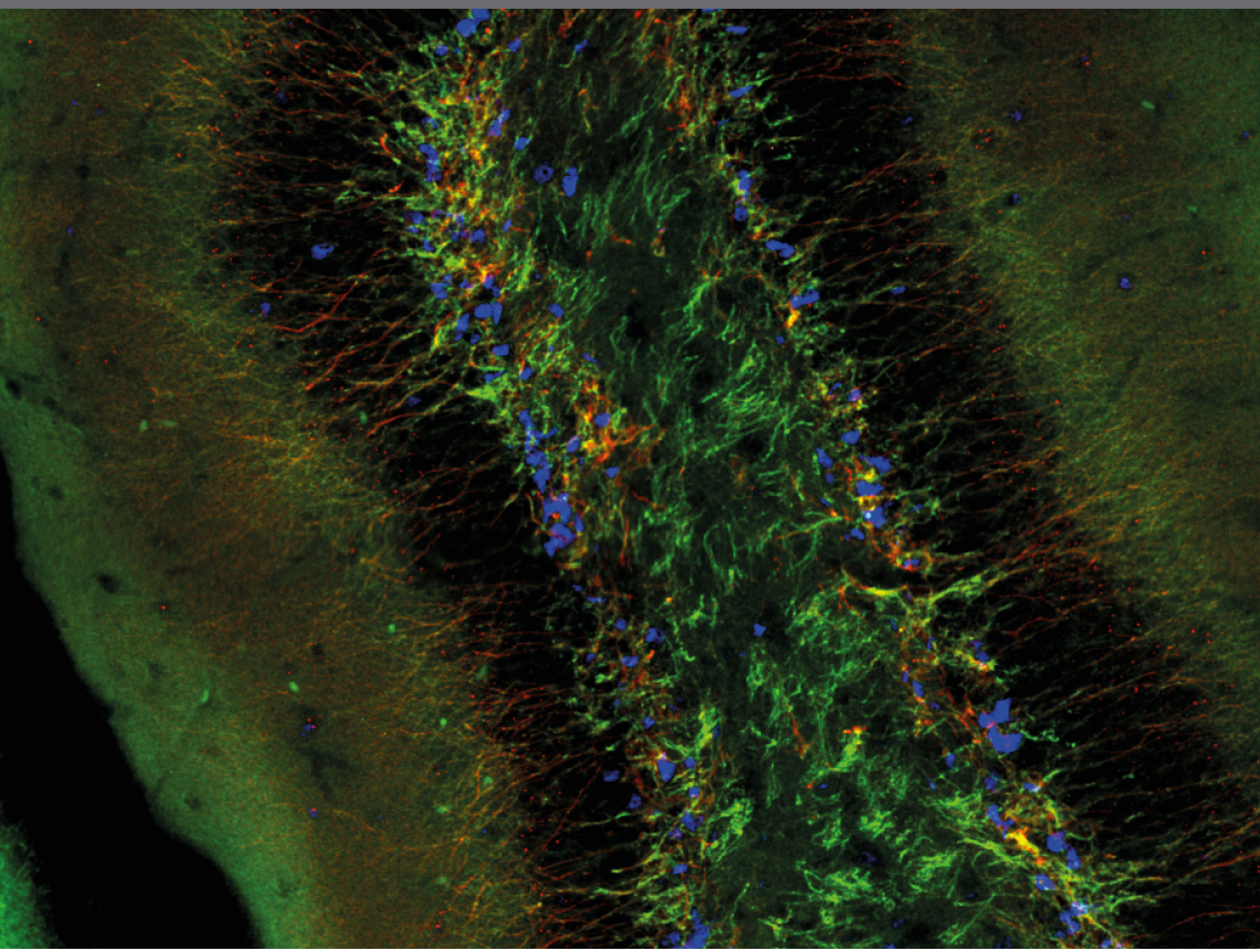

frontiers Research Topics

frontiers

ISSN 1664-8714
ISBN 978-2-88966-634-8
DOI 10.3389/978-2-88966-634-8

About Frontiers

Frontiers is more than just an open-access publisher of scholarly articles: it is a pioneering approach to the world of academia, radically improving the way scholarly research is managed. The grand vision of Frontiers is a world where all people have an equal opportunity to seek, share and generate knowledge. Frontiers provides immediate and permanent online open access to all its publications, but this alone is not enough to realize our grand goals.

Frontiers Journal Series

The Frontiers Journal Series is a multi-tier and interdisciplinary set of open-access, online journals, promising a paradigm shift from the current review, selection and dissemination processes in academic publishing. All Frontiers journals are driven by researchers for researchers; therefore, they constitute a service to the scholarly community. At the same time, the Frontiers Journal Series operates on a revolutionary invention, the tiered publishing system, initially addressing specific communities of scholars, and gradually climbing up to broader public understanding, thus serving the interests of the lay society, too.

Dedication to Quality

Each Frontiers article is a landmark of the highest quality, thanks to genuinely collaborative interactions between authors and review editors, who include some of the world's best academicians. Research must be certified by peers before entering a stream of knowledge that may eventually reach the public - and shape society; therefore, Frontiers only applies the most rigorous and unbiased reviews.
Frontiers revolutionizes research publishing by freely delivering the most outstanding research, evaluated with no bias from both the academic and social point of view. By applying the most advanced information technologies, Frontiers is catapulting scholarly publishing into a new generation.

What are Frontiers Research Topics?

Frontiers Research Topics are very popular trademarks of the Frontiers Journals Series: they are collections of at least ten articles, all centered on a particular subject. With their unique mix of varied contributions from Original Research to Review Articles, Frontiers Research Topics unify the most influential researchers, the latest key findings and historical advances in a hot research area! Find out more on how to host your own Frontiers Research Topic or contribute to one as an author by contacting the Frontiers Editorial Office: frontiersin.org/about/contact

TROPISM, MAPPING, MODELING, OR THERAPY USING CANINE ADENOVIRUS TYPE 2 (CAV-2) VECTORS IN THE CNS

Topic Editors:
Eric J. Kremer, Université de Montpellier, France
Melissa R. Andrews, University of Southampton, United Kingdom
Iria Gonzalez Dopeso-Reyes, UMR5535 Institut de Génétique Moléculaire de Montpellier (IGMM), France
Mathieu Wolff, Centre National de la Recherche Scientifique (CNRS), France

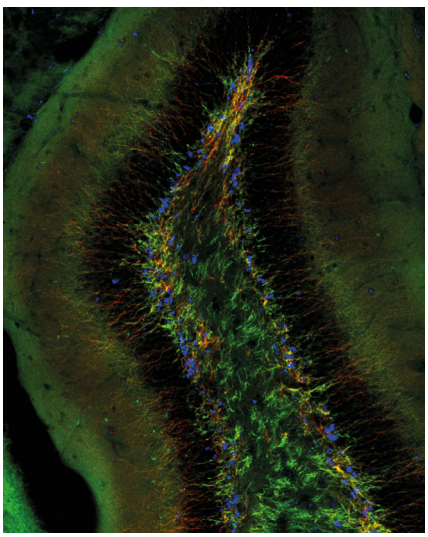

30-micrometers-thick coronal sections from a 1 month-old C57BL/6 mouse brain, containing the dentate gyrus. Immunofluorescent staining shows coxsackievirus adenovirus receptor immunoreactivity (green) in cells and projections in the hilus, subgranular zone, and granular and molecular layers; doublecortin immunoreactivity (red) in the subgranular zone and in the projections crossing the granular layer, and SRY-box 2 immunoreactive nuclei (blue) located in the subgranular zone (scale bar 250 µm).
Image: Iria Gonzalez-Dopeso Reyes.

Citation: Kremer, E. J., Andrews, M. R., Dopeso-Reyes, I. G., Wolff, M., eds. (2021). Tropism, Mapping, Modeling, or Therapy Using Canine Adenovirus Type 2 (CAV-2) Vectors in the CNS. Lausanne: Frontiers Media SA. doi: 10.3389/978-2-88966-634-8

Table of Contents

frontiers in Molecular Neuroscience

EDITORIAL
published: 11 February 2021
doi: 10.3389/fnmol.2021.636476

Editorial: Tropism, Mapping, Modeling, or Therapy Using Canine Adenovirus Type 2 (CAV-2) Vectors in the CNS

Iria Gonzalez Dopeso-Reyes[1]*, *Mathieu Wolff*[2]*, *Melissa R. Andrews*[3]* and *Eric J. Kremer*[1]*

[1] Institut de Génétique Moléculaire de Montpellier, Université de Montpellier, CNRS, Montpellier, France, [2] Unité Mixte de Recherche 5287, Centre National de la Recherche Scientifique, INCIA, Université de Bordeaux, Bordeaux, France, [3] School of Biological Sciences, University of Southampton, Southampton, United Kingdom

Keywords: CAV-2, neural circuit tracing, gene transfer, Parkinson's disease, coxsackievirus adenovirus receptor, retrograde transport, DREADDs, optogenetics

Editorial on the Research Topic

Tropism, Mapping, Modeling, or Therapy Using Canine Adenovirus Type 2 (CAV-2) Vectors in the CNS

This Frontiers in Molecular Neuroscience Research Topic addresses tropism, mapping, modeling, and therapy using canine adenovirus (CAV-2) vectors in the CNS. Genetic modification of cells in the brain or spinal cord has undergone a revolution in the last decade, both in terms of furthering our understanding of brain structure/function and for therapeutic reasons. The current collection of viral vectors gives scientists a multifunctional kit to target neurons in many brain structures. Approximately 20 years ago, we demonstrated the capacity of CAV-2 vectors to preferentially infect neurons and their high retrograde transport capacity (Soudais et al., 2001). Richard Palmiter's lab was one of the first to take advantage of CAV-2 vector retrograde transport and addressed the physiological functions of the substantia nigra (Hnasko et al., 2005, 2006). The evolution of gene transfer vectors for the CNS has not abated. In this *Research Topic*, our goal was to provide a readily accessible collection of reviews and primary studies that epitomize the advantages and drawbacks of CAV-2 vectors in the mammalian CNS.

For some neuroscientists, the idiosyncrasies of each vector platform are confusing because the best choice will depend upon their unique question(s). The first question is likely "*Which vector is best to infect neurons?*" While adenoviral vectors can use numerous cell surface molecules to eventually infect cells (Arnberg, 2012), most of the >200 types have not been tested in the CNS. The uniqueness with CAV-2 is that for all intents and purposes it depends only on a cell adhesion molecule called "coxsackievirus and adenovirus receptor" (CAR) (Soudais et al., 2001, Salinas et al., 2009). Fortunately, CAR is highly conserved, and all mammals appear to express CAR on neurons in the brain parenchyma (Wehbi et al.). CAV-2 vectors have been used efficiently in rodents (Morceau et al.; Martel et al.; Cerpa et al.; Kakava-Georgiadou et al.), dogs (Cubizolle et al., 2014), and non-human primates (NHP) (di Caudo et al., reviewed by Lasbleiz et al.). Not only are CAV-2 vectors efficient but they also appear to drive highly selective expression, which is sometimes a concern with AAV-based conditional constructs with leakage of gene expression, prompting the need to either work out the optimal virus titration (Morceau et al.) or rely on CAV-2 vectors and transgenic lines (Cerpa et al.).

Edited by:
Ildikó Rácz,
University Hospital Bonn, Germany

Reviewed by:
Mitsuhiro Hashimoto,
Fukushima Medical University, Japan

***Correspondence:**
Iria Gonzalez Dopeso-Reyes
iria.gonzalez-dopeso-reyes@igmm.cnrs.fr
Mathieu Wolff
mathieu.wolff@u-bordeaux.fr
Melissa R. Andrews
m.r.andrews@soton.ac.uk
Eric J. Kremer
eric.kremer@igmm.cnrs.fr

Received: *01 December 2020*
Accepted: *05 January 2021*
Published: *11 February 2021*

Citation:
Dopeso-Reyes IG, Wolff M, Andrews MR and Kremer EJ (2021) Editorial: Tropism, Mapping, Modeling, or Therapy Using Canine Adenovirus Type 2 (CAV-2) Vectors in the CNS. Front. Mol. Neurosci. 14:636476. doi: 10.3389/fnmol.2021.636476

The second question is likely to be— "*Which vector has the capacity to harbor my expression cassette of interest?*" E1/E3-deleted CAV-2 vectors have a cloning capacity >7 kbp, while helper-dependent CAV-2 vectors (HD-CAV2) have a cloning capacity up to 36 kbp (del Rio et al.). This characteristic sets CAV-2 vectors apart from others (except HSV vectors, which have a theoretical capacity of 150 kb). By exploiting this characteristic, di Caudo et al. and Mestre-Francés et al. (2019) created vectors harboring a leucine-rich repeat kinase 2 (LRRK2) cassette containing a point mutation (G2019S) to produce genetic NHP models of Parkinson's disease (reviewed by Lasbleiz et al.).

The third issue typically concerns the type of neuron that needs to be targeted. CAR is present mainly but not exclusively in the axons (Wehbi et al.) of different neuronal populations (reviewed by Lavoie and Liu), allowing one to target different types of neurons in different areas of the CNS in rodents and the peripheral nervous system in primates (Bohlen et al.). If one combines the presence of CAR and a specific promoter, transgene expression can be targeted to cholinergic interneurons (Martel et al.) or neurons in the locus coeruleus (Hirschberg et al., 2017; Xiang et al., 2019; Hayat et al., 2020). Furthermore, Lavoie and Liu have compiled a list of possible neuronal subtypes (glutamatergic, dopaminergic, catecholaminergic, serotoninergic, oxytonic, and GABAergic) that have been effectively transduced by CAV-2 vectors and they also point out that the lack of infection of some projecting neuron types is possible.

The ability of the neuronal pre-synapse to endocytose CAV-2 particles and confuse them for cargo destined for transport to the soma (retrograde transport) has provided neuroscientists with one of the first efficient vectors to address neuronal circuitry. How the 100 billion neurons, via the trillions of synapses, in a human brain interact, and how a given subset influences behavior may never be understood. However, this daunting task has not stopped many from trying to use less complex systems to create a rough blueprint as a starting point. In addition to circuitry, the advent of opto- and chemogenetics now allows one to address the function of selected neuronal populations (Cerpa et al.).

Finally, CAV-2 vectors (both E1/E3-deleted and HD) are also capable of long-term expression (del Rio et al.; Hirschberg et al., 2017). A study of the transcriptional pathways affected by HD-CAV2 demonstrated that there was a modest modulation of genes involved in the immune response, intracellular trafficking, and transcriptional regulation (reviewed by del Rio et al.).

In summary, the future of neuron-targeted gene transfer has many options—and in particular, CAV-2 vectors have many favorable characteristics.

AUTHOR CONTRIBUTIONS

IGD-R, MW, MA, and EK wrote the manuscript, edited, and approved of the manuscript.

FUNDING

Work in Andrews lab is funded by the Biotechnology and Biological Sciences Research Council and the International Foundation for Research in Paraplegia. Work in the Kremer lab was support by the LabEx EpiGenMed, an Investissements d'avenir program, Université de Montpellier, the Agence Nationale de la Recherche (ANR), ERA-Net (E-Rare) Joint Transnational Call, the Fondation pour la Recherche Médicale/Fondation Alzheimer's, and l'Institut de Génétique Moléculaire de Montpellier. The funders had no role in study design, data collection and analysis, decision to publish, or preparation of the manuscript.

ACKNOWLEDGMENTS

We thank all the authors that contributed to this Research Topic.

REFERENCES

Arnberg, N. (2012). Adenovirus receptors: implications for targeting of viral vectors. *Trends Pharmacol. Sci*. 33, 442–448. doi: 10.1016/j.tips.2012.04.005

Cubizolle, A., Serratrice, N., Skander, N., Colle, M. A., Ibanes, S., Gennetier, A., et al. (2014). Corrective GUSB transfer to the canine mucopolysaccharidosis VII brain. *Mol. Ther*. 22, 762–773. doi: 10.1038/mt.2013.283

Hayat, H., Regev, N., Matosevich, N., Sales, A., Paredes-Rodriguez, E., Krom, A. J., et al. (2020). Locus coeruleus norepinephrine activity mediates sensory-evoked awakenings from sleep. *Sci. Adv*. 6:eaaz4232. doi: 10.1126/sciadv.aaz4232

Hirschberg, S., Li, Y., Randall, A., Kremer, E. J., and Pickering, A. E. (2017). Functional dichotomy in spinal- vs prefrontal-projecting locus coeruleus modules splits descending noradrenergic analgesia from ascending aversion and anxiety in rats. *Elife*. 6:e29808. doi: 10.7554/eLife.29808

Hnasko, T. S., Perez, F. A., Scouras, A. D., Stoll, E. A., Gale, S. D., Luquet, S., et al. (2006). Cre recombinase-mediated restoration of nigrostriatal dopamine in dopamine-deficient mice reverses hypophagia and bradykinesia. *Proc. Natl. Acad. Sci. U.S.A*. 103, 8858–8863. doi: 10.1073/pnas.0603081103

Hnasko, T. S., Sotak, B. N., and Palmiter, R. D. (2005). Morphine reward in dopamine-deficient mice. *Nature* 438, 854–857. doi: 10.1038/nature04172

Mestre-Francés, N., Serratrice, N., Gennetier, A., Devau, G., Cobo, S., Trouche, S., et al. (2019). Exogenous LRRK2G2019S induces parkinsonian-like pathology in a nonhuman primate. *JCI Insight* 3:98202. doi: 10.1172/jci.insight.98202

Salinas, S., Bilsland, L. G., Henaff, D., Weston, A. E., Keriel, A., Schiavo, G., et al. (2009). CAR-associated vesicular transport of an adenovirus in motor neuron axons. *PLoS Pathog*. 5:e1000442. doi: 10.1371/journal.ppat.1000442

Soudais, C., Laplace-Builhe, C., Kissa, K., and Kremer, E. J. (2001). Preferential transduction of neurons by canine adenovirus vectors and their efficient retrograde transport *in vivo*. *FASEB J*. 15, 2283–2285. doi: 10.1096/fj.01-0321fje

Xiang, L., Harel, A., Gao, H., Pickering, A. E., Sara, S. J., and Wiener, S. I. (2019). Behavioral correlates of activity of optogenetically identified locus coeruleus noradrenergic neurons in rats performing T-maze tasks. *Sci Rep*. 9:1361. doi: 10.1038/s41598-018-37227-w

Conflict of Interest: The authors declare that the research was conducted in the absence of any commercial or financial relationships that could be construed as a potential conflict of interest.

frontiers in Molecular Neuroscience

MINI REVIEW
published: 11 February 2019
doi: 10.3389/fnmol.2019.00010

Combining Gene Transfer and Nonhuman Primates to Better Understand and Treat Parkinson's Disease

*Christelle Lasbleiz[1], Nadine Mestre-Francés[1], Gina Devau[1], Maria-Rosario Luquin[2], Liliane Tenenbaum[3], Eric J. Kremer[4] and Jean-Michel Verdier[1]**

[1]MMDN, University of Montpellier, EPHE, INSERM, U1198, PSL University, Montpellier, France, [2]Department of Neurology, Clinica Universidad de Navarra, Pamplona, Spain, [3]Laboratory of Molecular Neurotherapies and NeuroModulation, Clinical Neuroscience Department, Lausanne University Hospital, Lausanne, Switzerland, [4]Institut de Génétique Moléculaire de Montpellier, University of Montpellier, CNRS, Montpellier, France

Parkinson's disease (PD) is a progressive CNS disorder that is primarily associated with impaired movement. PD develops over decades and is linked to the gradual loss of dopamine delivery to the striatum, *via* the loss of dopaminergic (DA) neurons in the substantia nigra pars compacta (SNpc). While the administration of L-dopa and deep brain stimulation are potent therapies, their costs, side effects and gradual loss of efficacy underlines the need to develop other approaches. Unfortunately, the lack of pertinent animal models that reproduce DA neuron loss and behavior deficits—in a timeline that mimics PD progression—has hindered the identification of alternative therapies. A complementary approach to transgenic animals is the use of nonhuman primates (NHPs) combined with the overexpression of disease-related genes using viral vectors. This approach may induce phenotypes that are not influenced by developmental compensation mechanisms, and that take into account the personality of animals. In this review article, we discuss the combination of gene transfer and NHPs to develop "genetic" models of PD that are suitable for testing therapeutic approaches.

Keywords: Parkinson's disease, primate, CAV vectors, gene transfer, dopaminergic neurons

OPEN ACCESS

Edited by:
Jean-Marc Taymans, Institut National de la Santé et de la Recherche Médicale (INSERM), France

Reviewed by:
Masahiko Takada, Kyoto University, Japan
Hui-Yun Chang, National Tsing Hua University, Taiwan

****Correspondence:***
Jean-Michel Verdier
jean-michel.verdier@ephe.psl.eu

Received: *02 November 2018*
Accepted: *14 January 2019*
Published: *11 February 2019*

Citation:
Lasbleiz C, Mestre-Francés N, Devau G, Luquin M-R, Tenenbaum L, Kremer EJ and Verdier J-M (2019) Combining Gene Transfer and Nonhuman Primates to Better Understand and Treat Parkinson's Disease. Front. Mol. Neurosci. 12:10. doi: 10.3389/fnmol.2019.00010

INTRODUCTION

Parkinson's disease (PD) is a disorder of the CNS primarily due to the degeneration of nigro-striatal dopaminergic (DA) neurons. Early symptoms are movement-related, including shaking, rigidity, slowness of movement, postural instability and difficulty with walking. Collectively, these symptoms are called "parkinsonism". However, non-motor symptoms, such as depression and apathy, which are attributed to the degeneration of the mesolimbic mesocortical DA pathway [neurons of the ventral tegmental area (VTA) projecting to the *nucleus accumbens*, Lewis et al., 2003; Carriere et al., 2014; Dujardin and Lopes, 2014; Dujardin et al., 2014], frequently appear before the motor symptoms (**Figure 1**). In addition to fine-tuning of motor function, these pathways are also involved in reward (motivation), pleasure, compulsion and perseveration. Later, sensory, sleep, emotional problems, depression and dementia may arise in the late stages. Regarding the latter, the degeneration of non-DA neurons (e.g., serotoninergic) are thought to contribute to depression (Tan et al., 2011).

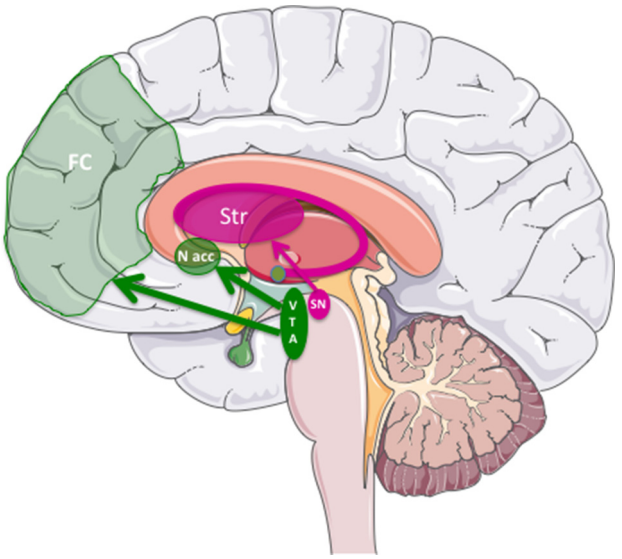

FIGURE 1 | The three major dopaminergic (DA) pathways in the brain linked to Parkinson's Disease (PD). The nigrostriatal pathway was DA cells from substantia nigra pars compacta (SNpc) project into the striatum (in dark pink). The mesolimbic/mesocortical pathway, which corresponds to the projection of the midbrain ventral tegmental area (VTA) to the *nucleus accumbens* (N. Acc) in the limbic areas, and to the frontal cortex (FC), respectively.

These early neuropsychiatric manifestations often precede motor symptoms, which appear when approximately 70% of the substantia nigra pars compacta (SNpc) DA neurons are lost or are unable to deliver dopamine to the striatum. This implies that PD is, in part, an axonopathy (O'Keeffe and Sullivan, 2018). Finally, cognitive symptoms like dementia and hallucinations tend to appear in the late phases of the disease and are related to perturbation of the mesocortial pathway, which connects the VTA to the prefrontal cortex. Eventually, deficits in the noradrenergic, serotoninergic and acetylcholinergic systems also appear. Clearly, early diagnosis will be of utmost importance for disease prevention/reversal.

A handful of genes are involved in monogenic (recessive or dominant) forms of PD. Together these genes account for around 30% of familial forms and 3%–5% of sporadic cases (Klein and Westenberger, 2012). Among these PD-related genes, α-synuclein (SNCA) and leucine-rich repeat kinase 2 (*LRRK2* or *PARK8*) or are the best characterized because over-expression and/or mutations in *SNCA* and *LRRK2* are responsible for autosomal-dominant PD forms. A mutation in *SCNA* that causes an A53T change was identified in four families (Polymeropoulos et al., 1997). Since then, other mutations, duplication and triplication of this gene have been linked to PD (Deng and Yuan, 2014). LRRK2^{G2019S} is the most common mutation in familial and sporadic PD. LRRK2 mutations are also found in sporadic cases further supporting the prominent role of this gene in PD aetiology. Finally, disease evolution of patients with LRRK2 mutations, including the accumulation of Lewy bodies, are clinically indistinguishable from those with idiopathic PD (Gasser, 2009). Familial forms of PD are slowly providing clues to underlying mechanisms of neurodegeneration.

While some drugs have markedly improved parkinsonism, their efficacy often declines as PD progresses. To date, there are no long-term disease-modifying treatments available for the 10 million people worldwide suffering from PD. Therefore, using pertinent models that allow the scientific community to develop new approaches are of utmost importance to combat PD.

ACUTE AND CHRONIC MODELS OF PD

One bottleneck associated with identifying therapeutic options for PD is the lack of a robust and pertinent animal model. While many models give potential results on a given aspect of parkinsonism, none fully recapitulate the pathognomonic lesions of PD (Dawson et al., 2010). Two broad categories of models are being used: neurotoxin-based (acute) and genetic-based (chronic) models. Neurotoxin models are the most popular. They can be produced by the use of the toxin 6-hydroxydopamine (6-OHDA), which preferentially kills DA neurons by production of free radicals (Przedborski et al., 1995), or 1-methyl-4-phenyl-1, 2, 3, 6-tetrahydropyridine (MPTP); Schober, 2004), which interferes with the mitochondrial metabolism, also producing free radicals (Petroske et al., 2001) and strong neuroinflammation (Luchtman et al., 2009, 2012). In addition to the loss of dopamine in the nigrostriatal DA system, they also reach extrastriatal regions, such as the subcortex and brainstem (Bezard et al., 2013). While we have learned much from toxin-induced PD models, their use in the development of disease-modifying therapies is challenging. A well-recognized caveat of toxin-induced PD models is that they mainly cause the degeneration of the nigrostriatal DA pathway, which induces robust motor symptoms, but poorly recapitulate symptoms related to most, but not all, pathways (Brown et al., 2012). These models, although very useful to test motor deficits or L-dopa responsiveness (Dawson et al., 2002), remain acute models where the progressive DA cell death is absent, and poorly mimic PD progression over time (Hattori and Sato, 2007). To circumvent these drawbacks many labs have opted for the creation of transgenic mice, widely based on *SNCA* and *LRRK2* mutants. However, transgenic *SNCA* mice, based on missenses mutations A30P, E46K or A53T, have led to limited parkinsonism (Deng and Yuan, 2014), especially in terms of nigrostriatal degeneration (Chesselet, 2008; Dawson et al., 2010). On the other side, the current cohort of *LRRK2* transgenic mice induce mild, if any, degeneration of nigrostriatal DA neurons, Lewy body formation, or behavior effects (Ramonet et al., 2011; Blesa and Przedborski, 2014). Of note though, *LRRK2* overexpression does accelerate the pathological consequences of *SNCA*^{A53T} in double transgenic mice (Lin et al., 2009). The latter study also suggests that the LRRK2 protein affects the intracellular trafficking and accumulation of SNCA protein. A transgenic rat overexpressing the G2019S mutation impaired dopamine uptake but did not show any nigral DA cell loss and striatal dopamine contents in aged rats (Zhou et al., 2011). Interestingly, transgene expression in adult animals using viral vectors can

induce pronounced phenotypes in rodents, presumably by circumventing developmental compensatory effects, and by producing high level of transgene expression. In particular, vector-mediated expression of native or mutant SNCA can lead to DA neuron cell death and motor symptoms. Cognitive symptoms such as spatial learning and memory deficits (Hall et al., 2013), depression (Caudal et al., 2015) and emotional memory impairment, are influenced by VTA neurons (Alvarsson et al., 2016) in rats. In conclusion, animal models that recapitulate the early and late, motor and non-motor symptoms, within a time frame suitable to evaluate PD-modifying treatments, are still needed.

VIRAL VECTOR-MEDIATED PD EFFECTS IN NONHUMAN PRIMATES

Nonhuman primates (NHPs) are particularly relevant in preclinical research because they share several genetic, physiological and anatomical similarities with humans. NHPs display complex cognitive functions, complex motor skills and a highly developed cerebral cortex (Verdier et al., 2015). Equally important, NHPs can be studied under controlled and humane experimental conditions. Interestingly, aged rhesus monkeys can naturally display a significant loss of tyrosine-hydroxylase and dopamine-transporter immunoreactivity correlated with motor impairments (Emborg et al., 1998). Furthermore, aged-related SNCA increase in rhesus monkeys has been observed in the nigral pathway (Chu and Kordower, 2007). These observations led to the idea that aged NHPs are at the threshold to develop a PD and, as a consequence, constitute a model of choice. Several viral vectors have been used to drive the development of PD in NHPs. Vector-mediated transgenesis is also versatile and transposable between species. Taking nothing away from the ground-breaking work performed in rodents, we believe that NHPs are needed to unravel PD induction, progression, therapeutic strategies (Emborg, 2007), and understand long-term pathophysiological, biochemical and behavioral anomalies. To develop these models, intracerebral injection of viral vectors bearing mutated *SNCA* or *LRRK2* have been tested for modeling "genetic" PD. Monkeys overexpressing simian or human SNCA coding for a protein with the A53T change *via* adeno-associated virus (AAV) vectors exhibit motor impairment and neuropathological features of PD including but not limited to: head position bias, loss of TH- and VMAT2-positive innervation throughout caudate nucleus and putamen, dystrophic neurites and swollen axons, SNCA-positive inclusions (Kirik et al., 2003). AAV vectors have been successfully used for expression of human $SNCA^{A53T}$ in cynomolgus macaque SN, and led to a 50% loss of nigral DA neurons (Koprich et al., 2016). Lentivirus vectors expression of $SNCA^{A53T}$ into the SN of rhesus monkeys resulted in more neuronal pathology and chronicity in monkey brains than in mouse brains (Yang et al., 2015). Of note, NHPs are also responsive to dopamine replacement therapies, and show complications resulting from long-term use such as dyskinesia and motor fluctuations when the medication is not working well.

In contrast to the small (∼16 kDa) SNCA protein, the LRRK2 protein is ∼250 kDa with at least seven different functional domains (Taymans and Greggio, 2016). The G2019S change located in the kinase domain, leads to a hyperkinase activity. LRRK2 was recently shown to be involved in the endoplasmic reticulum to Golgi export. Interestingly, this function is altered in the PD-related $LRRK2^{R1441C}$ mutation located in the GTPase domain (Cho et al., 2014).

HELPER-DEPENDENT CANINE ADENOVIRUS FOR DEVELOPING NEW PD MODELS

The *LRRK2* cDNA is about 8 kb and therefore a vector with an appropriately large cloning capacity is needed, and precludes its efficient expression in AAV and lentivirus vectors. A handful of attempts have been made to develop animal models expressing $LRRK2^{G2019S}$ *via* viral vectors. To date, three vector platforms have been used to deliver the $LRRK2^{G2019S}$ cDNA: human adenovirus type 5 (HAd5; Dusonchet et al., 2011; Tsika et al., 2014) were used in rats, herpes simplex virus (HSV) were used in mice. The HAd5-$LRRK2^{G2019S}$ vector was injected into the striatum of rodents and due to its preferential transduction of glia cells and poor retrograde transport, the direct effect of $LRRK2^{G2019S}$ on DA neurons in the nigra could not be addressed. Using a HSV vectors expressing LRRK2 or $LRRK2^{G2019S}$, Lee et al. (2010) showed that the hyperkinase activity of $LRRK2^{G2019S}$ was responsible for the PD phenotype, and that LRRK2 kinase inhibitors provide a potential neuroprotective treatment for PD. Interestingly, they also showed that overexpression of wild type LRRK2 caused neurite shortening *in vitro*.

Clearly, the ability to efficiently and simultaneously deliver expression cassettes to multiple regions of the brain could be a notable plus for PD. Taking nothing away from the encouraging results when using HSV vectors (Goverdhana et al., 2005; Lee et al., 2010), we believe that we can improve PD modeling by using helper-dependent (HD) canine adenovirus (CAV-2; Junyent and Kremer, 2015; **Figure 2**). HD CAV-2 vectors have a unique combination of characteristics that make it ideally suited for PD modeling: CAV-2 vectors preferentially transduce neurons in rodent and NHPs, have no long-term impact on adult of newborn neuron homeostasis, have a 30 kb cloning capacity. Following injection in the rodent and NHP striatum, CAV-2 efficiently transits into afferent (axonal projections into the striatum) structures and is ≥100-fold more efficient than HAd5 vectors. This is particularly pertinent for PD modeling because efficient and stable gene transfer to DA neurons *via* injections into the SN is pernicious because DA neurons are particularly sensitive to stress (Albert et al., 2017). Due to the efficient retrograde transport of CAV-2 vectors in DA neurons (Soudais et al., 2001b; Schwarz et al., 2015), HD-LRRK2 vector can be delivered in the striatum, thus bypassing the potential damage incurred by SN injections.

HD CAV-2 vectors lead to long-term expression in the brain: transgene expression was stable for >1 year post-transduction (Soudais et al., 2001b) and cellular protein expression showed

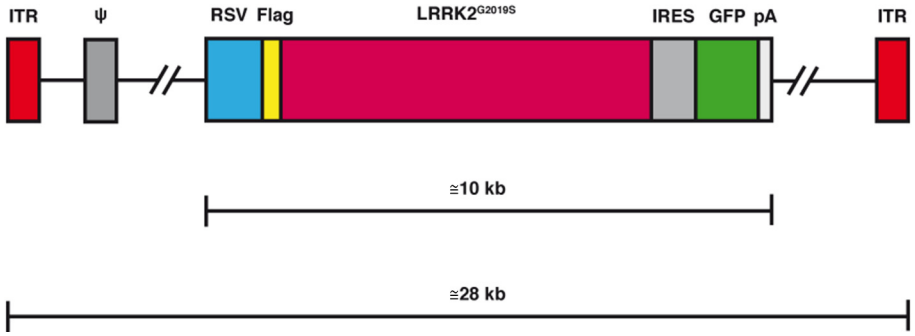

FIGURE 2 | Schematic representation of the helper-dependent (HD) canine adenovirus-2 (CAV-2) vector expressing leucine-rich repeat kinase 2 (*LRRK2*)^{G2019S}. While the HD genome is devoid of all viral coding sequences, it still retains the 200 bp inverted terminal repeat (ITR) at each end and the 150 bp packaging signal (ψ) at the left end of the genome. To create a stable capsid the genome must fill the interior of the capsid which therefore requires it to be 95%-105% of the 32 kbp wild type genome. Depending on the size of the expression cassette [here it contains the 600 bp Rous sarcoma virus early promoter (RSV), an internal ribosome entry signal (IRES), a green fluorescent protein cDNa 5GF] the *LRRK2* cDNA and a 250 polyA signal (pA), the remaining sequence is made up of noncoding intronic sequence from the human genome.

no change. These data demonstrate the low immunogenicity of HD CAV-2. Finally, scalable high titre production is also possible (Junyent and Kremer, 2015). We have invested significantly in optimizing CAV-2 vector cloning, creation and production parameters (Kremer et al., 2000; Soudais et al., 2001a; Fernandes et al., 2013, 2015a,b; Ibanes and Kremer, 2013), understanding CAV-2 uptake and trafficking (Soudais et al., 2000, 2001b; Chillon and Kremer, 2001; Martin-Touaux et al., 2002; Salinas et al., 2009), the physiological role of CAV-2's receptor (Seiradake et al., 2006; Schoehn et al., 2008; Salinas et al., 2010; Rademacher et al., 2012; Piersanti et al., 2013; Kremer and Nemerow, 2015; Loustalot et al., 2015), and the *in vivo* use of the vectors [Junyent and Kremer, 2015 and del Rio et al. (in this Research Topics issue)]. HD CAV-2 vectors are therefore ideal for *LRRK2* cDNA delivery.

NEW NHP MODELS OF PD

LRRK2^{G2019S} Expression in the Lemurian Primate *Microcebus murinus*

By complementing and extending the work performed in rodents, NHPs can help unravel PD induction, progression, therapeutic strategies (Emborg, 2007), and understand long-term pathophysiological, biochemical and behavioral anomalies. Although several type of NHPs are used to study neurodegenerative diseases (Verdier et al., 2015) the use of NHPs is time demanding, expensive, and the number of available animals for research is limited. To circumvent these issues, the *Microcebus murinus* (or gray mouse lemur) has the notable advantages to be small and efficiently bred in captivity. *M. murinus* are ideally for cerebral ageing and neurodegenerative studies because they develops complex behavioral (emotional), cognitive, and motor tests [(Joly et al., 2004, 2006, 2014; Picq, 2007; Trouche et al., 2010; Picq et al., 2012); for a review article, see also (Languille et al., 2012)], and also through transcriptomic studies (Abdel Rassoul et al., 2010) and transmissibility of neurodegenerative diseases (Mestre-Francés et al., 2012) or for gene transfer (Alba et al., 2012). In addition, its brain structure is similar to that of the humans, with a relative proportion of each region.

Recently, we generated HD CAV-2 vectors containing a LRRK2^{G2019S} expression cassette (HD-LRRK2^{G2019S}) that we injected unilaterally into the putamen of *M. murinus*. We found preferential transduction of neurons at the injection site, and in numerous areas harboring neurons that project into the striatum. The long-term expression leads to the progressive unilateral loss of DA cells in the SNpc accounting for up to 30%–40% a decreased of the DA fibers, dystrophic neurites and swollen axons, characteristic of neurodegeneration. This neurodegeneration was accompanied by dopamine loss in the striatum, and PD-like motor symptoms (bradykinesia, rigidity, and difficulty in prehension; Mestre-Francés et al., 2018).

LRRK2^{G2019S} Expression in Macaques

The promising outcomes obtained in the *M. murinus* model, prompted us to determine if CAV-2 vectors were also effective gene transfer tools in the *Macaca fascicularis* brain, and if CAV-2–mediated expression of LRRK2^{G2019S} in the SN neurons could induce pathological features associated with PD in a more complex NHP model. Our study demonstrated the neuronal tropism, retrograde transport, biodistribution, and efficacy of CAV-2 vectors expressing GFP in the *M. fascicularis* brain (Di Caudo et al., in preparation). Furthermore, we also demonstrated that CAV-2-mediated HD-LRRK2^{G2019S} expression in the SN leads to the loss of DA cells, neurite dystrophy, axon swelling and mitochondrial abnormalities. Unfortunately, animals injected with HD-LRRK2^{G2019S} into the striatum did not develop clear parkinsonian features, but they exhibited a significant reduction of striatal F-dopa uptake, indicating that they represent an early stage of the disease.

Together, these data demonstrate that robust PD NHP models can be generated using HD CAV-2 vectors and in turn could allow detailed evaluation of the therapeutic options for PD motor, emotional, and cognitive deficits.

VIRAL VECTORS FOR DEVELOPING DISEASE-MODIFYING TREATMENTS

While currently available treatments can temporarily relieve the symptoms, they have little influence on the neurodegenerative process.

Neurotropic factors (NFs), which mediate pro-survival effects on neurons, potentially constitute a disease-modifying option. However, the results obtained with NFs are controversial, and largely depend on the model. For instance, in an AAV-SNCA-injected rat, the delivery of AAV-GDNF (glial cell line-derived neurotrophic factor), 2–3 weeks before AAV-SNCA injection, failed to demonstrate a neuroprotective effect (Decressac et al., 2012). In this case, *SNCA* overexpression resulted in Ret downregulation and disruption of GDNF signaling. However, a recent study demonstrated that Ret is not downregulated in PD patients (Su et al., 2017). In other studies, the therapeutic potential of NFs was demonstrated in toxin injected (6-OHDA and MPTP) rodents and NHPs, in which NFs reduced motor symptoms (Bilang-Bleuel et al., 1997; Kirik et al., 2000; Kordower et al., 2000, 2006; Eslamboli et al., 2003; Su et al., 2009). Following these encouraging results, clinical trials were conducted using AAV2-GDNF (still ongoing) or AAV2-neurturin (NRTN; Marks et al., 2010; Warren Olanow et al., 2015). Although the AAV2-NRTN trials demonstrated acceptable tolerance, after a 1-year follow-up, no significant improvement was observed in the "Unified PD Rating Scale" (UPDRS). However, *post hoc* analyses suggested that a subgroup of patients had beneficial effects (Marks et al., 2010). Post-mortem analysis of four patients showed that although surviving DA neurons were still present in the SN, very few co-stained with NRTN. These observations suggested that retrograde transport was inefficient (Bartus et al., 2011, 2015). Strikingly, these results were not predicted by the pre-clinical animal models used to establish the clinical protocol (MPTP-treated NHPs and 6-OHDA-injected rats) in which the surviving nigro-striatal DA neurons still had functional projections proficient for retrograde transport and could be efficiently rescued. In a subsequent study (Kordower et al., 2013), analysis of brains from untreated PD patients at different stages, showed that the putamen innervation had almost totally disappeared at 4 years post-diagnosis, whereas numerous DA neurons cell bodies were still present in the SNpc. Because most of the patients enrolled in the AAV2-NRTN trial were more than 5 years post-diagnosis, it is likely that their putaminal DA innervation had been lost or was dysfunctional. Although unsuccessful, the AAV2-NTRN trial was informative since it allowed: (i) to identify the limitations of the toxin-induced models; (ii) to suggest that disease-interfering treatments should be administered before disappearance the DA fibers; and (iii) supported enrolment of patients at earlier disease stages in gene therapy trials.

Therefore, disease-modifying treatments will need animal models that more faithfully recapitulate the mechanisms underlying the progression of PD, and should be administered at the earliest possible stage.

CONCLUDING REMARKS

No animal model manifests all the characteristics of PD in humans, i.e., SNCA aggregation, DA reduction, progressive DA cell death, motor and non-motor symptoms. If transgenic models offer tremendous advantages over toxin-induced models, the overexpression of human disease causing mutated genes should be kept within the range of physiological levels. Viral vector-mediated local transgenesis offers the advantage to allow adjusting the transgene copy number to avoid confounding effects of a non-physiological overdosage. Clearly though it is difficult, if not impossible, to argue that NHP will not be the most informative path towards testing PD therapies. As underlined by Blesa and Przedborski (2014), *models are just models*, and should answer the question asked, not all the questions. Because NHPs have their own personality each animal can produce different emotional, motor, or cognitive behavior (that is why they are their own control). In addition, NHPs allow us to monitor early phases of the disease and follow-up. The combination of gene therapy and the use of NHPs should open new route to a disease-modifying treatment of PD.

DATA AVAILABILITY

The datasets generated for this study are available on request to the corresponding author.

AUTHOR CONTRIBUTIONS

CL, M-RL, LT, EK, and J-MV wrote this review article. NM-F and GD edited and revised it.

FUNDING

This work was supported in part by France Parkinson's (EK), BrainCAV (EC FP7 contract #292222; EK, J-MV, NM-F), BrainVector (EC FP7 contract #286071; EK), Université de Montpellier (EK, J-MV), the Region Languedoc Roussillon (EK), IGMM (EK), and LabEx EpiGenMed, an Investissements d'Avenir Program (PIA), ANR-10-LABX-12-01 (EK), MMDN (J-MV), Instituto de Salud Carlos III (PI15/01816; M-RL), INSERM and Swiss National Foundation (Contract #31003A_179527; LT), Institut National de la Santé et de la Recherche Médicale (INSERM; NM-F, J-MV).

REFERENCES

Abdel Rassoul, R., Alves, S., Pantesco, V., De Vos, J., Michel, B., Perret, M., et al. (2010). Distinct transcriptome expression of the temporal cortex of the primate *Microcebus murinus* during brain aging versus Alzheimer's disease-like pathology. *PLoS One* 5:e12770. doi: 10.1371/journal.pone.0012770

Alba, R., Bradshaw, A. C., Mestre-Francés, N., Verdier, J.-M., Henaff, D., and Baker, A. H. (2012). Coagulation factor X mediates adenovirus type 5 liver gene transfer in non-human primates (*Microcebus murinus*). *Gene Ther* 19, 109–113. doi: 10.1038/gt.2011.87

Albert, K., Voutilainen, M. H., Domanskyi, A., and Airavaara, M. (2017). AAV vector-mediated gene delivery to substantia nigra dopamine neurons:

implications for gene therapy and disease models. *Genes Basel.* 8:63. doi: 10.3390/genes8020063

Alvarsson, A., Caudal, D., Björklund, A., and Svenningsson, P. (2016). Emotional memory impairments induced by AAV-mediated overexpression of human α-synuclein in dopaminergic neurons of the ventral tegmental area. *Behav. Brain Res.* 296, 129–133. doi: 10.1016/j.bbr.2015.08.034

Bartus, R. T., Herzog, C. D., Chu, Y., Wilson, A., Brown, L., Siffert, J., et al. (2011). Bioactivity of AAV2-neurturin gene therapy (CERE-120): differences between Parkinson's disease and nonhuman primate brains. *Mov. Disord.* 26, 27–36. doi: 10.1002/mds.23442

Bartus, R. T., Kordower, J. H., Johnson, E. M. Jr., Brown, L., Kruegel, B. R., Chu, Y., et al. (2015). Post-mortem assessment of the short and long-term effects of the trophic factor neurturin in patients with α-synucleinopathies. *Neurobiol. Dis.* 78, 162–171. doi: 10.1016/j.nbd.2015.03.023

Bezard, E., Yue, Z., Kirik, D., and Spillantini, M. G. (2013). Animal models of Parkinson's disease: limits and relevance to neuroprotection studies. *Mov. Disord.* 28, 61–70. doi: 10.1002/mds.25108

Bilang-Bleuel, A., Revah, F., Colin, P., Locquet, I., Robert, J.-J., Mallet, J., et al. (1997). Intrastriatal injection of an adenoviral vector expressing glial-cell-line-derived neurotrophic factor prevents dopaminergic neuron degeneration and behavioral impairment in a rat model of Parkinson disease. *Proc. Natl. Acad. Sci. U S A* 94, 8818–8823. doi: 10.1073/pnas.94.16.8818

Blesa, J., and Przedborski, S. (2014). Parkinson's disease: animal models and dopaminergic cell vulnerability. *Front. Neuroanat.* 8:155. doi: 10.3389/fnana.2014.00155

Brown, C. A., Campbell, M. C., Karimi, M., Tabbal, S. D., Loftin, S. K., Tian, L. L., et al. (2012). Dopamine pathway loss in nucleus accumbens and ventral tegmental area predicts apathetic behavior in MPTP-lesioned monkeys. *Exp. Neurol.* 236, 190–197. doi: 10.1016/j.expneurol.2012.04.025

Carriere, N., Besson, P., Dujardin, K., Duhamel, A., Defebvre, L., Delmaire, C., et al. (2014). Apathy in Parkinson's disease is associated with nucleus accumbens atrophy: a magnetic resonance imaging shape analysis. *Mov. Disord.* 29, 897–903. doi: 10.1002/mds.25904

Caudal, D., Alvarsson, A., Björklund, A., and Svenningsson, P. (2015). Depressive-like phenotype induced by AAV-mediated overexpression of human α-synuclein in midbrain dopaminergic neurons. *Exp. Neurol* 273, 243–252. doi: 10.1016/j.expneurol.2015.09.002

Chesselet, M.-F. (2008). *In vivo* alpha-synuclein overexpression in rodents: a useful model of Parkinson's disease? *Exp. Neurol.* 209, 22–27. doi: 10.1016/j.expneurol.2007.08.006

Chillon, M., and Kremer, E. J. (2001). Trafficking and propagation of canine adenovirus vectors lacking a known integrin-interacting motif. *Hum. Gene Ther.* 12, 1815–1823. doi: 10.1089/104303401750476302

Cho, H. J., Yu, J., Xie, C., Rudrabhatla, P., Chen, X., Wu, J., et al. (2014). Leucine-rich repeat kinase 2 regulates Sec16A at ER exit sites to allow ER-Golgi export. *EMBO J.* 33, 2314–2331. doi: 10.15252/embj.201487807

Chu, Y., and Kordower, J. H. (2007). Age-associated increases of α-synuclein in monkeys and humans are associated with nigrostriatal dopamine depletion: is this the target for Parkinson's disease? *Neurobiol. Dis.* 25, 134–149. doi: 10.1016/j.nbd.2006.08.021

Dawson, T. M., Ko, H. S., and Dawson, V. L. (2010). Genetic animal models of Parkinson's disease. *Neuron* 66, 646–661. doi: 10.1016/j.neuron.2010.04.034

Dawson, T., Mandir, A., and Lee, M. (2002). Animal models of PD: pieces of the same puzzle? *Neuron* 35, 219–222. doi: 10.1016/S0896-6273(02)00780-8

Decressac, M., Kadkhodaei, B., Mattsson, B., Laguna, A., Perlmann, T., and Bjorklund, A. (2012). α-Synuclein-induced down-regulation of Nurr1 disrupts GDNF signaling in nigral dopamine neurons. *Sci. Transl. Med.* 4:163ra156. doi: 10.1126/scitranslmed.3004676

Deng, H., and Yuan, L. (2014). Genetic variants and animal models in SNCA and Parkinson disease. *Ageing Res. Rev.* 15, 161–176. doi: 10.1016/j.arr.2014.04.002

Dujardin, K., and Lopes, R. (2014). Apathy and impaired recognition of emotion: are they related in Parkinson's disease? *J. Neurol. Neurosurg. Psychiatry* 85:1061. doi: 10.1136/jnnp-2013-307224

Dujardin, K., Langlois, C., Plomhause, L., Carette, A.-S., Delliaux, M., Duhamel, A., et al. (2014). Apathy in untreated early-stage Parkinson disease: relationship with other non-motor symptoms. *Mov. Disord.* 29, 1796–1801. doi: 10.1002/mds.26058

Dusonchet, J., Kochubey, O., Stafa, K., Young, S. M. Jr., Zufferey, R., Moore, D. J., et al. (2011). A rat model of progressive nigral neurodegeneration induced by the Parkinson's disease-associated G2019S mutation in LRRK2. *J. Neurosci.* 31, 907–912. doi: 10.1523/JNEUROSCI.5092-10.2011

Emborg, M. E. (2007). Nonhuman primate models of Parkinson's disease. *ILAR J.* 48, 339–355. doi: 10.1093/ilar.48.4.339

Emborg, M. E., Ma, S. Y., Mufson, E. J., Levey, A. I., Taylor, M. D., Brown, W. D., et al. (1998). Age-related declines in nigral neuronal function correlate with motor impairments in rhesus monkeys. *J. Comp. Neurol.* 401, 253–265. doi: 10.1002/(SICI)1096-9861(19981116)401:2<253::AID-CNE7>3.0.CO;2-X

Eslamboli, A., Cummings, R. M., Ridley, R. M., Baker, H. F., Muzyczka, N., Burger, C., et al. (2003). Recombinant adeno-associated viral vector (rAAV) delivery of GDNF provides protection against 6-OHDA lesion in the common marmoset monkey *(Callithrix jacchus)*. *Exp. Neurol.* 184, 536–548. doi: 10.1016/j.expneurol.2003.08.007

Fernandes, P., Almeida, A. I., Kremer, E. J., Alves, P. M., and Coroadinha, A. S. (2015a). Canine helper-dependent vectors production: implications of Cre activity and co-infection on adenovirus propagation. *Sci. Rep.* 5:9135. doi: 10.1038/srep09135

Fernandes, P., Santiago, V. M., Rodrigues, A. F., Tomás, H., Kremer, E. J., Alves, P. M., et al. (2013). Impact of E1 and Cre on adenovirus vector amplification: developing MDCK CAV-2-E1 and E1-Cre transcomplementing cell lines. *PLoS ONE* 8:e60342. doi: 10.1371/journal.pone.0060342

Fernandes, P., Simão, D., Guerreiro, M. R., Kremer, E. J., Coroadinha, A. S., and Alves, P. M. (2015b). Impact of adenovirus life cycle progression on the generation of canine helper-dependent vectors. *Gene Ther.* 22, 40–49. doi: 10.1038/gt.2014.92

Gasser, T. (2009). Molecular pathogenesis of Parkinson disease: insights from genetic studies. *Expert Rev. Mol. Med.* 11:e22. doi: 10.1017/s1462399409001148

Goverdhana, S., Puntel, M., Xiong, W., Zirger, J. M., Barcia, C., Curtin, J. F., et al. (2005). Regulatable gene expression systems for gene therapy applications: progress and future challenges. *Mol. Ther.* 12, 189–211. doi: 10.1016/j.ymthe.2005.03.022

Hall, H., Jewett, M., Landeck, N., Nilsson, N., SchagerlÖf, U., Leanza, G., et al. (2013). Characterization of cognitive deficits in rats overexpressing human alpha-synuclein in the ventral tegmental area and medial septum using recombinant adeno-associated viral vectors. *PLoS One* 8:e64844. doi: 10.1371/journal.pone.0064844

Hattori, N., and Sato, S. (2007). Animal models of Parkinson's disease: similarities and differences between the disease and models. *Neuropathology* 27, 479–483. doi: 10.1111/j.1440-1789.2007.00842.x

Ibanes, S., and Kremer, E. J. (2013). Canine adenovirus type 2 vector generation *via* I-Sce1-mediated intracellular genome release. *PLoS One* 8:e71032. doi: 10.1371/journal.pone.0071032

Joly, M., Ammersdörfer, S., Schmidtke, D., and Zimmermann, E. (2014). Touchscreen-Based Cognitive Tasks Reveal Age-Related Impairment in a Primate Aging Model, the Grey Mouse Lemur (*Microcebus murinus*). *PLoS One* 9:e109393. doi: 10.1371/journal.pone.0109393

Joly, M., Deputte, B., and Verdier, J. M. (2006). Age effect on olfactory discrimination in a non-human primate, *Microcebus murinus*. *Neurobiol. Aging* 27, 1045–1049. doi: 10.1016/j.neurobiolaging.2005.05.001

Joly, M., Michel, B., Deputte, B., and Verdier, J.-M. (2004). Odor discrimination assessment with an automated olfactometric method in a prosimian primate, *Microcebus murinus*. *Physiol. Behav.* 82, 325–329. doi: 10.1016/j.physbeh.2004.03.019

Junyent, F., and Kremer, E. J. (2015). CAV-2—why a canine virus is a neurobiologist's best friend. *Curr. Opin. Pharmacol.* 24, 86–93. doi: 10.1016/j.coph.2015.08.004

Kirik, D., Annett, L. E., Burger, C., Muzyczka, N., Mandel, R. J., and Björklund, A. (2003). Nigrostriatal α-synucleinopathy induced by viral vector-mediated overexpression of human α-synuclein: a new primate model of Parkinson's disease. *Proc. Natl. Acad. Sci. U S A* 100, 2884–2889. doi: 10.1073/pnas.0536383100

Kirik, D., Rosenblad, C., Bjorklund, A., and Mandel, R. J. (2000). Long-term rAAV-mediated gene transfer of GDNF in the rat Parkinson's model: intrastriatal but not intranigral transduction promotes functional

regeneration in the lesioned nigrostriatal system. *J. Neurosci.* 20, 4686–4700. doi: 10.1523/JNEUROSCI.20-12-04686.2000

Klein, C., and Westenberger, A. (2012). Genetics of Parkinson's disease. *Cold Spring Harb. Perspect. Med.* 2:a008888. doi: 10.1101/cshperspect.a008888

Koprich, J. B., Johnston, T. H., Reyes, G., Omana, V., and Brotchie, J. M. (2016). Towards a Non-Human Primate Model of Alpha-Synucleinopathy for Development of Therapeutics for Parkinson's Disease: Optimization of AAV1/2 Delivery Parameters to Drive Sustained Expression of Alpha Synuclein and Dopaminergic Degeneration in Macaque. *PLoS ONE* 11:e0167235. doi: 10.1371/journal.pone.0167235

Kordower, J. H., Emborg, M. E., Bloch, J., Ma, S. Y., Chu, Y., Leventhal, L., et al. (2000). Neurodegeneration prevented by lentiviral vector delivery of GDNF in primate models of Parkinson's disease. *Science* 290, 767–773. doi: 10.1126/science.290.5492.767

Kordower, J. H., Herzog, C. D., Dass, B., Bakay, R. A., Stansell, J. 3rd, Gasmi, M., et al. (2006). Delivery of neurturin by AAV2 (CERE-120)-mediated gene transfer provides structural and functional neuroprotection and neurorestoration in MPTP-treated monkeys. *Ann. Neurol.* 60, 706–715. doi: 10.1002/ana.21032

Kordower, J. H., Olanow, C. W., Dodiya, H. B., Chu, Y., Beach, T. G., Adler, C. H., et al. (2013). Disease duration and the integrity of the nigrostriatal system in Parkinson's disease. *Brain J. Neurol.* 136, 2419–2431. doi: 10.1093/brain/awt192

Kremer, E. J., and Nemerow, G. R. (2015). Adenovirus tales: from the cell surface to the nuclear pore complex. *PLoS Pathog* 11:e1004821. doi: 10.1371/journal.ppat.1004821

Kremer, E. J., Boutin, S., Chillon, M., and Danos, O. (2000). Canine adenovirus vectors: an alternative for adenovirus mediated gene transfer. *J. Virol.* 74, 505–512. doi: 10.1128/jvi.74.1.505-512.2000

Languille, S., Blanc, S., Blin, O., Canale, C. I., Dal-Pan, A., Devau, G., et al. (2012). The grey mouse lemur: a non-human primate model for ageing studies. *Ageing Res. Rev.* 11, 150–162. doi: 10.1016/j.arr.2011.07.001

Lee, B. D., Shin, J.-H., VanKampen, J., Petrucelli, L., West, A. B., Ko, H. S., et al. (2010). Inhibitors of leucine-rich repeat kinase-2 protect against models of Parkinson's disease. *Nat. Med.* 16, 998–1000. doi: 10.1038/nm.2199

Lewis, S. J., Dove, A., Robbins, T. W., Barker, R. A., and Owen, A. M. (2003). Cognitive impairments in early Parkinson's disease are accompanied by reductions in activity in frontostriatal neural circuitry. *J. Neurosci* 23, 6351–6356. doi: 10.1523/JNEUROSCI.23-15-06351.2003

Lin, X., Parisiadou, L., Gu, X. L., Wang, L., Shim, H., Sun, L., et al. (2009). Leucine-rich repeat kinase 2 regulates the progression of neuropathology induced by Parkinson's-disease-related mutant alpha-synuclein. *Neuron* 64, 807–827. doi: 10.1016/j.neuron.2009.11.006

Loustalot, F., Kremer, E. J., and Salinas, S. (2015). The intracellular domain of the coxsackievirus and adenovirus receptor differentially influences adenovirus entry. *J. Virol* 89, 9417–9426. doi: 10.1128/jvi.01488-15

Luchtman, D. W., Meng, Q., and Song, C. (2012). Ethyl-eicosapentaenoate (E-EPA) attenuates motor impairments and inflammation in the MPTP-probenecid mouse model of Parkinson's disease. *Behav. Brain Res.* 226, 386–396. doi: 10.1016/j.bbr.2011.09.033

Luchtman, D. W., Shao, D., and Song, C. (2009). Behavior, neurotransmitters and inflammation in three regimens of the MPTP mouse model of Parkinson's disease. *Physiol. Behav.* 98, 130–138. doi: 10.1016/j.physbeh.2009.04.021

Marks, W. J. Jr., Bartus, R. T., Siffert, J., Davis, C. S., Lozano, A., Boulis, N., et al. (2010). Gene delivery of AAV2-neurturin for Parkinson's disease: a double-blind, randomised, controlled trial. *Lancet Neurol.* 9, 1164–1172. doi: 10.1016/S1474-4422(10)70254-4

Martin-Touaux, E., Puech, J. P., Château, D., Emiliani, C., Kremer, E. J., Raben, N., et al. (2002). Muscle as a putative producer of acid alpha-glucosidase for glycogenosis type II gene therapy. *Hum. Mol. Genet* 11, 1637–1645. doi: 10.1093/hmg/11.14.1637

Mestre-Francés, N., Nicot, S., Rouland, S., Biacabe, A. G., Quadrio, I., Perret-Liaudet, A., et al. (2012). Oral transmission of L-type bovine spongiform encephalopathy in primate model. *Emerging Infect. Dis.* 18, 142–145. doi: 10.3201/eid1801.111092

Mestre-Francés, N., Serratrice, N., Gennetier, A., Devau, G., Cobo, S., Trouche, S. G., et al. (2018). Exogenous LRRK2G2019S induces parkinsonian-like pathology in a nonhuman primate. *JCI Insight* 3:e98202. doi: 10.1172/jci.insight.98202

O'Keeffe, G. W., and Sullivan, A. M. (2018). Evidence for dopaminergic axonal degeneration as an early pathological process in Parkinson's disease. *Parkinsonism Relat. Disord.* 56, 9–15. doi: 10.1016/j.parkreldis.2018.06.025

Petroske, E., Meredith, G. E., Callen, S., Totterdell, S., and Lau, Y. S. (2001). Mouse model of Parkinsonism: a comparison between subacute MPTP and chronic MPTP/probenecid treatment. *Neuroscience* 106, 589–601. doi: 10.1016/s0306-4522(01)00295-0

Picq, J. L. (2007). Aging affects executive functions and memory in mouse lemur primates. *Exp. Gerontol.* 42, 223–232. doi: 10.1016/j.exger.2006.09.013

Picq, J. L., Aujard, F., Volk, A., and Dhenain, M. (2012). Age-related cerebral atrophy in nonhuman primates predicts cognitive impairments. *Neurobiol. Aging* 33, 1096–1109. doi: 10.1016/j.neurobiolaging.2010.09.009

Piersanti, S., Astrologo, L., Licursi, V., Costa, R., Roncaglia, E., Gennetier, A., et al. (2013). Differentiated neuroprogenitor cells incubated with human or canine adenovirus, or lentiviral vectors have distinct transcriptome profiles. *PLoS One* 8:e69808. doi: 10.1371/journal.pone.0069808

Polymeropoulos, M. H., Lavedan, C., Leroy, E., Ide, S. E., Dehejia, A., Dutra, A., et al. (1997). Mutation in the alpha-synuclein gene identified in families with Parkinson's disease. *Science* 276, 2045–2047. doi: 10.1126/science.276.5321.2045

Przedborski, S., Levivier, M., Jiang, H., Ferreira, M., Jackson-Lewis, V., Donaldson, D., et al. (1995). Dose-dependent lesions of the dopaminergic nigrostriatal pathway induced by intrastriatal injection of 6-hydroxydopamine. *Neuroscience* 67, 631–647. doi: 10.1016/0306-4522(95)00066-r

Rademacher, C., Bru, T., McBride, R., Robison, E., Nycholat, C. M., Kremer, E. J., et al. (2012). A Siglec-like sialic-acid-binding motif revealed in an adenovirus capsid protein. *Glycobiology* 22, 1086–1091. doi: 10.1093/glycob/cws073

Ramonet, D., Daher, J. P., Lin, B. M., Stafa, K., Kim, J., Banerjee, R., et al. (2011). Dopaminergic neuronal loss, reduced neurite complexity and autophagic abnormalities in transgenic mice expressing G2019S mutant LRRK2. *PLoS ONE* 6:e18568. doi: 10.1371/journal.pone.0018568

Salinas, S., Bilsland, L. G., Henaff, D., Weston, A. E., Keriel, A., Schiavo, G., et al. (2009). CAR-associated vesicular transport of an adenovirus in motor neuron axons. *PLoS Pathog* 5:e1000442. doi: 10.3410/f.1162577.624132

Salinas, S., Schiavo, G., and Kremer, E. J. (2010). A hitchhiker's guide to the nervous system: the complex journey of viruses and toxins. *Nat. Rev. Microbiol.* 8, 645–655. doi: 10.1038/nrmicro2395

Schober, A. (2004). Classic toxin-induced animal models of Parkinson's disease: 6-OHDA and MPTP. *Cell Tissue Res.* 318, 215–224. doi: 10.1007/s00441-004-0938-y

Schoehn, G., El Bakkouri, M., Fabry, C. M., Billet, O., Estrozi, L. F., Le, L., et al. (2008). Three-dimensional structure of canine adenovirus serotype 2 capsid. *J. Virol.* 82, 3192–3203. doi: 10.1128/jvi.02393-07

Schwarz, L. A., Miyamichi, K., Gao, X. J., Beier, K. T., Weissbourd, B., DeLoach, K. E., et al. (2015). Viral-genetic tracing of the input-output organization of a central noradrenaline circuit. *Nature* 524, 88–92. doi: 10.1038/nature14600

Seiradake, E., Lortat-Jacob, H., Billet, O., Kremer, E. J., and Cusack, S. (2006). Structural and mutational analysis of human Ad37 and canine adenovirus 2 fiber heads in complex with the D1 domain of coxsackie and adenovirus receptor. *J. Biol. Chem.* 281, 33704–33716. doi: 10.1074/jbc.m605316200

Soudais, C., Boutin, S., and Kremer, E. J. (2001a). Characterization of cis-acting sequences involved in canine adenovirus packaging. *Mol. Ther.* 3, 631–640. doi: 10.1006/mthe.2001.0263

Soudais, C., Boutin, S., Hong, S. S., Chillon, M., Danos, O., Bergelson, J. M., et al. (2000). Canine adenovirus type 2 attachment and internalization: Coxsackievirus-adenovirus receptor, alternative receptors and an RGD-independent pathway. *J. Virol.* 74, 10639–10649. doi: 10.1128/jvi.74.22.10639-10649.2000

Soudais, C., Laplace-Builhe, C., Kissa, K., and Kremer, E. J. (2001b). Preferential transduction of neurons by canine adenovirus vectors and their efficient retrograde transport *in vivo*. *FASEB J* 15, 2283–2285. doi: 10.1096/fj.01-0321fje

Su, X., Fischer, D. L., Li, X., Bankiewicz, K., Sortwell, C. E., and Federoff, H. J. (2017). Alpha-Synuclein mRNA is not increased in sporadic PD and alpha-

synuclein accumulation does not block GDNF signaling in Parkinson's disease and disease models. *Mol. Ther. J. Am. Soc. Gene Ther.* 25, 2231–2235. doi: 10.1016/j.ymthe.2017.04.018

Su, X., Kells, A. P., Huang, E. J., Lee, H. S., Hadaczek, P., Beyer, J., et al. (2009). Safety evaluation of AAV2-GDNF gene transfer into the dopaminergic nigrostriatal pathway in aged and parkinsonian rhesus monkeys. *Hum. Gene Ther.* 20, 1627–1640. doi: 10.1089/hum.2009.103

Tan, S. K., Hartung, H., Sharp, T., and Temel, Y. (2011). Serotonin-dependent depression in Parkinson's Disease: a role for the subthalamic nucleus? *Neuropharmacology* 61, 387–399. doi: 10.1016/j.neuropharm.2011.01.006

Taymans, J.-M., and Greggio, E. (2016). LRRK2 kinase inhibition as a therapeutic strategy for Parkinson's Disease, where do we stand? *Curr. Neuropharmacol.* 14, 214–225. doi: 10.2174/1570159X13666151030102847

Trouche, S. G., Maurice, T., Rouland, S., Verdier, J. M., and Mestre-Francés, N. (2010). The three-panel runway maze adapted to Microcebus murinus reveals age-related differences in memory and perseverance performances. *Neurobiol. Learn. Mem.* 94, 100–106. doi: 10.1016/j.nlm.2010.04.006

Tsika, E., Kannan, M., Foo, C. S., Dikeman, D., Glauser, L., Gellhaar, S., et al. (2014). Conditional expression of Parkinson's disease-related R1441C LRRK2 in midbrain dopaminergic neurons of mice causes nuclear abnormalities without neurodegeneration. *Neurobiol. Dis.* 71, 345–358. doi: 10.1016/j.nbd.2014.08.027

Verdier, J. M., Acquatella, I., Lautier, C., Devau, G., Trouche, S. G., Lasbleiz, C., et al. (2015). Lessons from the analysis of nonhuman primates for understanding human aging and neurodegenerative diseases. *Front. Neurosci.* 9:64. doi: 10.3389/fnins.2015.00064

Warren Olanow, C., Bartus, R. T., Baumann, T. L., Factor, S., Boulis, N., Stacy, M., et al. (2015). Gene delivery of neurturin to putamen and substantia nigra in Parkinson disease: A double-blind, randomized, controlled trial. *Ann. Neurol.* 78, 248–257. doi: 10.1002/ana.24436

Yang, W., Wang, G., Wang, C.-E., Guo, X., Yin, P., Gao, J., et al. (2015). Mutant alpha-synuclein causes age-dependent neuropathology in monkey brain. *J. Neurosci.* 35, 8345–8358. doi: 10.1523/jneurosci.2727-15.2015

Zhou, H., Huang, C., Tong, J., Hong, W. C., Liu, Y.-J., and Xia, X.-G. (2011). Temporal expression of mutant LRRK2 in adult rats impairs dopamine reuptake. *Int. J. Biol. Sci.* 7, 753–761. doi: 10.7150/ijbs.7.753

Conflict of Interest Statement: The authors declare that the research was conducted in the absence of any commercial or financial relationships that could be construed as a potential conflict of interest.

frontiers in Molecular Neuroscience

ORIGINAL RESEARCH
published: 28 February 2019
doi: 10.3389/fnmol.2019.00049

An Intersectional Approach to Target Neural Circuits With Cell- and Projection-Type Specificity: Validation in the Mesolimbic Dopamine System

*Nefeli Kakava-Georgiadou[1], Maria M. Zwartkruis[1,2], Clara Bullich-Vilarrubias[1,2], Mieneke C. M. Luijendijk[1], Keith M. Garner[1], Geoffrey van der Plasse[1] and Roger A. H. Adan[1,3]**

[1] Division of Neuroscience, Department of Translational Neuroscience, Brain Center Rudolf Magnus, University Medical Center Utrecht, Utrecht, Netherlands, [2] Master's Program Neuroscience and Cognition, Utrecht University, Utrecht, Netherlands, [3] Institute of Neuroscience and Physiology, The Sahlgrenska Academy at the University of Gothenburg, Gothenburg, Sweden

Development of tools to manipulate activity of specific neurons is important for dissecting the function of neural circuits. Viral vectors and conditional transgenic animal lines that target recombinases to specific cells facilitate the successful manipulation and recording of specific subsets of neurons. So far, it has been possible to target neuronal subtypes within a certain brain region based on transcriptional control regions from a gene selectively expressed in those cells or based upon its projections. Nevertheless, there are only a few tools available that combine this and target a neuronal subtype within a projection. We tested a viral vector system, consisting of a canine adenovirus type 2 expressing a Cre-dependent Flp recombinase (CavFlexFlp) and an adeno-associated viral (AAV) vector expressing a Flp-dependent cDNA, which targets neurons in a subtype- and projection-specific manner. As proof of principle we targeted expression of a Designer Receptor Exclusively Activated by Designer Drugs (DREADD) to the dopamine neurons of the mesolimbic projection, which allows the transient activation of neurons by the ligand Clozapine-N-Oxide (CNO). We validated that the system specifically targets dopamine neurons and that chemogenetic activation of these neurons induces an increase in locomotor activity. We thus validated a valuable tool that allows *in vivo* neuronal activation in a projection- and subtype-specific manner.

Keywords: VTA, dopamine, DREADD, chemogenetics, Cav2, canine, CNO, Flp

OPEN ACCESS

Edited by:
Eric J. Kremer, UMR5535 Institut de Génétique Moléculaire de Montpellier (IGMM), France

Reviewed by:
Fabio Marti, Institut National de la Santé et de la Recherche Médicale (INSERM), France
Yuchio Yanagawa, Gunma University, Japan

***Correspondence:**
Roger A. H. Adan
r.a.h.adan@umcutrecht.nl

Received: *19 November 2018*
Accepted: *11 February 2019*
Published: *28 February 2019*

Citation:
Kakava-Georgiadou N, Zwartkruis MM, Bullich-Vilarrubias C, Luijendijk MCM, Garner KM, van der Plasse G and Adan RAH (2019) An Intersectional Approach to Target Neural Circuits With Cell- and Projection-Type Specificity: Validation in the Mesolimbic Dopamine System. Front. Mol. Neurosci. 12:49. doi: 10.3389/fnmol.2019.00049

INTRODUCTION

Investigating the roles of specific subsets of neurons in behavior is a major challenge in neuroscience. To this end, several genetic tools have been developed for manipulation of neuronal activity *in vivo*. Common tools for transient activation or inactivation of neurons are opto- and chemogenetics. Optogenetics utilizes expression of light-sensitive ion channels which are selectively activated by light at a precise millisecond scale, causing neuronal depolarization, thereby mimicking the physiological function of neurons through action potentials (Fenno et al., 2011). Chemogenetics, on the other hand, allows for a longer-lasting but still transient manipulation of neuronal activity, via expression of Designer

Receptors Exclusively Activated by Designer Drugs (DREADDs). Mutated human muscarinic receptors are the most commonly used DREADDs and are exclusively activated by designer drugs such as Clozapine-N-Oxide (CNO), which – in most cases – are administered systemically to the animals (Roth, 2016). Chemogenetic tools are used to transiently activate or inhibit neurons and determine their role in behavior or mimic physiological or pathological situations of general neuronal hyper- or hypo-activity.

The further development of genetic tools to more efficiently and specifically target neural specific cells will help neuroscientists to gain knowledge about the role of specific neurons in behavior and disease.

The most common strategy to express chemogenetic tools in the central nervous system (CNS) is to use viral vectors, such as the adeno-associated virus (AAV) as well as viral vectors that allow retrograde transfer, such as canine adenovirus type 2 (Cav2) (Davidson and Breakefield, 2003; Betley and Sternson, 2011; Gholizadeh et al., 2013; Junyent and Kremer, 2015). The development of the Cre/lox system has facilitated the successful delivery and expression of these tools in either a subtype or projection-specific manner. For example, the combination of Cre-dependent DREADDs with the retrograde viral vector Cav2-Cre injected in an output region permits projection- (but not subtype-) specific circuit manipulation (Boender et al., 2014; Augur et al., 2016). Instead, the delivery of Cre-dependent hM3D(Gq) DREADD in Cre-driver mouse or rat lines allows for the subtype- (but not projection-) specific activation of neurons with CNO (Krashes et al., 2011; Atasoy et al., 2012; Boekhoudt et al., 2016). Since DREADDs are also expressed in neuronal terminals, by using a subtype-specific system and locally applying CNO with a cannula in the output region, it is possible to activate neuronal subtypes in a subtype- and projection-specific manner (Stachniak et al., 2014; Verharen et al., 2018). Nevertheless, this technique is invasive to the animal – since it requires the placement of the cannula – and is time-consuming due to the time it takes to deliver CNO compared to an i.p. injection. Finally, even though the location and spread of viral expression can be assessed post-mortem, it is not possible to assess these parameters for drug delivery and there is also a possibility of off-target activation of passing fibers of neurons that belong to a different projection.

We aimed to further develop and validate a strategy that facilitates projection- and subtype- specific delivery of DREADD in neuronal subtypes. As a model system we targeted ventral tegmental area (VTA) dopamine neurons that project to the Nucleus Accumbens (NAc). We created a DREADD viral vector which we use in a double conditional system in order to achieve projection- and subtype-specific activation. To this end, we used TH::Cre rats, in which Cre recombinase is expressed in Tyrosine Hydroxylase neurons (a marker for dopamine neurons in the VTA). In these rats we injected: (1) CavFlexFlp in the NAc, which delivers the recombinase flippase (Flp) retrogradely in a Cre-dependent manner, thereby expressing Flp in all TH^+ neurons that project to NAc (Schwarz et al., 2015) and (2) a new Flp-dependent Gq-coupled DREADD [frt-DREADDq] in the VTA, which brings expression of this DREADD in dopamine cells in the VTA > NAc projection. We assessed the ability of the system to specifically target mesolimbic dopamine neurons and tested the efficacy of the system to manipulate behavior.

MATERIALS AND METHODS

Animals

Adult TH::Cre ($^{+/-}$) and ($^{-/-}$) rats on a Long-Evans background [provided by K. Deisseroth (Witten et al., 2011)] and adult Pvalb-2A-FlpO-D ($^{+/-}$) and ($^{-/-}$) mice (022730, Jackson Laboratories) on a C57Bl/6J background were used. Male and female animals that were used for immunohistochemical assessment only were housed socially and kept under a normal 12:12 h light-dark cycle with lights off at 19:00. For behavior experiments male rats were housed individually and kept under a reverse 12:12 h light-dark cycle with lights off at 07:00. All animals were kept at room temperature (21 ± 2°C) and 40–60% of humidity conditions. They were provided with chow and water *ad libitum*. All experiments were approved by the Animal Ethics Committee of Utrecht University and conducted in agreement with Dutch laws (Wet op de Dierproeven, 1996; revised 2014) and European regulations (Guideline 86/609/EEC; Directive 2010/63/EU).

Plasmid Construction and Viruses

Plasmids pAAV-EF1a-DIO-hM3D(Gq)-mCherry and pAAV-hSyn-dF-HA-KORD-IRES-mCitrine (pAAV-frt-KORD-mCitrine), gifts from Bryan Roth (Addgene plasmids #50460 and #65417), were digested with restriction enzymes AscI and NheI and hM3D(Gq):mCherry insert and pAAV-hSyn-dF backbone were ligated to generate plasmid pAAV-hSyn-frt-hM3D(Gq):mCherry. PCR with forward primer 5'-GCTAGCATGGTGAGCAAGGGCGAG-3' (Additional AscI restriction site on 5' end) and reverse primer 5'-GGCGCGCCTTACTTGTACAG-3' was performed on pAAV-EF1a-DIO-hM3D(Gq)-mCherry, the product was ligated into pGEMT.easy (Promega) and after restriction digest with AscI and NheI the mCherry insert was ligated into backbone pAAV-hSyn-dF, to generate plasmid pAAV-hSyn-frt-mCherry. The sequence of the constructs was confirmed with Sanger sequencing. Plasmid pAAV-hSyn-DIO-mCarMyc_f-ChetaHA_r (pAAV-mCAR) was provided by Li et al. (2018).

Serotype 5 AAV viruses were generated as described earlier (Backer, 2010), except that the vectors pAAV-hSyn-frt-hM3D(Gq):mCherry, pAAV-hSyn-frt-mCherry, pAAV-frt-KORD-mCitrine, and pAAV-mCAR were co-transfected with the pDP5 plasmid (Grimm et al., 2003) at a molar ratio of 1:1, resulting in AAV vectors rAAV5-hSyn-frt-hM3D(Gq):mCherry (frt-DREADDq), rAAV5-hSyn-frt-mCherry (frt-mCherry), rAAV5-frt-KORD-IRES-mCitirine (frt-KORD), rAAV5-mCAR (AAV-mCAR). Serotype 8 virus was generated by co-transfecting plasmids pAAV-hSyn-frt-hM3D(Gq):mCherry, pAR-8 (provided by M. Sena Esteves) and pXX-680 [provided by R. Samulski (Grieger et al., 2016)], at a molar ratio of 1:1:1 to create vector rAAV8-hSyn-frt- hM3D(Gq):mCherry. The plasmid pAAV-EF1a-Cre

(gift from Karl Deisseroth, addgene plasmid # 55636) was co-transfected with the plasmid pAAV2-retro helper (gift from Alla Karpova and David Schaffer, addgene plasmid # 81070) and plasmid pXX-680 at a molar ratio of 1:1:1 to create vector retro-AAV2-Cre (Retro-Cre). Titer of viruses was determined using real-time PCR (qPCR) with primers binding on the wPRE element or mCherry. CAV-FLEx^{loxP}-Flp (CavFlexFlp) and Cav2-Cre were purchased from IGMM, Montpellier, France and rAAV5-hSyn-DIO-hM3D(Gq):mCherry (lox-DREADDq) was purchased from UNC Vector Core and Addgene (Addgene viral prep # 44361-AAV5).

Stereotaxic Surgeries

All viruses were injected on the same day, except for rAAV5-mCAR, which was injected 2 weeks prior to the rest of the viruses. Rats were anesthetized with an intramuscular injection of hypnorm (0.315 mg/kg fentanyl and 10 mg/kg fluanisone, Janssen Pharmaceutica, Beerse, Belgium). Mice were anesthetized with ketamine (75 mg/kg, Narketan) and medetomidine (1 mg/kg, Seda Start). Animals were placed on a stereotaxic apparatus (David Kopf Instruments, Tujunga, United States or Configuration Stereotaxic, SGL Manip 18° – 68U801, UNO, Netherlands) and a small incision was made along the midline of the skull. Viruses were injected using a 34G stainless steel needle connected to 10 μl Hamilton syringe at a rate of 0.2 μL/min. In PV-FlpO mice, 1 μL of rAAV5-hSyn-frt-hM3D(Gq):mCherry (2×10^{12}g.c./ml) was injected into the ventral hippocampus (−3.50 mm anteroposterior (AP), ± 2.90 mm mediolateral (ML) from Bregma, and −4.70 mm dorsoventral (DV) from the skull, no angle). In rats, 0.3–1 μl of CAV-FLEx^{loxP}-Flp (2.8×10^{12}g.c./ml) or Cav2-Cre or retroCre (2×10^{12}g.c./ml) or saline (0,9% NaCl) were bilaterally injected into the NAc (+1.20 mm anteroposterior (AP), ± 2.80 mm mediolateral (ML) from Bregma, and -7.50 mm dorsoventral (DV) from the skull, at an angle of 10°) and rAAV5-mCAR or rAAV5-hSyn-frt-KORD-IRES-mCitrine or rAAV5-hSyn-DIO-hM3D(Gq):mCherry (2×10^{12}g.c./ml) or rAAV5-hSyn-frt-hM3D(Gq):mCherry or rAAV5-hSyn-frt-mCherry ($2.5–5 \times 10^{12}$g.c./ml) into the VTA (-5.60 mm AP, ± 1.30 mm ML from Bregma, and -8.20 mm DV from the skull, at an angle of 5°). After injection, the needle was maintained at its injection position for 15 min. After surgery, carprofen was administered for pain relief (5 mg/kg per day for 3 days, subcutaneous, s.c.) and saline (1 ml/100 g in rats and 0.4 ml/10 g in mice, once, s.c.).

Histology

Mice used in **Figure 1A** were perfused 2 weeks after surgery. Rats used in **Figures 1B,C**, 2A,B,D were perfused 7, 4, 5, 7, and 7 weeks after the last surgery, respectively. Rats used in **Figure 2E** were from various experiments and they were perfused 7 to 17 weeks after surgery, timepoints balanced between groups. Animals were sacrificed with a sodium pentobarbital overdose (200 mg/mL, Euthanimal, Alfasan BV, Netherlands). Animals were perfused with ice-cold 1× phosphate buffered saline (PBS) pH 7.3, followed by ice-cold 4% paraformaldehyde (PFA) in 1×PBS pH 7.3. Brains were removed and incubated overnight in 4% PFA, then transferred consecutively to 20% for 1 day and 30% for 2 days sucrose solution in 1×PBS. After the brains had sunk in the sucrose solution, they were snap-frozen by isopentane immersion and stored at −80°C. Coronal sections were sliced at 40 μm thickness in a cryostat (Leica, Germany).

Immunohistochemistry

Sections were blocked with 10% normal goat serum (NGS), 1% Triton X-100 in 1×PBS, followed by overnight incubation with primary antibodies (1:500 mouse anti-TH, MAB318, Milipore; 1:750 rabbit anti-dsRed,632496, Clontech; 1:500 rabbit anti-TH, Ab152, Milipore; 1:1000 chicken anti-GFP, ab13970, Abcam) in 3% NGS, 0,25% Triton X-100 in 1× PBS. Sections were incubated with the secondary antibodies (1:500 goat anti-mouse 488,ab150113, Abcam; 1:500 goat anti-rabbit 568,ab175471, Abcam; 1:500 goat anti-chicken 488, ab150169, Abcam) for 1 h at room temperature and DAPI (1:1000 in PBS 1×) for 15'. Between all steps sections were washed three times for 5–10 min in PBS 1×. Sections were then mounted on microscope glasses, let to dry and covered with Fluorsave Reagent (345789, Calbiochem).

Imaging and Image Analysis

For quantifications of specificity and efficiency, pictures were taken at 20× magnification at a confocal microscope (Olympus Fluoview FV1000, Olympus, Japan). Cells were manually counted using the Cell Counter plugin of ImageJ. For intensity analysis, 10× magnification pictures were taken with an epi-fluorescent microscope (Zeiss Scope A1, ZEISS, Germany). Intensity was measured on ImageJ and background fluorescence was subtracted. All images within a figure part (e.g., in 1C) were taken with the same exposure and brightness and contrast were altered in the same levels.

Drugs

Clozapine-N-oxide (CNO; kindly provided by Bryan Roth and NIMH or purchased from AK scientific Cat. No. AMTA056) was dissolved in sterile saline (0.9% NaCl). All injections were given intra-peritoneally (i.p.) at 1 ml per kg body weight, and CNO solution was kept at 4°C in between injections, for a maximum of 1 week.

Locomotor Activity

At 4 weeks after surgery rats were acclimatized for 1 h to PhenoTyper® 9000 cages (Noldus IT, Wageningen, Netherlands), 43 × 43 × 90 cm, equipped with infrared video cameras in the top to monitor locomotor activity, and to intraperitoneal (i.p.) injections with sterile saline (0.9% NaCl) for at least two times before starting with testing. Behavioral testing started at least 5 weeks after surgery, to allow virus expression to reach its maximum. On the day of the testing, at 10:00 or 13:00 (counterbalanced between groups), rats were habituated to the PhenoTyper cages for 30 min, injected i.p. with CNO or vehicle (saline) counterbalanced between groups and locomotor activity was recorded for 2 h after injections. The test was repeated 48 h after the first test day and rats that previously received CNO, now received saline and vice versa. Locomotor activity was recorded

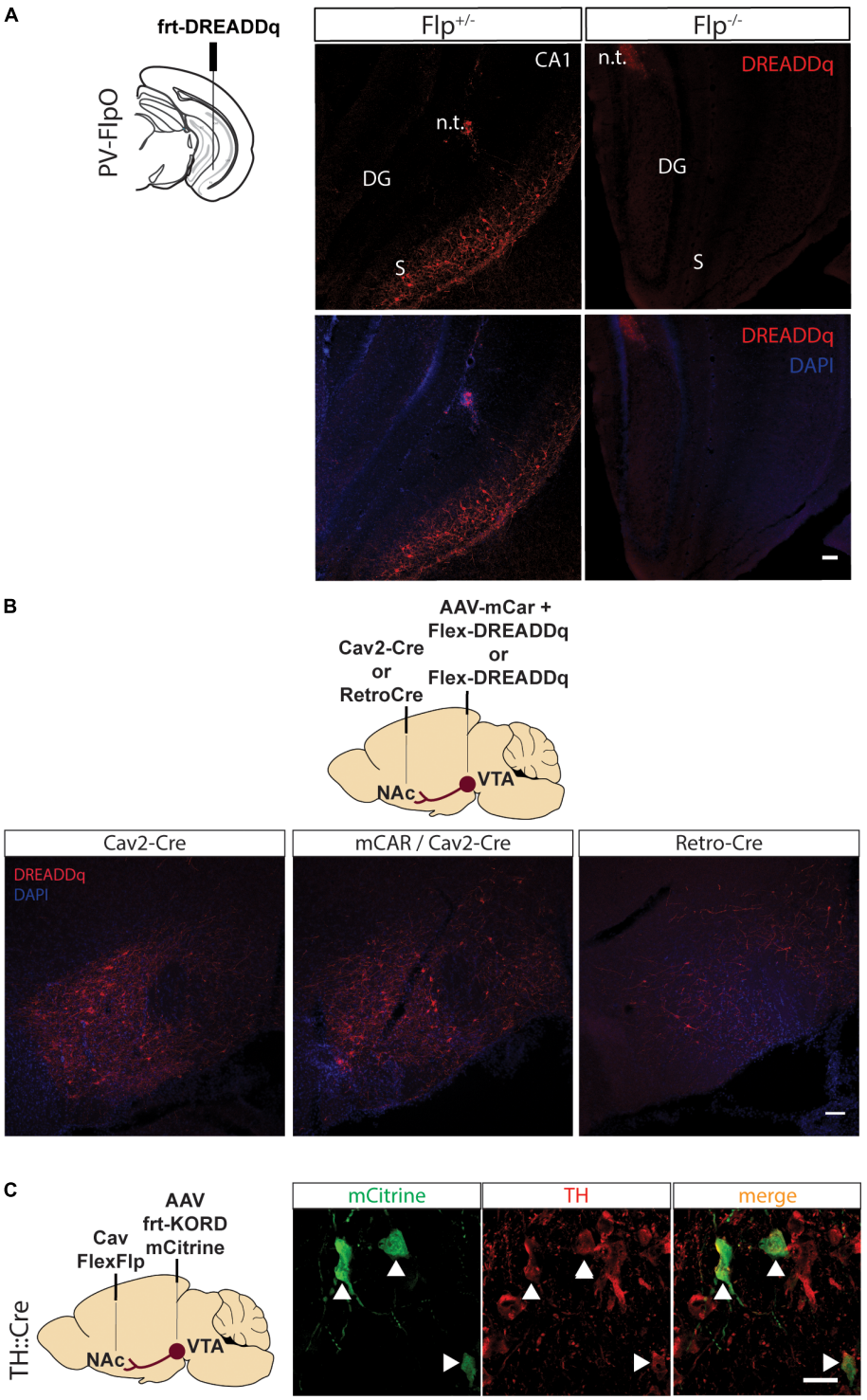

FIGURE 1 | Pilot testing of viral vectors. **(A)** PV-FlpO$^{+/-}$ and $^{-/-}$ mice were injected in the ventral hippocampus with frt-DREADDq. Immunohistochemistry against mCherry (fused to DREADDq) showed expression of DREADDq in sections from ventral hippocampus of PV-FlpO$^{+/-}$ but not of PV-FlpO$^{-/-}$ littermates. **(B)** Rats were injected in the NAc and VTA with a combination of Cav2-Cre and lox-DREADDq (Cav2-Cre) or Cav2-Cre and lox-DREADDq with AAV-mCAR (mCAR/Cav2-Cre) or Retro-Cre and lox-DREADDq (Retro-Cre) respectively. Immunohistochemical detection of mCherry (fused to DREADDq) showed no difference in expression levels between Cav2-Cre and mCAR/Cav2-Cre, whereas Retro-Cre brought lower levels of mCherry expression. **(C)** TH::Cre rats were injected with CavFlexFlp and frt-KORD-mCitrine in the NAc and VTA, respectively, so that VTA>NAc dopamine neurons would be targeted. Immunohistochemistry against mCitrine (green) and TH (red) showed co-localization of the mCitrine^{+} with TH^{+} neurons (white arrows). n.t., needle tract; CA1, field CA1 of the hippocampus; DG, Dentate Gyrus; S, Subiculum.

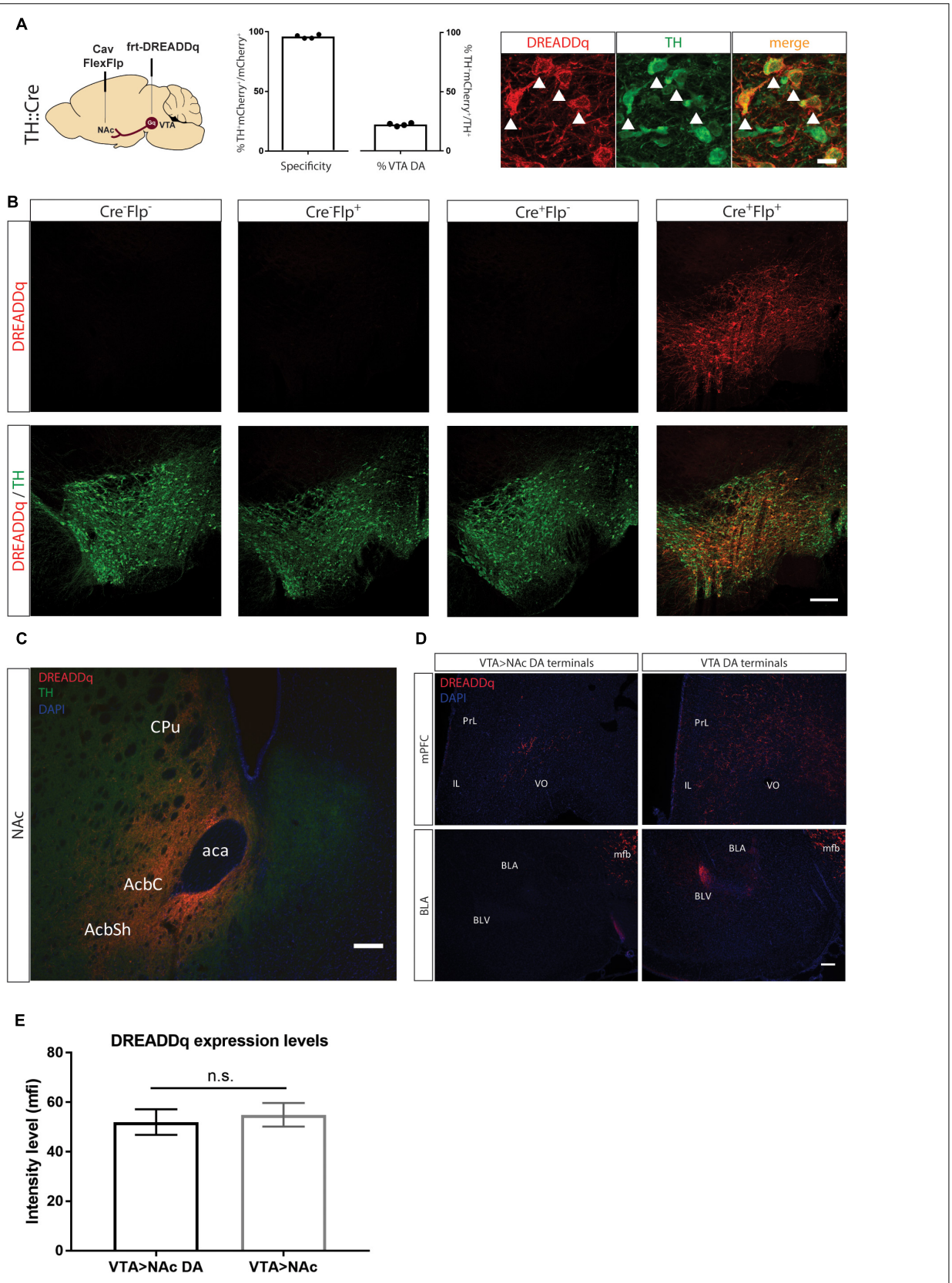

FIGURE 2 | Continued

FIGURE 2 | Targeting VTA>NAc dopamine neurons with DREADDq. **(A)** TH::Cre$^{+/-}$ rats were injected in the NAc and VTA with CavFlexFlp and frt-DREADDq, respectively. Co-staining for mCherry (fused to DREADDq, red) and TH (green), showed co-localization (white arrows), with 22,2% ± 0,6 of the total VTA TH$^+$ neurons targeted (% mCherry$^+$TH$^+$ / total TH$^+$) and specificity of 95,9% ± 0,8 (% mCherry$^+$TH$^+$ / total mCherry$^+$). **(B)** TH::Cre$^{-/-}$ rats were injected with frt-DREADDq in the VTA (Cre$^-$Flp$^-$) or with CavFlexFlp in the NAc and frt-DREADDq in the VTA (Cre$^-$Flp$^+$); TH:Cre$^{+/-}$ rats were injected with frt-DREADDq in the VTA (Cre$^+$Flp$^-$) or with CavFlexFlp in the NAc and frt-DREADDq in the VTA (Cre$^+$Flp$^+$); Immunohistochemical detection of mCherry (fused to DREADDq) showed no expression of DREADDq in Cre$^-$Flp$^-$, Cre$^-$Flp$^+$ and Cre$^+$Flp$^-$ rats, whereas in Cre$^+$Flp$^+$ rats DREADDDq was expressed in the VTA. **(C)** Fibers positive for mCherry (red) were detected in the NAc shell and core, where TH$^+$ fibers are also detected (green) in TH::Cre$^{+/-}$ rats injected in the NAc and VTA with CavFlexFlp and frt-DREADDq, respectively. **(D)** In TH::Cre$^{+/-}$ rats injected in the VTA with lox-DREADDq (VTA DA) fibers positive for mCherry (fused to DREADDq) were detected in the mPFC and the BLA (panels on the right), whereas in TH::Cre$^{+/-}$ rats injected in the NAc and VTA with CavFlexFlp and frt-DREADDq, respectively few or no mCherry$^+$ fibers were detected in the mPFC and the BLA, respectively (panels on the left). **(E)** Expression levels of DREADDq were measured by quantification of mCherry intensity (as mean fluorescent intensity – mfi) in TH::Cre$^{+/-}$ rats injected in the NAc and VTA with CavFlexFlp and frt-DREADDq, respectively (VTA>NAc DA) and TH::Cre$^{-/-}$ rats injected in the NAc and VTA with Cav2-Cre and lox-DREADDq, respectively (VTA>NAc). No difference was found between VTA>NAc DA and VTA>NAc targeting (unpaired *t*-test; $t(25) = 0{,}4093$, $p = 0.6858$); Data represented as mean ± SEM; ns, not significant; Cpu, Caudate putamen; AcbC, Accumbens nucleus, Core; AcbSh, Accumbens nucleus, Shell; aca, anterior commissure; PrL, Prelimbic cortex; IL, Infralimbic cortex; VO, Ventral Orbital cortex; BLA, Basolateral Amygdaloid nucleus, anterior; BLV, Basolateral Amygdaloid nucleus, ventral; mfb, medial forebrain bundle.

at 25 samples per second, and was analyzed with EthoVision XT11.5 (Noldus IT, Wageningen, Netherlands). Movement tracks of the animals' center point were smoothed by locally weighted scatterplot smoothing.

Statistical Analyses

Statistical analyses were performed with GraphPad Prism 7.0 and IBM SPSS version 13. Data was checked for normality and non-parametric tests were performed when data did not follow a Gaussian distribution. Rats with unilateral or no expression were excluded from analysis of locomotor activity.

RESULTS

In order to achieve projection- and subtype-specific expression of transgenes, we utilized a double conditional system comprising of a Cre-driver rat expressing Cre in tyrosine hydroxylase positive cells (TH::Cre), the retrograde virus CAV-FLEx^{loxP}-Flp (CavFlexFlp) in the Nucleus Accumbens (NAc), which infects neurons at their terminals and expresses Flp only in the presence of Cre, and an AAV virus expressing a transgene only in the presence of Flp in the ventral tegmental area (VTA). In order to test this system's specificity and efficiency, we applied it to dopaminergic neurons of the mesolimbic projection and assessed histological and behavioral parameters.

Pilot Testing of Viral Vectors

As a first step to test the system, we performed a series of pilot experiments to assess the specificity of Flp-dependent transgene expression and to find the most efficient way to target the VTA>NAc projection.

First, we created an rAAV5-frt-hM3D(Gq):mCherry (frt-DREADDq), a Flp-dependent DREADD receptor which allows transient activation of neurons when CNO is administered. This virus was expressed when injected into the ventral hippocampus of parvalbumin (PV)-FlpO$^{+/-}$ mice but not in wild-type (PV-FlpO$^{-/-}$) littermates (**Figure 1A**), therefore confirming that it is expressed only in the presence of Flp recombinase.

In an effort to find the most efficient viral vector system to target VTA>NAc projection neurons, we tested novel tools that are known to increase retrograde transfer. Canine adenovirus 2 (Cav2) vectors are robustly used in neuroscience to target projections. Therefore, we injected Cav2-Cre in the NAc and Cre-dependent lox-DREADDq in the VTA (Cav2-Cre). In a second group of rats we aimed to increase Cav uptake by inducing expression of coxsackievirus and adenovirus receptor (CAR) in the neuronal terminals of the VTA>NAc projection, by injecting the VTA with AAV-mCAR 2 weeks prior the injections of Cav2-Cre in the NAc and lox-DREADDq in the VTA of rats (mCar/Cav2-Cre) (Li et al., 2018). Finally, in a third group of rats we injected Retro-Cre (a virus expressing Cre packaged in the retro-AAV2 variant) (Tervo et al., 2016) in the NAc and lox-DREADDq in the VTA (Retro-Cre). We compared the expression of DREADDq between these three groups. Overall, we observed equal levels of expression of DREADDq in the mCar/Cav2-Cre and Cav2-Cre groups and much lower levels in the Retro-Cre group (**Figure 1B**). Therefore, using a Cav2 was the most efficient way in our hands to target the VTA>NAc projection in rats.

CavFlexFlp retrogradely delivers Flp in a Cre-dependent manner (Schwarz et al., 2015). In order to assess the specificity of this vector, we injected CavFlexFlp in the NAc and a previously established frt-KORD-mCitrine (Vardy et al., 2015) into the VTA of TH::Cre rats. VTA TH$^+$ (dopamine) neurons stained for mCitrine with a specificity of 91,15% ± 0,95 (mean ± SEM, $n = 2$, **Figure 1C**).

We thus demonstrated the specificity of each of the vectors which we aimed to combine in subsequent experiments.

Targeting VTA>NAc Dopamine Neurons With DREADDq

We next injected CavFlexFlp in the NAc and rAAV5- or rAAV8-frt-DREADDq in the VTA of TH::Cre rats ($n = 2$/group). We did not observe differences in expression between the two serotypes, suggesting similar infection efficacy of the two different viral coats and therefore combined the results. 22,2% ± 0,6 of the total VTA TH$^+$ neurons were targeted with a specificity of 95,9% ± 0,8 (**Figure 2A**). In all subsequent experiments serotype 5 was used.

To further confirm the specificity of the viral vector system, we determined expression of mCherry in the absence of either or both of the recombinases Cre (by using a non-transgenic littermate) and Flp (by injecting saline instead of CavFlexFlp), the presence of which is essential for expression. We found no expression in all three control conditions (**Figure 2B**).

Next, we explored whether there is expression of DREADDq in the projection terminal sites of mesolimbic dopamine neurons in the NAc. We found robust expression of mCherry (fused to DREADDq) in the NAc core and shell (**Figure 2C**) as well as along the needle tract in the dorsomedial part of the striatum (not shown).

Moreover, we examined two more major output sites of VTA dopamine neurons: the medial prefrontal cortex (mPFC) and basolateral amygdala (BLA) in order to assess if VTA>NAc dopamine neurons make collaterals to these regions (Lammel et al., 2008; Yetnikoff et al., 2014). We found fewer or no DREADDq^{+} fibers in the mPFC and BLA, respectively, in TH::Cre rats injected with frt-DREADDq and CavFlexFlp in the VTA and the NAc, respectively (VTA>NAc DA) compared to TH::Cre rats injected with DIO-Gq in the VTA (VTA DA) (**Figure 2D**).

Considering that dopamine neurons form a subpopulation of the VTA>NAc projection, we expected that fewer neurons would express DREADDq when targeting the VTA>NAc DA projection compared to targeting the VTA>NAc projection. In a pilot experiment, we found that in TH::Cre rats injected with CavFlexFlp in the NAc and frt-DREADDq in the VTA (VTA>NAc DA), the total number of DREADDq^{+} neurons in the VTA was 645 ± 51 (mean ± SEM, n = 2). In Long-Evans rats injected with Cav2-Cre in the NAc and lox-DREADDq in the VTA (VTA>NAc), 661,5 ± 74,25 (mean ± SEM; n = 2) DREADDq^{+} neurons were counted in the VTA. To further investigate whether there is a difference in expression levels, we measured DREADDq expression in larger groups of animals, by quantifying intensity of mCherry, which is fused to DREADDq. We found no difference in DREADDq expression levels between VTA>NAc DA and VTA DA groups (unpaired t-test; $t(25)$ = 0,4093, p = 0.6858, **Figure 2E**). Therefore, we concluded that targeting neurons at a subtype- and projection-specific level was as efficient as targeting neurons at a projection-specific level.

Activation of VTA>NAc DA Neurons Increases Locomotor Activity

Next, we aimed to investigate the efficiency of the system to manipulate behavior. Chemogenetic activation of VTA DA neurons or VTA>NAc neurons leads to locomotor hyperactivity (Boender et al., 2014; Boekhoudt et al., 2016). Therefore, we used locomotor activity as an outcome measure in order to assess the efficiency of the system to drive behavior.

We injected CavFlexFlp and frt-DREADDq into the NAc and VTA of TH::Cre$^{+/-}$ rats, respectively (n = 13, Gq group). As controls we used TH::Cre$^{-/-}$ rats (n = 5, Cre^{-} group) as well as TH::Cre$^{+/-}$ rats injected instead with frt-mCherry (n = 4, Gq^{-} group). After at least 5 weeks, we measured the distanced moved in 2 h after CNO and vehicle i.p. administration.

There was no effect of CNO administration on locomotor activity in neither the Cre^{-} group (Friedman test; $\chi^2(5)$ = 0.4, p = 0.9537) or the Gq^{-} group (Friedman test; $\chi^2(4)$ = 4.5, p = 0.1250). Therefore, we merged the two groups in order to increase the power in subsequent analyses (n = 9, Ctl group).

Activation of mesolimbic dopamine neurons with CNO (at 0.3 and 1.0 mg/kg) significantly increased distance moved in 2 h after injection in the Gq group (Friedman test; $\chi^2(13)$ = 0.333, p = 0.0002; Dunn's multiple comparisons *post hoc* test: Saline vs. CNO 0.3 mg/kg p = 0.0004; Saline vs. CNO 1.0 mg/kg p = 0.0017), whereas CNO had no effect in the Ctl group (Friedman test; ($\chi^2(9)$ = 1.556, p = 0.5690) (**Figure 3**).

DISCUSSION

We here assessed a novel tool that targets and allows to transiently activate neurons in a subtype- and projection-specific manner. We demonstrate that the combination of CavFlexFlp with AAV-frt-DREADDq specifically targets mesolimbic dopamine neurons in TH::Cre rats. We also show that CNO increases locomotor activity, showing that sufficient numbers of mesolimbic dopamine neurons were brought under chemogenetic control using this strategy.

In particular, we created a Flp-dependent hM3D(Gq) DREADD which is only expressed in the presence of Flp recombinase (**Figure 1A**). Next, we assessed which is the most efficient viral vector to target the VTA>NAc projection.

Cav2 viruses use coxsackievirus and adenovirus receptors (CAR) in neuronal terminals to infect neurons. Therefore, enhancing expression of CAR may enhance Cav2 tropism, resulting in higher expression of DREADDq. To this end, we targeted the VTA>NAc projection with Cav2-Cre in the NAc and a combination of AAV-mCAR and lox-DREADDq in the VTA (Li et al., 2018). We did not observe differences in expression of

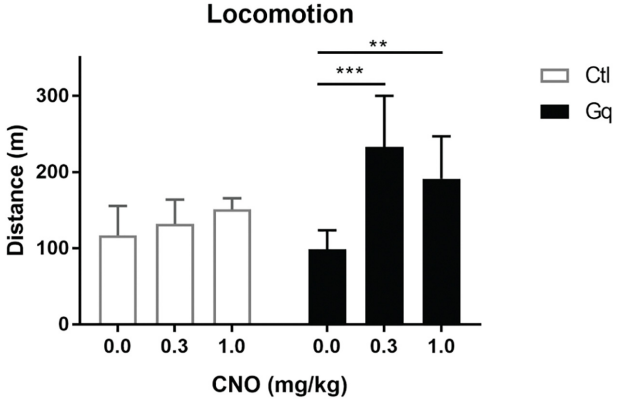

FIGURE 3 | Activation of VTA>NAc DA neurons increases locomotor activity. Gq rats were TH::Cre$^{+/-}$ rats injected in the NAc and VTA with CavFlexFlp and frt-DREADDq, respectively (n = 13); Ctl rats were either TH::Cre$^{+/-}$ rats injected in the NAc and VTA with CavFlexFlp and frt-mCherry, respectively, or TH::Cre$^{-/-}$ rats injected in the NAc and VTA with CavFlexFlp and frt-DREADDq, respectively (total n = 9); CNO administration did not increase locomotor activity in Ctl rats (Friedman test; $\chi^2(9)$ = 1.556, p = 0.5690), whereas CNO significantly increased locomotor activity in Gq rats (Friedman test; $\chi^2(13)$ = 0.333, p = 0.0002; Dunn's multiple comparisons *post hoc* test: Saline vs. CNO 0.3 mg/kg p = 0.0004; Saline vs. CNO 1.0 mg/kg p = 0.0017); Data represented as median with interquartile range; $^{**}P < 0.01$, $^{***}P < 0.001$.

DREADDq after targeting mCAR in the VTA compared to just injecting Cav2-Cre in the NAc, suggesting that VTA dopamine neurons are sensitive enough to be infected by Cav and infection is not further increased by expressing CAR. Another tool for retrograde delivery is a retro-AAV2 carrying Cre recombinase (Tervo et al., 2016). We injected Retro-Cre in the NAc and lox-DREADDq in the VTA and observed that Retro-Cre was less efficient than the previous tools to target the VTA to NAc projection in rats (**Figure 1B**). This data shows that Cav2 is the most efficient way to target the VTA>NAc projection in rats, without the need for a prior injection with AAV-mCAR.

Next, we expressed DREADDq in the dopamine neurons of the VTA>NAc projection by targeting the VTA with frt-DREADDq and the NAc with retrograde Cre-dependent Flp (CavFlexFlp) in TH::Cre rats, and showed that DREADDq is only expressed when both Cre and Flp are present (**Figure 2B**). We also show that terminals in the NAc express DREADDq using this strategy (**Figure 2C**). We found no expression of DREADDq in the BLA, showing that the dopamine neurons targeted in this study do not make collaterals to this region. Moreover, we found very low expression in the mPFC which might be collaterals, but we cannot exclude that this was caused by spread of CavFlexFlp (**Figure 2D**). Even though this is not a major finding, we confirmed previous studies that mostly show that VTA>NAc dopamine projection neurons do not make collaterals to PFC or BLA (Lammel et al., 2008; Yetnikoff et al., 2014). Nevertheless, we cannot exclude the possibility that there might be collaterals to the regions investigated or other regions in the brain (Aransay et al., 2015). However, it is beyond the aims of this study to investigate this further.

In our hands, we did not find a difference in DREADDq expression levels between VTA>NAc and VTA>NAc DA targeting, despite the fact that dopamine neurons constitute around 80% of the VTA>NAc projection (**Figure 2E**). This suggests that efficacy to target specifically dopamine neurons in the VTA>NAc projection is not compromised when two recombinases (Cre and Flp) rather than one (Cre) need to be active to achieve proper recombination.

Dopamine-specific expression of DREADDq in the midbrain, as well as VTA>NAc expression of DREADDq drives CNO-induced locomotor activity (Wang et al., 2013; Boender et al., 2014; Boekhoudt et al., 2016). While our work was in preparation, it was shown that chemogenetic deactivation of VTA>NAc DA neurons in TH-Cre mice, after injection of CavFlexFlp in the NAc and Flp-dependent hM4D(Gi) in the VTA, results in reduction in cocaine-induced hyperlocomotion (Runegaard et al., 2018). In line with this, we found that chemogenetic activation of VTA>NAc DA neurons in rats induced a hyperactive phenotype. In particular, administration of CNO increased locomotor activity around twofold compared to Saline in the Gq (VTA>NAc DA) group but not in the control group (**Figure 3**). The twofold increase in locomotor activity is at a similar magnitude with the increase observed in Boender et al. (2014), when projection-specific (VTA>NAc) activation was induced. Nevertheless, Boekhoudt et al. (2016) observed a sevenfold increase when activating either VTA DA or VTA>NAc neurons at the same CNO doses as we used. One explanation for why we did not observe such an increase is that during VTA DA activation more populations of DA neurons contribute to the hyperactive phenotype. Secondly, the additional activation of GABA neurons, which constitute around 20% of the VTA>NAc projection, might contribute to the higher increase in locomotor activity when VTA>NAc neurons are chemogenetically activated. Another explanation might be that Boekhoudt et al. (2016) tested locomotion in the homecage, in which the baseline locomotion was already at lower levels when testing, whereas we tested the effect of CNO activation in a more novel environment, with 30 min habituation prior to injection. Finally, the lower magnitude of increase that we observed might be due to lower efficiency of the system to target neurons. We injected frt-DREADDq in the VTA at lower titers ($2.5–5 \times 10^{12}$ g.c./mL) compared to the titers of lox-DREADDq injected by Boekhoudt et al. (2016) ($6.4–8 \times 10^{12}$ g.c./mL). The lower amount of genomic copies might explain a lower efficiency of expression. In the future, in order to target more neurons, higher titers of frt-DREADDq could be applied but with caution, because specificity could be compromised.

In conclusion, we tested and validated cell-type and projection- specific systems to transiently activate neurons and study behavior. We showed that combining CavFlexFlp and AAV-frt-DREADDq in TH::Cre transgenic rats specifically targets VTA>NAc dopamine neurons and that activation by CNO increases locomotor activity. The usefulness of this strategy remains to be determined for other VTA dopamine projections. This system has great potential to be applied in a variety of Cre-transgenic lines to target, record, and manipulate the activity of specific cell-types in different projections. Increasing the efficiency of the system might be achieved by increasing titers and using more efficient tools for retrograde delivery.

DATA AVAILABILITY

The datasets generated for this study are available on request to the corresponding author.

AUTHOR CONTRIBUTIONS

NK-G, GvdP, and RA conceptualized the manuscript. NK-G, MZ, CB-V, ML, and KG performed the experiments. NK did analysis of the data. NK and RA prepared the original draft. All authors reviewed the manuscript.

FUNDING

This project was funded by the European Union Seventh Framework Programme under grant agreement number 607310 (Nudge-IT).

ACKNOWLEDGMENTS

We thank Frank Meye for discussing the manuscript and giving feedback.

REFERENCES

Aransay, A., Rodríguez-López, C., García-Amado, M., Clascá, F., and Prensa, L. (2015). Long-range projection neurons of the mouse ventral tegmental area: a single-cell axon tracing analysis. *Front. Neuroanat.* 9:59. doi: 10.3389/fnana.2015.00059

Atasoy, D., Betley, J. N., Su, H. H., and Sternson, S. M. (2012). Deconstruction of a neural circuit for hunger. *Nature* 488, 172–177. doi: 10.1038/nature11270

Augur, I. F., Wyckoff, A. R., Aston-Jones, G., Kalivas, P. W., and Peters, J. (2016). Chemogenetic activation of an extinction neural circuit reduces cue-induced reinstatement of cocaine seeking. *J. Neurosci.* 36, 10174–10180. doi: 10.1523/JNEUROSCI.0773-16.2016

Backer, M. W. A. (2010). *Optimization of Viral Vector Technology to Study Gene Function in the Hypothalamus*. Available at: http://dspace.library.uu.nl/handle/1874/44371 [accessed April 21, 2014].

Betley, J. N., and Sternson, S. M. (2011). Adeno-Associated viral vectors for mapping, monitoring, and manipulating neural circuits. *Hum. Gene Ther.* 22, 669–677. doi: 10.1089/hum.2010.204

Boekhoudt, L., Omrani, A., Luijendijk, M. C. M., Wolterink-Donselaar, I. G., Wijbrans, E. C., van der Plasse, G., et al. (2016). Chemogenetic activation of dopamine neurons in the ventral tegmental area, but not substantia nigra, induces hyperactivity in rats. *Eur. Neuropsychopharmacol.* 26, 1784–1793. doi: 10.1016/j.euroneuro.2016.09.003

Boender, A. J., de Jong, J. W., Boekhoudt, L., Luijendijk, M. C. M., van der Plasse, G., and Adan, R. A. H. (2014). Combined use of the canine adenovirus-2 and DREADD-technology to activate specific neural pathways in vivo. *PLoS One* 9:e95392. doi: 10.1371/journal.pone.0095392

Davidson, B. L., and Breakefield, X. O. (2003). Viral vectors for gene delivery to the nervous system. *Nat. Rev. Neurosci.* 4, 353–364. doi: 10.1038/nrn1104

Fenno, L., Yizhar, O., and Deisseroth, K. (2011). The development and application of optogenetics. *Annu. Rev. Neurosci.* 34, 389–412. doi: 10.1146/annurev-neuro-061010-113817

Gholizadeh, S., Tharmalingam, S., Macaldaz, M. E., and Hampson, D. R. (2013). Transduction of the central nervous system after intracerebroventricular injection of adeno-associated viral vectors in neonatal and juvenile mice. *Hum. Gene Ther. Methods.* 24, 205–213. doi: 10.1089/hgtb.2013.076

Grieger, J. C., Soltys, S. M., and Samulski, R. J. (2016). Production of recombinant adeno-associated virus vectors using suspension HEK293 cells and continuous harvest of vector from the culture media for GMP FIX and FLT1 clinical vector. *Mol. Ther.* 24, 287–297. doi: 10.1038/mt.2015.187

Grimm, D., Kay, M. A., and Kleinschmidt, J. A. (2003). Helper virus-free, optically controllable, and two-plasmid-based production of adeno-associated virus vectors of serotypes 1 to 6. *Mol. Ther.* 7, 839–850. doi: 10.1016/S1525-0016(03)00095-9

Junyent, F., and Kremer, E. J. (2015). CAV-2—why a canine virus is a neurobiologist's best friend. *Curr. Opin. Pharmacol.* 24, 86–93. doi: 10.1016/j.coph.2015.08.004

Krashes, M. J., Koda, S., Ye, C., Rogan, S. C., Adams, A. C., Cusher, D. S., et al. (2011). Rapid, reversible activation of AgRP neurons drives feeding behavior in mice. *J. Clin. Invest.* 121, 1424–1428. doi: 10.1172/JCI46229

Lammel, S., Hetzel, A., Häckel, O., Jones, I., Liss, B., and Roeper, J. (2008). Unique properties of mesoprefrontal neurons within a dual mesocorticolimbic dopamine system. *Neuron* 57, 760–773. doi: 10.1016/j.neuron.2008.01.022

Li, S.-J., Vaughan, A., Sturgill, J. F., and Kepecs, A. (2018). A viral receptor complementation strategy to overcome CAV-2 tropism for efficient retrograde targeting of neurons. *Neuron* 98, 905.e5–917.e5. doi: 10.1016/j.neuron.2018.05.028

Roth, B. L. (2016). DREADDs for neuroscientists. *Neuron* 89, 683–694. doi: 10.1016/j.neuron.2016.01.040

Runegaard, A. H., Sørensen, A. T., Fitzpatrick, C. M., Jørgensen, S. H., Petersen, A. V., Hansen, N. W., et al. (2018). Locomotor- and reward-enhancing effects of cocaine are differentially regulated by chemogenetic stimulation of gi-signaling in dopaminergic neurons. *eNeuro* 5:ENEURO.0345-17.2018. doi: 10.1523/ENEURO.0345-17.2018

Schwarz, L. A., Miyamichi, K., Gao, X. J., Beier, K. T., Weissbourd, B., DeLoach, K. E., et al. (2015). Viral-genetic tracing of the input-output organization of a central noradrenaline circuit. *Nature* 524, 88–92. doi: 10.1038/nature14600

Stachniak, T. J., Ghosh, A., and Sternson, S. M. (2014). Chemogenetic synaptic silencing of neural circuits localizes a hypothalamus→midbrain pathway for feeding behavior. *Neuron* 82, 797–808. doi: 10.1016/j.neuron.2014.04.008

Tervo, D. G. R., Hwang, B.-Y., Viswanathan, S., Gaj, T., Lavzin, M., Ritola, K. D., et al. (2016). A designer AAV variant permits efficient retrograde access to projection neurons. *Neuron* 92, 372–382. doi: 10.1016/j.neuron.2016.09.021

Vardy, E., Robinson, J. E., Li, C., Olsen, R. H. J., DiBerto, J. F., Giguere, P. M., et al. (2015). A new DREADD facilitates the multiplexed chemogenetic interrogation of behavior. *Neuron* 86, 936–946. doi: 10.1016/j.neuron.2015.03.065

Verharen, J. P. H., de Jong, J. W., Roelofs, T. J. M., Huffels, C. F. M., van Zessen, R., Luijendijk, M. C. M., et al. (2018). A neuronal mechanism underlying decision-making deficits during hyperdopaminergic states. *Nat. Commun.* 9:731. doi: 10.1038/s41467-018-03087-1

Wang, S., Tan, Y., Zhang, J.-E., and Luo, M. (2013). Pharmacogenetic activation of midbrain dopaminergic neurons induces hyperactivity. *Neurosci. Bull.* 29, 517–524. doi: 10.1007/s12264-013-1327-x

Witten, I. B., Steinberg, E. E., Lee, S. Y., Davidson, T. J., Zalocusky, K. A., Brodsky, M., et al. (2011). Recombinase-driver rat lines: tools, techniques, and optogenetic application to dopamine-mediated reinforcement. *Neuron* 72, 721–733. doi: 10.1016/j.neuron.2011.10.028

Yetnikoff, L., Lavezzi, H. N., Reichard, R. A., and Zahm, D. S. (2014). An update on the connections of the ventral mesencephalic dopaminergic complex. *Neuroscience* 282, 23–48. doi: 10.1016/j.neuroscience.2014.04.010

Conflict of Interest Statement: The authors declare that the research was conducted in the absence of any commercial or financial relationships that could be construed as a potential conflict of interest.

frontiers in Molecular Neuroscience

REVIEW
published: 29 March 2019
doi: 10.3389/fnmol.2019.00071

CAV-2 Vector Development and Gene Transfer in the Central and Peripheral Nervous Systems

*Danila del Rio[1†], Bertrand Beucher[2†], Marina Lavigne[1†], Amani Wehbi[1], Iria Gonzalez Dopeso-Reyes[1], Isabella Saggio[3,4] and Eric J. Kremer[1]**

[1] Institut de Génétique Moléculaire de Montpellier, University of Montpellier, CNRS, Montpellier, France, [2] PVM, BioCampus, CNRS, INSERM, University of Montpellier, Montpellier, France, [3] Department of Biology and Biotechnology "C. Darwin", Sapienza University of Rome, Rome, Italy, [4] Institute of Structural Biology, School of Biological Sciences, Nanyang Technological University, Singapore, Singapore

The options available for genetic modification of cells of the central nervous system (CNS) have greatly increased in the last decade. The current panoply of viral and nonviral vectors provides multifunctional platforms to deliver expression cassettes to many structures and nuclei. These cassettes can replace defective genes, modify a given pathway perturbed by diseases, or express proteins that can be selectively activated by drugs or light to extinguish or excite neurons. This review focuses on the use of canine adenovirus type 2 (CAV-2) vectors for gene transfer to neurons in the brain, spinal cord, and peripheral nervous system. We discuss (1) recent advances in vector production, (2) why CAV-2 vectors preferentially transduce neurons, (3) the mechanism underlying their widespread distribution via retrograde axonal transport, (4) how CAV-2 vectors have been used to address structure/function, and (5) their therapeutic applications.

Keywords: adenovirus, CAV-2, coxsackievirus and adenovirus receptor, vectors, neurons, gene therapy, disease modeling, circuits

OPEN ACCESS

Edited by:
Valery Grinevich, German Cancer Research Center (DKFZ), Germany

Reviewed by:
Françoise Muscatelli, Institut National de la Santé et de la Recherche Médicale (INSERM), France
Jonathan Nassi, Inscopix, United States

****Correspondence:***
Eric J. Kremer
eric.kremer@igmm.cnrs.fr

† These authors have contributed equally to this work

Received: *29 November 2018*
Accepted: *07 March 2019*
Published: *29 March 2019*

Citation:
del Rio D, Beucher B, Lavigne M, Wehbi A, Gonzalez Dopeso-Reyes I, Saggio I and Kremer EJ (2019) CAV-2 Vector Development and Gene Transfer in the Central and Peripheral Nervous Systems. Front. Mol. Neurosci. 12:71. doi: 10.3389/fnmol.2019.00071

UNDERSTANDING STRUCTURE AND FUNCTION BY MODIFICATION OF CELLS IN THE CENTRAL AND PERIPHERAL NERVOUS SYSTEM

The human brain contains about 80 billion neurons and trillions of synapses. How a given subset of neurons influences behavior and cognition will never be completely understood. Nevertheless, many are trying to use less complex nervous systems to provide a rough blueprint of how these interactions could influence behavior. Chemical tracers have been used to map circuits and connections in the brain for decades (Vercelli et al., 2000; Carter and Shieh, 2015). Combining circuitry data with functional analyses based on the effect of ablation, diseases, infections, or injury of a given population of neurons also provides insight into the physiological role of some brain regions (Caeyenberghs et al., 2017). This foundation is now being built upon by the advent of gene transfer tools that modify cells at the injection site, modify neurons that synapse to those that are transduced at the injection site (via anterograde transsynaptic transport), or modify neurons that project into the injection site via retrograde transport of the vector.

Some of the current approaches to understand the function of neuronal subsets exploit chemo- and optogenetics (Adamantidis et al., 2015; Roth, 2016); they have further refined our understanding of the mammalian brain. Gene transfer tools that effectively target cells at the site of injection, as well as those in connected regions, are now available to deliver expression

cassettes coding for chemo- and optogenetic proteins that extinguish or excite neurons. Moreover, the limitations in gene transfer efficacy are now frequently overcome by using novel and modified viral vectors.

CLINICAL GENE THERAPY

Gene therapy, i.e., using genetic material as a drug, can transiently or permanently endow target cells with novel or curative functions. Gene therapy approaches include, but are not limited to, gene replacement, gene correction, modifying mRNA stability, producing alternative gene products that reduce or increase the efficacy of cellular pathways, or endow cells with novel functions. The cornerstone in the optimization of *in vivo* gene transfer has been the steady improvement of vector design, delivery and expression kinetics. Viral vectors, which exploit natural uptake of viruses by cells, can be targeted to specific tissues by diverse means, including vector choice, vector tropism, the delivery mechanism, and/or modifying their expression parameters.

The *raison d'être* for clinical gene therapy targeting the central nervous system (CNS) is the unquantifiable impact on the patient and his/her entourage. Second comes the economic impact of neurodegenerative diseases, which often incurs costs for decades. Gene therapy to target neurodegeneration is particularly attractive given the insidious evolution of CNS diseases that deprive patients of their humanity. Here, neurodegeneration is defined by conditions that result in the loss of nerve structure/function that affects cognition, memory, or motor control. Among the hundreds of neurodegenerative disorders, considerable attention has been paid to the most common, in particular Parkinson's and Alzheimer's disease. Nonetheless, therapies for numerous brain diseases are in pre-clinical or Phase I/II/III stages. Examples include lysosomal storage disorders (e.g., Sly syndrome; Hunter's, Batten's disease), Huntington's disease, childhood epilepsies (e.g., Dravet syndrome), leukodystrophies (e.g., Canavan disease), and motor control diseases (e.g., amyotrophic lateral sclerosis, spinocerebellar ataxia) (Piguet et al., 2017).

The major challenges for therapy of neurodegenerative disease are (1) targeting the correct population of cells (neurons, astrocytes, and/or microglia) in the desired structure(s), (2) repair of damaged or deteriorating neurons, (3) maintaining healthy and/or corrected cells alive in potentially toxic environments, (4) modifying enough target cells to make a clinical impact, (5) maintaining therapeutic levels of expression for decades, and/or (6) endowing the brain with self-repair capabilities. Self-repair will likely be the *Holy Grail* of brain gene therapy and may require the combination of vector-mediated and cell-based therapy. Indeed, because neurogenesis and astrogenesis continue throughout our lifetime, they could be combined with gene transfer for therapeutic approaches.

PANOPLY OF VIRAL VECTORS

The number of viruses, or virus-like particles, that can be used to develop gene transfer tools is nearly limitless. Virologists divide vectors either by the type of genome they contain (single-stranded, double-stranded, segmented, linear or circular, RNA, or DNA) or by Families (which is used here). Some of the current vectors are made from the families *Adenoviridae* (adenovirus), *Retroviridae* (γ-retroviruses, HIV and other lentiviruses), *Poxviridae* (pox viruses, vaccinia virus), *Togaviridae* (α viruses/Semliki and SV-40), *Rhabdoviridae* (e.g., rabies virus), *Baculoviridae* (baculovirus), *Parvoviridae* (e.g., adeno-associated viruses), *Herpesviridae* (herpes simplex virus, cytomegalovirus, Epstein–Barr virus), and *Hepadnaviridae* (hepatitis B virus). The "virus-to-vector" transition includes using an unmodified capsid/envelope or altering it by borrowing pieces from another virus or a cell, or by adding moieties based on structure-based designs (Gao et al., 2005; Li et al., 2008; Kremer and Nemerow, 2015).

It is difficult to offer a balanced and critical analysis of the pros and cons of a viral vector without extensive experience in its production and *in vivo* use. While we have first-hand experience with adeno-associated viruses, γ-retroviruses, lentiviruses, baculoviruses, and picornaviruses, our expertise is with generating and using vectors derived from human and nonhuman adenoviruses. Therefore, here we provide an update of canine adenovirus type 2 (CAV-2) vectors for gene transfer to the central and peripheral nervous system (Junyent and Kremer, 2015).

Adenoviridae

Adenovirus (Ad) infections occur in all human populations regardless of health standards (Lion, 2014). During repeated encounters, we generally develop multifaceted humoral and cellular immune responses (Perreau and Kremer, 2006; Kremer and Van De Perre, 2015; Mennechet et al., 2015; Eichholz et al., 2016; Tran et al., 2018). Nevertheless, many human Ad (HAd) types routinely establish persistent subclinical infection by mechanisms that are beginning to be identified (Zheng et al., 2016; Tran et al., 2018). As of 2018, approximately 90 types of Ad have been isolated from humans (Hage et al., 2017). They are broadly classed into 7 species (A–G), based on serology, agglutination characteristics, and genome sequences. Notably, species B and E arose via transmission from monkeys and great apes (Hoppe et al., 2015). There are also >300 nonhuman Ads that remain, for the most part, poorly characterized. The number of nonhuman Ads, isolated from mammals, reptiles, birds, and fish, will certainly continue to increase.

As a general rule, all Ads have an approximately 90 nm diameter, icosahedral, proteinaceous shell (i.e., they are nonenveloped) that encapsidates a linear, double-stranded DNA genome of 36 ± 8 kilobase pairs (Kremer and Nemerow, 2015). An increasing number of human and nonhuman Ads are being tested for their potential as a gene transfer tools (Duffy et al., 2018). The versatility of Ad genome and capsid parts allows one to create vectors for either short-term immunogenic responses (e.g., vaccines) or long-term stable transgene expression (e.g., for therapy for neurodegenerative diseases). It is worth noting that very few reports exist describing

the efficacy of the majority of Ad vectors in the brain, spinal cord, or peripheral nervous system.

WHY A VECTOR FROM A CANINE ADENOVIRUS?

It is not surprising that vectors derived from viruses that generate a multi-faceted immune response in humans are not ideal candidates for clinical gene transfer. To reduce or circumvent immune-related drawbacks, numerous strategies have been used, including the induction of tolerance, immunosuppression, chemical and genetic modifications of the capsid (Nettelbeck et al., 2004; Lu et al., 2006; Kreppel and Kochanek, 2008; Toivonen et al., 2009; Prill et al., 2011). In the early 1990's, Klonjkowski et al. (1997) initiated the creation of canine type 2 (CAdV-2 or more commonly referred to as CAV-2) vectors (Paillard, 1997). At that time, CAV-2 was the only nonhuman Ad that had been sequenced and produced as a vaccine for domestic dogs. An attenuated strain (Manhattan) of CAV-2 is still used as a vaccine against the more virulent CAV-1. Only in 1999 was a replication-defective CAV-2 vector isolated free of wild type CAV-2 (Kremer et al., 2000). Similar to most HAd vectors, CAV-2 was made replication-defective by deleting the early region 1 (E1). This codes for transactivating factors needed to upregulate viral gene expression and downregulate host cell genes (Horwitz, 1996; Berk, 2005). Thus, CAV-2 vectors must be propagated in CAV-2 E1-transcomplementing canine cells.

Democratizing CAV-2 Vector Development – SLiCE and Dice With I-SceI

The development of replication-defective CAV-2 vectors was quite a challenge in the mid 1990's. Similar to the human cell lines 293 and 911 (Fallaux et al., 1998; Shaw et al., 2002) that express the human Ad2 E1 region, we generated a canine cell line that expressed the CAV-2 E1 region, notably because CAV-2 does not propagate efficiently in human cells. While generating this canine cell line was relatively straightforward, selecting a clone for vector production was only possible when we created the vector.

At the time, recombinant vectors were created through homologous recombination between two DNA fragments transfected into transcomplementing cells (Kremer and Perricaudet, 1995). However, canine cells are notoriously difficult to transfect with linear, 32 kbp DNA fragments (efficiency typically $< 3\%$). This precluded the use of homologous recombination in cells and in turn, vector isolation and production. The breakthrough in CAV-2 vector generation occurred when we adapted homologous recombination in bacteria, which is now routinely used to insert an expression cassette into a plasmid containing the HAd vectors. This strategy uses a shuttle plasmid together with a plasmid containing the Ad genome in *recAB*$^+$-competent bacteria, typically BJ5183 cells. While homologous recombination in BJ5183 cells works for CAV-2 vector construction, it was ∼100-fold less efficient using the equivalent fragment from the human HAd type 5 (HAd5) genome. To circumvent this problem, we now use seamless ligation cloning extract (SLiCE) strategy (Zhang et al., 2012). Briefly, SLiCE was initially developed using an extract of the bacterial strain PPY, which contains λ prophage Red/ET recombination system, to mediate recombination between a DNA insert and a linearized vector. It is also possible to generate SLiCE extracts with the commonly-used bacterial strains DH5a, DH10b, XL10-gold or SURE2 (Motohashi, 2015). We find that SLiCE is an efficient, simple, inexpensive, and rapid method for cloning expression cassettes into a 32 kbp plasmid containing the CAV-2 genome. Expression cassettes are inserted directly into either the E1, the E3 (which codes for proteins involved in limiting the immune response to the infected cells and is dispensable for vector use), or the E1 and E3 regions in less than 1 week. Notably, SLiCE eliminates the need for the shuttle plasmid used in the commercially available "AdEasy system" (**Figure 1**).

The second step is generating viral vectors from the plasmid that contains the recombinant vector genome. As mentioned above, canine cells are poorly transfected with linear 32 kbp DNA fragments. To circumvent this, we adapted another technique based on the use of I-SceI activity in DKE1 cells (Ibanes and Kremer, 2013). We generated DKSce1 cells constitutively expressing I-SceI fused to the hormone binding domain of the oestrogen receptor (ER). I-SceI is a yeast endonuclease that recognizes an 18 bp sequence (Choulika et al., 1994). In the absence of the ER ligand 4-OH tamoxifen, the I-SceI-ER protein remains cytoplasmic, thereby avoiding potential damage to the cellular genome. The 18 bp I-SceI recognition site was inserted flanking the CAV-2 genome in the plasmid backbone, and freshly prepared supercoiled plasmid DNA increases transfection efficacy to $> 50\%$ in DKSce1 cells. 4-OH-tamoxifen-mediated nuclear translocation of the I-SceI-ER allows excision of the vector genome from the circular plasmid (Ibanes and Kremer, 2013). Restriction by I-SceI is a prerequisite because an Ad genome needs two free ends to initiate replication. This technical advance increased CAV-2 vector generation from plasmid DNA by <1,000-fold. The combination of SLiCE and I-SceI allows us to generate, under optimal conditions, a CAV-2 vector deleted in the E1 and/or E3 regions in 17 days (**Figure 1**).

The Production and Advantages of Helper-Dependent CAV-2 Vectors

E1/E3-deleted CAV-2 vectors have numerous advantages: a cloning capacity of >7 kbp; can be purified in high titers ($>10^{13}$ physical particles/ml) in a basic research laboratory; the highest ratio of infectious units/physical particles reported for any viral vector (>1:3) (Kremer et al., 2000); weak recognition by both the adaptive immune response in rats and pre-existing immunity in humans (Perreau and Kremer, 2005, Kremer, 2006; Perreau et al., 2007a,b). However, larger expression cassettes are needed in some cases. In these cases, helper-dependent (HD) CAV-2 vectors (Soudais et al., 2004) are useful. HD vectors lack all

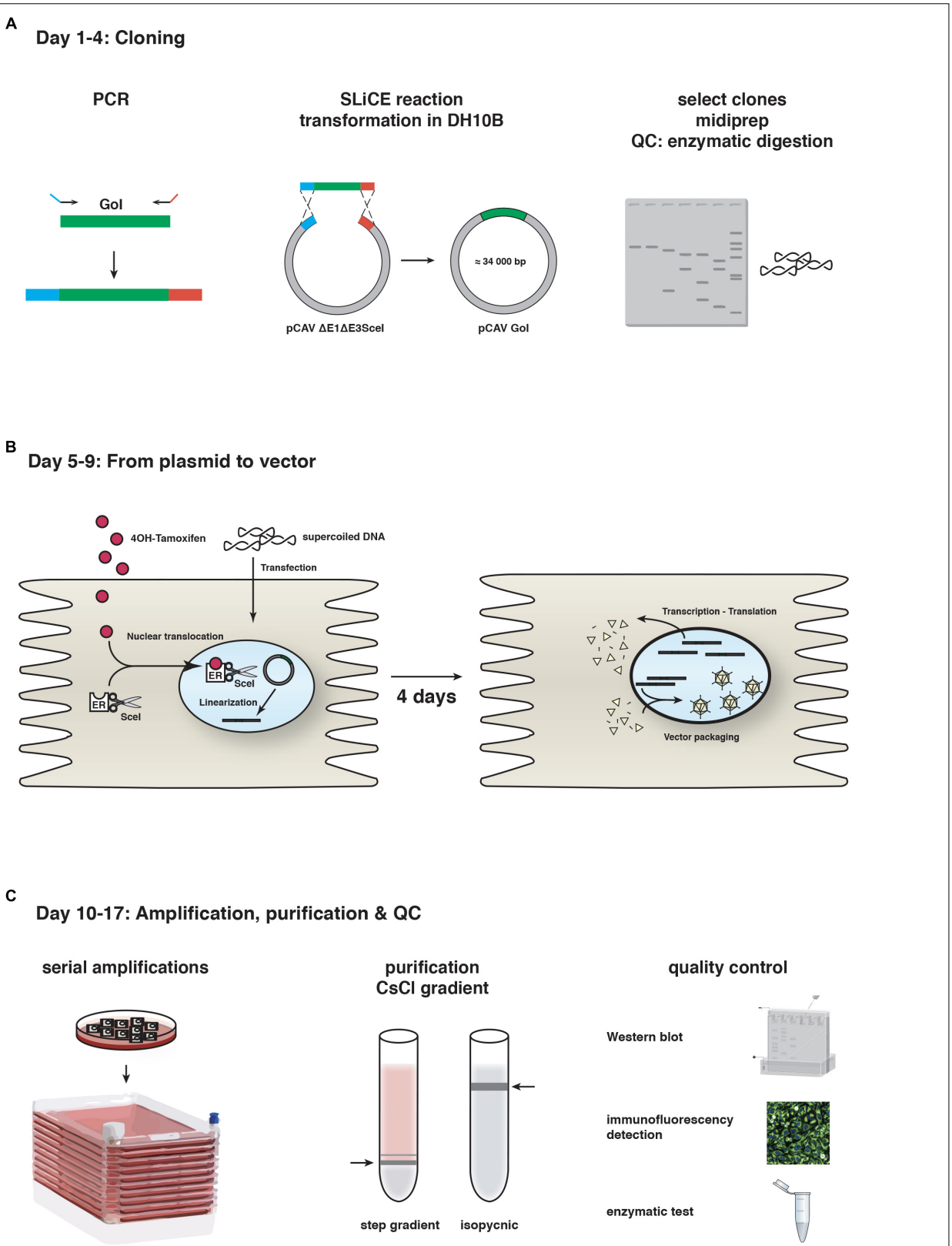

FIGURE 1 | CAV-2 vector production. A schematic representation of the steps and timeline for **(A)** cloning using SLiCE, **(B)** vector generation from plasmid using SceI-expressing cells, and **(C)** vector amplification in cell factories, purification and quality control (QC). GoI, gene of interest.

regions coding for viral proteins but retain the inverted terminal repeats (ITRs) and packaging signal (ψ) (Brunetti-Pierri and Ng, 2016). The 198 bp CAV-2 ITRs are needed for DNA polymerase to initiate genome replication. The 150 bp CAV-2 ψ (Soudais et al., 2001a) is bound by proteins that initiate the insertion of the linear genome into the capsid (Alba et al., 2011). HD vectors, also called high-capacity (HC), gutted, or gutless, can accommodate DNA inserts of up to 36 kbp. In most tissues, HD vectors increased the duration of transgene expression (Morral et al., 1998; Amalfitano and Parks, 2002; Kreppel and Kochanek, 2004; Brunetti-Pierri et al., 2007; Ariza et al., 2014; Cubizolle et al., 2014; Serratrice et al., 2014; Brunetti-Pierri and Ng, 2016). Given their characteristics, these vectors further improve *in vivo* safety and efficacy for long-term treatment of neurodegenerative diseases.

To generate HD vectors, cloning can be performed in *E. coli* via classic digestion/ligations, homologous recombination, or via SLiCE. Whether the 95–105% genome size limit for HAd5 vectors (i.e., minimum genome size of ∼34 kbp and a maximum of 38 kbp) applies to the 32 kbp CAV-2 genome and capsid is unknown. As in the case of E1-deleted CAV-2 vector generation, the HD genome is transfected into DKE1 cells that are co-infected with an E1-deleted "helper" vector, which provides the viral proteins in *trans* during the 36 h propagation cycle. While both HD and helper genomes replicate, helper genome packaging is prevented by flanking its ψ with the 34 bp *lox* sequences together with expression of Cre recombinase by the cells or the helper vector (Kochanek et al., 1996; Morsy et al., 1998). *Ipso facto*, Cre excises the helper's ψ, leading to preferential packaging of the HD vector genome.

Unfortunately, constitutive expression of Cre recombinase in DKE1 cells (DKCre cells) decreases cell viability, protein expression by the E1 region, and production of HD CAV-2 vectors (Fernandes et al., 2015a; Simão et al., 2016). Multiple amplification steps are needed to produce HD CAV-2 vectors, which also hampers robust production and in turn the availability of high quality preps. This led us to analyze the progression of the HD vector propagation cycle (Fernandes et al., 2015b). Paulo Fernandes found that the helper genome replicates faster during HD vector production compared to E1-deleted vectors alone. This is mirrored by increased expression of the CAV-2 polymerase, pre-terminal protein, and structural proteins. While genome packaging resembles that of E1-deleted vectors, more immature capsids are generated during HD production. This leads to a fourfold increase in the physical-to-infectious particles ratio, as well as augmented autophagy and cell death, which further compromises productivity. One potential approach to improve HD CAV-2 production is a helper vector with a floxed ψ, which also expresses a transcriptionally-regulated CreERT2 cassette (Gonzalez-Aparicio et al., 2011). This vector would allow the use of DKSceI cells for HD CAV-2 vector production and potentially increase both production and the infectious units/physical particle ratio.

CAV-2 PREFERENTIALLY TRANSDUCES NEURONS DUE TO CAR EXPRESSION

The tropism of a virus is usually associated with the clinical symptoms. However, the tropism of viral vectors does not *a priori* mimic that of their virus of origin. Similar to the tropism of HAd5, CAV-2 is thought to preferentially infect the upper respiratory track in Canidae and Ursidae. In dogs, CAV-2 causes a mild disease called "kennel cough" (Wright et al., 1972). In the case of a vector, cellular and tissue targets are a function of multiple factors: (1) the mode of injection (e.g., intravenous, subcutaneous, intradermal, intramuscular, intranasal, intracerebral, intrathecal. . .), (2) host physiology (e.g., when the blood brain barrier closes), (3) capsid modifications, (4) interaction with extracellular components (5) fluid flow dynamics, and other factors. Upon intracerebral and intramuscular injection, CAV-2 vectors preferentially transduce neurons (Soudais et al., 2001b). When a CAV-2 vector expressing GFP (CAVGFP) was placed in the olfactory cavity, which is predominantly lined with columnar epithelial cells, sensory olfactory neurons were preferentially transduced. Injection in the hindleg muscle in newborn mice led to poor transduction of myofibers but a surprising specificity for the innervating motoneurons via retrograde axonal transport (Soudais et al., 2001b, 2004; Salinas et al., 2017). Similarly, following injection into the highly innervated diaphragm, few muscle cells were transduced but a significant number of neuromuscular junctions were GFP^+, again demonstrating a preference for motoneurons and axonal retrograde transport of CAV-2 (Soudais et al., 2001b). When injected into the rodent brain parenchyma, CAV-2 vectors preferentially transduced neurons at the site of injection, as well as the neurons that project into this area (see **Box 1**). Following injection in the striatum, dopaminergic neurons of the *substantia nigra pars compacta* (SNpc), thalamic neurons, and cortical neurons (layer IV) of the ipsilateral and contralateral neocortex are transduced (Soudais et al., 2001b; Hnasko et al., 2005; Kremer, 2005; Bru et al., 2010).

We also injected a HD CAV-2 vector expressing GFP (HD-GFP) in the *Microcebus murinus* caudate nucleus (Mestre-Francés et al., 2018). *M. murinus,* commonly called the gray mouse lemur, is small nocturnal primate from Madagascar, whose brain structure and organization are comparable to that of the human brain. *M. murinus* have been bred in captivity since the 1960s, with lifespan of $\geq$ 10 years. This primate is increasingly used to study aging, Alzheimer's disease (including amyloid-β vaccination) (Trouche et al., 2009), and identification of cognitive deficits (Kraska et al., 2009; Trouche et al., 2010). Due to captive breeding programs, *M. murinus* is one of the few primates allowed by current European regulations for research. After HD-GFP injection in the striatum, GFP^+ somata and processes were found at the injection site, throughout the frontal and occipital cortex in both hemispheres, in the *SNpc* of both hemispheres, and in the ipsilateral basal nuclei of Meynert. The dense GFP signal surrounding the injection site was consistent with transduction of striatal

BOX 1 | Recent examples of CAV-2 vector use.

- The Adan lab used the same tools to identify the ventral tegmental area (VTA) to nucleus accumbens pathway. In some cases, this approach can circumvent the need to implement glass fibers for optogenetic stimulation and complements the use of transgenic Cre mice (Boender et al., 2014).
- Using a similar approach, Carter et al. (2013) demonstrated that the neural circuit from the parabrachial nucleus to the central nucleus of the amygdala is involved in the suppression of appetite.
- Lerner et al. (2015) used CAV-2 vectors to identify two distinct nigrostriatal DA circuits with differing in inputs, outputs, biophysical properties, and environmental information representations. Both circuits independently control information representations streaming through *SNpc* and each provides a generalizable framework for brain-wide mapping of diverse populations of neurons defined by multiple independent types of features (Lerner et al., 2015).
- The Maren lab showed that medial prefrontal cortex-thalamic nucleus reuniens circuits inhibit the expression of Pavlovian fear memories in rats, a function that influences adaptive emotional regulation (Ramanathan et al., 2018).
- By using CAV-2 vectors and DREADD-mediated inhibition of laterodorsal tegmentum excitatory cholinergic inputs to the VTA, the Barik lab in Marseilles characterized a neuro-circuitry implicated in depressive-like disorders (Fernandez et al., 2018).
- The Huberman lab explored how our internal state is merged with our visual perception of an impending threat to drive an adaptive behavioral response. They showed that the nucleus reuniens, nuclei of the ventral midline thalamus, and the xiphoid nucleus (Xi) are implicated in controlling behavioral responses to visual threats (Salay et al., 2018).
- In Bordeaux, Senn et al. (2014) showed using CAV-2 vectors and optogenetics that dorsal medial prefrontal cortex that projects to the lateral and ventrolateral periaqueductal gray circuits are necessary for discriminating a previously threatening context from a neutral context.
- Using CAV-2 vectors and chemogenetic silencing of the lateral hypothalamus-lateral habenula pathway, the Mameli lab showed that aversive stimuli such as foot-shocks drive hypothalamus-to-habenula excitation to promote escape behavior in mice (Lecca et al., 2017).
- The Stuber lab showed that in addition to intra-cortical connectivity, prefrontal cortical projection neurons innervate subcortical structures that contribute to reward-seeking behaviors. Using CAV-2 retrograde transport for bidirectional optogenetic manipulation of these neurons allowed them to demonstrate that stimulation of corticostriatal neurons promotes conditioned reward-seeking behavior after learning. By contrast, activity in corticothalamic neurons suppresses both the acquisition and expression of conditioned reward seeking (Otis et al., 2017).
- The locus coeruleus (LC) projects to almost the entire neuro-axis and plays a role in learning and memory, pain, motivation, strategic behavior, and arousal. The LC is the principal noradrenergic nucleus in the CNS and is the main source of noradrenergic innervation to the spinal dorsal horn, forming part of an analgesic circuit (Li et al., 2016; Hirschberg et al., 2017). It was unclear whether the LC acts functionally as a single global effector or as discrete modules. Specifically, while spinal-projections from LC neurons can exert analgesic actions, it was unknown whether they can act independently of ascending LC projections. The Pickering lab unraveled this dichotomy using CAV-2 uptake at axon terminals and a pharmaco-selective actuator module (PSAM) to selectively target LC neurons with spinal (LC→SC) or prefrontal cortex (LC→PFC) projections (Li et al., 2016; Hirschberg et al., 2017). Activation of the LC→SC module produced robust, lateralized anti-nociception while activation of LC→PFC produced aversion. In a neuropathic pain model, LC→SC activation reduced hind-limb sensitization and induced conditioned place preference. By contrast, activation of LC→PFC exacerbated spontaneous pain, produced aversion and increased anxiety-like behavior.
- Still in the LC, the Johansen lab examined how the circuit and neural-coding features of this neuromodulatory system regulates aversive emotional learning and behavioral flexibility in rats. They described a modular organization containing distinct neural projection patterns and coding properties for flexible specification of opposing behavioral learning states. An amygdala-projecting group promoted aversive learning, while a medial prefrontal cortex-projecting group extinguished aversive responses (Uematsu et al., 2017).
- The Nir lab examined how LC activity modulates sensory-evoked awakenings, testing whether reduced LC activity mediates sensory disconnection occurring in sleep. Optogenetic LC excitation using CAV-2-mediated ChR2 modulated arousal as shown by sleep-wake transitions, EEG desynchronization, and pupil dilation. Sounds presented on a background of weaker LC excitation (not awakening by itself) led animals to wake up frequently. Next, Hayat et al. (2019) silenced LC activity using a CAV-2 vector harboring a soma-targeted anion-conducting channelrhodopsin (stGtACR2) under the control of the PRS promoter and showed that it effectively silences LC activity and constricts pupils. Brief LC silencing around auditory stimulation reduced sound-evoked awakenings, showing that LC activity is both necessary and sufficient for modulating sensory-evoked arousal threshold (Hayat et al., 2019).
- Using CAV-2 vectors, targeted lesion, optogenetic, and chemogenetic stimulation of central amygdala of mice, the de Araujo lab identified coordinated circuits emanating from the central amygdala that control the efficiency of prey capture and the ability to deliver fatal bites to prey. Coordinated control of cervical and mandibular musculatures was mediated by a central amygdala projection to the reticular formation in the brainstem. By contrast, prey pursuit was mediated by projections to the midbrain periaqueductal gray matter (Han et al., 2017). The de Araujo lab also showed how the gut-brain neuronal circuitry regulates of motivational and emotional states. Using CAV-2 vector to infect gut-innervating vagal sensory neurons and optogenetics they found that right, but not left, vagal sensory ganglion activation sustained self-stimulation behavior, conditioned flavor and place preferences, and induced dopamine release from *SNpc* cells (Han et al., 2018).
- Asokan et al. (2018) examined how the layer 5 cortical neurons coordinate integrative auditory processing and adaptive behaviors. Using CAV-2 vectors they showed that auditory corticofugal neurons that innervate the inferior colliculus have widespread targets throughout the forebrain.
- The Tye lab has used CAV-2 vectors to identify and characterize several pathways (Allsop et al., 2014; Tye, 2014; Namburi et al., 2015; Beyeler et al., 2016; Vander Weele et al., 2018). These pathways include the medial prefrontal cortex projections to the dorsal periaqueductal gray (Vander Weele et al., 2018); the basolateral amygdala neurons during the retrieval of associative memories via synapse in the nucleus accumbens, the central amygdala, or ventral hippocampus (Namburi et al., 2015; Beyeler et al., 2016).
- At the Friedrich Miescher Institute for Biomedical Research in Basel, the Arber lab characterized motor collateral organization between the spinal cord and neurons in the brainstem. Pivetta et al. revealed a widespread and diverse network of spinal dual-axon neurons, with coincident input to forelimb motor neurons and the lateral reticular nucleus in the brainstem (Pivetta et al., 2014; Ruder et al., 2016). The Lüthi lab functionally characterized the connections of basal nucleus of the amygdala – medial prefrontal cortex (Vogel et al., 2016) and in particular the prelimbic and infralimbic subdivisions in fear generation and extinction.
- The Grinevich lab used CAV-2 vectors to separate magno- versus parvocellular oxytocin neurons and hypothalamic paraventricular neurons projecting to the supraoptic nuclei, and spinal cord deep laminae of L5 projections to cell bodies of oxytocin neurons in the paraventricular nuclei and their axonal projections in close proximity to somas and dendrites of magnocellular oxytocin neurons of the supraoptic nuclei (Eliava et al., 2016).
- The Arenkiel lab showed that the arcuate nucleus, receives cholinergic, and noncholinergic diagonal band of Broca projections to regulate appetite (Herman et al., 2016).
- The Chester lab used the retrograde transport of CAV-2 from the central nucleus of the amygdala and the dorsal reticular formation in the medulla to the parabrachial nucleus to help characterize a brainstem circuit that controls escape responses to select noxious stimuli (Barik et al., 2018).

neurons and afferent axons from other brain areas. In some animals, the vector leaked into the ventricles/cerebral spinal fluid and transduced $SOX2^+$ cells lining the lateral ventricles. It is unknown if these $SOX2^+$ cells were equivalent to the neural precursor cells infected by CAV-2 in the mouse brain (Salinas et al., 2017).

In the *M. murinus* brain, the total number of GFP^+ neurons at 6 months was equivalent to that at 2 weeks, demonstrating that the vectors led to long-term expression of a potentially immunogenic protein (GFP) (Mestre-Francés et al., 2018). These authors also quantified TH^+/GFP^+ neurons in the *SNpc* following vector deposit at a single coordinate in the caudate nucleus, and found a transduction efficacy of approximately 70% in the 3,000 TH^+ neurons/hemisphere. Thus, these data demonstrate that in the primate brain CAV-2 vectors preferentially transduce neurons, are transported to afferent structures, and allow stable expression of a foreign protein.

CAV-2 IS RETROGRADELY TRANSPORT (FROM THE AXON TIP TO THE SOMA)

As in the rodent brain (Zussy et al., 2016), expression of the coxsackievirus and adenovirus receptor (CAR) is restricted to neurons in the *M. murinus* brain parenchyma (Salinas et al., 2013; Mestre-Francés et al., 2018). While the transduction profile in the *M. murinus* brain is similar to that of the rodent brain, efficacy is globally better. CAV-2 infects neurons by binding to CAR at axon terminals (Salinas et al., 2009, 2010), however, the density and distribution of CAR along the surface of axons has not been extensively characterized. In most regions of the mouse brain, anti-CAR staining appears as small puncta along axons and dendrites (Zussy et al., 2016). Moreover, CAR is found in the presynapse fraction of synaptosome preparations from adult mouse, *M. murinus* and human brains (Zussy et al., 2016). While CAV-2 can efficiently enter a neuron via presynaptic termini, other entry sites are possible, but the efficacy is unknown (Schwarz and Luo, 2015).

Another aspect about CAV-2 vectors is that the preference for neuronal subtypes is not fully characterized. While CAV-2 infects many classes of neurons, such as motor, sensory, parasympathetic, GABAergic, cholinergic, norepinephrine (NE), and dopamine (DA) neurons (**Figure 2** and **Box 1**; Hnasko et al., 2006; Salinas et al., 2009; Beier et al., 2015; Schwarz et al., 2015; Li et al., 2016; Uematsu et al., 2017), some neurons may not express CAR and are therefore transduced less efficiently if at all. A potential example of this is the comparison of CAV-2 vectors to an engineered AAV vector (AAV-retro) selected for its capacity for *in vivo* retrograde transport from the mouse basal pontine nuclei (Tervo et al., 2016). While the study provided no information with respect to dose, volume, number of animals, or controls, they concluded that CAV-2 vectors poorly infected these neurons and therefore did not induce significant cortical expression of GFP in Rosa26-LSL-H2B-eGFP mice after injection in the basal pontine nuclei.

Axonal transport is essential for neuronal homeostasis, as its impairment can be linked with neurodegenerative disorders (Hinckelmann et al., 2013; Millecamps and Julien, 2013; Gibbs et al., 2015; Grosch et al., 2016). Some viruses, including rabies, herpes simplex type I, and poliovirus, as well as tetanus toxin, use axonal transport to access the soma of neurons in the CNS (Salinas et al., 2010). Live-cell imaging and cell biology approaches allowed us to characterize the mechanisms regulating CAV-2 entry and transport in primary rodent motor neurons (Salinas et al., 2009; Henaff et al., 2011; Simão et al., 2015). CAV-2 trafficking occurs in pH neutral endosomes, which allows long-range transport in an environment that precludes pH-induced conformational changes of the capsid and endosomal escape. Interestingly, tetanus toxin and other viruses, along with neurotropic factors and their receptors, are transported in these endosomal structures (Salinas et al., 2010; Schmieg et al., 2014).

HOW CAV-2 HAS BEEN USED FOR MPS THERAPY AND TO MODEL NEURODEGENERATIVE DISORDERS

Treating Mucopolysaccharidoses Type IIIA and VII

Mucopolysaccharidoses (MPSs) are a group of rare, autosomal recessive disorders caused by deficiencies in the catabolism of glycosaminoglycans (GAGs) (Mehta and Winchester, 2012).

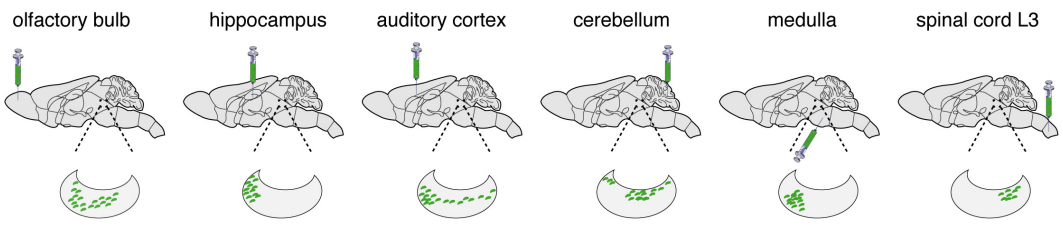

FIGURE 2 | LC transduction. While working with the laboratories of Liqun Luo [100], Tony Pickering (Li et al., 2016; Hirschberg et al., 2017), and Johan Johansen (Uematsu et al., 2017), we have used the retrograde transport of CAV-2 vectors to characterize the connections and functions of the LC. Here we present some of the results showing LC connectivity as determined by CAV-2 retrograde transport. The green syringe shows where CAVGFP was injected. The kidney shaped blow up represents the LC and green dots are GFP positive soma.

Several MPSs are associated with neuropathologies presenting variable clinical symptoms (Eto and Ohashi, 2002). For MPS brain therapy, the majority of cells do not need to be transduced by a therapeutic vector due to the phenomenon of cross-correction (Neufeld, 2011). Nevertheless, transduced cells must be dispersed throughout the brain to generate local factories that secrete enzymes. Thus, multiple injections throughout the brain must be combined with a vector that is capable of widespread brain distribution. For these reasons, CAV-2 vectors are ideal candidates for gene transfer. Indeed, CAV-2 vectors have been tested for their ability to improve neuropathological changes associated with MPS IIIA and MPS VII (Lau et al., 2010; Ariza et al., 2014; Cubizolle et al., 2014; Serratrice et al., 2014).

Neonatal administration of CAV-2 vectors harboring a N-sulfoglucosamine sulfohydrolase expression cassette produced both dose-dependent and widespread transgene expression that persisted for at least 20 weeks and prevented memory and learning deficits in mice (Lau et al., 2010). By contrast, introduction of the same vectors in the thalamus and ventricles of adult MPS IIIA mice resulted in limited duration of N-sulfoglucosamine sulfohydrolase expression (Lau et al., 2012). There are several potential reasons for this: the adult MPS IIIA mouse brain is primed by damage-associated molecular pattern molecules (Yang et al., 2017) and GAGs that induce chronic inflammation and likely "trained immunity" (Mehta and Winchester, 2012; Saeed et al., 2014; Netea et al., 2016; Netea and van der Meer, 2017). This inflammatory-primed environment would render vector injection less benign and the detection of a pathogen-associated molecule, like the double-stranded DNA genome of a vector in the cytoplasm, would likely amplify an immune response.

This hypothesis is supported by the work from Ariza et al. (2014), who also showed that transient immune suppression dramatically improves the duration of transgene expression in the MPS VII mouse brain. MPS VII is caused by deficient ß-glucuronidase activity, which results in the partial degradation of chondroitin sulfate, dermatan sulfate, heparan sulfate, and gangliosides (Ray et al., 1999; Heuer et al., 2001). We demonstrated that a CAV-2 vector containing a ß-glucuronidase expression cassette restores global ß-glucuronidase activity, reduces GAG accumulation, and corrects both the enlarged storage vesicle and irregular lysosome morphology in the brains of MPS VII mice and the ∼200-fold larger MPS VII dog (beagle) brain (Ariza et al., 2014; Cubizolle et al., 2014). Equally relevant, this approach improved cognitive functions of MPS VII mice (Ariza et al., 2014). In contrast to a study using AAV vectors for MPS I/III therapy (Ellinwood et al., 2011), transient immunosuppression was sufficient when using HD CAV-2.

Using CAV-2 Vectors to Model Parkinson's Disease in Nonhuman Primates

Vector-mediated gene transfer can also be used to better understand neurodegenerative diseases. Due to the efficient infection of DA neurons in the *SNpc* following injection in the striatum (Soudais et al., 2001b, 2004; Hnasko et al., 2005, 2006; Mestre-Francés et al., 2018), Parkinson's disease modeling is an attractive target for CAV-2 vectors. Like the NE neurons in the *locus coeruleus*, CAV-2 vectors can transduced > 90% of the rat or 70% of *M. murinus* DA neurons in the *SNpc* following injection into striatum (Soudais et al., 2001b, 2004; Mestre-Francés et al., 2018). Vector-mediated gene transfer can complement transgenic rodents and/or drug-induced disease models that have been invaluable, yet imperfect, for unraveling the mechanism of numerous brain and systemic disorders. The general consensus is that the lack of robust Parkinson's disease animals reproducing its complex characteristics hampers progress in both the understanding of pathogenic mechanisms and identification of therapies. MPTP (1-methyl-4-phenyl-1,2,3,6-tetrahydropyridine)-induced Parkinson's disease in primates is often used to test the efficacy of therapeutic approaches. However, MPTP induces acute and toxic injury to DA cells and poorly mimics the progressive course of Parkinson's disease. In addition, MPTP injections do not lead to the definitive Parkinson's disease pathological hallmarks of α-synuclein (α-syn) aggregates and Lewy body formation (Beal, 2010). One approach is to express LRRK2^{G2019S}, the most common dominant-negative mutation in patients with familiar and sporadic Parkinson's disease. The LRRK2 cDNA is ∼7.5 kbp, i.e., too large for AAV and lentivirus vectors. By contrast, the LRRK2 cDNA is readily cloned into a HD CAV-2 or herpes virus vector (Lee et al., 2010). Injection of CAV-LRRK2^{G2019S} into the brain of *M. murinus* induced Parkinson's disease-like motor symptoms, swelling and loss of neurites, dystrophic neurons, and reduced tyrosine hydroxylase immunoreactivity in the putamen (Mestre-Francés et al., 2018; Lasbleiz et al., 2019).

NETWORKS, CIRCUITS, PAIN, AND BEHAVIOR

Networks: Tracing the Relationship Between Input and Output (TRIO)

Deciphering how neural circuits are anatomically organized with respect to input and output connections is instrumental in understanding how the brain processes information. TRIO is a technique to map input–output connections in a selected region (Beier et al., 2015; Schwarz et al., 2015). To trace neural pathways, TRIO uses the combinatorial power of CAV-2, AAV, and rabies virus vectors (**Figure 3**). Briefly, an AAV2 vector, which preferentially infects cells at the site of injection, contains genes for an engineered receptor for a pseudo-typed rabies virus and a fluorescent protein (e.g., mCherry). The open reading frames for the receptor and mCherry in the AAV vector are in reverse orientation (3′–5′) and flanked by double-inverted oriented (DIO) lox sequences (i.e., a DIO cassette). Thus, an AAV-infected neuron must contain Cre recombinase for the receptor and mCherry to be expressed. Cre is delivered by CAV*Cre*, which is injected at a site that may contain axonal

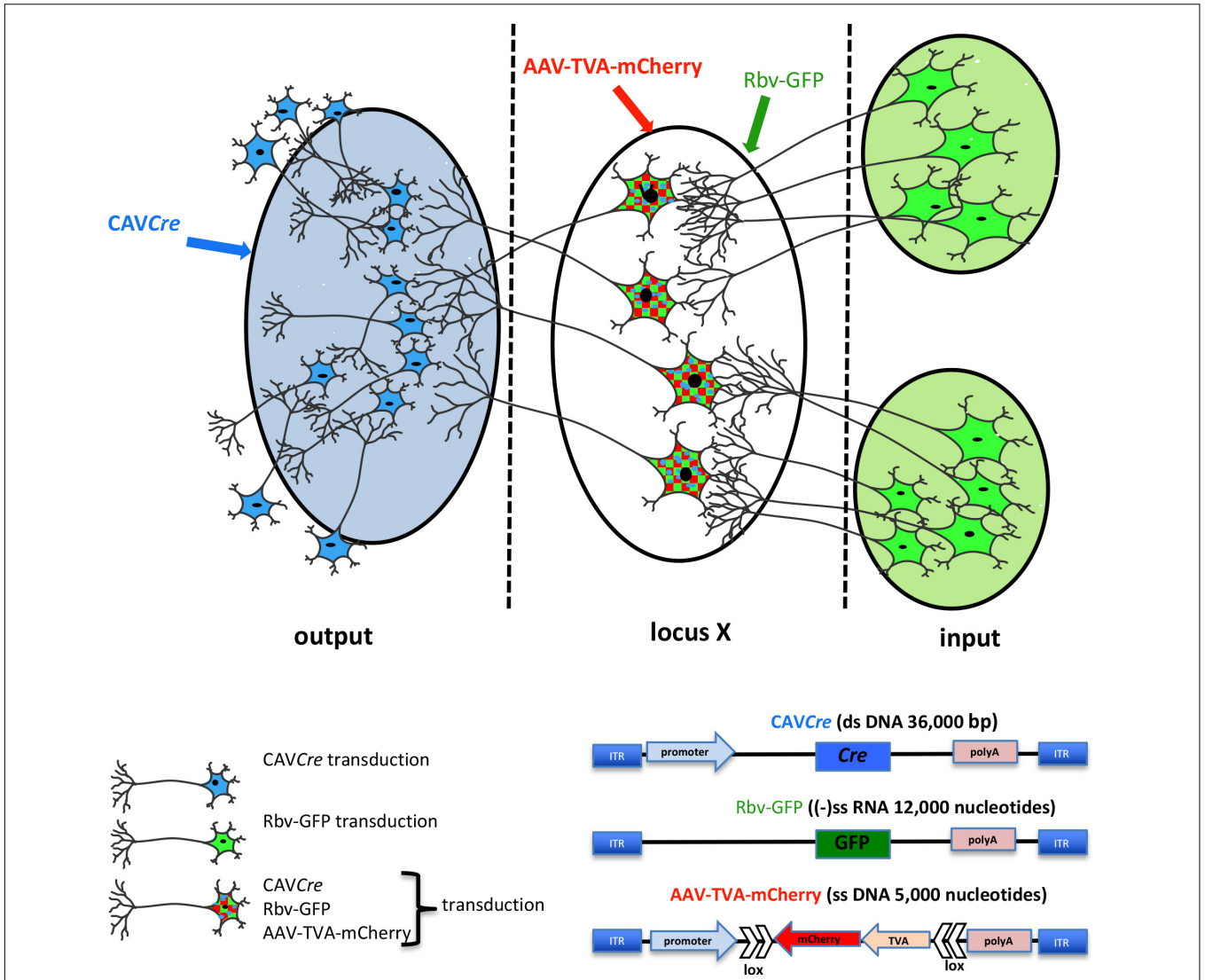

FIGURE 3 | TRIO: tracing the relationship between input and output neural circuits. Three viral vectors are used. CAV-2, a nonenveloped capsid containing an ~32 kbp double-stranded DNA genome; AAV, a nonenveloped capsid containing a single-stranded DNA genome of ~5,000 nucleotides: and a rabies virus, an enveloped particle containing negative single-stranded RNA genome. TRIO takes advantage of the retrograde transport capacity of CAV-2 vectors, the local transduction of neurons without significant retrograde transport of the AAV vector, and the transsynaptic transport of rabies vector. In this schema, CAV*Cre* (in blue) and AAV-TVA-mCherry (in red), containing the receptor for the rabies virus (TVA) and mCherry flanked by double inverted lox sequences, are injected in the respective locations (shaded blue for CAV*Cre*, locus X/unshaded oval for the AAV). AAV vectors need ~2 weeks to generate the second strand of their genome. It is then that Cre expression induces the expression the rabies virus receptor by flipping the expression cassette to "on." All mCherry$^+$ cells have been transduced by CAV*Cre* and AAV-TVA-mCherry, which identifies the output connection of locus X. Rbv-GFP is then injected at the same coordinates of the AAV injections (locus X unshaded oval). Only mCherry positive cells, which also express TVA for the pseudo-typed rabies vector can be transduced, therefore mCherry$^+$ and GFP$^+$ cells have been transduced by all three vectors. Rbv-GFP then undergoes a round of replication, and new particles are transported into neurons that synapse to the infected cell. GFP$^+$/mCherry$^-$ cells identify input regions.

projection of the neurons infected by the AAV vector. This combination allows one to identify the output of the neurons in the locus/region/structure targeted by the AAV injections, because these cells become mCherry$^+$. To identify which cells synapse to the AAV and CAV*Cre* infected neurons (which now express the receptor for the pseudo-typed rabies virus also), one injects the rabies vector that harbors a GFP expression cassette. Here, infection is restricted to the subset of cells expressing its receptor, i.e., only cells infected with both CAV*Cre* and AAV vectors. The rabies vector turns these cells yellow (mCherry + GFP = yellow), and is capable of a single replication cycle, transcytosis, and retrograde transport to synapsing neurons. Cre$^+$/mCherry$^+$/GFP$^+$ cells are infected by the three vectors, while GFP$^+$ cells synapse to the neurons at the injection site. TRIO, as well as a more complex version called cTRIO (Beier et al., 2015; Schwarz et al., 2015), allows identification

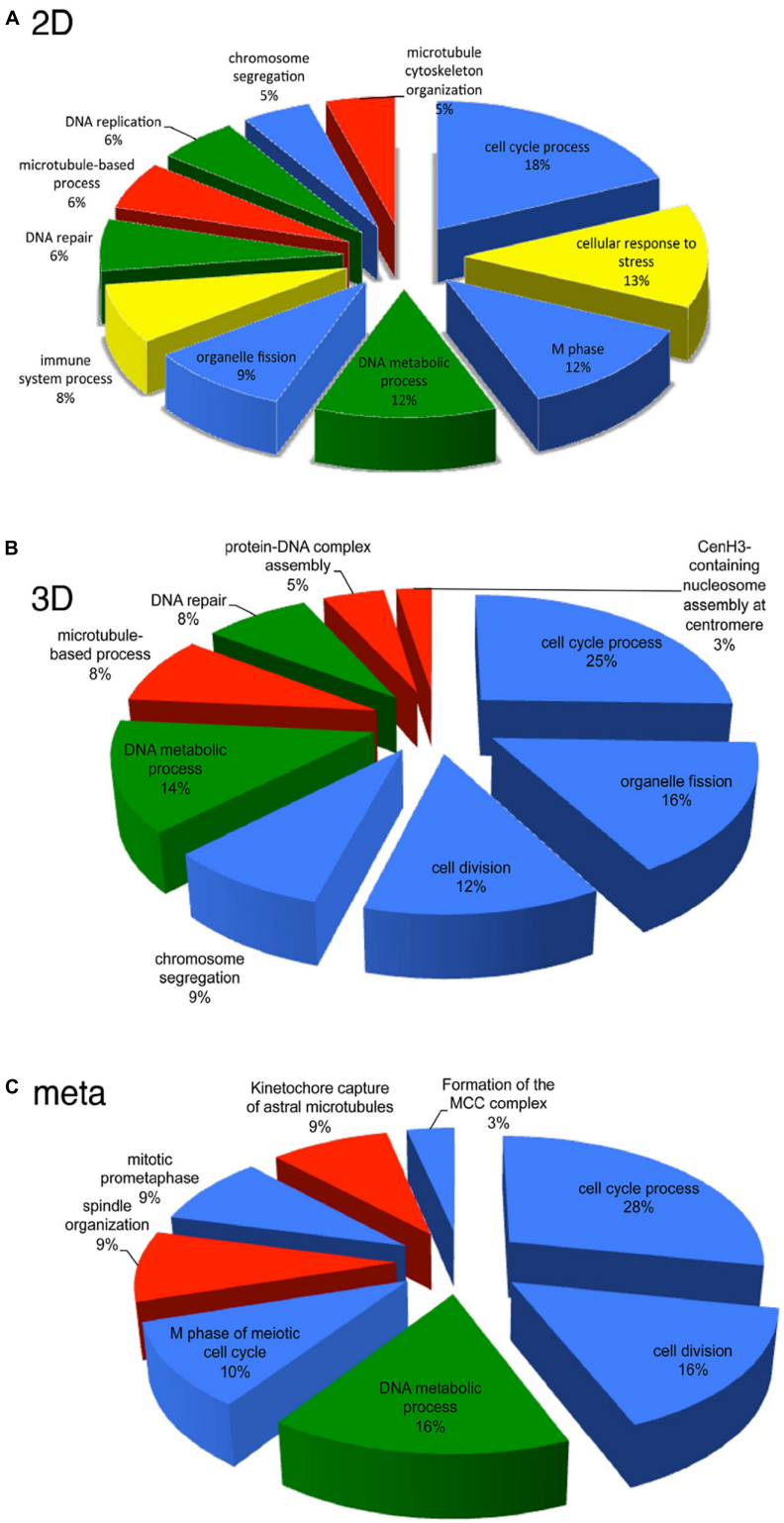

FIGURE 4 | Transcriptional pathways affected by HD-CAV-2 in human neuron *in vitro* and *M. murinus* neurons *in vivo*. **(A,B)** Functional transcriptional signature of HD-CAV-2 in classic 2D cultures **(A)** or 3D bioreactor cultures **(B)** from differentiated human midbrain progenitor cells obtained by *in silico* G-profiler analysis of microarray data on RNA extracted at 5 days post-vector addition. **(C)** Meta-analysis of functional signature of HD-CAV-2 in 2D or 3D cultures on RNA extracted at 5 days post-vector addition and of RNA extracted from *M. murinus* striatum at 24 h and 28 days after HD-CAV-2 stereotaxic injection. Green – DNA metabolism related functions; red – microtubule related processes; yellow – immune response related processes; blue – cell division/organization related functions.

of the relationship between input and output circuits, thereby improving our understanding of normal brain function and potentially diseases like depression, addiction, and schizophrenia.

Functional Characterization of Circuits

When an anatomical circuit has been identified and/or characterized it can be targeted for functional analyses. Previously, the complexity of neural anatomy, i.e., many thousands of neurons synapsing with thousands of other neurons, made identifying the involvement of a given neuronal pathway in a specific behavior a daunting challenge. Combining optogenetics (e.g., channelrhodopsins, a family of proteins that function as light-gated ion channels) (Adamantidis et al., 2015), DREADDs (designer receptor exclusively activated by designer drugs) (Roth, 2016) and retrograde vector transport allows specific targeting and manipulation of neural pathways. In turn, these tools have improved our understanding of how the activity of specific neuronal pathways can act as determinants of behavior (Sara, 2009; Takeuchi et al., 2016). Often, optogenetic and DREADD technologies are used in knock-in mice expressing Cre, which limits their applicability. As suggested by Nair et al. (2013), using these technologies together with Cre-expressing viral vectors, e.g., CAV-2, provides a way to target specific neural pathways with cellular resolution. These options include (1) combining CAV*Cre* and a second viral vector containing a Cre-inducible (DIO) DREADD/channelrhodopsin expression cassette, (2) using CAV*Cre* in knock-in mice with a DIO DREADD/channelrhodopsin expression cassette, or (3) injecting CAVFlexFlp vector harboring a Flippase-inducible Ce expression cassette into a knock-in mouse expressing DIO DREADD/channelrhodopsin in a subset of neurons (e.g., under transcriptional control) (Beier et al., 2015; Schwarz et al., 2015). Any of these approaches would allow the activation of a group of neurons in one area of the nervous system that innervate a distal area.

COULD CAV-2 VECTOR INFECTION PERTURB NEURON FUNCTION?

One way to measure the influence of viral vectors on tissue homeostasis is to characterize the changes in the transcriptional signature. This approach helps dissect the interplay between vectors and host-specific cells, predict vector impact, and identify vector-specific responses (Piersanti et al., 2013, 2015). Global transcriptional analyses were used to analyze the impact of E1/E3-deleted and HD vectors on human cells (Simão et al., 2016). DNA chips were used to assess the transcriptional changes in lung fibroblasts induced by HAd5 compared to AAV5 particles (Stilwell et al., 2003; Stilwell and Samulski, 2004). Furthermore, transcriptome analyses corroborate *in vivo* data indicating that AAVs have a quantifiably different effect on host cells compared HAds. Such analyses also showed that the activation of the innate response by group C HAdVs is affected by HAd-factor X (FX) complexes (Doronin et al., 2012).

BOX 2 | Take home messages.

- CAV-2 vectors preferentially transduce neurons in the rodent, canine, and primate brain due to the neuronal expression of CAR in the brain parenchyma.
- Uptake at axons and delivery to the somata (retrograde transport) occurs via pH neutral multitasking endosomal vesicles.
- Previously cumbersome, CAV-2 vector cloning, generation and production are now straightforward due to SLiCE and I-Sce1-ER expression in transcomplementing cells.
- The payload/cloning capacity of E1/E3-deleted CAV-2 vectors is >7 kbp.
- Transgene expression from E1/E3-deleted CAV-2 vectors is stable for at least 6 months in rats.
- The payload/cloning capacity of HD CAV-2 vectors is > 30 kbp.
- Transgene expression from HD CAV-2 vectors is stable for at least 12 months in rodents and in primates.
- When E1/E3-deleted CAV-2 vectors transduce neural precursor or neural stem cells, the cells still efficiently integrate into the existing circuits.
- HD CAV-2 vectors do not significantly perturb the transcriptome of human NPCs or neurons in the NHP brain.
- CAV-2 vectors have been used to: treat mucopolysaccharidoses in the mouse and dog, model Parkinson's disease in NHPs by expressing a hyperactive kinase form of LRRK2, and used by numerous groups to understand and explore neuronal networks.

Given the potential of HD CAV-2, DNA chips were used to characterize the influence of HD CAV-2, HD HAd5, and lentivirus vectors on transcription in human midbrain neuroprogenitor cells differentiated into dopaminergic neurons and propagated in 2D cultures (Piersanti et al., 2013, 2015; Mestre-Francés et al., 2018). The three viral vectors differentially affected the transcriptome, activating pro-survival genes and slightly altering neuron morphogenesis. While HD CAV-2 did not negatively affect neuronal development, it did induce an innate immune response. HD CAV-2 induced a lower transcriptional response when compared to HD HAd5 and lentivirus vectors. The HD CAV-2 transcriptional signature was further refined using 3D human neurospheres. These neurospheres were generated from midbrain progenitors and display multiple characteristics of human brain (Brito et al., 2012; Gualda et al., 2014; Simão et al., 2015). The effect of HD CAV-2 on the transcriptome in neurospheres was similar to that observed in the 2D culture system, with the notable addition of centromeric- and microtubule-related genes in 3D cultures. Finally, DNA chips were used to analyze transcriptional alterations in brain tissue of *M. murinus* following stereotaxic injection of the HD-CAV-2 into the caudate nucleus. The vector induced a modest modulation of genes involved in the immune response, intracellular trafficking and transcriptional regulation. Comparing the data sets from the three model systems (2D and 3D midbrain cultures and *M. murinus* brains) reveals that HD CAV-2 specifically modulates genes related to the cell cycle, microtubule organization and DNA metabolism (**Figure 4**). We hypothesize that the effects on microtubule-related genes is due to the interaction of the CAV-2 fiber with CAR, while the DNA damage response reflects activation of host DNA-damage repair systems by free viral DNA ends in the transduced cells. The modest effect on genes involved in the immune response could also be related to the immunogenicity of GFP.

CONCLUSION

Viral vectors will continue to help advance the characterization of brain function, circuitry and neural plasticity. Our understanding of the capabilities of CAV-2 vectors, their titers, and cloning capacity are assets that will allow users to create multiple and/or complex cassettes under transcriptional or post-translational control to explore the healthy and diseased brain (**Box 2**).

Nevertheless, there are caveats. As mentioned above, we do not know the transduction efficiency of all neuronal types. Because CAV-2 relies on CAR for uptake and transport, CAR-negative neurons will be poorly transduced. In another report in this Research Topic series, Iria Gonzales Dopeso-Reyes will show that the CAR expression pattern in mice, rats, microcebes and macaques varies considerably. One way to circumvent the lack of CAR expression by some neurons is the approach developed by Li et al. (2018). They used a receptor complementation strategy via an AAV vector to express CAR in candidate projection neurons. Exogenous CAR expression mediated by the AAV vector increased CAV-2 retrograde labeling efficacy. However, a confounding issue is our rudimentary understanding of the neuronal functions of CAR. Exogenous expression of CAR, which can be recruited to activate synapses (Zussy et al., 2016), might affect neuronal function and downstream cognitive assays.

Another approach to increase CAR-tropic virus infection is the use of nanovesicles covered with CAR (marketed by Takara^{TM}). The CAR-coated nanovesicles fuse with the plasma membrane of cells to transiently allow CAV-2 attachment and internalization. Whether the CAR-covered nanovesicles can be used in the mammalian brain has not been reported. *In vivo* use of nanovesicles could create complications because all cells would likely take up the microvesicles, thereby obviating the preferential transduction of neurons by CAV-2 vectors. Yet, neuron-specific transgene expression could be controlled by using appropriate promoters driving the expression cassette. If nanovesicles were used to characterize neuronal circuits, the exogenous CAR would need to be trafficked to distal regions of the axons. Finally, exogenous CAR could affect neuronal function and downstream cognitive assays. We found that, after CAR depletion in the striatum, its replacement takes approximately 2 weeks (Zussy et al., 2016). This suggests, but does not directly demonstrate, that CAR is relatively stable and its aberrant expression could have long-term effects on neuron homeostasis.

A third approach is modifying the CAV-2 capsid to preferentially target neuronal subtypes. Numerous methods have been developed to modify the tropism of adenoviruses. These include swapping fiber knobs from other types and adding ligands into the fiber, penton base, hexon, or protein IX by inserting a sequence into their open reading frame. Finally, one could create a "bi-polar" recombinant protein with one end that binds the fiber knob and the other end that targets a cell surface moiety. Several reviews describe these and other approaches (Arnberg, 2012; Yoon et al., 2016; Yamamoto et al., 2017; Zhang and Ehrhardt, 2017).

AUTHOR CONTRIBUTIONS

All authors contributed to writing and figure design.

FUNDING

Funding Work in the Kremer lab has been provided in part by the European commission (FP7 BrainVector #222992, BrainVector #286071), EpiGenMed (an "Investissements d'avenir" program, ANR-10-LABX-12-01), La Fondation pour la Recherche Médicale, E-Rare (Grant # ANR-17-RAR3-0001-01), La Region Occitanie (ALDOCT 000411-2018001118), and the ANR (GOAL: ANR-14-CE13-0014-03).

ACKNOWLEDGMENTS

We thank EKL members for constructive comments. We thank the technological platforms in Montpellier (MRI, RHEM, and RAM) for histology, image acquisition and analysis. CAV-2 vectors can be obtained from the Plateforme de Vectorologie de Montpellier (https://www.pvm.cnrs.fr/plateau-igmm/), a nonprofit service of the CNRS BioCampus.

REFERENCES

Adamantidis, A., Arber, S., Bains, J. S., Bamberg, E., Bonci, A., Buzsáki, G., et al. (2015). Optogenetics: 10 years after ChR2 in neurons - Views from the community. *Nat. Neurosci.* 18, 1202–1212. doi: 10.1038/nn.4106

Alba, R., Cots, D., Ostapchuk, P., Bosch, A., Hearing, P., and Chillon, M. (2011). Altering the Ad5 packaging domain affects the maturation of the Ad particles. *PLoS One* 6:e19564. doi: 10.1371/journal.pone.0019564

Allsop, S. A., Vander Weele, C. M., Wichmann, R., and Tye, K. M. (2014). Optogenetic insights on the relationship between anxiety-related behaviors and social deficits. *Front. Behav. Neurosci.* 8:241. doi: 10.3389/fnbeh.2014.00241

Amalfitano, A., and Parks, R. J. (2002). Separating fact from fiction: assessing the potential of modified adenovirus vectors for use in human gene therapy. *Curr. Gene Ther.* 2, 111–133.

Ariza, L., Giménez-Llort, L., Cubizolle, A., Pagès, G., García-Lareu, B., Serratrice, N., et al. (2014). Central nervous system delivery of helper-dependent canine adenovirus corrects neuropathology and behavior in mucopolysaccharidosis type VII mice. *Hum. Gene Ther.* 25, 199–211. doi: 10.1089/hum.2013.152

Arnberg, N. (2012). Adenovirus receptors: Implications for targeting of viral vectors. *Trends Pharmacol. Sci.* 33, 442–448. doi: 10.1016/j.tips.2012.04.005

Asokan, M. M., Williamson, R. S., Hancock, K. E., and Polley, D. B. (2018). Sensory overamplification in layer 5 auditory corticofugal projection neurons following cochlear nerve synaptic damage. *Nat. Commun.* 9:2468. doi: 10.1038/s41467-018-04852-y

Barik, A., Thompson, J. H., Seltzer, M., Ghitani, N., and Chesler, A. T. (2018). A brainstem-spinal circuit controlling nocifensive behavior. *Neuron* 100, 1491–1503.e3. doi: 10.1016/j.neuron.2018.10.037

Beal, F. (2010). Parkinson's disease: a model dilemma. *Nature* 466, S8–S10. doi: 10.1038/466S8a

Beier, K., Steinberg, E., Deloach, K., Xie, S., Miyamichi, K., Schwarz, L., et al. (2015). Circuit architecture of VTA dopamine neurons revealed by systematic input-output mapping. *Cell* 162, 622–634. doi: 10.1016/j.cell.2015.07.015

Berk, A. J. (2005). Recent lessons in gene expression, cell cycle control, and cell biology from adenovirus. *Oncogene* 24, 7673–7685. doi: 10.1038/sj.onc.1209040

Beyeler, A., Namburi, P., Glober, G. F., Simonnet, C., Calhoon, G. G., Conyers, G. F., et al. (2016). Divergent routing of positive and negative information from the amygdala during memory retrieval. *Neuron* 90, 348–361. doi: 10.1016/j.neuron.2016.03.004

Boender, A. J., de Jong, J. W., Boekhoudt, L., Luijendijk, M. C., van der Plasse, G., and Adan, R. A. (2014). Combined use of the canine adenovirus-2 and DREADD-technology to activate specific neural pathways in vivo. *PLoS One* 9:e95392. doi: 10.1371/journal.pone.0095392

Brito, C., Simão, D., Costa, I., Malpique, R., Pereira, C. I., Fernandes, P., et al. (2012). Generation and genetic modification of 3D cultures of human dopaminergic neurons derived from neural progenitor cells. *Methods* 56, 452–460. doi: 10.1016/j.ymeth.2012.03.005

Bru, T., Salinas, S., and Kremer, E. J. (2010). An update on canine adenovirus type 2 and its vectors. *Viruses* 2, 2134–2153. doi: 10.3390/v2092134

Brunetti-Pierri, N., and Ng, P. (2016). "Helper-dependent adenoviral vectors," in *Adenoviral Vectors for Gene Therapy*, 2nd Edn, ed. D. Curiel 423–450. doi: 10.1016/B978-0-12-800276-6.00017-6

Brunetti-Pierri, N., Stapleton, G. E., Palmer, D. J., Zuo, Y., Mane, V. P., and Finegold, M. J. (2007). Pseudo-hydrodynamic delivery of helper-dependent adenoviral vectors into non-human primates for liver-directed gene therapy. *Mol. Ther.* 15, 732–740.

Caeyenberghs, K., Verhelst, H., Clemente, A., and Wilson, P. H. (2017). Mapping the functional connectome in traumatic brain injury: What can graph metrics tell us? *Neuroimage* 160, 113–123. doi: 10.1016/j.neuroimage.2016.12.003

Carter, M., and Shieh, J. (2015). "'Visualizing neural structure,'" in *Guide to Research Techniques in Neuroscience*, eds M. Carter and J. Shieh (Cambridge, MA: Academic Press), 145–166. doi: 10.1016/B978-0-12-800511-8.00006-X

Carter, M. E., Soden, M. E., Zweifel, L. S., and Palmiter, R. D. (2013). Genetic identification of a neural circuit that suppresses appetite. *Nature* 503, 111–116. doi: 10.1038/Nature12596

Choulika, A., Perrin, A., Dujon, B., and Nicolas, J. F. (1994). The yeast I-Sce I meganuclease induces site-directed chromosomal recombination in mammalian cells. *C. R. Acad. Sci. III* 317, 1013–1019.

Cubizolle, A., Serratrice, N., Skander, N., Colle, M. A., Ibanes, S., Gennetier, A., et al. (2014). Corrective GUSB transfer to the canine mucopolysaccharidosis VII brain. *Mol. Ther.* 22, 762–773. doi: 10.1038/mt.2013.283

Doronin, K., Flatt, J. W., Di Paolo, N. C., Khare, R., Kalyuzhniy, O., Acchione, M., et al. (2012). Coagulation factor X activates innate immunity to human species C adenovirus. *Science* 338, 795–798. doi: 10.1126/science.1226625

Duffy, M. R., Alonso-Padilla, J., John, L., Chandra, N., Khan, S., Ballmann, M. Z., et al. (2018). Generation and characterization of a novel candidate gene therapy and vaccination vector based on human species D adenovirus type 56. *J. Gen. Virol.* 99, 135–147. doi: 10.1099/jgv.0.000978

Eichholz, K., Bru, T., Tran, T. T. P., Fernandes, P., Welles, H., Mennechet, F. J. D., et al. (2016). Immune-complexed adenovirus induce AIM2-mediated pyroptosis in human dendritic cells. *PLoS Pathog.* 12:e1005871. doi: 10.1371/journal.ppat.1005871

Eliava, M., Melchior, M., Knobloch-Bollmann, H. S., Wahis, J., da Silva Gouveia, M., Tang, Y., et al. (2016). A new population of parvocellular oxytocin neurons controlling magnocellular neuron activity and inflammatory pain processing. *Neuron* 89, 1291–1304. doi: 10.1016/J.NEURON.2016.01.041

Ellinwood, N. M., Ausseil, J., Desmaris, N., Bigou, S., Liu, S., Jens, J. K., et al. (2011). Safe, efficient, and reproducible gene therapy of the brain in the dog models of Sanfilippo and Hurler syndromes. *Mol. Ther.* 19, 251–259. doi: 10.1038/mt.2010.265

Eto, Y., and Ohashi, T. (2002). Novel treatment for neuronopathic lysosomal storage diseases–cell therapy/gene therapy. *Curr. Mol. Med.* 2, 83–89.

Fallaux, F. J., Bout, A., van der Velde, I., van den Wollenberg, D. J., Hehir, K. M., Keegan, J., et al. (1998). New helper cells and matched early region 1-deleted adenovirus vectors prevent generation of replication-competent adenoviruses. *Hum. Gene Ther.* 9, 1909–1917.

Fernandes, P., Almeida, A. I., Kremer, E. J., Alves, P. M., and Coroadinha, A. S. (2015a). Canine helper-dependent vectors production: Implications of Cre activity and co-infection on adenovirus propagation. *Sci. Rep.* 5:9135. doi: 10.1038/srep09135

Fernandes, P., Simaõ, D., Guerreiro, M. R., Kremer, E. J., Coroadinha, A. S., and Alves, P. M. (2015b). Impact of adenovirus life cycle progression on the generation of canine helper-dependent vectors. *Gene Ther.* 22, 40–49. doi: 10.1038/gt.2014.92

Fernandez, S. P., Broussot, L., Marti, F., Contesse, T., Mouska, X., Soiza-Reilly, M., et al. (2018). Mesopontine cholinergic inputs to midbrain dopamine neurons drive stress-induced depressive-like behaviors. *Nat. Commun.* 9:4449. doi: 10.1038/s41467-018-06809-7

Gao, G., Vandenberghe, L. H., and Wilson, J. M. (2005). New recombinant serotypes of AAV vectors. *Curr. Gene Ther.* 5, 285–297.

Gibbs, K. L., Greensmith, L., and Schiavo, G. (2015). Regulation of axonal transport by protein kinases. *Trends Biochem. Sci.* 40, 597–610. doi: 10.1016/j.tibs.2015.08.003

Gonzalez-Aparicio, M., Mauleon, I., Alzuguren, P., Bunuales, M., Gonzalez-Aseguinolaza, G., San Martin, C., et al. (2011). Self-inactivating helper virus for the production of high-capacity adenoviral vectors. *Gene Ther.* 18, 1025–1033. doi: 10.1038/gt.2011.58

Grosch, J., Winkler, J., and Kohl, Z. (2016). Early degeneration of both dopaminergic and serotonergic axons – a common mechanism in Parkinson's disease. *Front. Cell. Neurosci.* 10:293. doi: 10.3389/fncel.2016.00293

Gualda, E. J., Simao, D., Pinto, C., Alves, P. M., and Brito, C. (2014). Imaging of human differentiated 3D neural aggregates using light sheet fluorescence microscopy. *Front. Cell. Neurosci.* 8:221. doi: 10.3389/fncel.2014.00221

Hage, E., Dhingra, A., Liebert, U. G., Bergs, S., Ganzenmueller, T., and Heim, A. (2017). Three novel, multiple recombinant types of species of human mastadenovirus D (HAdV-D 73, 74 & 75) isolated from diarrhoeal faeces of immunocompromised patients. *J. Gen. Virol.* 98, 3037–3045. doi: 10.1099/jgv.0.000968

Han, W., Tellez, L. A., Perkins, M. H., Perez, I. O., Qu, T., Ferreira, J., et al. (2018). A neural circuit for gut-induced reward. *Cell* 175, 665–678.e23. doi: 10.1016/j.cell.2018.08.049

Han, W., Tellez, L. A., Rangel, M. J., Motta, S. C., Zhang, X., Perez, I. O., et al. (2017). Integrated control of predatory hunting by the central nucleus of the amygdala. *Cell* 168, 311–324.e18. doi: 10.1016/j.cell.2016.12.027

Hayat, H., Regev, N., Matosevich, N., Sales, A., Paredes, E., Krom, A., et al. (2019). *Locus-Coeruleus Norepinephrine Activity Gates Sensory-Evoked Awakenings from Sleep. bioRxv.* Available at: https://doi.org/10.1101/539502

Henaff, D., Salinas, S., and Kremer, E. J. (2011). An adenovirus traffic update: from receptor engagement to the nuclear pore. *Future Microbiol.* 6, 179–192. doi: 10.2217/fmb.10.162

Herman, A. M., Ortiz-Guzman, J., Kochukov, M., Herman, I., Quast, K. B., Patel, J. M., et al. (2016). A cholinergic basal forebrain feeding circuit modulates appetite suppression. *Nature* 538, 253–256. doi: 10.1038/nature19789

Heuer, G. G., Skorupa, A. F., Prasad Alur, R. K., Jiang, K., and Wolfe, J. H. (2001). Accumulation of abnormal amounts of glycosaminoglycans in murine mucopolysaccharidosis type VII neural progenitor cells does not alter the growth rate or efficiency of differentiation into neurons. *Mol. Cell. Neurosci.* 17, 167–178. doi: 10.1006/mcne.2000.0917

Hinckelmann, M. V., Zala, D., and Saudou, F. (2013). Releasing the brake: restoring fast axonal transport in neurodegenerative disorders. *Trends Cell Biol.* 23, 634–643. doi: 10.1016/j.tcb.2013.08.007

Hirschberg, S., Li, Y., Randall, A., Kremer, E. J., and Pickering, A. E. (2017). Functional dichotomy in spinal-vs prefrontal-projecting locus coeruleus modules splits descending noradrenergic analgesia from ascending aversion and anxiety in rats. *eLife* 6:e29808. doi: 10.7554/eLife.29808.001

Hnasko, T. S., Perez, F. A., Scouras, A. D., Stoll, E. A., Gale, S. D., Luquet, S., et al. (2006). Cre recombinase-mediated restoration of nigrostriatal dopamine in dopamine-deficient mice reverses hypophagia and bradykinesia. *Proc. Natl. Acad. Sci. U.S.A.* 103, 8858–8863. doi: 10.1073/pnas.0603081103

Hnasko, T. S., Sotak, B. N., and Palmiter, R. D. (2005). Morphine reward in dopamine-deficient mice. *Nature* 438, 854–857.

Hoppe, E., Pauly, M., Gillespie, T. R., Akoua-Koffi, C., Hohmann, G., Fruth, B., et al. (2015). Multiple cross-species transmission events of human adenoviruses (HAdV) during hominine evolution. *Mol. Biol. Evol.* 32, 2072–2084. doi: 10.1093/molbev/msv090

Ibanes, S., and Kremer, E. (2013). Canine adenovirus type 2 vector generation via I-Sce1-mediated intracellular genome release. *PLoS One* 8:e71032. doi: 10.1371/journal.pone.0071032

Junyent, F., and Kremer, E. J. (2015). CAV-2 - Why a canine virus is a neurobiologist's best friend. *Curr. Opin. Pharmacol.* 24, 86–93. doi: 10.1016/j.coph.2015.08.004

Klonjkowski, B., Gilardi-Hebenstreit, P., Hadchouel, J., Randrianarison, V., Boutin, S., Yeh, P., et al. (1997). A recombinant E1-deleted canine adenoviral vector capable of transduction and expression of a transgene in human-derived cells and in vivo. *Hum. Gene Ther.* 8, 2103–2115. doi: 10.1089/hum.1997.8.17-2103

Kochanek, S., Clemens, P. R., Mitani, K., Chen, H. H., Chan, S., and Caskey, C. T. (1996). A new adenoviral vector: replacement of all viral coding sequences with 28 kb of DNA independently expressing both full-length dystrophin and beta-galactosidase. *Proc. Natl. Acad. Sci. U.S.A.* 93, 5731–5736.

Kraska, A., Dorieux, O., Picq, J. L., Petit, F., Bourrin, E., Chenu, E., et al. (2009). Age-associated cerebral atrophy in mouse lemur primates. *Neurobiol. Aging.* 32, 894–906. doi: 10.1016/j.neurobiolaging.2009.05.018

Kremer, E. J. (2005). Gene transfer to the central nervous system: Current state of the art of the viral vectors. *Curr. Genomics* 6, 13–37. doi: 10.2174/1389202053202111

Kremer, E. J., Boutin, S., Chillon, M., and Danos, O. (2000). Canine adenovirus vectors: an alternative for adenovirus-mediated gene transfer. *J. Virol.* 74, 505–512. doi: 10.1128/JVI.74.1.505-512.2000

Kremer, E. J., and Nemerow, G. R. (2015). Adenovirus tales: from the cell surface to the nuclear pore complex. *PLoS Pathog.* 11:e1004821. doi: 10.1371/journal.ppat.1004821

Kremer, E. J., and Perricaudet, M. (1995). Adenovirus and adeno-associated virus mediated gene transfer. *Br. Med. Bull.* 51, 31–44. doi: 10.1093/oxfordjournals.bmb.a072951

Kremer, E. J., and Van De Perre, P. (2015). Ebola vaccines based on adenovirus vectors and risk of HIV. *BMJ* 350:h1307. doi: 10.1136/bmj.h1307

Kreppel, F., and Kochanek, S. (2004). Long-term transgene expression in proliferating cells mediated by episomally maintained high-capacity adenovirus vectors. *J. Virol.* 78, 9–22.

Kreppel, F., and Kochanek, S. (2008). Modification of adenovirus gene transfer vectors with synthetic polymers: a scientific review and technical guide. *Mol. Ther.* 16, 16–29. doi: 10.1038/sj.mt.6300321

Lasbleiz, C., Mestre-Frances, N., Devau, G., Luquin-Piudo, M., Tenenbaum, L., Kremer, E. J., et al. (2019). Combining gene transfer and nonhuman primates to better understand and treat Parkinson's disease. *Front. Mol. Neurosci.* 12:10. doi: 10.3389/fnmol.2019.00010

Lau, A. A., Hopwood, J. J., Kremer, E. J., and Hemsley, K. M. (2010). SGSH gene transfer in mucopolysaccharidosis type IIIA mice using canine adenovirus vectors. *Mol. Genet. Metab.* 100, 168–175. doi: 10.1016/j.ymgme.2010.02.006

Lau, A. A., Rozaklis, T., Ibanes, S., Luck, A. J., Beard, H., Hassiotis, S., et al. (2012). Helper-dependent canine adenovirus vector-mediated transgene expression in a neurodegenerative lysosomal storage disorder. *Gene* 491, 53–57. doi: 10.1016/j.gene.2011.09.004

Lecca, S., Meye, F. J., Trusel, M., Tchenio, A., Harris, J., Schwarz, M. K., et al. (2017). Aversive stimuli drive hypothalamus-to-habenula excitation to promote escape behavior. *eLife* 6:e30697. doi: 10.7554/eLife.30697

Lee, B. D., Shin, J.-H., VanKampen, J., Petrucelli, L., West, A. B., Ko, H. S., et al. (2010). Inhibitors of leucine-rich repeat kinase-2 protect against models of Parkinson's disease. *Nat. Med.* 16, 998–1000. doi: 10.1038/nm.2199

Lerner, T. N. N., Shilyansky, C., Davidson, T. J. J., Evans, K. E. E., Beier, K. T. T., Zalocusky, K. A. A., et al. (2015). Intact-brain analyses reveal distinct information carried by SNc dopamine subcircuits. *Cell* 162, 635–647. doi: 10.1016/j.cell.2015.07.014

Li, S.-J., Vaughan, A., Sturgill, J. F., and Kepecs, A. (2018). A viral receptor complementation strategy to overcome CAV-2 tropism for efficient retrograde targeting of neurons. *Neuron* 98, 905–917.e5. doi: 10.1016/j.neuron.2018.05.028

Li, W., Asokan, A., Wu, Z., Van Dyke, T., DiPrimio, N., Jarrod, J. S., et al. (2008). Engineering and selection of shuffled AAV genomes: a new strategy for producing targeted biological nanoparticles. *Mol. Ther.* 16, 1252–1260. doi: 10.1038/mt.2008.100

Li, Y., Hickey, L., Perrins, R., Werlen, E., Patel, A. A., Hirschberg, S., et al. (2016). Retrograde optogenetic characterization of the pontospinal module of the locus coeruleus with a canine adenoviral vector. *Brain Res.* 1641, 274–290. doi: 10.1016/j.brainres.2016.02.023

Lion, T. (2014). Adenovirus infections in immunocompetent and immunocompromised patients. *Clin. Microbiol. Rev.* 27, 441–462. doi: 10.1128/CMR.00116-13

Lu, Z. Z., Ni, F., Hu, Z. B., Wang, L., Wang, H., Zhang, Q. W., et al. (2006). Efficient gene transfer into hematopoietic cells by a retargeting adenoviral vector system with a chimeric fiber of adenovirus serotype 5 and 11p. *Exp. Hematol.* 34, 1171–1182. doi: 10.1016/j.exphem.2006.05.005

Mehta, A., and Winchester, B. (eds) (2012). *Lysosomal Storage Disorders: A Practical Guide*. Oxford: John Wiley & Sons.

Mennechet, F. J. D., Tran, T. T. P., Eichholz, K., Van De Perre, P., and Kremer, E. J. (2015). Ebola virus vaccine: Benefit and risks of adenovirus-based vectors. *Expert Rev. Vaccines* 14, 1471–1478. doi: 10.1586/14760584.2015.1083429

Mestre-Francés, N., Serratrice, N., Gennetier, A., Devau, G., Cobo, S., Trouche, S., et al. (2018). Exogenous LRRK2G2019S induces parkinsonian-like pathology in a nonhuman primate. *JCI Insight* 3:98202. doi: 10.1172/jci.insight.98202

Millecamps, S., and Julien, J. P. (2013). Axonal transport deficits and neurodegenerative diseases. *Nat. Rev. Neurosci.* 14, 161–176. doi: 10.1038/nrn3380

Morral, N., Parks, R. J., Zhou, H., Langston, C., Schiedner, G., Quinones, J., et al. (1998). High doses of a helper-dependent adenoviral vector yield supraphysiological levels of alpha1-antitrypsin with negligible toxicity. *Hum. Gene Ther.* 9, 2709–2716.

Morsy, M. A., Gu, M. C., Motzel, S., Zhao, J., Lin, J., Su, Q., et al. (1998). An adenoviral vector deleted for all viral coding sequences results in enhanced safety and extended expression of a leptin transgene. *Proc. Natl. Acad. Sci. U.S.A.* 95, 7866–7871.

Motohashi, K. (2015). A simple and efficient seamless DNA cloning method using SLiCE from *Escherichia coli* laboratory strains and its application to SLiP site-directed mutagenesis. *BMC Biotechnol.* 15:47. doi: 10.1186/s12896-015-0162-8

Nair, S. G., Strand, N. S., and Neumaier, J. F. (2013). DREADDing the lateral habenula: a review of methodological approaches for studying lateral habenula function. *Brain Res.* 1511, 93–101. doi: 10.1016/j.brainres.2012.10.011

Namburi, P., Beyeler, A., Yorozu, S., Calhoon, G. G., Halbert, S. A., Wichmann, R., et al. (2015). A circuit mechanism for differentiating positive and negative associations. *Nature* 520, 675–678. doi: 10.1038/nature14366

Netea, M. G., Joosten, L. A. B., Latz, E., Mills, K. H. G., Natoli, G., Stunnenberg, H. G., et al. (2016). Trained immunity: a program of innate immune memory in health and disease. *Science.* 352:aaf1098. doi: 10.1126/science.aaf1098

Netea, M. G., and van der Meer, J. W. M. (2017). Trained immunity: an ancient way of remembering. *Cell Host Microbe* 21, 297–300. doi: 10.1016/j.chom.2017.02.003

Nettelbeck, D. M., Rivera, A. A., Kupsch, J., Dieckmann, D., Douglas, J. T., Kontermann, R. E., et al. (2004). Retargeting of adenoviral infection to melanoma: combining genetic ablation of native tropism with a recombinant bispecific single-chain diabody (scDb) adapter that binds to fiber knob and HMWMAA. *Int. J. Cancer* 108, 136–145. doi: 10.1002/ijc.11563

Neufeld, E. F. (2011). From serendipity to therapy. *Annu. Rev. Biochem.* 80, 1–15. doi: 10.1146/annurev.biochem.031209.093756

Otis, J. M., Namboodiri, V. M. K. K., Matan, A. M., Voets, E. S., Mohorn, E. P., Kosyk, O., et al. (2017). Prefrontal cortex output circuits guide reward seeking through divergent cue encoding. *Nature* 543, 1–19. doi: 10.1038/nature21376

Paillard, F. (1997). Advantages of nonhuman adenoviruses versus human adenoviruses. *Hum. Gene Ther.* 8, 2007–2009.

Perreau, M., Guérin, M. C., Drouet, C., and Kremer, E. J. (2007a). Interactions between human plasma components and A xenogenic adenovirus vector: reduced immunogenicity during gene transfer. *Mol. Ther.* 15, 1998–2007. doi: 10.1038/sj.mt.6300289

Perreau, M., and Kremer, E. J. (2005). Frequency, proliferation, and activation of human memory T cells induced by a nonhuman adenovirus. *J. Virol.* 79, 14595–14605. doi: 10.1128/JVI.79.23.14595-14605.2005

Perreau, M., and Kremer, E. J. (2006). The conundrum between immunological memory to adenovirus and their use as vectors in clinical gene therapy. *Mol. Biotechnol.* 34, 247–256.

Perreau, M., Mennechet, F., Serratrice, N., Glasgow, J. N., Curiel, D. T., Wodrich, H., et al. (2007b). Contrasting effects of human, canine, and hybrid adenovirus vectors on the phenotypical and functional maturation of human

dendritic cells: implications for clinical efficacy. *J. Virol.* 81, 3272–3284. doi: 10.1128/JVI.01530-06

Piersanti, S., Astrologo, L., Licursi, V., Costa, R., Roncaglia, E., Gennetier, A., et al. (2013). Differentiated neuroprogenitor cells incubated with human or canine adenovirus, or lentiviral vectors have distinct transcriptome profiles. *PLoS One* 8:e69808. doi: 10.1371/journal.pone.0069808

Piersanti, S., Burla, R., Licursi, V., Brito, C., La Torre, M., Alves, P. M., et al. (2015). Transcriptional response of human neurospheres to helper-dependent CAV-2 vectors involves the modulation of DNA damage response, microtubule and centromere gene groups. *PLoS One* 10:e0133607. doi: 10.1371/journal.pone.0133607

Piguet, F., Alves, S., and Cartier, N. (2017). Clinical gene therapy for neurodegenerative diseases: past, present, and future. *Hum. Gene Ther.* 28, 988–1003. doi: 10.1089/hum.2017.160

Pivetta, C., Esposito, M. S., Sigrist, M., and Arber, S. (2014). Motor-circuit communication matrix from spinal cord to brainstem neurons revealed by developmental origin. *Cell* 156, 537–548. doi: 10.1016/J.Cell.2013.12.014

Prill, J.-M., Espenlaub, S., Samen, U., Engler, T., Schmidt, E., Vetrini, F., et al. (2011). Modifications of adenovirus hexon allow for either hepatocyte detargeting or targeting with potential evasion from Kupffer cells. *Mol. Ther.* 19, 83–92. doi: 10.1038/mt.2010.229

Ramanathan, K. R., Jin, J., Giustino, T. F., Payne, M. R., and Maren, S. (2018). Prefrontal projections to the thalamic nucleus reuniens mediate fear extinction. *Nat. Commun.* 9:4527. doi: 10.1038/s41467-018-06970-z

Ray, J., Scarpino, V., Laing, C., and Haskins, M. E. (1999). Biochemical basis of the beta-glucuronidase gene defect causing canine mucopolysaccharidosis VII. *J. Hered.* 90, 119–123.

Roth, B. L. (2016). DREADDs for neuroscientists. *Neuron* 89, 683–694. doi: 10.1016/j.neuron.2016.01.040

Ruder, L., Takeoka, A., and Arber, S. (2016). Long-distance descending spinal neurons ensure quadrupedal locomotor stability. *Neuron* 92, 1063–1078. doi: 10.1016/j.neuron.2016.10.032

Saeed, S., Quintin, J., Kerstens, H. H. D., Rao, N. A., Aghajanirefah, A., Matarese, F., et al. (2014). Epigenetic programming of monocyte-to-macrophage differentiation and trained innate immunity. *Science* 345:1251086. doi: 10.1126/science.1251086

Salay, L. D., Ishiko, N., and Huberman, A. D. (2018). A midline thalamic circuit determines reactions to visual threat. *Nature* 557, 183–189. doi: 10.1038/s41586-018-0078-2

Salinas, S., Bilsland, L. G., Henaff, D., Weston, A. E., Keriel, A., Schiavo, G., et al. (2009). CAR-associated vesicular transport of an adenovirus in motor neuron axons. *PLoS Pathog.* 5:e1000442. doi: 10.1371/journal.ppat.1000442

Salinas, S., Junyent, F., Core, N., Cremer, H., and Kremer, E. J. (2017). What is CAR doing in the middle of the adult neurogenic road? *Neurogenesis* 4:e1304790. doi: 10.1080/23262133.2017.1304790

Salinas, S., Schiavo, G., and Kremer, E. J. (2010). A hitchhiker's guide to the nervous system: The complex journey of viruses and toxins. *Nat. Rev. Microbiol.* 8, 645–655. doi: 10.1038/nrmicro2395

Salinas, S., Zussy, C., Loustalot, F., Henaff, D., Menendez, G., Morton, P. E., et al. (2013). Disruption of the coxsackievirus and adenovirus receptor-homodimeric interaction triggers lipid microdomain- and dynamin-dependent endocytosis and lysosomal targeting. *J. Biol. Chem.* 289, 680–695. doi: 10.1074/jbc.M113.518365

Sara, S. J. (2009). The locus coeruleus and noradrenergic modulation of cognition. *Nat. Rev. Neurosci.* 10, 211–223. doi: 10.1038/nrn2573

Schmieg, N., Menendez, G., Schiavo, G., and Terenzio, M. (2014). Signalling endosomes in axonal transport: travel updates on the molecular highway. *Semin. Cell Dev. Biol.* 27, 32–43. doi: 10.1016/j.semcdb.2013.10.004

Schwarz, L., Miyamichi, K., Gao, X. J., Beier, K. T., Weissbourd, B., DeLoach, K., et al. (2015). Viral-genetic tracing of the input–output organization of a central noradrenaline circuit. *Nature* 524, 88–92. doi: 10.1038/nature14600

Schwarz, L. A., and Luo, L. (2015). Organization of the locus coeruleus-norepinephrine system. *Curr. Biol.* 25, R1051–R1056. doi: 10.1016/j.cub.2015.09.039

Senn, V., Wolff, S. B. E., Herry, C., Grenier, F., Ehrlich, I., Gründemann, J., et al. (2014). Long-range connectivity defines behavioral specificity of amygdala neurons. *Neuron* 81, 428–437. doi: 10.1016/j.neuron.2013.11.006

Serratrice, N., Cubizolle, A., Ibanes, S., Mestre-Francès, N., Bayo-Puxan, N., Creyssels, S., et al. (2014). Corrective GUSB transfer to the canine mucopolysaccharidosis VII cornea using a helper-dependent canine adenovirus vector. *J. Control. Release* 181, 22–31. doi: 10.1016/j.jconrel.2014.02.022

Shaw, G., Morse, S., Ararat, M., and Graham, F. L. (2002). Preferential transformation of human neuronal cells by human adenoviruses and the origin of HEK 293 cells. *FASEB J.* 1, 869–871.

Horwitz, M. S. (1996). "Adenoviridae," in *Fields Virology*, 3rd Edn, eds B. Knipe, D. Howley (Philadelphia, MA: Lippincott Williams & Wilkins), 2111–2171.

Simão, D., Pinto, C., Fernandes, P., Peddie, C. J., Piersanti, S., Collinson, L. M., et al. (2016). Evaluation of helper-dependent canine adenovirus vectors in a 3D human CNS model. *Gene Ther.* 23, 86–94. doi: 10.1038/gt.2015.75

Simão, D., Pinto, C., Piersanti, S., Weston, A., Peddie, C. J., Bastos, A. E. P., et al. (2015). Modeling human neural functionality *in vitro*: three-dimensional culture for dopaminergic differentiation. *Tissue Eng. Part A* 21, 654–668. doi: 10.1089/ten.tea.2014.0079

Soudais, C., Boutin, S., and Kremer, E. (2001a). Characterization of cis-acting sequences involved in canine adenovirus packaging. *Mol. Ther.* 3, 631–640. doi: 10.1006/mthe.2001.0263

Soudais, C., Laplace-Builhe, C., Kissa, K., and Kremer, E. J. (2001b). Preferential transduction of neurons by canine adenovirus vectors and their efficient retrograde transport in vivo. *FASEB J.* 15, 2283–2285. doi: 10.1096/fj.01-0321fje

Soudais, C., Skander, N., and Kremer, E. (2004). Long-term in vivo transduction of neurons throughout the rat CNS using novel helper-dependent CAV-2 vectors. *FASEB J.* 18, 391–393. doi: 10.1096/fj.03-0438fje

Stilwell, J. L., McCarty, D. M., Negishi, A., Superfine, R., and Samulski, R. J. (2003). Development and characterization of novel empty adenovirus capsids and their impact on cellular gene expression. *J. Virol.* 77, 12881–12885.

Stilwell, J. L., and Samulski, R. J. (2004). Role of viral vectors and virion shells in cellular gene expression. *Mol. Ther.* 9, 337–346.

Takeuchi, T., Duszkiewicz, A. J., Sonneborn, A., Spooner, P. A., Yamasaki, M., Watanabe, M., et al. (2016). Locus coeruleus and dopaminergic consolidation of everyday memory. *Nature* 537, 357–362. doi: 10.1038/nature19325

Tervo, D. G. R., Hwang, B.-Y., Viswanathan, S., Gaj, T., Lavzin, M., Ritola, K. D., et al. (2016). A designer AAV variant permits efficient retrograde access to projection neurons. *Neuron* 92, 1–11. doi: 10.1016/j.neuron.2016.09.021

Toivonen, R., Suominen, E., Grenman, R., and Savontaus, M. (2009). Retargeting improves the efficacy of a telomerase-dependent oncolytic adenovirus for head and neck cancer. *Oncol. Rep.* 21, 165–171.

Tran, T. T. P., Eichholz, K., Amelio, P., Moyer, C., Nemerow, G. R., Perreau, M., et al. (2018). Humoral immune response to adenovirus induce tolerogenic bystander dendritic cells that promote generation of regulatory T cells. *PLoS Pathog.* 14: e1007127. doi: 10.1371/journal.ppat.1007127

Trouche, S. G., Asuni, A., Rouland, S., Wisniewski, T., Frangione, B., Verdier, J. M., et al. (2009). Antibody response and plasma Abeta1-40 levels in young *Microcebus murinus* primates immunized with Abeta1-42 and its derivatives. *Vaccine* 27, 957–964. doi: 10.1016/j.vaccine.2008.12.012

Trouche, S. G., Maurice, T., Rouland, S., Verdier, J. M., and Mestre-Frances, N. (2010). The three-panel runway maze adapted to *Microcebus murinus* reveals age-related differences in memory and perseverance performances. *Neurobiol. Learn. Mem.* 94, 100–106. doi: 10.1016/j.nlm.2010.04.006

Tye, K. M. (2014). Neural circuit reprogramming: a new paradigm for treating neuropsychiatric disease? *Neuron* 83, 1259–1261. doi: 10.1016/j.neuron.2014.08.022

Uematsu, A., Tan, B., Ycu, E., Cuevas, J., Koivumaa, J., Junyent, F., et al. (2017). Modular organization of the brainstem noradrenaline system coordinates opposing learning states. *Nat. Neurosci.* 20, 1602–1611. doi: 10.1038/nn.4642

Vander Weele, C. M., Siciliano, C. A., Matthews, G. A., Namburi, P., Izadmehr, E. M., Espinel, I. C., et al. (2018). Dopamine enhances signal-to-noise ratio in cortical-brainstem encoding of aversive stimuli. *Nature* 563, 397–401. doi: 10.1038/s41586-018-0682-1

Vercelli, A., Repici, M., Garbossa, D., and Grimaldi, A. (2000). Recent techniques for tracing pathways in the central nervous system of developing and adult mammals. *Brain Res. Bull.* 51, 11–28. doi: 10.1016/S0361-9230(99)00229-4

Vogel, E., Krabbe, S., Gründemann, J., Wamsteeker Cusulin, J. I., and Lüthi, A. (2016). Projection-specific dynamic regulation of inhibition in amygdala microcircuits. *Neuron* 91, 644–651. doi: 10.1016/j.neuron.2016.06.036

Wright, N. G., Cornwell, H. J., Thompson, H., Armitage, A., and Morrison, I. (1972). Canine adenovirus respiratory disease: isolation of infectious canine hepatitis virus from natural cases and the experimental production of the disease. *Vet. Rec.* 90, 411–416.

Yamamoto, Y., Nagasato, M., Yoshida, T., and Aoki, K. (2017). Recent advances in genetic modification of adenovirus vectors for cancer treatment. *Cancer Sci.* 108, 831–837. doi: 10.1111/cas.13228

Yang, D., Han, Z., and Oppenheim, J. J. (2017). Alarmins and immunity. *Immunol. Rev.* 280, 41–56. doi: 10.1111/imr.12577

Yoon, A.-R., Hong, J., Kim, S. W., and Yun, C.-O. (2016). Redirecting adenovirus tropism by genetic, chemical, and mechanical modification of the adenovirus surface for cancer gene therapy. *Expert Opin. Drug Deliv.* 13, 1–16. doi: 10.1517/17425247.2016.1158707

Zhang, W., and Ehrhardt, A. (2017). Getting genetic access to natural adenovirus genomes to explore vector diversity. *Virus Genes* 53, 675–683. doi: 10.1007/s11262-017-1487-2

Zhang, Y., Werling, U., and Edelmann, W. (2012). SLiCE: a novel bacterial cell extract-based DNA cloning method. *Nucleic Acids Res.* 40:e55. doi: 10.1093/nar/gkr1288

Zheng, Y., Stamminger, T., and Hearing, P. (2016). E2F/Rb family proteins mediate interferon induced repression of adenovirus immediate early transcription to promote persistent viral infection. *PLoS Pathog.* 12:e1005415. doi: 10.1371/journal.ppat.1005415

Zussy, C., Loustalot, F., Junyent, F., Gardoni, F., Bories, C., Valero, J., et al. (2016). Coxsackievirus adenovirus receptor loss impairs adult neurogenesis, synapse content, and hippocampus plasticity. *J. Neurosci.* 36, 9558–9571. doi: 10.1523/JNEUROSCI.0132-16.2016

Conflict of Interest Statement: The authors declare that the research was conducted in the absence of any commercial or financial relationships that could be construed as a potential conflict of interest.

frontiers in Neuroanatomy

ORIGINAL RESEARCH
published: 18 September 2019
doi: 10.3389/fnana.2019.00084

Transduction of Craniofacial Motoneurons Following Intramuscular Injections of Canine Adenovirus Type-2 (CAV-2) in Rhesus Macaques

Martin O. Bohlen[1], Hala G. El-Nahal[1] and Marc A. Sommer[1,2]*

[1] Department of Biomedical Engineering, Duke University, Durham, NC, United States, [2] Department of Neurobiology, Duke University School of Medicine, Durham, NC, United States

Reliable viral vector-mediated transgene expression in primate motoneurons would improve our ability to anatomically and physiologically interrogate motor systems. We therefore investigated the efficacy of replication defective, early region 1-deleted canine adenovirus type-2 (CAV-2) vectors for mediating transgene expression of fluorescent proteins into brainstem motoneurons following craniofacial intramuscular injections in four rhesus monkeys (*Macaca mulatta*). Vector injections were placed into surgically identified and isolated craniofacial muscles. After a 1- to 2-month survival time, animals were sacrificed and transgene expression was assessed with immunohistochemistry in the corresponding motoneuronal populations. We found that injections of CAV-2 into individual craniofacial muscles at doses in the range of $\sim 10^{10}$ to 10^{11} physical particles/muscle resulted in robust motoneuronal transduction and expression of immunohistochemically identified fluorescent proteins across multiple animals. By using different titers in separate muscles, with the resulting transduction patterns tracked via fluorophore expression and labeled motoneuron location, we established qualitative dose-response relationships in two animals. In one animal that received an atypically high titer (5.7×10^{11} total CAV-2 physical particles) distributed across numerous injection sites, no transduction was detected, likely due to a retaliatory immune response. We conclude that CAV-2 vectors show promise for genetic modification of primate motoneurons following craniofacial intramuscular injections. Our findings warrant focused attention toward the use of CAV-2 vectors to deliver opsins, DREADDs, and other molecular probes to improve genetics-based methods for primate research. Further work is required to optimize CAV-2 transduction parameters. CAV-2 vectors encoding proteins could provide a new, reliable route for modifying activity in targeted neuronal populations of the primate central nervous system.

Keywords: canine adenovirus type-2 (CAV-2), adenovirus, motoneurons, oculomotor, monkey, primate, gene therapy

OPEN ACCESS

Edited by:
Melissa R. Andrews, University of Southampton, United Kingdom

Reviewed by:
Anja Kerstin Ellen Horn, Ludwig Maximilian University of Munich, Germany
Angel M. Pastor, University of Seville, Spain

****Correspondence:***
Martin O. Bohlen
martin.bohlen@duke.edu

Received: *12 July 2019*
Accepted: *02 September 2019*
Published: *18 September 2019*

Citation:
Bohlen MO, El-Nahal HG and Sommer MA (2019) Transduction of Craniofacial Motoneurons Following Intramuscular Injections of Canine Adenovirus Type-2 (CAV-2) in Rhesus Macaques. Front. Neuroanat. 13:84. doi: 10.3389/fnana.2019.00084

INTRODUCTION

Replication defective, early region 1-deleted canine adenovirus type 2 (CAV-2) vectors are an increasingly important tool for neurological research due to CAV-2's neuronal tropism and capacity to retrogradely label neurons projecting to the injection sites. This is particularly true for non-human primate research, where CAV-2 has increasingly been used for anatomical investigations and perturbation of neuronal circuits.

Early work found that CAV-2 efficiently and preferentially transduces to cultured motoneurons. CAV-2-GFP injected into the gastrocnemius of newborn mice produced motoneuronal labeling within the ventral horn of the lumbosacral spinal cord 24-days post-injection (Soudais et al., 2001). This and other work suggested that CAV-2 binds to the coxsackie and adenovirus receptor (CAR) (Soudais et al., 2000, 2001; Loustalot et al., 2016). Injections into the tibialis anterior, gastrocnemius, and diaphragm muscles of mice resulted in no transduction to the muscle fibers but did yield transduction in the motoneurons (Soudais et al., 2001; Salinas et al., 2009). This is likely because in mature, non-pathological (i.e., normal) muscles, CAR expression is confined to neuromuscular junctions (Shaw et al., 2004; Sinnreich et al., 2005).

In an elegant series of experiments, Salinas et al. (2009) provided compelling evidence that, in cell culture, once bound to CAR, CAV-2 undergoes rapid clathrin-mediated formation endosomes in the first 5 min. At the motoneuronal terminals, once internalized, Salinas and colleagues observed a ∼30-min period where the intracellular CAV-2 containing endosomes oscillated locally at the region of internalization, before undergoing long-range retrograde axonal transportation. In the same series of experiments, injections of CAV-2 into the tibialis anterior and gastrocnemius muscles of mice revealed the presence of internalized CAV-2 positive endosomes in axons of the sciatic nerve following an 8-h survival period (Salinas et al., 2009).

In addition to CAV-2's efficacy at transducing motoneurons via injections into muscles, there is a growing body of evidence demonstrating its utility when injected into brain areas. Intracerebral injection of CAV-2 labels neurons both locally at the injection site and retrogradely in areas that project to the injection site (reviewed in Box 1 of Del Rio et al., 2019). In primates, CAV-2 has proven effective for transducing genes into multiple regions of the central nervous system, for example in the Cd of *Microcebus murinus* using helper-dependent CAV-GFP (Mestre-Frances et al., 2018).

Given the accruing evidence for CAV-2's efficacy as a vector, our goal was to test the ability of CAV-2 to retrogradely label primate motoneurons following intramuscular craniofacial injections, with a focus on the extraocular musculature. The extraocular muscles, in particular, provide a unique and sensitive testbed for characterizing viral vectors for their capacity to deliver their genomic payload to targeted cellular populations, for two reasons. First is their unique pattern of innervation. The extraocular muscles receive two patterns of innervation: 80–90% of the muscle fibers receive nervous input at a single point in the middle third (or belly) of the muscle, while the remaining muscle fibers receive multiple neuromuscular junctions from the origin of the muscle fiber at the back of the orbit through to the muscle's insertion into the globe (Spencer and Porter, 1988, 2006). This unique innervation pattern provides the opportunity to target injections to separate classes of fibers within the same muscle. Second, in primates, the neurons forming the single neuromuscular junctions, called singly innervating fiber or "SIF" motoneurons, are found within the cytoarchitectonic boundaries of the three extraocular motor nuclei. In contrast, the neurons forming the multiple neuromuscular junctions, called multiply innervating fiber or "MIF" motoneurons, are found in the periphery of the respective three extraocular motor nuclei. *Oculomotor nucleus*: The medial and inferior rectus motoneurons cap the oculomotor nucleus by sitting on its dorsomedial periphery; this division has been termed the C-group (Büttner-Ennever et al., 2001; Tang et al., 2015). Also, the MIF motoneurons of the inferior oblique and superior rectus sit sandwiched between the two oculomotor nuclei, on the midline; this division of these motoneuronal pools has been termed the S-group (Büttner-Ennever et al., 2001). *Trochlear nucleus*: Superior oblique MIF motoneurons sit on the dorsal cap of the trochlear nucleus. *Abducens nucleus*: MIF motoneurons of the lateral rectus sit in the ventral, medial and dorsal peripheries of the abducens nucleus (Büttner-Ennever et al., 2001). Together, these two features of extraocular motor units – unique patterns of muscle innervation and distinct motoneuronal pools – make the oculomotor system favorable for characterizing viral vectors and optimizing techniques of intramuscular viral injections.

The parameters of most interest to us were injection location and the propensity for a vector to diffuse from the injection site. Both are critical parameters to consider, as the proximity of the vector to the neuromuscular junction may play a critical role in determining whether an injected vector is able to successfully transduce motoneuronal terminals. In the case of *in vivo* muscle injections, the ∼25 nm AAV (Colella et al., 2018) or ∼100 nm CAV-2 capsids (Schoehn et al., 2008) must diffuse from the injection site through the tightly organized intramuscular and extracellular spaces to reach their receptors on the motoneuronal terminals. During the interval between depositing the vectors into the muscle and the vector binding to its receptor, the vector must survive an immunological gauntlet that is initiated as soon as the needle

Abbreviations: 4, fourth ventricle; C, cochlear nucleus; CA, cerebral aqueduct; CAV-2, Canine Adenovirus type-2; Cd, caudate nucleus; CG, central gray/periaqueductal gray; CL, centrolateral thalamic nucleus; CM, centromedian thalamic nucleus; Cn, cochlear nucleus; cp, cerebral peduncle; IC, inferior colliculus, III, oculomotor nucleus; InC, interstitial nucleus of Cajal; IO, inferior olive; IP, interpeduncular nucleus; IR, inferior rectus; IVn, trochlear nerve; LD, laterodorsal thalamic nucleus; LGN, lateral geniculate nucleus; ll, lateral lemniscus; LR, lateral rectus; M, masseter; mcp, middle cerebellar peduncle; MD, mediodorsal thalamic nucleus; MGN, medial geniculate nucleus; MLF, medial longitudinal fasciculus; MR, medial rectus; ObOc, orbicularis oculi; PAG, periaqueductal gray; PC, posterior commissure; PT, pretectum; Pul, pulvinar; Py, pyramids; RN, red nucleus; Rt, reticular thalamic nucleus; RTP, reticulotegmental pontine nucleus; SC, superior colliculus; scp, superior cerebellar peduncle; SN, substantia nigra; SO, superior oblique; SR, superior rectus; V, trigeminal nucleus; VI, abducens nucleus; VII, facial motor nucleus; VIIn, facial motor nerve; VL, ventrolateral thalamic nucleus; Vn, spinal trigeminal nerve; VPL, ventral posterolateral thalamic nucleus; VPM, ventral posteromedial thalamic nucleus.

is inserted. The act of injecting the muscle causes trauma and extravasation of several immune system agents (Tidball, 2017; Sass et al., 2018). To improve their odds of motoneuronal transduction, Williams et al. (2018) performed low-threshold electrical stimulation of skeletal muscles in three macaques. They assumed that areas in which the largest contractions were elicited following the smallest stimulation parameters were the sites of neuromuscular junctions, and injected adeno-associated virus, serotype 6 (AAV6) at these locations. This resulted in muscle fasciculations when the peripheral nerves were optically illuminated. This technique has yet to be tested with CAV-2.

Here we analyzed the capacity of CAV-2 to transduce fluorescent proteins into motoneurons following craniofacial intramuscular injections in rhesus macaques. In three of four animals tested, CAV-2 transduced its genes into motoneurons reliably. In general, efficacy was a function of dose (number of particles). The results confirm the efficacy of CAV-2 for transduction of cranial motoneurons in primates and illustrate the usefulness of the uniquely innervated extraocular muscles as a testbed for viral transduction.

MATERIALS AND METHODS

Animals

Four rhesus macaques (*Macaca mulatta*) were included in this investigation (**Table 1**). All procedures were in accordance with the NIH Guide for the Care and Use of Laboratory Animals and approved by the Duke University IACUC. Some animals received additional intraparenchymal injections that are not reported here. All animals included in the current report received additional viral injections placed in the other extraocular muscles. These injections included different serotypes of adeno-associated virus (AAV), herpes simplex virus (HSV) and lentivirus. No other adenovirus was tested besides CAV-2.

Viral Vectors

All CAV-2 vectors came from the Platform de Vectorology de Montpellier (PVM). Viruses were shipped in dry ice and stored at −80°C until they were used. To minimize the number of freeze-thaws, aliquots were made following the first thaw for an injection, rather than upon receipt of the stock virus. **Table 2** lists the vectors used and relevant parameters of the injection procedures. To test dose responses, custom titers of CAV-2 were created by diluting stock titers with Dulbecco's phosphate buffered saline (MilliporeSigma, St. Louis, MO, United States; D8537/MDL number: MFCD00131855).

TABLE 1 | Case information for the animals.

Animal	Age (Years)	Sex	Survival Duration (Days)	Weight (kgs)	Total CAV-2 Particles Injected
M18-01	19	M	23	10.2	5.2×10^{10}
M18-02	18	M	63	8.6	5.7×10^{11}
M18-03	10	F	60	5.6	4.2×10^{11}
M19-01	11	F	50	8.9	1.6×10^{11}

Surgical Procedures

Dexamethasone (2.0 mg/kg, IM) or Solu-Medrol (15.0 mg/kg, IM) was administered 24 h prior to surgery and immediately before surgery for mild immunosuppression. Animals were sedated with ketamine hydrochloride (3.0 mg/kg, IM) and dexdomitor (0.075 mg/kg, IM), then a surgical plane of anesthesia was maintained using 1–3% isoflurane and oxygen. All surgical procedures were carried out under aseptic conditions using sterile techniques.

Supraorbital Approach

Orbicularis oculi and superior rectus muscle injections required a surgical approach from the superior orbit. Animals were first placed into a stereotaxic frame (Kopf Instruments, Tujunga, CA, United States) and 0.5–1.0 ml of 0.25% bupivacaine was administered cutaneously along a planned incision line on the supraorbital ridge. Next, the incision was made, forming a small tissue flap that revealed the supraorbital insertion point of the annular orbicularis oculi. A second incision was made just inferior to the insertion point to reveal the superior retroorbital space and provide access to the levator palpebrae superioris, superior rectus, and superior oblique muscles. Blunt dissection was used to identify and isolate each muscle. Once isolated, muscles were looped with suture to allow for clean, precise injections. Injections were made by pushing a sharp needle attached to an appropriately sized Hamilton syringe (10–100 μl) through the insertion, toward the belly of each muscle. As the needle traversed the muscle, care was taken to avoid exiting the epimysium with the needle point. Once the needle point was in position, small bolus injections were made along the length of the needle track as it was slowly retracted from the muscle. In larger volume injections, the muscle expanded noticeably as the viral vector solution was dispensed along the injection track. To inject the orbicularis oculi, a very thin muscle that sits inside the eyelid, a sharp Hamilton syringe was inserted into the lateral aspect of the tissue flap and pushed medially through the lid. Once again, small bolus injections were placed along the length of the needle track as it was slowly withdrawn. Following injections, the retroorbital space was thoroughly washed with sterile saline. The orbicularis oculi was sutured back to its supraorbital insertion and the dermal incision was reapproximated and sutured along the supraorbital ridge.

Conjunctival Approach

Muscles in the inferior half of the orbit were approached via the conjunctiva. Animals were placed on their back and a small incision was made through the conjunctiva near the corneal junction around the bottom two thirds of the eye. Tissues were blunt dissected to reveal the insertion points of the three targeted muscles: the medial, lateral and inferior recti. These muscles were injected using the same procedure described above. Once injections were made, the site was flushed with sterile saline, the conjunctiva was reapproximated, and ophthalmic ointment was

TABLE 2 | Injection information.

Animal	Vector	Stock Titer (pp/μl)	No. CAV-2 Particles Injected	Injection Volume (μl)	Injection Location	Degree of Motoneuron Labeling
M18-01	CAV-2-CMV-mCitrine	2.9×10^9	5.2×10^{10}	18	ObOc	++++
M18-02	CAV-2-CMV-mCitrine	2.9×10^9	7.2×10^{10}	25	SR	0
	CAV-2-CMV-DsRedII	5.4×10^9	2.7×10^{10}	25	MR	0
	CAV-2-CMV-DsRedII	5.4×10^9	7.0×10^{10}	25	LR	0
	CAV-2-CMV-mCitrine	2.9×10^9	3.0×10^{10}	15	ObOc	0
	CAV-2-hChAT-GFP	1.0×10^{10}	4×10^{11}	40	M	0
M18-03	CAV-2-CMV-mCitrine	2.9×10^9	1.4×10^{10}	15	ObOc	+
	CAV-2-CMV-mCitrine	6.5×10^9	7.8×10^{10}	12	SR	++
	CAV-2-hChAT-GFP	1.0×10^{10}	2.4×10^{11}	24	IR	Inconclusive
	CAV-2-CMV-DsRedII	5.4×10^9	6.2×10^{10}	22	LR	+
	CAV-2-CMV-DsRedII	5.4×10^9	2.4×10^{10}	22	MR	+
M19-01	CAV-2-CMV-DsRedII	5.4×10^9	1.1×10^{11}	20	MR	+++
	CAV-2-CMV-DsRedII	5.4×10^9	5.6×10^{10}	20	LR	++

applied to the eye. No sutures were necessary as the conjunctiva heals without them.

Masseter

For masseter muscle injections, the surgeon digitally located the muscle belly. The overlying skin was then injected with 0.5 ml of 0.25% bupivacaine and then a small incision was made to reveal the muscle. Viral injections were made into the masseter as described above, then dermal layers were reapproximated and sutured.

At the end of surgery, a second cutaneous injection (0.5–1.0 ml) of 0.25% bupivacaine was administered along incision lines. Before exiting the surgical suit, all personnel removed their personal protective equipment (PPE) and sprayed their shoe-bottoms with RescueTM (Virox Technologies Inc., Oakville, ON, Canada). Postoperatively, animals received buprenorphine SR (0.2 mg/kg, IM) for analgesia. Additionally, either dexamethasone (1.0 mg/kg, IM for 3 days, then 0.5 mg/kg, IM every other day for 7 days) or Solu-Medrol (15.0 mg/kg, IM for 2 days, then 10.0 mg/kg, IM for 3 days, then 5.0 mg/kg, IM for 2 days, then 1.0 mg/kg, IM for 3 days) was administered. Post-operatively, animals were housed in an isolated room for a minimum of 48 h to prevent any potential shedding of vectors that could sensitize naïve animals to the viruses being used. Experimenters, staff, and veterinarians that entered the colony room housing the injected animals were not allowed to enter any other colony rooms for 12–48 h. Personnel removed all PPE before leaving the colony room, immediately sprayed down their shoes with RescueTM outside of the room, and thoroughly washed their hands with soap and water. Following isolation, animals were returned to their home colony room but were not allowed access to any other animals in the room unless the cage-mate had already received viral injections. In general, the injected animals were always the last to be worked with during the day, and if there was a need to go back to work with naïve animals, PPE was changed. Post-operative recovery was uneventful and, during the survival periods, no symptoms of neural deficits were observed.

Histology

After viral injections, animals survived long enough to allow for transduction and subsequent expression of fluorescent proteins (23–63 days, **Table 1**). Then we performed euthanasia and perfusion, tissue preparation, and immunohistochemistry.

Euthanasia and Perfusion

At the end of the survival period, animals were sedated with ketamine hydrochloride (3.0 mg/kg, IM) and then administered a lethal dose of pentobarbital (50.0 mg/kg, IP). Animals were then transcardially perfused with 4 L of chilled 0.1 M, pH 7.4 phosphate buffered saline (PBS), followed by 4 L of 4% paraformaldehyde in 0.1 M, pH 7.4 PBS.

Tissue Preparation

After perfusion, the brain was extracted, stereotaxically cut into blocks, and post-fixed in 4% paraformaldehyde in 0.1 M, pH 7.4 PBS at 4°C overnight. Blocks were then cryoprotected in PBS containing 30% sucrose at 4°C with agitation. Once sunk, blocks were cut into 75-μm-thick coronal sections using a freezing stage sliding microtome (American Optical Company, Buffalo, NY, United States) and stored in PBS at 4°C. For processing, sections were divided into 6 rostral to caudal series, with ∼450 μm between adjacent sections in the series.

Immunohistochemistry

Due to variability in the intensity and quality of signal that was provided through unaided epifluorescence across cases, and to avoid fading of the fluorescent signal over time, we opted to perform immunohistochemical amplification. This provided a standardized method for visualizing the degree of intracellular labeling, while also establishing a fade-resistant anatomical signal. Serial, free-floating sections were rinsed in 0.1 M, pH 7.4 PBS then, to block endogenous peroxidase activity, they were placed in 0.3% H_2O_2 in PBS solution. Following a second PBS wash, sections were placed in a solution of 0.25% Triton X-100 in PBS. Afterward, sections were moved to a 1% BSA/0.25% Triton X-100 in PBS solution to prevent non-specific antibody binding. Sections were then ready for incubation with primary antibody.

Anti-green fluorescent protein (GFP)/mCitrine

Despite differences in spectral characteristics, mCitrine and GFP have very high amino acid sequence homology which causes primary antibodies against GFP to also bind to YFP family proteins (including mCitrine). Therefore, to detect CAV-2 mediated expression of mCitrine, sections were incubated in a solution of biotinylated goat anti-GFP (1:1000, Rockland Immunochemicals Inc., Limerick, PA, United States; 600-106-215) in 1% BSA/0.25% Triton X-100 in PBS for 1–3 h at room temperature, then ∼48 h at 4°C with agitation. Sections were then rinsed with PBS and incubated with biotinylated rabbit anti-goat IgG secondary antibody (Vector Laboratories, INC., Burlingame, CA, United States; PK6105) for 1.5 h at room temperature.

Anti-DsRedII

For visualization of the RFP family of fluorophores, sections were incubated in rabbit anti-RFP conjugated to horseradish peroxidase (1:300, Rockland Immunochemicals Inc., Limerick, PA, United States; 600-403-379) or rabbit anti-RFP (1:300, Rockland Immunochemicals Inc., Limerick, PA, United States; 600-401-379) in a 1% BSA/0.25% Triton X-100 in PBS solution for 1–3 h at room temperature, then ∼48 h at 4°C. Next, sections were washed with PBS and incubated in biotinylated goat anti-rabbit IgG secondary antibody (Vector Laboratories, Inc., Burlingame, CA, United States; PK-6101) for 1.5 h at room temperature.

After antibody treatment, sections were transferred to an avidin-biotin-horseradish peroxidase complex (ABC) solution (Vector Laboratories, Inc., Burlingame, CA, United States; PK6105) for 1 h at room temperature. Sections were then rinsed with PBS and placed in 0.5% DAB/0.01% cobalt chloride/0.01% nickel ammonium sulfate in PBS solution for 20 min. Finally, to catalyze the reaction, 0.3% H_2O_2 was added to the solution. This produced a brown-black product in structures expressing the transgene. After a final PBS wash, sections were mounted to glass slides and allowed to dry overnight. Sections were then counterstained with thionin and dehydrated with graded ethanols then xylene. Sections were coverslipped using Cytoseal 60 (Thermo Fisher Scientific, Waltham, MA, United States).

Analyses

Low magnification drawings were made using a Bausch & Lomb projection microscope (Rochester, NY, United States). 10x medium and 100x high magnification drawings were made using drawing tubes mounted to a Zeiss Axioskop. Drawings were vectorized using CorelDRAW 2018. Digital photomicrographs were taken on a Keyence BZ-X800 (Itasca, IL, United States) affixed with a digital color camera, operated using Keyence BZ-H4XD software. When necessary, images were adjusted for brightness, contrast and color using Adobe Photoshop CS8 to provide the most accurate representation of how samples appeared under the microscope.

RESULTS

Intramuscular injections of CAV-2 were made into different craniofacial muscles of four rhesus macaques with the intent of assessing the vector's capacity for reliable uptake at the terminals of cranial nucleus motoneurons. In the first case, an 18 μl injection of CAV-2-CMV-mCitrine (5.2×10^{10} pp) was made into the left orbicularis oculi (**Figure 1A**). This was the only CAV-2 injection made in this animal, "M18-01" (**Table 2**). The injection resulted in fairly robust labeling of motoneurons in the dorsomedial division of the left facial motor nucleus (VII; **Figures 1B,C**). In addition to dense dendritic labeling, several labeled somata were observed (**Figure 1C**; example motoneuron in **Figure 1D**). CAV-2 retrogradely labeled soma and primary and secondary dendrites with some regularity. **Figure 2** shows photomicrographs from a neighboring section from the same case. A medium magnification photomicrograph (**Figure 2A**) shows an example labeled neuron and illustrates the density of dendritic labeling within the dorsomedial division of the facial motor nucleus. A higher magnification photomicrograph of the ventral labeling from the same section as in **Figure 2A** revealed labeled neuronal structures with numerous varicosities that were partitioned by fine filaments (**Figure 2B**, white arrowheads). In some regions, for example directly ventral toward the central core of the facial motor nucleus, a number of 90° bifurcations were observed (**Figure 2B**, white arrows). In this same region, there were a number of labeled neuronal structures presumed to be dendrites (**Figure 2B**, black arrow heads). In some instances, there were labeled neuronal structures that presented with morphology reflecting mildly beaded dendrites (**Figure 2B**, black arrowheads with a "*"). Finally, a presumed acutely angled dendritic branch is highlighted (**Figure 2B**, black arrow). In other regions, for example the ventrolateral portions of the facial motor nucleus, there were similar labeled morphological features with minimal branching (**Figure 2C**). Finally, we noted some gliosis in this case (**Figure 2D**). The dorsomedial division of the facial motor nucleus exhibited a marked increase in the presence of glia (**Figure 2D**, black arrows), suggesting a degree of neurotoxicity.

In the next animal, we attempted to study the dose-response relationship by injecting four different doses of CAV-2-CMV and one dose of CAV-2-hChAT into the left orbital musculature ("M18-02"; **Tables 1**, **2**). This animal received a total of 5.7×10^{11} pp of CAV-2, in addition to other injections placed intramuscularly and intraparenchymally (data not shown). The animal showed no transduction across all injections, which we suspect was due to an exaggerated immune response to the high viral load (see Discussion). The animal nevertheless remained asymptomatic through the survival period, exhibiting normal behavior and no overt signs of an immune reaction.

In the third animal, five injections into the orbital musculature were made again, but to decrease the presumed immune response, the total number of viral particles was reduced to 4.2×10^{11} ("M18-03"; **Tables 1**, **2**). First, 15 μl of CAV-2-CMV-mCitrine (1.4×10^{10} pp) injected into the left orbicularis oculi (**Figure 3A**) produced retrograde labeling of facial motor nucleus motoneurons (**Figures 3B,C**). There was a clear reduction both in the density of dendritic labeling and number of labeled soma compared to the first case (cf. **Figure 1C**), but the labeling was robust enough to allow visualization of somata, primary, secondary, and tertiary dendrites, while axonal labeling was sparse (**Figure 3D**).

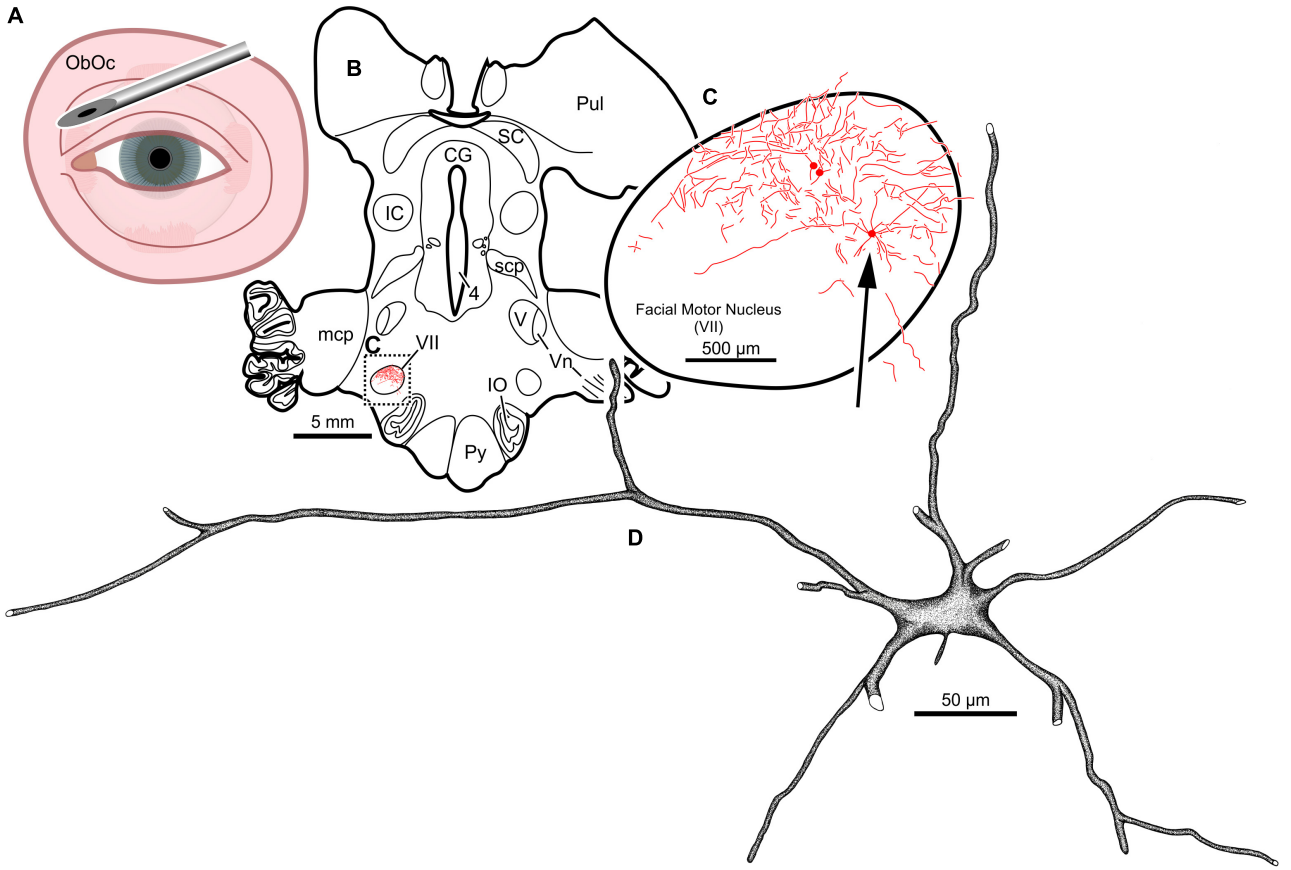

FIGURE 1 | Facial motoneuronal labeling following injection of CAV-2-CMV-mCitrine into the left orbicularis oculi. **(A)** Approximate angle and location of the orbicularis oculi injection **(B)** Low magnification view of the coronal section that contained the left facial motor nucleus, box in **(A)** indicates location of drawing shown in **(B)**. **(C)** A medium magnification view of the facial motor nucleus. CAV-2 mediated motoneuronal labeling was observed throughout the dorsomedial division of the facial motor nucleus. **(D)** A high magnification, camera lucida reconstruction of a single neuron from this case demonstrating the intracellular distribution of mCitrine expression. CAV-2 transgene expression resulted in the ability to visualize the somata, primary and secondary dendrites in addition to axonal labeling (*not illustrated*).

The second injection in this animal (M18-03) consisted of 12 µl CAV-2-CMV-mCitrine (7.8×10^{10} pp) placed into the left superior rectus muscle (**Figure 4A**). This produced retrograde labeling of superior rectus motoneurons, primarily on the midline between the two oculomotor nuclei (**Figures 4B,C,E,F**) which is known to be the territory of S-group MIF motoneurons of the superior rectus muscle. This injection resulted in the largest number of retrogradely labeled motoneurons in this animal. In addition to labeled somata, there were many labeled, short dendritic shoots running through the sections. Careful inspection of midline motoneuronal morphology, in known loci for superior rectus but not inferior rectus MIF motoneurons, revealed frequent labeling of the soma as well as primary, secondary and tertiary dendrites. Labeled axons were often observed exiting the oculomotor complex ventrally and could be observed within the fascicles of the oculomotor nerve (**Figures 4D,G**). This series also showed motoneuronal labeling within the oculomotor nucleus ipsilateral to the injected orbit (**Figure 4F**, indicated by *).

Third, 24 µl of CAV-2-hChAT-GFP (2.4×10^{11} pp) was injected into the left inferior rectus (**Figure 4A**) to test the hChAT promotor for its ability to provide transgene expression in motoneurons. The primary antibody, goat anti-GFP, is unable to discriminate between GFP and mCitrine labeling. The motoneuronal labeling in the left oculomotor nucleus, however, suggested that the hChAT promoter may have been effective.

The fourth injection in the same animal consisted of 22 µl of CAV-2-CMV-DsRedII (6.2×10^{10} pp) into the left lateral rectus muscle (**Figure 5A**). This resulted in retrograde labeling of lateral rectus motoneurons in the periphery of the left abducens nucleus (**Figures 5B,C**), a location attributed to MIF motoneurons of the lateral rectus in primates (Büttner-Ennever et al., 2001). While this injection produced more neuronal labeling compared to the lowest titer injection into the medial rectus from the same case, there was less viral transgene expressed from this injection compared to the higher titer injections in this animal (M18-03; **Figure 5C** compared to **Figures 4C,F**) and the animal that received a single CAV-2 injection (M18-01; **Figure 1C**). This injection labeled soma and primary, secondary and tertiary dendrites (**Figure 5D**).

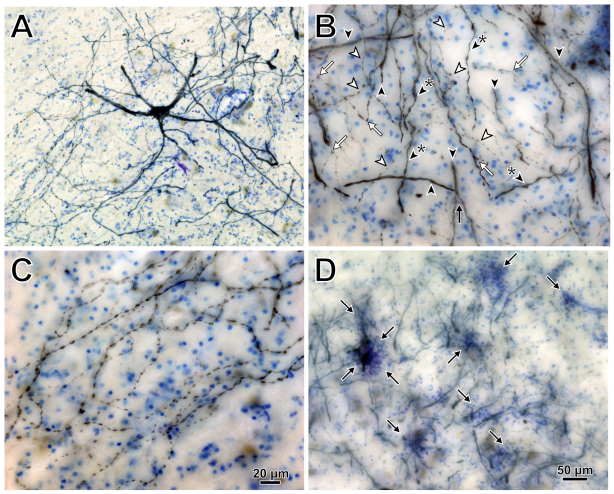

FIGURE 2 | Photomicrographs of CAV-2 mediated retrogradely labeled orbicularis oculi motoneuronal somata, dendrites and axons from the same case presented in **Figure 1**. **(A)** View of CAV-2 mediated motoneuronal labeling within the facial motor nucleus. **(B)** Labeling ventral to the dorsomedial division of the facial motor nucleus. **(C)** A large number of orbicularis oculi motoneuronal projections with varicosities were observed coalescing in the ventrolateral portion of the facial motor nucleus. **(D)** Low magnification view showing the distribution of glia (light blue) within the dorsomedial division of the facial motor nucleus; areas enriched with glia are highlighted with arrows. Photomicrographs **(A,D)** were taken at 20x, while **(B,C)** were taken at 40x. A = 12z, B = 9z, and D = 7z.

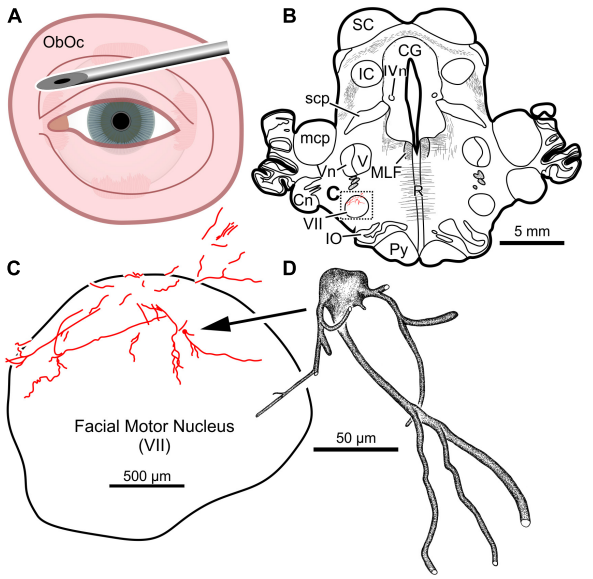

FIGURE 3 | Facial motoneuronal labeling following an injection of CAV-2-CMV-mCitrine into the left orbicularis oculi. **(A)** Approximate angle and location of orbicularis oculi injections. **(B)** Low magnification view of a representative section containing the left facial motor nucleus, box in **(B)** indicates location of drawing shown in **(C)**. **(C)** A medium magnification view of the facial motor nucleus. In this case, CAV-2 injected into the orbicularis oculi provided retrograde labeling, albeit to a lesser extent when compared to the first case. **(D)** A high magnification, camera lucida reconstruction of a single neuron from this case demonstrating the intracellular distribution of mCitrine expression of a single cell.

Finally, the fifth (and lowest dose) injection in this animal (M18-03) consisted of 22 µl of CAV-2-CMV-DsRedII (2.4×10^{10} pp) into the left medial rectus muscle (**Figure 6A**). During surgery, a large bolus was injected into the belly of the muscle, then multiple smaller injections were dispensed as the needle was withdrawn anteriorly. This injection resulted in generally weak labeling in the left oculomotor nucleus (**Figures 6B,C**). A few labeled cells were also observed just dorsal to the oculomotor nucleus, in the C-group (**Figures 6B,C**) where MIF motoneurons of the medial rectus reside. There was also labeling within the territory of the SIF medial rectus motoneurons, within the ventral oculomotor nucleus (**Figure 6C**). Only a few motoneurons were observed, and less dendritic labeling compared to even the lateral rectus injection. Careful morphological inspection of the MIF motoneurons revealed sparse dendritic labeling (**Figure 6D**).

To help compare across injections for this animal (M18-03), photomicrographs in **Figure 7** illustrate the quality and intensity of virally mediated labeling of motoneurons innervating the superior rectus muscle (high dose, 7.8×10^{10} pp; **Figure 7A**), lateral rectus muscle (medium dose, 6.2×10^{10} pp; **Figure 7B**), and medial rectus muscle (low dose, 2.4×10^{10} pp; **Figure 7C**). An example superior rectus motoneuron (white arrow; same cell illustrated in **Figure 4F**) featured numerous short, lightly labeled dendrites (black arrowheads) in the surrounding region (**Figure 7A**). An example lateral rectus motoneuron (white arrow; same cell illustrated in **Figure 5C**) had drastically less dendritic labeling in the surround (**Figure 7B**). Finally, an example medial rectus motoneuron (white arrow; same cell illustrated in **Figure 6C**) showed no obvious extraneous dendritic labeling (**Figure 7C**). Across all the CAV-2 injection sites of this case, no gliosis was found histologically in any of the respective nuclei.

Combined, the injections from the third animal (**Figures 3–6**) revealed an overall diminished degree of labeling, both in the number of cells and dendritic densities, compared to the first animal that only received a single CAV-2 injection (**Figures 1**, **2**). We hypothesized that the differences in motoneuronal labeling were a result of the sum of all CAV-2 injections rather than the titers being injected into individual muscles. To test this, we reduced the number of CAV-2 injections to only two extraocular muscles in a fourth animal ("M19-01"). A general increase in the number of cells and density of dendritic labeling would support the hypothesis. Also, to test whether differences in labeling were dose-related or muscle/nucleus-related, in this fourth animal we injected a higher dose into the medial rectus than into the lateral rectus (opposite to the procedure for M18-03).

The results of a 20 µl injection of CAV-2-CMV-DsRedII (1.1×10^{11} pp) placed into the left medial rectus muscle of animal M19-01 are shown in **Figure 8A**. This injection resulted in dense motoneuronal labeling around the left oculomotor nucleus (**Figure 8B**). A closer inspection of the somatic and dendritic distributions revealed heavy labeling along the dorsomedial edge

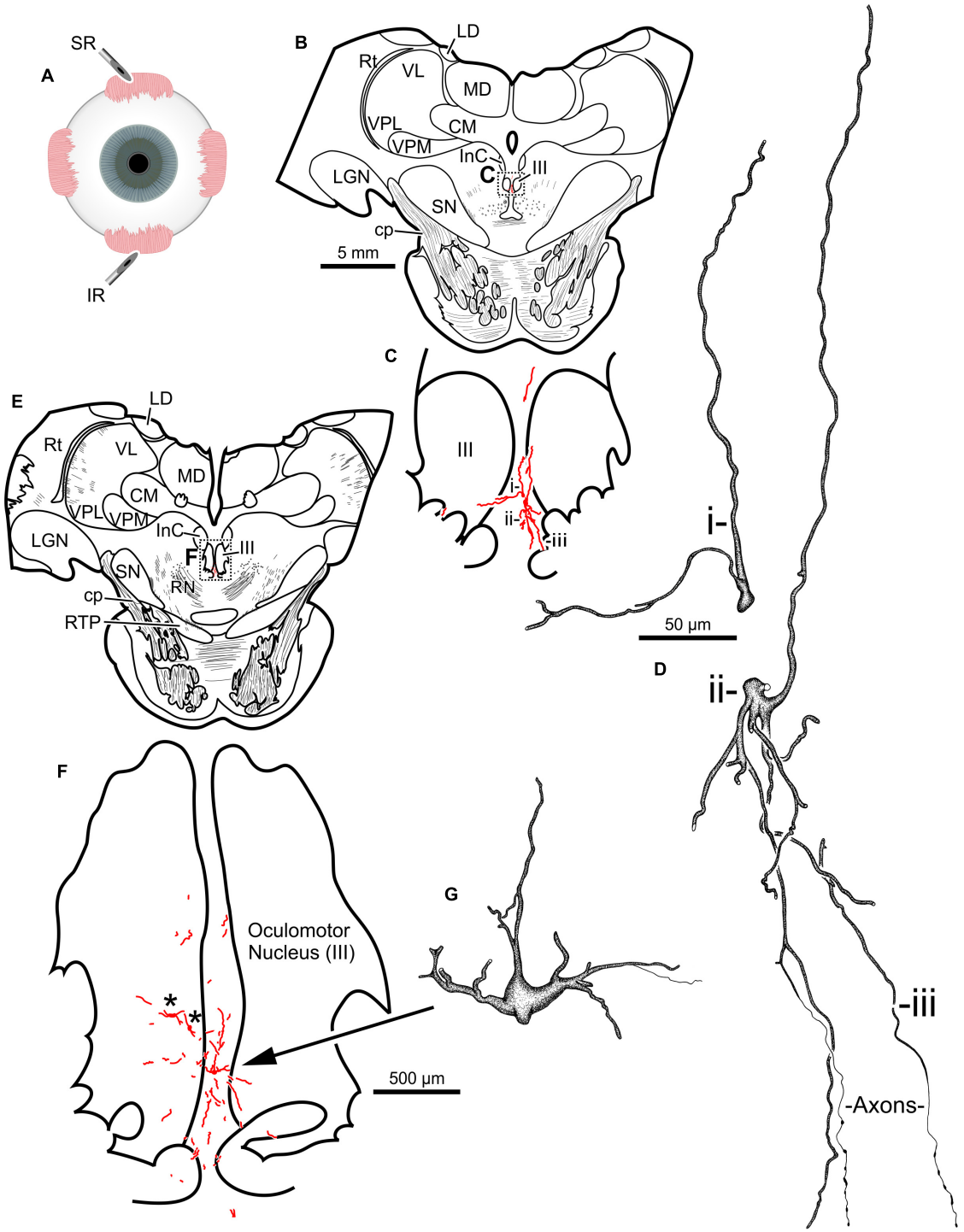

FIGURE 4 | An injection of CAV-2-CMV-mCitrine into the left superior rectus **(A)** resulted in motoneuronal labeling along midline, in the region of the S-group, between the left and right oculomotor nucleus. Low magnification views from representative sections containing the rostral **(B)** and more caudal **(E)** oculomotor nucleus, box in **(B)** indicates location of drawing shown in **(C)**, box in **(E)** indicates the location of the drawing shown in **(F)**. **(C,F)** Medium magnification views of the oculomotor nucleus and the distribution of superior rectus motoneuronal labeling within. * in **(F)** indicates potential inferior rectus motoneurons labeled in the left oculomotor nucleus. **(D,G)** High magnification, camera lucida reconstructions of single neurons from this case, demonstrating the intracellular distribution of mCitrine expression within single cells. Labeled neuronal structures (i, ii, and iii) in **(C)** are presented as high magnification in **(D)**. Magnifications are the same for **(B,E)**, **(C,F)** and **(D,G)**.

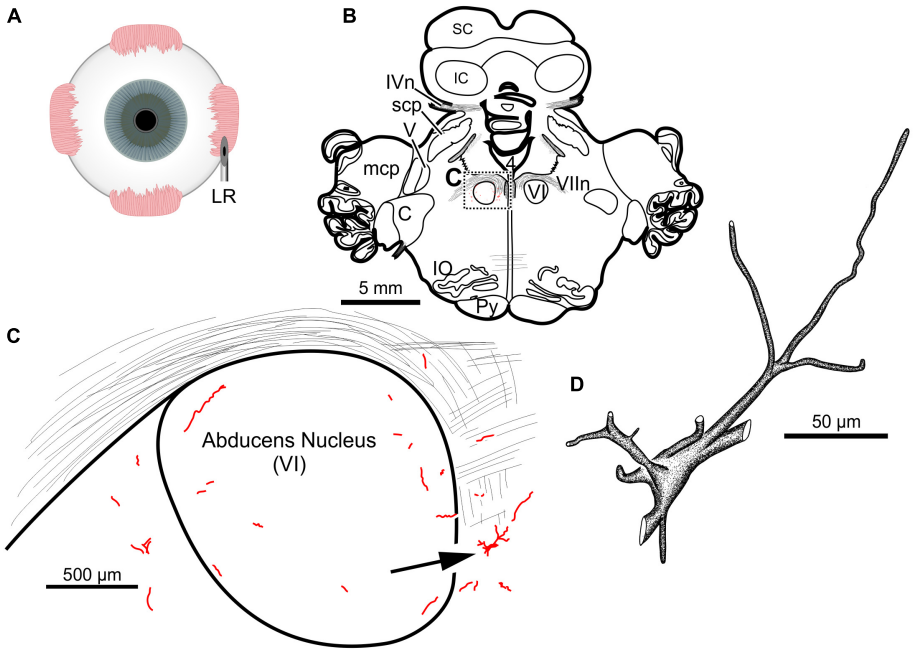

FIGURE 5 | An injection of CAV-2-CMV-DsRedII into the left lateral rectus **(A)** resulted in motoneuronal labeling predominantly in the periphery of the left abducens nucleus. **(B)** Low magnification view from a representative section containing the abducens nucleus, box in **(B)** indicates location of drawing shown in **(C)**. **(C)** A medium magnification view of the abducens nucleus and the distribution of lateral rectus motoneuronal labeling predominantly in the surround of the left abducens nucleus. **(D)** High magnification, camera lucida reconstruction of a single neuron from this case demonstrating the extent of intracellular DsRedII labeling expression within a single cell.

of the left oculomotor nucleus, the known location of the medial rectus MIF motoneurons (**Figure 8C**). Most of the dendrites projected ventrally, above the oculomotor nucleus and avoiding the oculomotor nucleus all together. A few dendrites, however, could be observed projecting laterally into the oculomotor nucleus (**Figure 8C**). In general, labeling was robust enough to visualize somata and primary and secondary dendrites from this injection (**Figure 8D**).

In the same animal (M19-01), 20 µl of CAV-2-CMV-DsRedII (5.6×10^{10} pp) was injected into the left lateral rectus (**Figure 9A**). This injection resulted in motoneuronal labeling within the left abducens nucleus (**Figure 9B**). Somatic and dendritic labeling was most frequently observed in the periphery of the abducens nucleus (**Figure 9C**). Close inspection of labeled cells revealed transgene expression throughout the somata and primary, secondary, and tertiary dendrites (**Figure 9D**).

Photomicrographs from the last presented case (M19-01) provide examples of the quality and intensity of CAV-2-mediated expression of DsRedII in medial and lateral rectus motoneurons (**Figure 10**). **Figure 10A** is a photomicrograph from the same section as presented in **Figure 8**, where injections into the medial rectus muscle resulted in well-labeled somata (**Figure 10A**, arrows) and dense dendritic labeling (**Figure 10A**, arrowheads) within the C-group around the oculomotor nucleus. Similarly, **Figure 10B** illustrates the intensity and distribution of labeling within the somata (**Figure 10B**, white arrows) and dendrites (**Figure 10B**, arrowheads) of motoneurons in the abducens nucleus. Overall, labeling was denser for the higher titer injection in medial rectus (**Figure 10A**) compared with the lower titer injection in lateral rectus (**Figure 10B**). Taken together with the results of animal M18-03, this indicates that labeling was a function of dose rather than the specific muscle/nucleus system.

Though not displayed in the reconstructions, across cases, labeled axons were observed within the fascicules of the oculomotor, trochlear, and facial motor nerves associated with each respective muscle.

DISCUSSION

The goal of the present work was to evaluate CAV-2's capacity to transduce exogenous genes into cranial nucleus motoneurons following intramuscular injection in non-human primates. Our histological assessments yielded three main conclusions: (1) The vector worked well to transduce genes into motoneurons of the ocular and facial cranial nuclei (animals M18-01, M18-03, and M19-01); (2) There was an effect of total viral load, with relatively small, single injections yielding the best labeling (M18-01) and larger injections in 2–3 muscles working adequately (M18-03 and M19-01). More extensive injections, however, yielded no transgene expression, presumably due to an immune response triggered by the total viral load (M18-02); (3) With total load constrained to avoid counterproductive immune responses, we found an increasing dose-response relationship over the range of $\sim 10^{10}$ to 10^{11} viral particles injected (animals M18-03 and M19-01). We will discuss these results in light

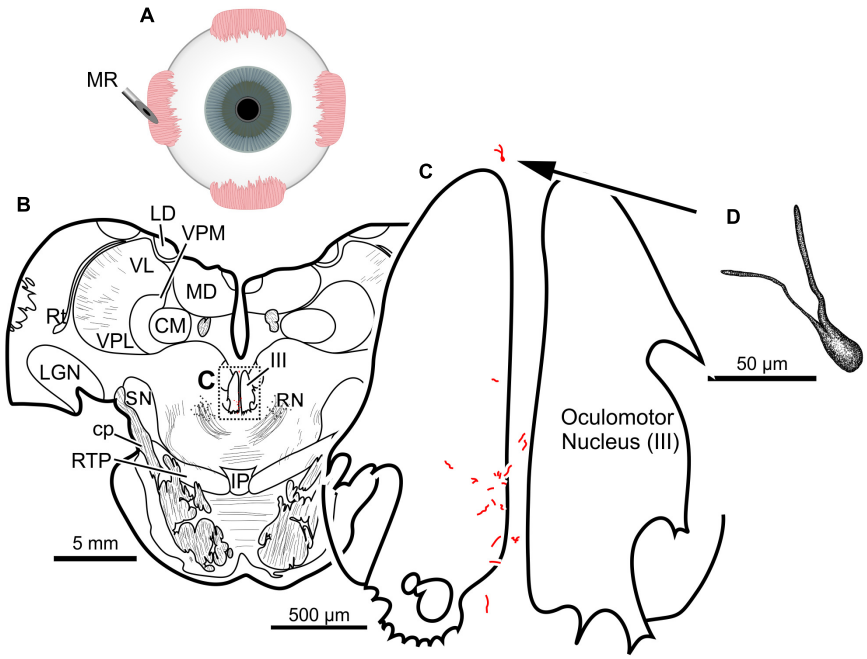

FIGURE 6 | An injection of CAV-2-CMV-DsRedII into the left medial rectus **(A)** resulted in motoneuronal labeling both within and outside the left oculomotor nucleus. **(B)** Low magnification view from a representative section containing the oculomotor nucleus, box in **(B)** indicates location of drawing shown in **(C)**. **(C)** A medium magnification view of the oculomotor nucleus and the distribution of medial rectus motoneuronal labeling within and to a lesser extent, outside the cytoarchitectonic boundaries of the left oculomotor nucleus. **(D)** High magnification, camera lucida reconstruction of a single neuron from this case demonstrating the intracellular distribution of DsRedII expression within a single cell. Based on its location, this neuron is a presumed medial rectus multiply innervating fiber motoneuron within the C-group region.

of prior results, address the relevance and limitations of the findings, and review important technical considerations when using CAV-2.

Motoneuronal Labeling Following Intramuscular CAV-2 Injections

The primary finding in this study is that intramuscular injections of CAV-2 reliably transduce cranial nucleus motoneurons in non-human primates. In cranial nuclei that innervate the extraocular musculature, most of the observed labeling was within the territories of MIF motoneurons (located in the periphery of the respective nuclei). We suspect that labeling of the MIF neuromuscular system was favored as a result of our injection approach. The needle was advanced into the muscle at its insertion and driven posteriorly toward the belly. Then, as the needle was withdrawn, small injections of CAV-2 were deposited along its path. Hence, most of the CAV-2 was not in the belly, where SIF neuromuscular junctions reside, but more toward the muscle insertions, where only MIF neuromuscular junctions are found. Correspondingly, we found that transduction was restricted to the relatively small zones in which MIF motoneurons reside, with little if any unintentional encroachment into the larger SIF motoneuron zones. This result provides direct evidence for little, if any, diffusion of the ∼100 nm CAV-2 capsids (Schoehn et al., 2008). If the capsids did not spread longitudinally within the injected muscle toward the belly, it is highly unlikely that they spread to other nearby, intact muscles. In future work, we aim to target both SIF and MIF motoneurons by injecting the central (belly) regions of extraocular muscles to involve the SIF as well as the MIF terminals. We expect that this will result in a drastic increase in the number of motoneurons that are labeled, both by transducing more MIF motoneurons and by adding transduction of SIF motoneurons. This point is substantiated by the medial rectus muscle injection illustrated in **Figure 6**, in which there was an effort to place more of the CAV-2 injection into the belly of the muscle before releasing virus along the needle track as it was withdrawn; this resulted in labeled motoneurons both within (SIF motoneuron zone) and around (MIF motoneuron zone) the oculomotor nucleus. This is further supported by previous anatomical work in which injections of conventional tracers confined to the insertion of the extraocular muscles resulted in predominantly MIF motoneuronal labeling, while belly injection or full muscle injections resulted in labeling of all motoneuronal populations (Büttner-Ennever et al., 2001; Büttner-Ennever and Horn, 2002). All of this emphasizes the usefulness of the extraocular neuromuscular systems as testbeds for the characterization of viral vectors and the development of viral vector techniques aimed at targeting motoneurons, due to the extraocular muscles' unique patterns of innervation.

Previous work on transduction of motoneurons following intramuscular injections focused on AAV vectors in spinal systems. Towne et al. (2010) made injections of

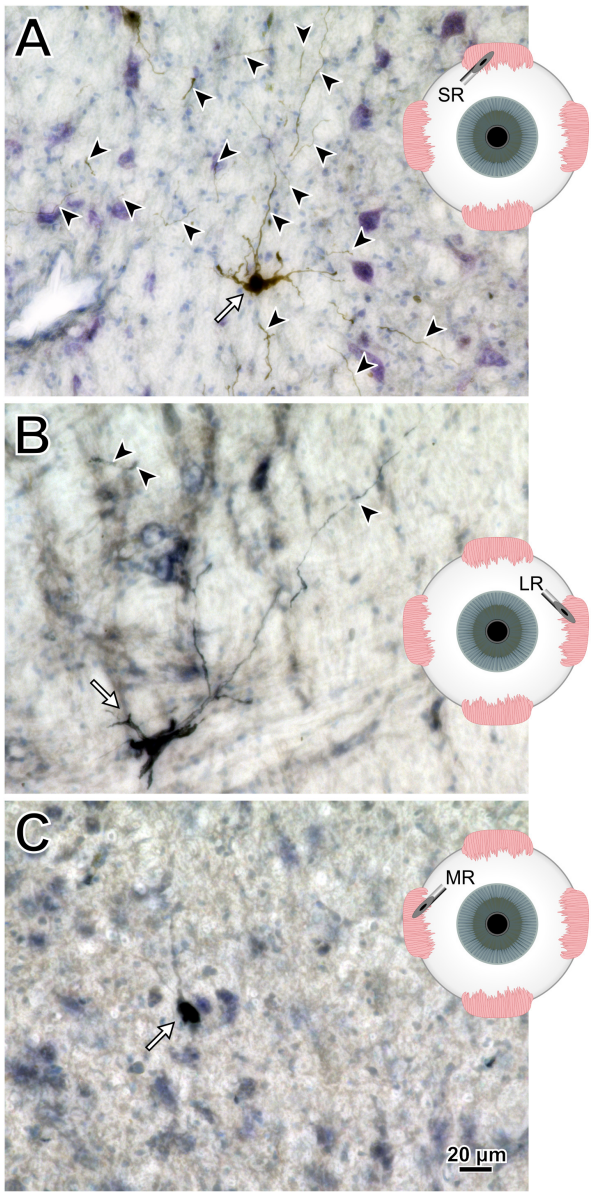

FIGURE 7 | M18-03 photomicrographs of motoneuronal labeling following different CAV-2 dosage injections into the **(A)** superior rectus, **(B)** lateral rectus, and **(C)** medial rectus muscles. Arrows indicate cells, arrowheads indicate dendritic labeling. Photomicrographs **(A–C)** were taken at 40x, A = 25z; B = 1z; C = 2z.

AAV6-CMV-glb-eGFP into the gastrocnemius muscle of three African green monkeys (*Chlorocebus sabaeus*). Following a 1-month survival period, they found robust fluorescent protein expression in alpha motor neurons within the ventral spinal cord. Using a similar approach, Williams et al. (2018) injected three rhesus macaques with either AAV6-hSyn-ChR2-eYFP or AAV6-hSyn-Chronos-eYFP. Post-injection, optical stimulation of the peripheral nerve produced visually observed fasciculations and electromyographic-detected activity that suggested effective gene expression. Thirteen-weeks post-injection, however, anatomical assessment revealed transgene expression only in the peripheral nerves. A major concern using AAV is that the time course of its expression can be highly variable (Maimon et al., 2017; Williams et al., 2018). More recently, Maimon et al. (2018) found that, in rats, the loss of AAV6-hSyn-ChR2(H124R) mediated protein expression in peripheral nerves was the result of an immunological response against the transgenes. This response resulted in motoneuronal cell death and muscle atrophy. Another downside of AAV6 is that it transduces both the motoneurons and the muscle cells (Towne et al., 2010). This could potentially provide a peripheral catalytic site for developing an immunological response against the transduced exogenous genes. We found strong evidence of CAV-2 transgene expression in motoneurons 2-months post-injection (**Table 1**), and helper-dependent CAV-2 vectors have been shown to provide constitutive expression over a year post-CAV-2 inoculation (Soudais et al., 2004). In general, CAV-2 shows little immunogenicity in rats, and human sera does not contain neutralizing antibodies (Perreau and Kremer, 2005; Perreau et al., 2007a,b). Further, since the CAV-2 receptor, CAR, is expressed only at the neuromuscular junctions, there is no non-specific uptake of the CAV-2 in the muscle cells; its transduction is restricted to the innervating motoneurons (Soudais et al., 2000, 2001; Salinas et al., 2009). Taken together, a conservative conclusion is that CAV-2 offers a reliable, alternative method to AAV6 for transducing motoneurons following intramuscular injection. With further development of CAV-2 vectors, including helper-dependent approaches, the vector could become a superior tool to AAV6 for basic research studies and gene therapies that target specific motoneuronal populations in non-human primates.

Dose Responses

A secondary aim of this work was to find an optimal CAV-2 dose that would provide maximal motoneuronal labeling while minimizing cytotoxicity. To this end, there are two dose responses to consider with the current work: the total number of viral particles injected, assessed by comparing across animals, and the viral loads injected into discrete muscles, assessed within animals. First, comparisons across animals suggested that the total number of viral capsids was an important variable (**Table 1**). The animal receiving the largest vector load, M18-02, received a total of 5.7×10^{11} pp but showed no anatomical evidence of transgene expression (**Table 2**). Animal M18-03 received a total of 4.2×10^{11} CAV-2 particles (**Figures 3–7**), which yielded motoneuronal labeling from all the injection sites, but with relatively weak intensity (**Table 2**). Animal M18-01 received a single muscle injection with a total of 5.2×10^{10} CAV-2 particles (**Figure 1**), which resulted in robust motoneuronal labeling, but also some gliosis (**Table 2**). Animal M19-01 received two intramuscular injections for a total of 1.6×10^{11} CAV-2 viral particles (**Figures 8–10**), which yielded moderately strong labeling of both respective motoneuronal populations (**Table 2**) and no signs of gliosis. In sum, the range from $\sim 10^{10}$ to 10^{11} particles yielded the best results. A good example of the total-dose effect is to visually compare the degree of motoneuronal labeling from injections of the

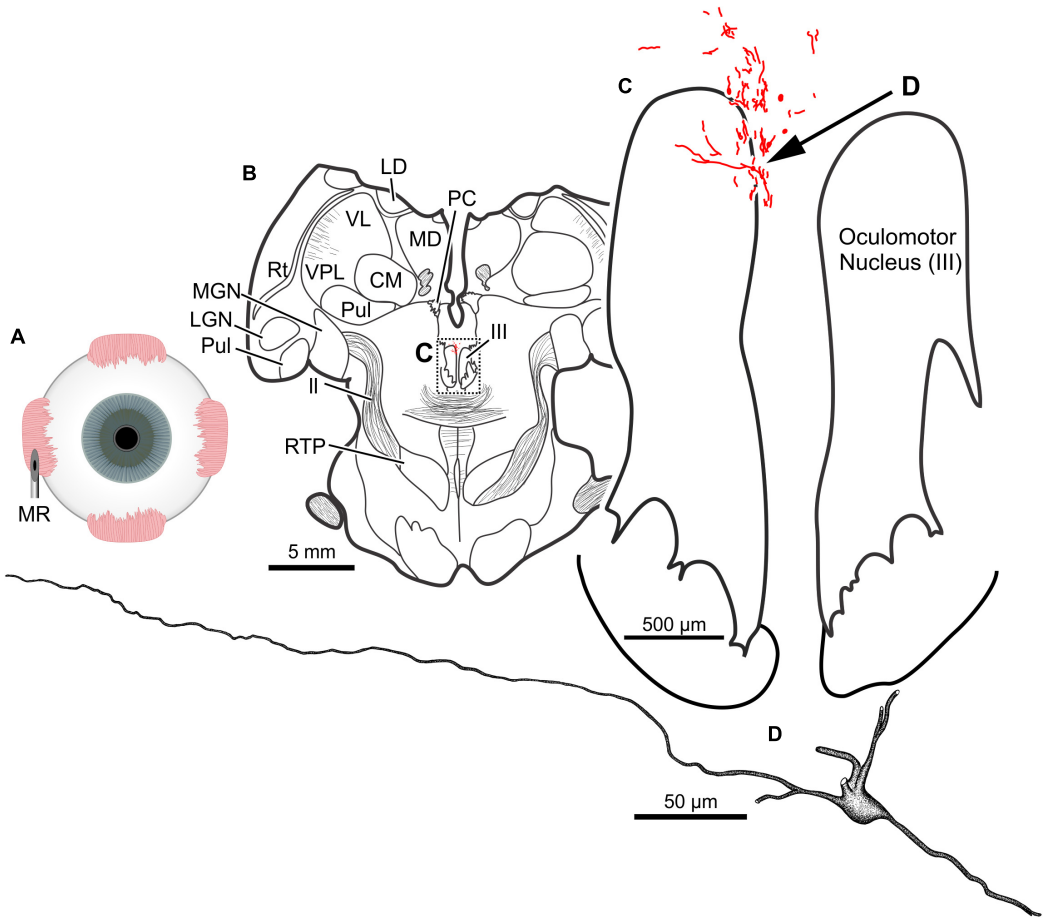

FIGURE 8 | An injection of CAV-2-CMV-DsRedII into the left medial rectus **(A)** resulted in motoneuronal labeling within and dorsomedial to the left oculomotor nucleus. **(B)** Low magnification view of a representative section containing the oculomotor nucleus, box in **(B)** indicates the location illustrated in **(C)**. **(C)** Medium magnification view of the oculomotor nucleus and the distribution of medial rectus motoneuronal DsRedII labeling. Arrow in **(C)** indicates the cell illustrated in **(D)**. **(D)** High magnification reconstruction of a single medial rectus motoneuron demonstrating the extent of motoneuronal labeling provided from an injection of CAV-2.

orbicularis oculi with relatively higher (**Figure 3C**) and lower doses (**Figure 1C**).

With total dose kept in the range $\sim 10^{10}$ to 10^{11} pp, allowing for transduction without an apparently counterproductive immune response, we could demonstrate within-animal dose response effects in which the transduction scaled with the dose. The clearest example was for animal M18-03, which received injections of different viral doses into different muscles, with the higher doses yielding better results. Injection of 7.8×10^{10} CAV-2 particles into the superior rectus resulted in labeling of the somata, dendrites, and axons of more motoneurons than injection of smaller viral loads into the lateral rectus (6.2×10^{10}) and medial rectus (2.4×10^{10}) as summarized in **Figures 7A–C**, respectively. The difference in labeling seemed related to dose, not muscle or nucleus, because in animal M19-01 we placed the highest dose in the medial rectus (1.1×10^{11}; **Figure 10A**) and again it yielded more pervasive labeling than a lower dose, this time placed in lateral rectus (5.6×10^{10}; **Figure 10B**). Based upon these results, we suspect that the optimal dose will likely be in the lower range of $\sim 10^{11}$ for total intramuscularly injected viral particles; if gliosis results, it should be preventable by dropping the dose to $\sim 10^{10}$ while still yielding robust transduction for the muscles tested.

The diminishing returns found for the highest total viral loads are probably related to stronger immune responses mounted in retaliation to the viral insults. While our experiments were not designed to explicitly test immune responses, in at least one case (M18-01; **Figures 1**, **2**), strong transduction co-occurred with clear gliosis as noted above. This could result from an immunological response that was reducing CAV-2 positive neurons, though it is unclear if this was a direct response or a secondary response to potential toxicity resultant from, for example, expression of the fluorophores (Stripecke et al., 1999; Taghizadeh and Sherley, 2008; Ansari et al., 2016). Other vectors have yielded similar results with more direct immunological explanations. For example, previous work with AAV showed that increasing the vector dose improves transduction, but counterintuitively, promotes the activation of T cells (Manno et al., 2006; Mingozzi et al., 2007; Mingozzi and High, 2011, 2013; Nathwani et al., 2011). Overall, the dose effect suggested

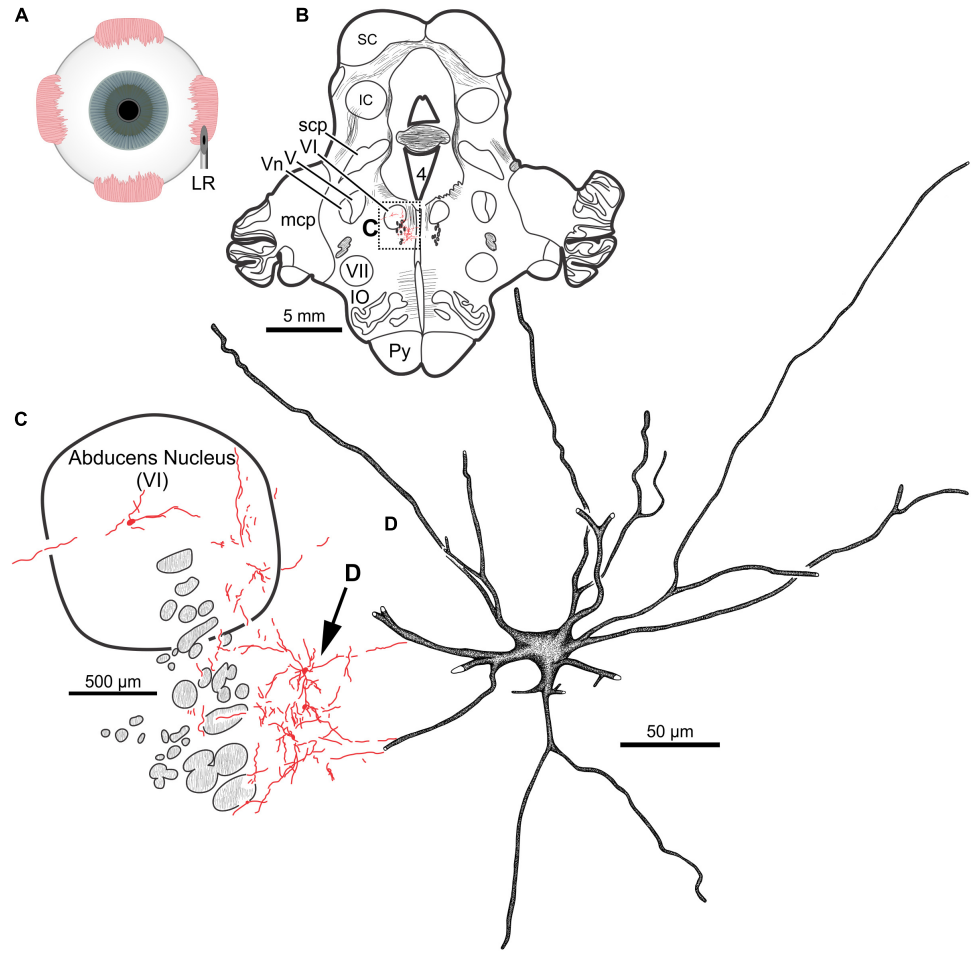

FIGURE 9 | An injection of CAV-2-CMV-DsRedII into the left lateral rectus **(A)** resulted in motoneuronal labeling within the left abducens nucleus. **(B)** Low magnification view of a representative section containing the abducens nucleus, box in **(B)** indicates the location illustrated in **(C)**. **(C)** Medium magnification view of the abducens nucleus and the distribution of labeled neuronal processes. Arrow in **(C)** indicates the cell illustrated in **(D)**. **(D)** High magnification reconstruction of a single lateral rectus motoneuron demonstrating the extent of DsRedII expression within a single motoneuron.

a complex interplay between the primate immune system and CAV-2. We tested only cranial nucleus motoneuron transduction, and it is unclear whether the optimal dose range suggested by our data generalize to other parts of the central nervous system. For any experiment using CAV-2 *in vivo*, it would seem important to establish dose-response curves to find the optimal dose for safe yet robust transgene expression in the specific, targeted cellular population.

Technical Considerations

A potential concern with regards to intramuscular injections is the spread of the viral vector from the injected muscle into the surrounding musculature. Based on our observations, this did not appear to be an issue. First, as noted above in §4.1, we found no evidence of spread even longitudinally within the injected muscles. If the capsids do not diffuse a few mm within the penetrated muscle, it is unlikely that they invade neighboring, intact muscles. Any viral spill would need to traverse the orbital space, penetrate the epimysium of another muscle, and then localize to motoneuronal terminals for transduction. Second, our impression was that the immunological response to peripheral viral injections could be stronger in some animals. As would be the case in humans, it is expected to have variable responses across subjects due to the different immunological background of each monkey. Given the volumes injected, the virally mediated labeling described here is far less than is expected from conventional tracer injections of similar volumes (Büttner-Ennever et al., 1981; Porter et al., 1983; Erichsen et al., 2014; Bohlen et al., 2017a). A potential explanation is that the viruses were neutralized soon after being injected into the muscle, and/or that chemical tracers are more readily diffuse throughout the injection site and therefore are capable of being taken up by more neuromuscular junctions. Third, the viral vectors carried different fluorophores that were strategically placed into muscles with neighboring motoneuronal pools. Crosstalk of viruses between the muscles would be noticeable via unexpected labeling in the cranial nuclei. The motoneurons innervating each extraocular muscle reside either in a separate

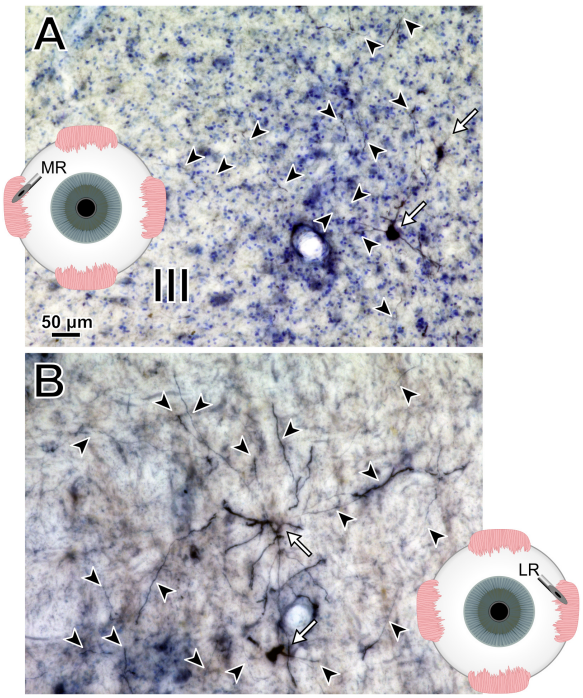

FIGURE 10 | M19-01 photomicrographs of motoneuronal labeling following different CAV-2 dosage injections into the **(A)** medial rectus and **(B)** lateral rectus muscles. Arrows indicate cells, arrowheads indicate dendritic labeling. Photomicrographs **(A,B)** were taken at 20x, A = 1z; B = 25z.

nucleus or, on average, in relatively segregated pools within the same nucleus: lateral rectus motoneurons reside in the abducens nucleus (VI), superior oblique motoneurons reside in the trochlear nucleus (IV), and motoneurons innervating the remaining four extraocular muscles and the levator reside in clustered pools within the oculomotor nucleus (III) with the medial rectus, inferior rectus and inferior oblique motoneurons sitting in pools within the oculomotor nucleus ipsilateral to the muscle they innervate, while the superior rectus motoneurons sit within the contralateral oculomotor nucleus to the orbit the innervate (Evinger, 1988; Büttner-Ennever et al., 2001; Bohlen et al., 2017b, 2019). The instance where this was an issue in the present study was the distinction between CAV-2-hChAT-GFP which was injected into the inferior rectus and CAV-2-CMV-mCitrine which was injected into the superior rectus. The epifluorescence would allow distinction between these two fluorophores, as would labeling of the whole motoneuronal populations. However, the method used for visualization in the present work was immunohistochemical amplification, in which the primary antibody, goat anti-GFP, recognizes both GFP and mCitrine. This left only the anatomical segregation of the two motoneuronal pools. Given that there were GFP positive neurons in the ipsilateral oculomotor nucleus, the known location of the inferior rectus motoneuronal pool, this strongly suggests that CAV-2-hChAT-GFP was able to successfully transduce and express GFP. In the same sections, there was clear motoneuronal labeling both on midline, in the region of the superior rectus MIF motoneurons, as well as labeling in the contralateral oculomotor nucleus (data not shown), a clear sign of superior rectus motoneuronal labeling. Finally, orbicularis oculi motoneurons reside in the dorsomedial division of the facial motor nucleus and masseter motoneurons are found in the trigeminal motor nucleus. Hence, although multiple viruses were injected into multiple muscles of the same orbit, there was no unexpected motoneuronal labeling observed within or across the respective nuclei. These check points provided confidence that a CAV-2 injection into a given muscle produced labeling only in the expected motoneuronal population, and not in others.

Though beyond the current body of work, there is a standing question of labeling with regards to the observed varicosities. It is unclear what these morphological features reflect in terms of the anatomy of labeled motoneurons. Specifically, are the varicosities reflective of bead-on-a-string axons, beaded dendrites, or both? Superficially, the morphological features are akin to the beads-on-a-string frequently observed in tracer-labeled axons, where fine filaments are intersected with boutonal enlargements. These sites of membranous enlargement are presumed to be sites containing vesicles, the molecular machinery necessary for the synaptic vesicular cycle, and anchoring proteins for maintaining pre- and post-synaptic alignment. Further, in the present work, we observed branching patterns that support axonal collateralization (**Figure 2B**; white filled arrows), where axonal collaterals frequently occur at obtuse or 90° angles and frequently maintain a similar size to the parental stem (Katz, 1985; Peters et al., 1991). In contrast, dendritic branches (**Figure 2B**; black filled arrow) frequently occur at acute angles and often the branch is smaller than the parental dendrite (Peters et al., 1991). Further, in the best labeled cases, CAV-2 provided fill of axons that could be observed coursing within the fascicles of respective nerves. On the other hand, the presentation of regular ovoid distensions along a dendrite (i.e., beaded dendrites) are assumed to reflect either a problem with the histological preparation or some neuropathology. As it relates to labeling using viruses, Ruigrok et al. (2016) reported gliosis surrounding a subset of rabies positive neurons following injections of rabies into fore- and hindlimb musculature of rats. These neurons appeared to be undergoing degeneration, and accompanying the degenerated neurons were dendrites with a beaded morphological presentation (see Figures 2E1-3 of Ruigrok et al., 2016). Following direct injections of rAAV2-CMV-GFP-TrkB.T1 into the facial motor nucleus, De Wit et al. (2006) also observed some dendritic beading in a subset of the transduced neurons. In the same report, the authors noted that in some cases the dendritic beading occurred throughout all dendrites including primary dendrites coming off the somata (not observed in the current report), while in other examples, beading of distal dendrites but not more proximal dendrites were observed (an occurrence not observed directly in single cells, but which is possible). The Catch-22 is that the cases with the densest labeling/fill were also the cases that, in general, showed the beading morphology and, in a subset of cases, gliosis. We expect that the labeling observed in our sections was likely a mix of axons and beaded dendrites. Fundamentally, more work needs to be

done to better understand these morphological features. Future work could use immunofluorescence with antibodies against myelin basic proteins to help determine whether the labeled neuronal structures are axons or dendrites. A more informative option may be to look at the ultrastructure of the labeled neuronal structures. This would not only allow for differentiation of dendritic and axonal structures but also could reveal unique pathological markers.

With regard to the variance in neuronal labeling, two other technical points are notable, as they may be important for optimizing viral vector-mediated transduction and transgene expression in motoneurons: post-injection survival duration and multiplicity of infection (MOI). It is possible that longer survival times could have led to more accumulation of fluorescent proteins that would have become detectable after superseding basal levels of detection. In its simplest form, MOI is a descriptor for the average number of virions infecting each cell (Shabram and Aguilar-Cordova, 2000), in this case, the average number of CAV-2 vectors that successfully transduced motoneurons. A higher MOI should result in overexpression of fluorescent proteins in targeted neurons and with that, an increased probability of immunological detection of the free ends of the CAV-2 genome in the nucleus (Del Rio et al., 2019), likely causing the apparent cytotoxicity. In other words, our results could reflect the low side of what is possible with CAV-2 in cranial motoneurons. The results here provide justification for a broader, systematic parametric study of CAV-2 transduction in macaque cranial nuclei, with the aim of optimizing the ability of CAV-2 vectors to find their receptor and control transgene expression (Perreau and Kremer, 2005; Perreau et al., 2007a,b).

Challenges and Potential Solutions to the Use of CAV-2 in Macaques

There is potential for CAV-2-mediated gene transfer in non-human primates to be exploited for expression of channelrhodopsin for optogenetics. Although some researchers have observed problems with the expression of channelrhodopsin during CAV-2 vector propagation (personal communication with E. J. Kremer), using neuron-specific promoters may circumvent this (Hirschberg et al., 2017). At present, there is a Cre-expressing CAV-2 that can be combined with a second virus containing a Cre-inducible channelrhodopsin or designer receptor exclusively activated by designer drugs (i.e., DREADDs) that works in primates (Del Rio et al., 2019). However, by requiring a second viral vector, this may decrease the number of neurons that are co-infected with both vectors, resulting in a diminished number of neurons expressing the mature, functional protein. Such an outcome would run counter to one of the main challenges in primate optogenetics: transduction and transgene expression in sufficient numbers of neurons to elucidate full circuits and affect behavior (Galvan et al., 2018). Therefore, the two-vector transactional techniques are less than ideal for primates in which reliable and robust expression is already a challenge.

As noted above in §4.1, one approach that may resolve many of the current issues involving both the immunogenicity and the reliable long-term expression of channelrhodopsin or DREADDs is to develop a helper-dependent (high-capacity, gutted or gutless) CAV-2 vector with the genetic payload of interest. In general, the development of helper-dependent vectors has eliminated many of the immunological issues while also providing constitutive expression over long periods of time in rodents and monkeys (O'Neal et al., 2000; Xiong et al., 2006; Barcia et al., 2007; Butti et al., 2008). More importantly, Soudais et al. (2004) found that a helper-dependent CAV-2 provided transgene expression for over a year without the aid of immunosuppression following intraparenchymal striatal injections in rats. Once a helper-dependent CAV-2 vector has been developed, an important step will be to replicate these findings in primates, requiring that animals survive and are tested at multiple time points for responsiveness to optical or pharmacological stimulation. Here again, the oculomotor system would be a good testbed, as there are established, highly sensitive methods for monitoring eye position in space (Robinson, 1963; Judge et al., 1980). All things considered, CAV-2 is emerging as an important viral vector for primate research, and shows promising clinical potential for its capacity to transduce therapeutic genes to motoneurons following intramuscular injections.

DATA AVAILABILITY

All datasets generated for this study are included in the manuscript and/or the supplementary files.

ETHICS STATEMENT

The animal study was reviewed and approved by the Duke University IACUC and Institutional Biosafety Committee.

AUTHOR CONTRIBUTIONS

MB, HE-N, and MS conceived the work and wrote the manuscript. MB and HE-N performed the surgeries and histology, and analyzed the data.

FUNDING

This work was supported by the Hartwell Biomedical Research Fellowship to MB, the Duke Institute for Brain Sciences Germinator Award to MO and MS, and the National Institutes of Health (NEI R21 EY030278 to MS).

ACKNOWLEDGMENTS

We thank Jessi Cruger and Duke lab animal facility veterinarians and staff for animal care and surgical technical assistance and the Platform de Vectorology de Montpellier (PVM) for providing the CAV-2 vectors.

REFERENCES

Ansari, A. M., Ahmed, A. K., Matsangos, A. E., Lay, F., Born, L. J., Marti, G., et al. (2016). Cellular GFP toxicity and immunogenicity: potential confounders in in vivo cell tracking experiments. *Stem Cell Rev.* 12, 553–559. doi: 10.1007/s12015-016-9670-8

Barcia, C., Jimenez-Dalmaroni, M., Kroeger, K. M., Puntel, M., Rapaport, A. J., Larocque, D., et al. (2007). One-year expression from high-capacity adenoviral vectors in the brains of animals with pre-existing anti-adenoviral immunity: clinical implications. *Mol. Ther.* 15, 2154–2163. doi: 10.1038/sj.mt.6300305

Bohlen, M. O., Bui, K., Stahl, J. S., May, P. J., and Warren, S. (2019). Mouse extraocular muscles and the musculotopic organization of their innervation. *Anat. Rec.* doi: 10.1002/ar.24141 [Epub ahead of print].

Bohlen, M. O., Warren, S., and May, P. J. (2017a). A central mesencephalic reticular formation projection to medial rectus motoneurons supplying singly and multiply innervated extraocular muscle fibers. *J. Comp. Neurol.* 525, 2000–2018. doi: 10.1002/cne.24187

Bohlen, M. O., Warren, S., Mustari, M. J., and May, P. J. (2017b). Examination of feline extraocular motoneuron pools as a function of muscle fiber innervation type and muscle layer. *J. Comp. Neurol.* 525, 919–935. doi: 10.1002/cne.24111

Butti, E., Bergami, A., Recchia, A., Brambilla, E., Franciotta, D., Cattalini, A., et al. (2008). Absence of an intrathecal immune reaction to a helper-dependent adenoviral vector delivered into the cerebrospinal fluid of non-human primates. *Gene Ther.* 15, 233–238. doi: 10.1038/sj.gt.3303050

Büttner-Ennever, J. A., Grob, P., Akert, K., and Bizzini, B. (1981). A transsynaptic autoradiographic study of the pathways controlling the extraocular eye muscles, using [125I]B-IIb tetanus toxin fragment. *Ann. N. Y. Acad. Sci.* 374, 157–170. doi: 10.1111/j.1749-6632.1981.tb30868.x

Büttner-Ennever, J. A., and Horn, A. K. (2002). The neuroanatomical basis of oculomotor disorders: the dual motor control of extraocular muscles and its possible role in proprioception. *Curr. Opin. Neurol.* 15, 35–43. doi: 10.1097/00019052-200202000-00007

Büttner-Ennever, J. A., Horn, A. K., Scherberger, H., and D'Ascanio, P. (2001). Motoneurons of twitch and nontwitch extraocular muscle fibers in the abducens, trochlear, and oculomotor nuclei of monkeys. *J. Comp. Neurol.* 438, 318–335. doi: 10.1002/cne.1318

Colella, P., Ronzitti, G., and Mingozzi, F. (2018). Emerging issues in AAV-mediated in vivo gene therapy. *Mol. Ther. Methods Clin. Dev.* 8, 87–104. doi: 10.1016/j.omtm.2017.11.007

De Wit, J., Eggers, R., Evers, R., Castrén, E., and Verhaagen, J. (2006). Long-term adeno-associated viral vector-mediated expression of truncated TrkB in the adult rat facial nucleus results in motor neuron degeneration. *J. Neurosci.* 26, 1516–1530. doi: 10.1523/JNEUROSCI.4543-05.2006

Del Rio, D., Beucher, B., Lavigne, M., Wehbi, A., Gonzalez Dopeso-Reyes, I., Saggio, I., et al. (2019). CAV-2 vector development and gene transfer in the central and peripheral nervous systems. *Front. Mol. Neurosci.* 12:71. doi: 10.3389/fnmol.2019.00071

Erichsen, J. T., Wright, N. F., and May, P. J. (2014). Morphology and ultrastructure of medial rectus subgroup motoneurons in the macaque monkey. *J. Comp. Neurol.* 522, 626–641. doi: 10.1002/cne.23437

Evinger, C. (1988). Extraocular motor nuclei: location, morphology and afferents. *Rev. Oculomot. Res.* 2, 81–117.

Galvan, A., Caiola, M. J., and Albaugh, D. L. (2018). Advances in optogenetic and chemogenetic methods to study brain circuits in non-human primates. *J. Neural Transm.* 125, 547–563. doi: 10.1007/s00702-017-1697-8

Hirschberg, S., Li, Y., Randall, A., Kremer, E. J., and Pickering, A. E. (2017). Functional dichotomy in spinal- vs prefrontal-projecting locus coeruleus modules splits descending noradrenergic analgesia from ascending aversion and anxiety in rats. *eLife* 6:e29808. doi: 10.7554/eLife.29808

Judge, S. J., Richmond, B. J., and Chu, F. C. (1980). Implantation of magnetic search coils for measurement of eye position: an improved method. *Vis. Res.* 20, 535–538. doi: 10.1016/0042-6989(80)90128-5

Katz, M. J. (1985). Axonal branch shapes. *Brain Res.* 361, 70–76. doi: 10.1016/0006-8993(85)91276-4

Loustalot, F., Kremer, E. J., and Salinas, S. (2016). Membrane dynamics and signaling of the coxsackievirus and adenovirus receptor. *Int. Rev. Cell Mol. Biol.* 322, 331–362. doi: 10.1016/bs.ircmb.2015.10.006

Maimon, B. E., Diaz, M., Revol, E. C. M., Schneider, A. M., Leaker, B., Varela, C. E., et al. (2018). Optogenetic peripheral nerve immunogenicity. *Sci. Rep.* 8:14076. doi: 10.1038/s41598-018-32075-0

Maimon, B. E., Zorzos, A. N., Bendell, R., Harding, A., Fahmi, M., Srinivasan, S., et al. (2017). Transdermal optogenetic peripheral nerve stimulation. *J. Neural Eng.* 14:034002. doi: 10.1088/1741-2552/aa5e20

Manno, C. S., Pierce, G. F., Arruda, V. R., Glader, B., Ragni, M., Rasko, J. J., et al. (2006). Successful transduction of liver in hemophilia by AAV-Factor IX and limitations imposed by the host immune response. *Nat. Med.* 12, 342–347. doi: 10.1038/nm1358

Mestre-Frances, N., Serratrice, N., Gennetier, A., Devau, G., Cobo, S., Trouche, S. G., et al. (2018). Exogenous LRRK2G2019S induces parkinsonian-like pathology in a nonhuman primate. *JCI Insight* 3:98202. doi: 10.1172/jci.insight.98202

Mingozzi, F., and High, K. A. (2011). Immune responses to AAV in clinical trials. *Curr. Gene Ther.* 11, 321–330. doi: 10.2174/156652311796150354

Mingozzi, F., and High, K. A. (2013). Immune responses to AAV vectors: overcoming barriers to successful gene therapy. *Blood* 122, 23–36. doi: 10.1182/blood-2013-01-306647

Mingozzi, F., Maus, M. V., Hui, D. J., Sabatino, D. E., Murphy, S. L., Rasko, J. E., et al. (2007). CD8(+) T-cell responses to adeno-associated virus capsid in humans. *Nat. Med.* 13, 419–422. doi: 10.1038/nm1549

Nathwani, A. C., Tuddenham, E. G., Rangarajan, S., Rosales, C., McIntosh, J., Linch, D. C., et al. (2011). Adenovirus-associated virus vector-mediated gene transfer in hemophilia B. *N. Engl. J. Med.* 365, 2357–2365. doi: 10.1056/NEJMoa1108046

O'Neal, W. K., Zhou, H., Morral, N., Langston, C., Parks, R. J., Graham, F. L., et al. (2000). Toxicity associated with repeated administration of first-generation adenovirus vectors does not occur with a helper-dependent vector. *Mol. Med.* 6, 179–195. doi: 10.1007/bf03402113

Perreau, M., Guerin, M. C., Drouet, C., and Kremer, E. J. (2007a). Interactions between human plasma components and a xenogenic adenovirus vector: reduced immunogenicity during gene transfer. *Mol. Ther.* 15, 1998–2007. doi: 10.1038/sj.mt.6300289

Perreau, M., Mennechet, F., Serratrice, N., Glasgow, J. N., Curiel, D. T., Wodrich, H., et al. (2007b). Contrasting effects of human, canine, and hybrid adenovirus vectors on the phenotypical and functional maturation of human dendritic cells: implications for clinical efficacy. *J. Virol.* 81, 3272–3284. doi: 10.1128/JVI.01530-06

Perreau, M., and Kremer, E. J. (2005). Frequency, proliferation, and activation of human memory T cells induced by a nonhuman adenovirus. *J. Virol.* 79, 14595–14605. doi: 10.1128/JVI.79.23.14595-14605.2005

Peters, A., Palay, S. L., and Webster, H. (1991). *The Fine Structure of the Nervous System: Neurons and Their Supporting Cells*, 3rd Edn, New York, NY: Oxford University Press.

Porter, J. D., Guthrie, B. L., and Sparks, D. L. (1983). Innervation of monkey extraocular muscles: localization of sensory and motor neurons by retrograde transport of horseradish peroxidase. *J. Comp. Neurol.* 218, 208–219. doi: 10.1002/cne.902180208

Robinson, D. A. (1963). A method of measuring eye movement using a scleral search coil in a magnetic field. *IEEE Trans. Biomed. Eng.* 10, 137–145. doi: 10.1109/tbmel.1963.4322822

Ruigrok, T. J., van Touw, S., and Coulon, P. (2016). Caveats in transneuronal tracing with unmodified rabies virus: an evaluation of aberrant results using a nearly perfect tracing technique. *Front. Neural Circuits* 10:46. doi: 10.3389/fncir.2016.00046

Salinas, S., Bilsland, L. G., Henaff, D., Weston, A. E., Keriel, A., Schiavo, G., et al. (2009). CAR-associated vesicular transport of an adenovirus in motor neuron axons. *PLoS Pathog.* 5:e1000442. doi: 10.1371/journal.ppat.1000442

Sass, F. A., Fuchs, M., Pumberger, M., Geissler, S., Duda, G. N., Perka, C., et al. (2018). Immunology guides skeletal muscle regeneration. *Int. J. Mol. Sci.* 19:E835. doi: 10.3390/ijms19030835

Schoehn, G., El Bakkouri, M., Fabry, C. M., Billet, O., Estrozi, L. F., Le, L., et al. (2008). Three-dimensional structure of canine adenovirus serotype 2 capsid. *J. Virol.* 82, 3192–3203. doi: 10.1128/JVI.02393-07

Shabram, P., and Aguilar-Cordova, E. (2000). Multiplicity of infection/multiplicity of confusion. *Mol. Ther.* 2, 420–421. doi: 10.1006/mthe.2000.0212

Shaw, C. A., Holland, P. C., Sinnreich, M., Allen, C., Sollerbrant, K., Karpati, G., et al. (2004). Isoform-specific expression of the Coxsackie and adenovirus receptor (CAR) in neuromuscular junction and cardiac intercalated discs. *BMC Cell Biol.* 5:42. doi: 10.1186/1471-2121-5-42

Sinnreich, M., Shaw, C. A., Pari, G., Nalbantoglu, J., Holland, P. C., and Karpati, G. (2005). Localization of coxsackie virus and adenovirus receptor (CAR) in normal and regenerating human muscle. *Neuromuscul. Disord.* 15, 541–548. doi: 10.1016/j.nmd.2005.05.007

Soudais, C., Boutin, S., Hong, S. S., Chillon, M., Danos, O., Bergelson, J. M., et al. (2000). Canine adenovirus type 2 attachment and internalization: coxsackievirus-adenovirus receptor, alternative receptors, and an RGD-independent pathway. *J. Virol.* 74, 10639–10649. doi: 10.1128/jvi.74.22.10639-10649.2000

Soudais, C., Laplace-Builhe, C., Kissa, K., and Kremer, E. J. (2001). Preferential transduction of neurons by canine adenovirus vectors and their efficient retrograde transport in vivo. *FASEB J.* 15, 2283–2285. doi: 10.1096/fj.01-0321fje

Soudais, C., Skander, N., and Kremer, E. J. (2004). Long-term in vivo transduction of neurons throughout the rat CNS using novel helper-dependent CAV-2 vectors. *FASEB J.* 18, 391–393. doi: 10.1096/fj.03-0438fje

Spencer, R. F., and Porter, J. D. (1988). Structural organization of the extraocular muscles. *Rev. Oculomot. Res.* 2, 33–79.

Spencer, R. F., and Porter, J. D. (2006). Biological organization of the extraocular muscles. *Prog. Brain Res.* 151, 43–80. doi: 10.1016/S0079-6123(05)51002-1

Stripecke, R., del Carmen Villacres, M., Skelton, D. C., Satake, N., and Kohn, D. B. (1999). Immune response to green fluorescent protein: implications for gene therapy. *Gene Ther.* 6, 1305–1312. doi: 10.1038/sj.gt.3300951

Taghizadeh, R. R., and Sherley, J. L. (2008). CFP and YFP, but not GFP, provide stable fluorescent marking of rat hepatic adult stem cells. *J. Biomed. Biotechnol.* 2008:453590. doi: 10.1155/2008/453590

Tang, X., Büttner-Ennever, J. A., Mustari, M. J., and Horn, A. K. (2015). Internal organization of medial rectus and inferior rectus muscle neurons in the C group of the oculomotor nucleus in monkey. *J. Comp. Neurol.* 523, 1809–1823. doi: 10.1002/cne.23760

Tidball, J. G. (2017). Regulation of muscle growth and regeneration by the immune system. *Nat. Rev. Immunol.* 17, 165–178. doi: 10.1038/nri.2016.150

Towne, C., Schneider, B. L., Kieran, D., Redmond, D. E. Jr., and Aebischer, P. (2010). Efficient transduction of non-human primate motor neurons after intramuscular delivery of recombinant AAV serotype 6. *Gene Ther.* 17, 141–146. doi: 10.1038/gt.2009.119

Williams, J., Watson, A., Vazquez, A. L., and Schwartz, A. B. (2018). Viral-mediated optogenetic stimulation of peripheral motor nerves in non-human primates. *bioRxiv*. doi: 10.1101/261925

Xiong, W., Goverdhana, S., Sciascia, S. A., Candolfi, M., Zirger, J. M., Barcia, C., et al. (2006). Regulatable gutless adenovirus vectors sustain inducible transgene expression in the brain in the presence of an immune response against adenoviruses. *J. Virol.* 80, 27–37. doi: 10.1128/JVI.80.1.27-37.2006

Conflict of Interest Statement: The authors declare that the research was conducted in the absence of any commercial or financial relationships that could be construed as a potential conflict of interest.

frontiers in Molecular Neuroscience

BRIEF RESEARCH REPORT
published: 10 December 2019
doi: 10.3389/fnmol.2019.00303

Targeting Reciprocally Connected Brain Regions Through CAV-2 Mediated Interventions

Sarah Morceau[1,2†], *Robin Piquet*[1,2†], *Mathieu Wolff*[1,2*] *and Shauna L. Parkes*[1,2*]

[1]CNRS, INCIA, UMR 5287, Bordeaux, France, [2]Université de Bordeaux, INCIA, UMR 5287, Bordeaux, France

An important issue in contemporary neuroscience is to identify functional principles at play within neural circuits. The reciprocity of the connections between two distinct brain areas appears as an intriguing feature of some of these circuits. This organization has been viewed as "re-entry," a process whereby two or more brain regions concurrently stimulate and are stimulated by each other, thus supporting the synchronization of neural firing required for rapid neural integration. However, until relatively recently, it was not possible to provide a comprehensive functional assessment of such reciprocal pathways. In this Brief Research Report, we highlight the use of a chemogenetic strategy to target projection-defined neurons in reciprocally connected areas through CAV-2 mediated interventions in the rat. Specifically, we targeted the bidirectional pathways between the dorsomedial prefrontal cortex (dmPFC) and the mediodorsal thalamus, as well as those connecting the insular cortex (IC) and the basolateral complex of the amygdala (BLA). These data showcase the usefulness of CAV-2-related strategies to address circuit-level issues. Moreover, we illustrate the inherent limitation of Cre-dependent adeno-associated virues (AAVs) with "leaked" expression of the gene of interest in the absence of Cre and highlight the need for appropriate control conditions.

Keywords: neural circuits, DREADD, prefrontal cortex, thalamus, insular cortex, basolateral amygdala

OPEN ACCESS

Edited by:
Ildikó Rácz,
Universitätsklinikum Bonn, Germany

Reviewed by:
Gonzalo Flores,
Meritorious Autonomous University of Puebla, Mexico
Anthony E. Pickering,
University of Bristol, United Kingdom

***Correspondence:**
Mathieu Wolff
mathieu.wolff@u-bordeaux.fr
Shauna L. Parkes
shauna.parkes@u-bordeaux.fr

[†]*These authors have contributed equally to this work*

Received: *15 February 2019*
Accepted: *26 November 2019*
Published: *10 December 2019*

Citation:
Morceau S, Piquet R, Wolff M and Parkes SL (2019) Targeting Reciprocally Connected Brain Regions Through CAV-2 Mediated Interventions. Front. Mol. Neurosci. 12:303. doi: 10.3389/fnmol.2019.00303

INTRODUCTION

A fundamental challenge for systems neuroscience is to connect structure to function. This becomes more difficult when considering distributed neural circuits with complex connectivity. One particularly intriguing feature of many distributed neural circuits is the reciprocity of the connections between two of their key elements. Functionally, an influential account posits that this organization enables re-entry, a process whereby two or more brain regions concurrently stimulate and are stimulated by each other, thus supporting the synchronization of neural firing required for rapid neural integration (Edelman and Gally, 2013). This account assumes global functions for reciprocal pathways such as categorizing sensory inputs, manipulating mental constructs and generating motor commands (Edelman and Gally, 2013; Wolff and Vann, 2019) but does not address the directionality of the exchanges within such "re-entrant" pathways. The aim of this Brief Research Report is to highlight the versatility of a CAV2-mediated strategy

to target projection-defined neurons in reciprocally connected areas. We provide two such examples by using the CAV2-Cre vector and a Cre-dependent adeno-associated virus (AAV) carrying an inhibitory Designer Receptor Activated by Designer Drugs [DREADDs; hM4D(Gi); Armbruster et al., 2007] to target a thalamocortical circuit and the reciprocal connections between the gustatory portion of the insular cortex (IC) and the basolateral complex of the amygdala (BLA; Sripanidkulchai et al., 1984; McDonald, 1998; Yamamoto, 2006). Finally, we illustrate the known problem of Cre-independent transgene expression (e.g., Sjulson et al., 2016) at commonly used titrations to highlight the need for systematic control conditions in these types of interventions.

METHODS

We used an AAV carrying a floxed inhibitory DREADD receptor (hM4Di; Armbruster et al., 2007) and the retrograde CAV-2 vector (Junyent and Kremer, 2015) carrying the Cre recombinase to selectively express the inhibitory receptor in neurons based on their anatomical connectivity. First, we targeted the reciprocal connections between the mediodorsal thalamus (MD) and the dorsomedial prefrontal cortex (dmPFC), as shown in **Figures 1A,D**. Then, in a separate group of rats, we targeted the bidirectional pathways between the IC and the BLA, as shown in **Figures 2A,D**.

Animals and Housing Conditions

Twenty-four male Long Evans rats weighing 275 g to 300 g at surgery were obtained from Centre d'Elevage Janvier (France). Housing conditions were the same as previously described (Alcaraz et al., 2018; Parkes et al., 2018), in accordance with current laws and policies (French Council directive 2013-118, February 1, 2013 and European directive 2010-63, September 22, 2010). The experimental protocols received approval #5012053-A from the local Ethics Committee on December 7, 2012. Six rats were used to assess connections between the MD and the dmPFC (three for MD-to-dmPFC and three for dmPFC-to-MD connections) and six others to assess the insular-BLA circuit (three for IC-to-BLA and three for BLA-to-IC connections). Another set of 12 rats was used to generate the different control conditions (three for each titer conditions for single AAV injections and another three to test the IC-to-BLA projection with the most diluted AAV condition).

Surgery

Rats were anesthetized and prepared for stereotaxic surgery, as previously described (see Alcaraz et al., 2018; Parkes et al., 2018). For the thalamocortical circuit, CAV-2 and AAV were pressure injected (Picospritzer, General Valve Corporation, Fairfield, NJ, USA) into the brain through a glass micropipette (outside diameter: around 100 μm) and polyethylene tubing. In all cases, the needle was left in place 5 min after injection before slow retraction.

To target the MD-to-dmPFC pathway, 1 μl of 1×10^9 genomic copies/μl (gc/μl) of CAV2-Cre (Biocampus PVM, Montpellier, France) was injected bilaterally in the dmPFC at the following coordinates (in mm from Bregma): AP +3.2, ML ±0.6, DV −3.4 mm. In the same surgery session, 1 μl of 1×10^9 gc/μl of AAV8-hSyn-DIO-hM4Di-mCherry (UNC Vector Core, Chapel Hill, NC, USA) was injected bilaterally in MD at the following coordinates: AP −2.6, ML ±0.7 and DV −5.6. To target the dmPFC-to-MD pathway in a separate group of rats, virus injections were reversed, i.e., CAV-2 in the MD and AAV in the dmPFC. All injection parameters were the same, except for the mediolateral coordinates of AAV injection in the dmPFC, which were set at ±0.8 mm, to preferentially target cortical layers V and VI that project to the MD.

For the temporocortical circuit, CAV2 and AAV were microinjected (UMP3-1 and Micro4 Controller, World Precision Instruments) *via* a 10 μl NanoFil syringe with a blunt, 33 G needle. To target the BLA-to-IC pathway (**Figure 2A**), 0.25 μl of 1.21×10^{12} gc/μl of AAV8-hSyn-DIO-hM4Di-mCherry (Addgene plasmid, Viral Vector Production Unit, Universitat Autonoma de Barcelona, Spain) was injected bilaterally in BLA at two sites (in mm from Bregma): AP −2.0, ML ±4.6, DV −8.7 and AP −3.0, ML ±5.0, DV −8.7. In the same surgery session, 1 μl of 1×10^9 gc/μl of CAV2-Cre (Biocampus PVM, Montpellier, France) was injected bilaterally at two sites in IC (in mm from Bregma): AP +0.7, ML ±5.5, DV −7.4 and AP +1.7, ML ±5.0, DV −7.0. To target the IC-to-BLA pathway, virus injections were reversed, i.e., CAV-2 in BLA and AAV in IC (**Figure 2B**).

To determine the extent of Cre-independent viral expression, we also injected AAV8-hSyn-DIO-hM4Di-mCherry (Addgene, Cambridge, MA, USA) alone at three titrations in another set of rats. The IC-to-BLA pathway was selected for this control condition. We therefore injected 1 μl of 1.21×10^{12} gc/μl, 4.8×10^{11} gc/μl or 4.8×10^{10} gc/μl at two sites in the IC. We then tested whether the weakest AAV titration (4.8×10^{10} gc/μl) was still effective in promoting Cre-dependent expression by injecting the AAV8 in the IC and the CAV2-Cre in the BLA (0.25 μl of 1.21×10^{10} gc/μl injected at two sites).

Histology

For optimal viral expression, rats were perfused transcardially >1 month after surgery with 4% paraformaldehyde in 0.1 M phosphate buffer (PFA). Brains were kept in the same PFA solution overnight then, 40 μm sections were cut using a vibratome. Immunochemistry [fluorescent and non-fluorescent (DAB)] was performed to enhance mCherry staining. The fluorescent staining protocol is described in detail in Alcaraz et al., 2018. Briefly, sections were rinsed in 0.1 M phosphate-buffered saline (PBS), incubated in a blocking solution for 1 h, and then incubated with rabbit anti-RFP primary antibody (1:200 in blocking solution, Clinisciences, PM005) at 4°C for 48 h. The sections were then rinsed in PBS and placed in a bath containing goat anti-rabbit coupled to DyLight® 549 (1:200 in PBS, 2 h; Jackson ImmunoResearch, 111-025-003). Following rinses in PBS, sections were incubated in Hoechst solution for neuronal counterstaining (1:5,000 in PBS, 15 min, bisBenzimide H 33258, Sigma, B2883). Finally, sections were rinsed, mounted onto gelatin-coated slides and coverslipped with the anti-fading reagent Fluoromount® G (SouthernBiotech, 0100-01).

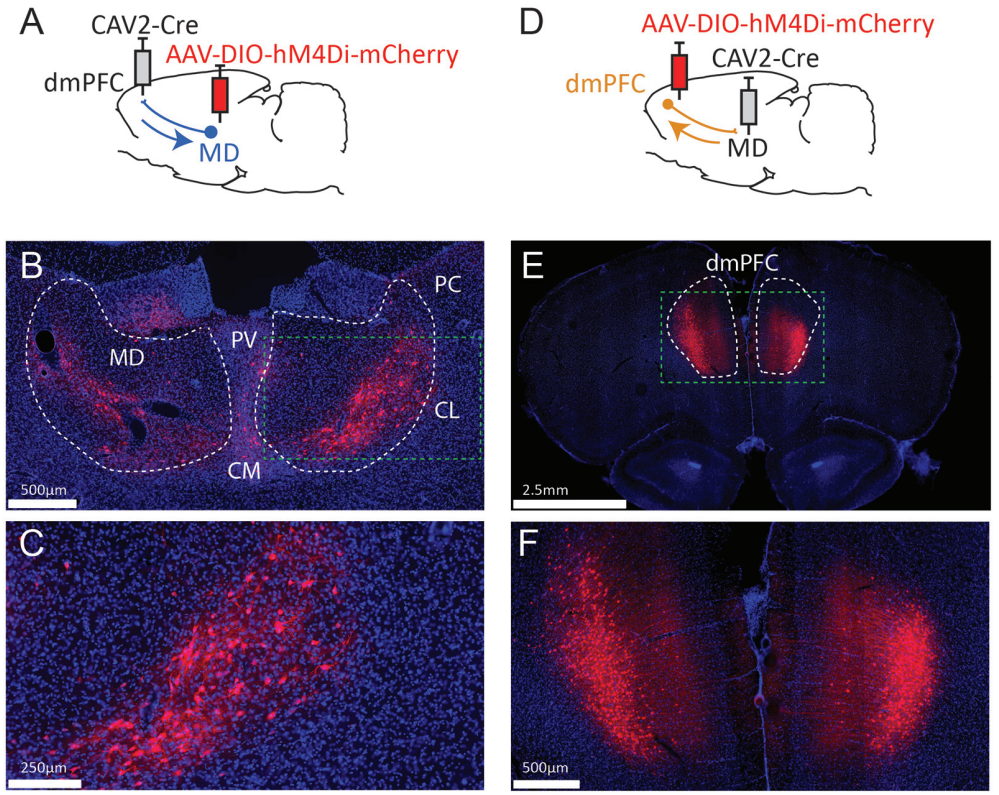

FIGURE 1 | Strategy to target projection-defined thalamic **(A)** or cortical **(D)** neurons. The resulting labeling appears consistent with the currently known connectivity both in the MD **(B,C)** and the dmPFC **(E,F)**. The green dotted lines in **(B,E)** correspond to the areas magnified in **(C,F)**, respectively. PV, paraventricular nucleus; CM, centromedial nucleus; PC, paracentral nucleus; CL, centrolateral nucleus; MD, mediodorsal thalamus; dmPFC, dorsomedial prefrontal cortex (A32d). Images were captured using a Nanozoomer slide scanner (Hamamatsu Photonics) and the NDP.view 2.0® freeware (Hamamatsu Photonics).

For non-fluorescent staining, floating sections were prepared by rinsing in 0.1 M PBS with 0.3% Triton X-100 (PBST; 5 × 5 min), and then in 0.5% H_2O_2 in 0.1 M PBST for 30 min. Following further rinsing in PBST, sections were incubated with rabbit anti-RFP (1:1,000 in PBST, Clinisciences, PM005) for 24 h at room temperature (RT). Then, the secondary antibody was applied (goat anti-rabbit biotinylated antibody, 1:1,000 in PBST containing 1% goat serum) and sections were incubated for 2 h at RT. Slices were then rinsed in PBST, incubated in avidine-biotinylated complex kit for 2 h at RT, rinsed in PBST and 0.05 M Tris buffer. Staining was revealed using 3,3′-Diaminobenzidine (DAB) solution (10 mg DAB + 50 ml 0.05 M Tris + 20 µl 30% H_2O_2) for 10 min. Finally, sections were rinsed, mounted and coverslipped with Eukitt (Sigma–Aldrich, St. Louis, MO, USA).

RESULTS

Connections Between the Medial Prefrontal Cortex and the Mediodorsal Thalamus

To target dmPFC-projecting MD cells, we injected an AAV carrying a floxed hM4Di receptor expression cassette in the MD and the retrograde CAV2-Cre in the dmPFC (**Figure 1A**). As a result, only thalamic cells projecting to the dmPFC should be infected by both vectors and therefore express mCherry and hM4Di. As shown in **Figures 1B,C**, the actual observations were consistent with this expectation as mCherry expression was more evident in the lateral portion of the MD, in agreement with our current knowledge of these thalamocortical projections (Groenewegen, 1988; Alcaraz et al., 2016). mCherry expression was also visible to some degree in adjacent dmPFC-projecting thalamic areas such as the intralaminar group (paracentral and centro-lateral nuclei, mostly) and, to some extent, the centro-medial and the paraventricular nuclei. In some cases, fluorescence was also observed in the habenula. Next, injection sites for the viral construct were reversed in a distinct set of rats (**Figure 1D**). This manipulation produced heavy labeling in deep layers of the dmPFC (**Figures 1E,F**). Importantly, this observation is consistent with the existence of abundant corticothalamic projections targeting the MD from cortical layers 5/6 (Gabbott et al., 2005).

Connections Between the Insular and the Basolateral Complex of the Amygdala

To target IC-projecting neurons in BLA, we injected the AAV carrying a floxed hM4Di receptor expression cassette in BLA

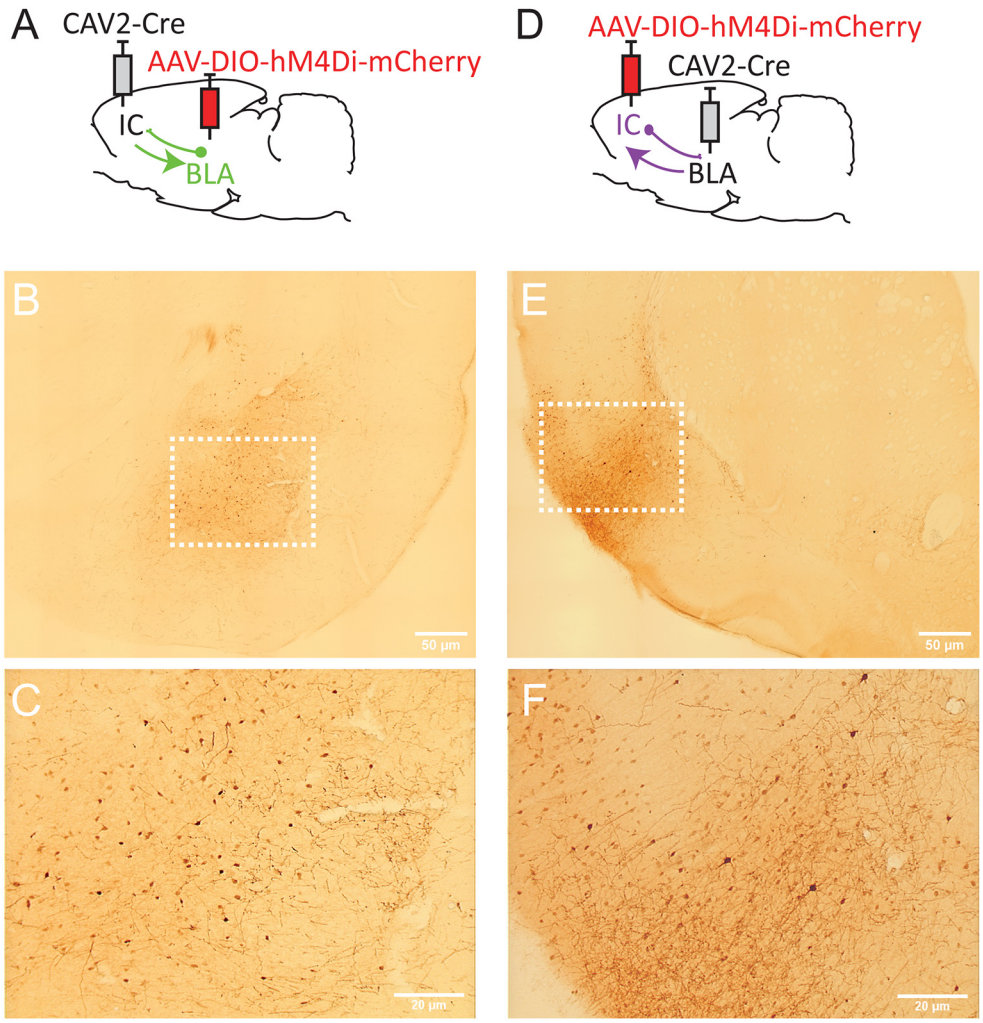

FIGURE 2 | Strategy to target projection-defined amygdala **(A)** or insular cortex (IC; **D**) neurons. mCherry labeling in the basolateral complex of the amygdala (BLA; **B,C**, Bregma −2.76 mm) and the IC (**E,F**; Bregma +1.92 mm). The white dotted lines in **(B,E)** correspond to the areas magnified in **(C,F)**, respectively. Images were captured using a Leitz laborlux S microscope (10× objective) equipped with a Nikon 3CCD color camera.

and the retrograde CAV2-Cre in IC (**Figure 2A**). Therefore, only amygdala cells projecting to the IC should be infected by both vectors and, thus, express mCherry and hM4Di. As shown in **Figures 2B,C**, we observed mCherry expression in the BLA and this expression was detected throughout the anteroposterior axis of the amygdala (between Bregma −2.04 and −3.48). Consistent with previous retrograde tracing studies (Sripanidkulchai et al., 1984), mCherry expression appeared to be greater in the basolateral (BL) and basomedial (BM) regions with less staining observed in the lateral amygdala however this was not formally quantified.

In a distinct group of rats, we reversed the location of the virus injections to study BLA-projecting neurons in the IC (**Figure 2D**). As shown in **Figures 2E,F**, we observed mCherry expression in most areas of IC, including agranular (dorsal and ventral) and dysgranular but little labeling in granular IC. We also observed some expression in the adjacent primary somatosensory cortex. mCherry expression was detected throughout the "gustatory IC" from Bregma +2.28 mm to 0.00 mm. This result is largely consistent with previous neuroanatomical tracing studies describing the connections from gustatory IC to the amygdala (see McDonald, 1998; Shi and Cassell, 1998).

Cre-Independent Expression Using AAV8-hSyn-DIO-hM4Di-mCherry

To provide an estimation of the Cre-independent expression that can be observed using this AAV, three rats received an injection of AAV only in the IC at 1.21×10^{12} gc/µl (**Figure 3A**), 4.8×10^{11} gc/µl (**Figure 3B**) or 4.8×10^{10} gc/µl (**Figure 3C**). We also injected three rats with the weakest AAV dilution (4.8×10^{10} gc/µl) in the IC and the CAV2-Cre in the BLA (**Figure 3D**) to ensure that labeling of BLA-projecting IC neurons could still be obtained with

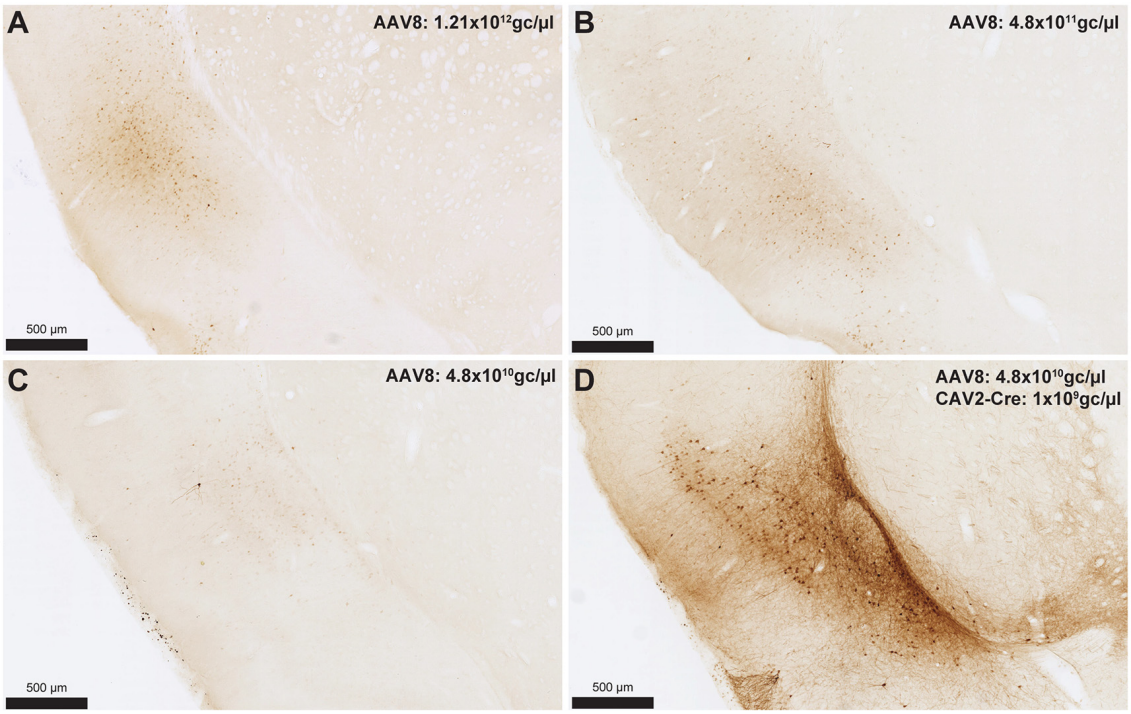

FIGURE 3 | Cre-independent expression across decreasing titers **(A–C)**. AAV8-hSyn-DIO-hM4Di-mCherry was injected at three different titers: 1.21×10^{12} gc/µl (**A**; same titer as used in **Figure 2**), 4.8×10^{11} gc/µl **(B)** or 4.8×10^{10} gc/µl **(C)**. The expression of mCherry in the presence of Cre is shown in **(D)** using the weakest adeno-associated virus (AAV) titer (i.e., titer used in **C**). Images were captured using a Nanozoomer slide scanner (Hamamatsu Photonics) and the NDP.view 2.0® freeware (Hamamatsu Photonics).

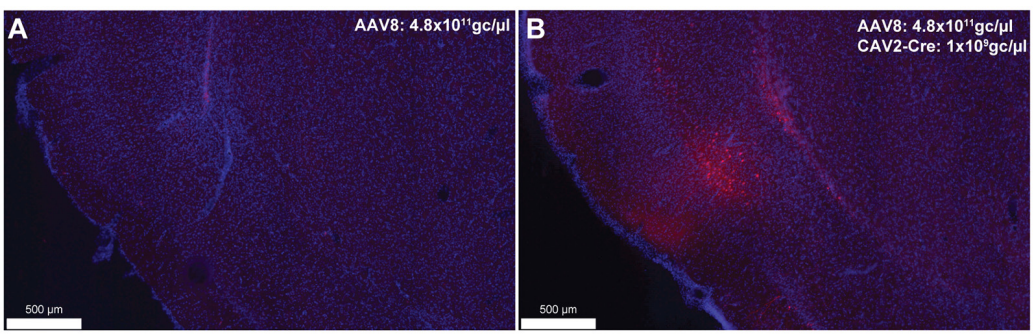

FIGURE 4 | Cre-independent **(A)** and Cre-dependent **(B)** expression using the same titer as **Figure 3B** (AAV8-hSyn-DIO-hM4Di-mCherry at 4.8×10^{11} gc/µl). The inspection of these figures demonstrates that the extent of Cre-independent expression can be underestimated in fluorescence. Images were captured using a Nanozoomer slide scanner (Hamamatsu Photonics) and the NDP.view 2.0® freeware (Hamamatsu Photonics).

a titer that minimized non-specific staining. As shown in **Figures 3A–C**, Cre-independent labeling was observed at all three titers. While this expression was not quantified, the amount of labeling seemed to decrease with the titer. It appears that at 4.8×10^{10} gc/µl minimal Cre-independent expression was observed (**Figure 3C**), while considerable Cre-dependent expression was preserved (**Figure 3D**). Finally, even at a titer where considerable leakage was observed in DAB amplification (4.8×10^{11} gc/µl; **Figure 3B**), immunofluorescence appeared insufficiently sensitive to reveal the Cre-independent expression (**Figure 4**), suggesting that this issue may be overlooked in similar studies that rely only on fluorescence.

DISCUSSION

Collectively, these data illustrate the use of the CAV2 vector to target neurons based on their anatomical connectivity in reciprocal thalamocortical and temporocortical pathways. In

both circuits, the labeling of projection-defined neurons was found to closely match the currently known architecture of these connections. For instance, in the MD, most labeled cells occupied the lateral segment of the structure, consistent with the fact that it is the most lateral portion of that structure that projects to the dmPFC (Groenewegen, 1988; Alcaraz et al., 2016). In the dmPFC, all labeled cells appeared to be in deep layers, again in agreement that deep but not superficial cortical layers project back to the MD (Gabbott et al., 2005). Similarly, in the gustatory IC, the majority of staining was found in dysgranular and agranular areas with little staining in the granular region, as previously described (Shi and Cassell, 1998). It should be noted that we also observed extensive labeling of fibers in the central nucleus of the amygdala, which again aligns with previous studies (Shi and Cassell, 1998). As expected, in the BLA-to-IC pathway, neuronal staining was detected throughout the anteroposterior axis and there appeared to be more labeled neurons in the basolateral nucleus than in the lateral nucleus (Sripanidkulchai et al., 1984), although this observation was not quantified.

Off-target transgene expression or "leakage" has been observed for a variety of genetically coded neuroscience tools (for a review see Sjulson et al., 2016). Here, we illustrated this limitation in AAVs carrying DREADDs and the fluorescent protein, mCherry. As expected, this Cre-independent expression appeared to reduce with weaker virus titers (**Figure 3**). Such leakage may be an issue that is specific to AAVs as Cerpa et al report in this Research Topic that no such leakage is observed when using the novel CAV2-DIO-DREADD vector in wild-type rats at a similar titration and volume. It should also be noted that the CAV2-Cre vector can infect axons of passage, which may potentially lead to Cre expression in regions that do not project to the site of injection (Schwarz et al., 2015). If an AAV is injected in areas from which such axons arise, neurons that do not connect to the site of injections of the CAV2-Cre vector may express the gene carried by the AAV. Finally, as previously reported (Sjulson et al., 2016), we observed that relying on fluorescence may underestimate the extent of both specific and Cre-independent expression. Indeed, a more sensitive method (such as DAB amplification) may be required to fully appreciate the extent of the leakage. These observations highlight the need for careful selection of the optimal AAV dosage and the importance of explicitly acknowledging and illustrating transgene leakage, using sufficiently sensitive detection methods.

Finally, the interventions described here in the thalamocortical circuit have been previously found to produce a specific impairment in an adaptive decision-making task, showing that thalamocortical and corticothalamic pathways support complementary but dissociable aspects of decision processes (Alcaraz et al., 2018). Thus, using CAV2 to target projection-defined neurons enabled us to identify the directionality of the functional exchanges within neural circuits as an important feature. However, as the vector is known to rely on the presence of its CAR receptor for initial infection (Bru et al., 2010; Zussy et al., 2016), detailing the expression of this receptor at brain-wide levels and in various species would be useful to predict its efficacy in other brain regions and pathways.

DATA AVAILABILITY STATEMENT

The datasets generated for this study are available on request to the corresponding authors.

ETHICS STATEMENT

Experiments were conducted in accordance with current laws and policies (French Council directive 2013-118, February 1, 2013 and European directive 2010-63, September 22, 2010). The experimental protocols received approval #5012053-A from the local Ethics Committee on December 7, 2012.

AUTHOR CONTRIBUTIONS

SM, RP, MW, and SP collected and analyzed the data. MW and SP wrote the manuscript. SM, RP, MW, and SP revised the manuscript and approved the final version.

FUNDING

This work was supported by a National Alliance for Research on Schizophrenia and Depression (NARSAD; Grant No. 27402) Young Investigator grant (Brain and Behavior Research Foundation) and a grant from the French agency for research (Agence Nationale de la Recherche) ANR-19-CE37-0004-07 awarded to SP and a NARSAD Independent Investigator grant (Brain and Behavior Research Foundation; Grant No. 26583) awarded to MW.

ACKNOWLEDGMENTS

The microscopy was performed, in part, at the Bordeaux Imaging Center (BIC), a service unit of the CNRS-INSERM and Bordeaux University and a member of the national infrastructure France BioImaging. The help of Jeremie Teillon (BIC) and Gilles Courtand (CNRS, INCIA) is acknowledged. We also acknowledge E. J. Kremer for generously donating the canine adenovirus type 2 (CAV-2) vector for these experiments.

REFERENCES

Alcaraz, F., Fresno, V., Marchand, A. R., Kremer, E. J., Coutureau, E., and Wolff, M. (2018). Thalamocortical and corticothalamic pathways differentially contribute to goal-directed behaviors in the rat. *Elife* 7:e32517. doi: 10.7554/eLife.32517

Alcaraz, F., Marchand, A. R., Courtand, G., Coutureau, E., and Wolff, M. (2016). Parallel inputs from the mediodorsal thalamus to the prefrontal cortex in the rat. *Eur. J. Neurosci.* 44, 1972–1986. doi: 10.1111/ejn.13316

Armbruster, B. N., Li, X., Pausch, M. H., Herlitze, S., and Roth, B. L. (2007). Evolving the lock to fit the key to create a family of G protein-coupled

receptors potently activated by an inert ligand. *Proc. Natl. Acad. Sci. U S A* 104, 5163–5168. doi: 10.1073/pnas.0700293104

Bru, T., Salinas, S., and Kremer, E. J. (2010). An update on canine adenovirus type 2 and its vectors. *Viruses* 2, 2134–2153. doi: 10.3390/v2092134

Edelman, G. M., and Gally, J. A. (2013). Reentry: a key mechanism for integration of brain function. *Front. Integr. Neurosci.* 7:63. doi: 10.3389/fnint.2013.00063

Gabbott, P. L., Warner, T. A., Jays, P. R., Salway, P., and Busby, S. J. (2005). Prefrontal cortex in the rat: projections to subcortical autonomic, motor and limbic centers. *J. Comp. Neurol.* 492, 145–177. doi: 10.1002/cne.20738

Groenewegen, H. J. (1988). Organization of the afferent connections of the mediodorsal thalamic nucleus in the rat, related to the mediodorsal-prefrontal topography. *Neuroscience* 24, 379–431. doi: 10.1016/0306-4522(88)90339-9

Junyent, F., and Kremer, E. J. (2015). CAV-2-why a canine virus is a neurobiologist's best friend. *Curr. Opin. Pharmacol.* 24, 86–93. doi: 10.1016/j.coph.2015.08.004

McDonald, A. J. (1998). Cortical pathways to the mammalian amygdala. *Prog. Neurobiol.* 55, 257–332. doi: 10.1016/s0301-0082(98)00003-3

Parkes, S. L., Ravassard, P. M., Cerpa, J. C., Wolff, M., Ferreira, G., and Coutureau, E. (2018). Insular and ventrolateral orbitofrontal cortices differentially contribute to goal-directed behavior in rodents. *Cereb. Cortex* 28, 2313–2325. doi: 10.1093/cercor/bhx132

Schwarz, L. A., Miyamichi, K., Gao, X. J., Beier, K. T., Weissbourd, B., Deloach, K. E., et al. (2015). Viral-genetic tracing of the input-output organization of a central noradrenaline circuit. *Nature* 524, 88–92. doi: 10.1038/nature14600

Shi, C. J., and Cassell, M. D. (1998). Cortical, thalamic and amygdaloid connections of the anterior and posterior insular cortices. *J. Comp. Neurol.* 399, 440–468. doi: 10.1002/(sici)1096-9861(19981005)399:4<440::aid-cne2>3.0.co;2-1

Sjulson, L., Cassataro, D., Dasgupta, S., and Miesenbock, G. (2016). Cell-specific targeting of genetically encoded tools for neuroscience. *Annu. Rev. Genet.* 50, 571–594. doi: 10.1146/annurev-genet-120215-035011

Sripanidkulchai, K., Sripanidkulchai, B., and Wyss, J. M. (1984). The cortical projection of the basolateral amygdaloid nucleus in the rat: a retrograde fluorescent dye study. *J. Comp. Neurol.* 229, 419–431. doi: 10.1002/cne.902290310

Wolff, M., and Vann, S. D. (2019). The cognitive thalamus as a gateway to mental representations. *J. Neurosci.* 39, 3–14. doi: 10.1523/jneurosci.0479-18.2018

Yamamoto, T. (2006). Neural substrates for the processing of cognitive and affective aspects of taste in the brain. *Arch. Histol. Cytol.* 69, 243–255. doi: 10.1679/aohc.69.243

Zussy, C., Loustalot, F., Junyent, F., Gardoni, F., Bories, C., Valero, J., et al. (2016). Coxsackievirus adenovirus receptor loss impairs adult neurogenesis, synapse content and hippocampus plasticity. *J. Neurosci.* 36, 9558–9571. doi: 10.1523/jneurosci.0132-16.2016

Conflict of Interest: The authors declare that the research was conducted in the absence of any commercial or financial relationships that could be construed as a potential conflict of interest.

frontiers in Molecular Neuroscience

MINI REVIEW
published: 27 February 2020
doi: 10.3389/fnmol.2020.00009

Canine Adenovirus 2: A Natural Choice for Brain Circuit Dissection

Andréanne Lavoie[1,2] *and Bao-hua Liu*[1,2]*

[1] Department of Biology, University of Toronto Mississauga, Mississauga, ON, Canada, [2] Department of Cell and Systems Biology, University of Toronto, Toronto, ON, Canada

Canine adenovirus-2 (CAV) is a canine pathogen that has been used in a variety of applications, from vaccines against more infectious strains of CAV to treatments for neurological disorders. With recent engineering, CAV has become a natural choice for neuroscientists dissecting the connectivity and function of brain circuits. Specifically, as a reliable genetic vector with minimal immunogenic and cytotoxic reactivity, CAV has been used for the retrograde transduction of various types of projection neurons. Consequently, CAV is particularly useful when studying the anatomy and functions of long-range projections. Moreover, combining CAV with conditional expression and transsynaptic tracing results in the ability to study circuits with cell- and/or projection-type specificity. Lastly, with the well-documented knowledge of viral transduction, new innovations have been developed to increase the transduction efficiency of CAV and circumvent its tropism, expanding the potential of CAV for circuit analysis.

Keywords: canine adenovirus 2, neural circuit, retrograde, circuit tracing, circuit function, cell type specificity, projection specificity

OPEN ACCESS

Edited by:
Mathieu Wolff,
Centre National de la Recherche Scientifique (CNRS), France

Reviewed by:
Sebastien Parnaudeau,
INSERM U1130 Neurosciences Paris Seine, France
Shauna L. Parkes,
Centre National de la Recherche Scientifique (CNRS), France

***Correspondence:**
Bao-hua Liu
baohua.liu@utoronto.ca

Received: *30 October 2019*
Accepted: *14 January 2020*
Published: *27 February 2020*

Citation:
Lavoie A and Liu B (2020) Canine Adenovirus 2: A Natural Choice for Brain Circuit Dissection. Front. Mol. Neurosci. 13:9. doi: 10.3389/fnmol.2020.00009

INTRODUCTION

Canine adenovirus-2 (CAV) is a non-human pathogen that causes a mild infectious respiratory disease in dogs known as "kennel cough." CAV was initially studied to develop a vaccine against canine adenoviruses-1, the cause of a severe liver disease in dogs, and proposed as a long-term gene therapy vector for neurological disorders (Kremer et al., 2000; Chillon and Kremer, 2001; Soudais et al., 2001). Since then, CAV has also attracted neuroscientists because of several advantageous properties for studying the anatomy and function of neural circuits (Junyent and Kremer, 2015; del Rio et al., 2019). Specifically, it is primarily the retrograde ability of CAV to deliver cargo genes via axon terminals that allow the investigation of the pattern and function of long-range projections

Abbreviations: ACC, anterior cingulate cortex; ACtx, auditory cortex; Amy, amygdala; Ath, auditory thalamus; BLA, basolateral amygdala; BPN, basal pontine nucleus; Cb, cerebellum; CeA, central amygdala; CLA, claustrum; CoA, cortical amygdaloid nucleus; Contra., contralateral; DBB, diagonal band of brocca; DCN, deep cerebellar nuclei; DG, dentate gyrus; DMH, dorsomedial hypothalamus; DRN, dorsal raphe nucleus; EC, entorhinal cortex; GC, gustatory cortex; HPC, hippocampus; IC, inferior colliculus; IO, inferior olive; LC, locus coeruleus; LH, lateral hypothalamus; LHb, lateral habenula; LS, lateral septum; LTDg, laterodorsal tegmentum; M1, primary motor cortex; MC, motor cortex; MdD, reticular formation; MDT, medial dorsal thalamus; Me, medulla; mPFC, medial prefrontal cortex; mPOA, medial preoptic area; NAc, nucleus accumbens; NG, nodose ganglia; NOT/DTN, complex of nucleus of optic tract and dorsal terminal nucleus; NRTP, nucleus reticularis tegmenti pontis; NTS, nucleus tractus solitaries; OB, olfactory bulb; OFC, orbitofrontal cortex; ORBvl, ventrolateral orbital cortex; PAG, periaqueductal gray; PBNl, lateral parabrachial nucleus; PCRt, parvocellular reticular formation; PFC, prefrontal cortex; PLC, prelimbic cortex; POm, posterior medial thalamic nucleus; preBötC, preBötzinger complex; PVN, hypothalamic paraventricular; PVT, paraventricular thalamus; RE, thalamic nucleus reuniens; RSP, retrosplenial cortex; SC, superior colliculus; SNc, substantia nigra pars compacta; SON, supraoptic nuclei; STN, subthalamic nucleus; TMN, tuberomammillary nucleus; VC, visual cortex; vMT, ventral midline thalamus; VTA, ventral tegmental area.

(Junyent and Kremer, 2015). In addition, CAV is useful for studying neural circuits because it has a high neuronal specificity and a strong compatibility with conditional gene expression (Kremer et al., 2000; Soudais et al., 2001; Junyent and Kremer, 2015). Furthermore, CAV is a reliable vector for long-term functional studies, since it mediates stable, lasting gene expression while sustaining low immunogenicity and cytotoxicity levels (Kremer et al., 2000; Chillon and Kremer, 2001; Soudais et al., 2001). This mini-review will summarize the properties that give CAV its edge, highlighting their utility in dissecting the connectivity and functions of neural circuits.

BENEFICIAL PROPERTIES OF CAV FOR CIRCUIT ANALYSIS

Canine adenovirus-2 viruses have been widely utilized in neuroscience due to their capability of infecting axon terminals via a retrograde mechanism and then driving gene expression at the somata. Owing to this retrograde capability, when injected into a brain region, CAV viruses transduce projection neurons which innervate the injection site, in addition to neurons at the injection site (Kremer et al., 2000; Chillon and Kremer, 2001; Soudais et al., 2001; Bru et al., 2010). CAV's retrograde capability relies on the coxsackievirus and adenovirus receptor (CAR) (Kremer et al., 2000; Chillon and Kremer, 2001; Soudais et al., 2001). CAR is a cell adhesion molecule necessary for the docking, internalization, endocytosis, and axonal transport of CAV viruses (Salinas et al., 2009). This receptor is highly enriched at presynaptic sites of neurons, but exists in low density in the somata and dendrites of neurons (Zussy et al., 2016). This domain-specific CAR expression gives rise to the retrograde transport of CAV, making it a powerful tool for mapping long-range connectivity between brain regions (Junyent and Kremer, 2015).

Another advantage of CAV for neuroscientists is that CAV vectors exhibit strong tropism, biasing neurons. For example, in the peripheral nervous system, CAV viruses preferentially transduced olfactory sensory neurons instead of the columnar epithelial cells (Bru et al., 2010). Moreover, when injected in the central nervous system, CAV strongly infects neurons but not non-neuronal types (Soudais et al., 2001; Bru et al., 2010). The molecular basis for this neuronal tropism is that CAR expression in the brain is primarily, if not exclusively, on neurons but not on astrocytes, oligodendrocytes, endothelium, or meningeal cells (Soudais et al., 2001; Persson et al., 2006). So far, in the central nervous system, CAV vectors have been successfully used to transduce various types of neurons in broad regions of the brain, demonstrating their wide applicability for studying neural circuits (**Table 1**). For example, CAV can transduce a variety of neurotransmitter systems, including, but not limited to, glutamatergic, dopaminergic, GABAergic, noradrenergic, oxytonergic, serotonergic, and cholinergic systems (**Table 1**). Furthermore, CAV has been successfully used in a broad diversity of cortical and subcortical projection pathways (**Table 1**). Even though rodents were used as the animal models in most of CAV applications in **Table 1**, recently, CAV was also successfully used in non-human primates (**Table 1**; Mestre-Francés et al., 2018; Bohlen et al., 2019; Dopeso-Reyes et al., 2019). These studies validate the applicability of CAV as a gene delivery tool in non-human primates, facilitating the investigation of neural circuits in a more human-relevant model.

Among a number of retrograde viruses (for example, rabies, lentivirus, and rAAV2-retro), what makes CAV viruses unique is their carrying capacity and physical size. In fact, CAV is the second largest retrograde virus with a 30–36 kb cloning capacity and ∼90 nm diameter, leading over rabies (1–3 kb) and lentivirus (9 kb) by 10- and 3-fold, respectively (Thompson and Towne, 2018). The large carrying load of CAV allows flexible, diverse, and creative design of cargo genes, which is particularly useful when dissecting neural circuits. For example, one can combine a variety of genes such as optogenetic tools, genetically encoded indicators of neuronal activity, fluorophores, large promoters, recombinases, LoxP/Flp sequences, and so on in one CAV vector (**Figure 1A**). Such combinations allow one to selectively label neurons according to cell type and/or projection, and they also facilitate efforts to monitor and perturb neural activity simultaneously (Soudais et al., 2004; Junyent and Kremer, 2015). Moreover, the large physical size of CAV provides advantages for neuroscientists performing stereotactic injections into small nuclei. CAV viruses (∼90 nm in diameter) remain near the injection site compared to smaller adeno-associated viruses (AAV) (22 nm in diameter). For instance, 0.25–0.5 μl of CAV spread on average by 200 μm from the center of the injection site, while 0.25 μl of rAAV2-retro spread four times more (Schwarz et al., 2015; Tervo et al., 2016). This restricted diffusion of CAV is useful when studying small structures, such as the complex of the nucleus of the optic tract and the dorsal terminal nucleus (NOT/DTN) (Liu et al., 2016), PAG (de Git et al., 2018) or CLA (Crick and Koch, 2005). It is worth noting that CAV cannot be injected with iontophoresis, which is commonly used to confine the spread of electrically charged AAV viruses (Gerhardt and Palmer, 1987), because the coat proteins of CAV are almost electrically neutral (10 times less charged than AAV viruses) (Karlin and Brendel, 1988; Chillon and Kremer, 2001).

For CAV to be an effective gene delivery tool, it should provide lasting, stable gene transduction. Indeed, to determine its viability for long-term experiments, Soudais et al. (2004) injected a CAV vector carrying green fluorescent protein (GFP) gene into multiple sites of the striatum in rats and indeed observed a high level of green fluorescent protein expression lasting for more than a year. In addition to rodents, CAV transduction led to a stable long-term transgene expression in a human stem-cell-derived 3D neural *in vitro* model (Simão et al., 2016), demonstrating its promise for functional experiments. Moreover, an ideal gene delivery vector should also avoid host immune responses and cytotoxicity. Indeed, CAV viruses are not human pathogens and do not induce significant cellular infiltration in rat brains (Soudais et al., 2004), nor in rhesus monkeys, unless abnormally high titers are used (Bohlen et al., 2019). Even a pre-existing immunity against human adenoviruses does not significantly affect CAV transduction (Klonjkowski et al., 1997; Kremer et al., 2000; Ibanes and Kremer, 2013). To further minimize the possible disruptions to normal neural processes caused by

TABLE 1 | Summary of cell types and circuit pathways where CAV had been used for circuit analysis.

System	Circuit	Effector	References
Cholinergic	DBB → arcuate nucleus	tdTomato	Herman et al., 2016
	LDTg → VTA	hM3D(Gq)-mCherry	Fernandez et al., 2018
	nuclei of Meynert → striatum	GFP	Soudais et al., 2004
Dopaminergic	SNc → striatum	GFP	Soudais et al., 2004
		TH	Sotak et al., 2005
			Robinson et al., 2007
		RG, TVA-mCherry, GFP, tdTomato, mGFP, SYP-mRuby, GCaMP6f	Lerner et al., 2015
	VTA → NAc	ArchT-GFP	Luo et al., 2018
		hM3D(Gq)-mCherry,	Boender et al., 2014
		hM3D(Gq)-mCherry,	Kakava-Georgiadou et al., 2019
		GFP, NBL10	Ekstrand et al., 2014
		eYFP	Reynolds et al., 2018
	VTA → (NAc, mPFC, Amy)	GFP	Beier et al., 2015
	(VTA, SNc) → Striatum	TH	Hnasko et al., 2006
	VTA → (NAc, BLA)		Fadok et al., 2010
	Midbrain human organoid	GFP	Brito et al., 2012
			Simão et al., 2016;
GABAergic	POA → (TMN, PFC)	GFP, RG,TVA-mCherry, mGFP, SYP-mRuby	Chung et al., 2017
	mPOA → (PAG, PVN, Amy, VTA)	ZsGreen, mCherry, myrGFP, RG, TVA-mCherry	Kohl et al., 2018
	CeA → (PCRt, PAG)	ChR2-mCherry, GFP	Han et al., 2017
	CeA→ PAG	RG, ArchT-GFP	Xu et al., 2016
	Cervical → lumbar	tdTomato, DTR, SynTag	Ruder et al., 2016
Glutamatergic	PLC → (NAc, Amy)	GCaMP6f, GFPL10	Murugan et al., 2017
	PLC → PVT	hM3D(Gq)-mCherry, hM4D(Gi)-mCherry	Campus et al., 2019
	GC → BLA	tdTomato	Lavi et al., 2018
	(HPC, mPFC) → LS	GFP, hM3D(Gq)-mCherry, hM4D(Gi)-mCherry	Parfitt et al., 2017
	Cervical → lumbar	tdTomato, DTR, SynTag	Ruder et al., 2016
	mPFC → PAG	ChR2-YFP	Vander Weele et al., 2018
	mPFC → NAc	hM3D(Gq)-mCherry, ChR2-eYFP	Augur et al., 2016
	mPFC → RE	hM4D(Gi)-mCherry	Ramanathan et al., 2018
	mPFC → MDT; MDT→ mPFC	hM4D(Gi)-mCherry	Alcaraz et al., 2018
	(contra. mPFC, MDT, HPC) → mPFC	hM3D(Gq)-mCherry, tdTomato	Miller et al., 2017
	PFC → (NAc, PVT)	GCaMP6; eYFP, ChR2-eYFP, eNpHR-eYFP	Otis et al., 2017
	ACC → HPC	eNpHR, eYFP	Rajasethupathy et al., 2015
	(ORBvl, VC, RSP, contra. ACC) → ACC	tdTomato	Chatterjee et al., 2018
	OFC → striatum	ChR2-eYFP	Hirokawa et al., 2019
	VC → NOT/DTN	tdTomato, DTR-GFP	Liu et al., 2016
	VC → SC	tdTomato	Zingg et al., 2017
	ACtx → IC	GCaMP6s	Asokan et al., 2018
		ChR2-mCherrry	Williamson and Polley, 2019
	(ACtx, Ath) → striatum	tdTomato, ChR2	Ponvert and Jaramillo, 2019
	MC → (contra. MC, Me) (OB, HPC, ACtx, Me) → LC	RG, GFP, TVA-mCherry	Schwarz et al., 2015
	MC → (Spinal cord, Contra. MC)	GCaMP6s, tdTomato	Kim et al., 2017
	EC → DG	ChR2-YFP, tdTomato	Leroy et al., 2017
	Periform cortex → (OB, CoA)	ChR2-YFP	Diodato et al., 2016
	Multiple cortices → BPN	eGFP	Tervo et al., 2016
	PBNl → (CeA, MdD)	hM4D(Gi)-mCherry	Carter et al., 2013
		hM4D(Gi)-mCherry, mCherry	Alhadeff et al., 2017
		hM3D(Gq), PLAP	Barik et al., 2018

(Continued)

TABLE 1 | Continued

System	Circuit	Effector	References
	vMT → (BLA, mPFC, NAc)	hM3D(Gq)-mCherry	Salay et al., 2018
	BLA → mPFC	tdTomato	Vogel et al., 2016
		ChR2-eNpHR-venus	Senn et al., 2014
		ChR2-mRubby, DsRed, GFP	Li et al., 2018
	BLA → (NAc, CeA, HPC)	ChR2-eYPF	Beyeler et al., 2016, 2018
		eNpHR-eYFP, eYFP	Namburi et al., 2015
	(Multiple cortices, SNc, basal nuclei of Meynert, Thalamic nuclei) → Striatum	GFP, LRRK2	Mestre-Francés et al., 2018*
	(DCN, IO, VN, NRTP, etc.) → Cb	GFP	Dopeso-Reyes et al., 2019*
	Pontine nuclei → vermis lobule	GFP, RG, TVA-mCherry	Wagner et al., 2019
	LH → LHb	hM4D(Gi)-mCherry, tdTomato	Lecca et al., 2017
	CLA → mPFC	tdTomato	Ährlund-Richter et al., 2019
	HPC → (CeA, BLA)	ChR2-eYFP, RG, TVA, ArchT-GFP, GFP, eNpHR-eYFP	Xu et al., 2016
	POm → M1	RG, GFP, TVA-mCherry	Mo and Sherman, 2019
	PVT → NAc	GCamP6s	Otis et al., 2019
	preBötC → LC	DTR	Yackle et al., 2017
Noradrenergic	LC → spinal cord	ChR2-mCherry	Li et al., 2016
	LC → (spinal cord, PFC)	PSAM-eGFP	Hirschberg et al., 2017
	LC → (ACtx, Cb, HPC, Me, OB)	RG, GFP, TVA-mCherry	Schwarz et al., 2015
	LC → (BLA, mPFC)	ChR2, mAG1, SYP-mCherry, ArchT-tdTomato	Uematsu et al., 2017
Oxytonergic	PVN → SON	eGFP; SYP-GFP ChR2-mCherry, hM4D(Gi)-mCherry	Eliava et al., 2016
Serotonergic	DRN → Amy	5-HT1b, GFP	Liu et al., 2015
	Raphe nuclei → NTS	Knockout Tph2	Wu et al., 2012
Non-canonical neurotransmitters	PVT → CeA	hM4D(Gi)-mCherry	Penzo et al., 2015
	CeA → LC	DTX	Andreoli et al., 2017
Periphery	Motor neurons → craniofacial muscle	GFP	Bohlen et al., 2019*
	NG → gut	GFP, rM3D(Gs)-mCherry	Han et al., 2018

*The citations in this table serve as examples of each type of studies. *Non-human primate studies.*

viral infection, CAV viral vectors were further engineered. For instance, the early region 1 (E1) gene, which is important for DNA replication, was deleted from CAV genome (Klonjkowski et al., 1997). The E1-deleted CAV is replication incompetent (Chartier et al., 1996; Fernandes et al., 2013) and thus causes negligible immune response in humans, non-human primates, and rodents at experimentally relevant titers (Kremer et al., 2000; Perreau and Kremer, 2005; Bohlen et al., 2019; Lau et al., 2019). Consequently, a large number of neurons can be transduced by E1-deleted CAV without being recognized and eliminated by immune cells (Kremer et al., 2000; Soudais et al., 2004; Perreau and Kremer, 2005; Lau et al., 2019).

Another line of evidence supporting the low cytotoxicity of CAV came from studies of neuronal morphology. CAV infection did not change the shape of the somata, the axonal arborization, the number of synaptic buttons, nor did it alter the ultrastructures of transduced neurons (Simão et al., 2016; Li et al., 2018). Interestingly, even with high multiplicity of infection (∼1,000 viral genomes/cell – which is 10–50× higher than normal; Hemmi et al., 1998), CAV did not disrupt the neuronal development of cultured cells, in contrast to both AAV and lentivirus (Piersanti et al., 2013). The long-lasting gene expression and negligible impact on the physiology of neurons make CAV a competent vector when expressing effectors for functional analyses. Indeed, CAV-Cre mediated the expression of effectors for chemogenetics (Augur et al., 2016; Roth, 2016; Alcaraz et al., 2018; Ramanathan et al., 2018), genetic ablation (Liu et al., 2016), and calcium imaging (Otis et al., 2017, 2019) for an intermediate time window, ranging from 2 weeks to a couple of months. Beyond 2 months, CAV can steadily express effectors for longer term functional analysis. For examples, CAV-mediated transduction of ChR2 in LC neurons remained stable for 6 months and was used to manipulate the sleep–wake transition of mice (Li et al., 2016). These experiments demonstrated the applicability of CAV for studying the physiology of neural circuits, with minimal effects on cellular health and circuit integrity.

APPLICATIONS

Canine adenovirus-2 is a powerful tool for mapping the input and output innervations of various types of projection neurons, and for recording or manipulating their activity. The simplest

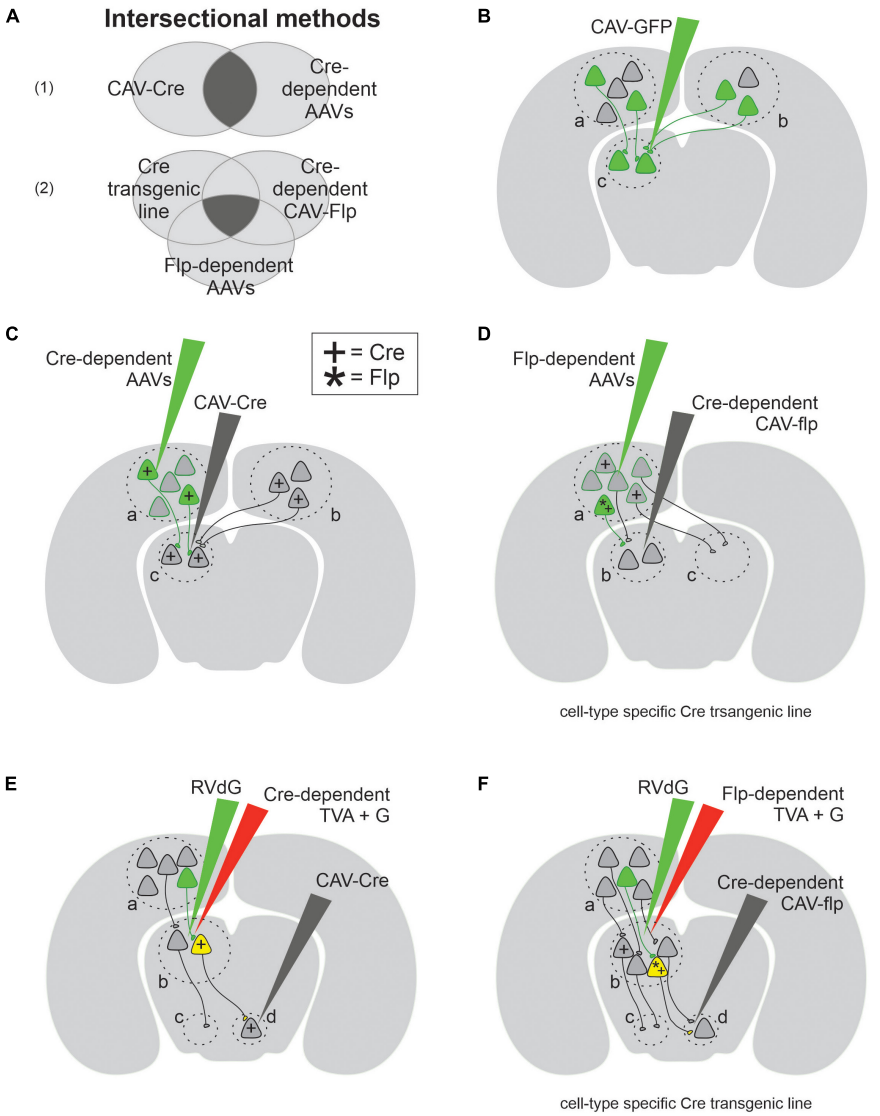

FIGURE 1 | Canine adenovirus type 2 (CAV-2) combined with genetic approaches allows a variety of experimental designs for circuit analyses. **(A)** Venn diagram of two intersectional methods: part **(A1)** provides projection-specific expression using two conditions, while part **(A2)** provides cell-type and projection-specific expression using three conditions. **(B)** The simplest experimental design that labels both local (area c) and projection neurons (areas a and b). **(C)** The schematics of experimental designs for projection-specific expression with the help of Cre (+) recombinase. **(D)** The schematics of experimental designs for cell-type and projection-specific expression with the help of both Cre (+) and Flp (*) recombinases. **(E)** The schematics of transsynaptic experimental design which selectively labels the input onto projection-specific neuronal population defined by retrograde CAV-Cre. **(F)** The schematics of transsynaptic experimental design which selectively labels the input onto cell-type and projection-specific neuronal population.

application of CAV involves transducing presynaptic and local neurons with either a fluorophore or an effector (**Figure 1B**). For instance, Li et al. (2016) revealed the existence of two separate neuronal populations in the rodent LC by injecting CAV carrying either red or green fluorophore in one of two known postsynaptic targets of LC neurons. Similarly, this straightforward experimental design was also used in non-human primates to express fluorescent proteins in neural pathways of interest, including motor neurons that innervate craniofacial muscles and midbrain neurons that project to the Cb (Bohlen et al., 2019; Dopeso-Reyes et al., 2019). This simple experimental design works well to tag projection neurons innervating a target of interest. However, on its own, CAV cannot be used to selectively target a single pathway, nor to report the anatomical origin of observed fluorescent axonal fibers. This limitation arises from the ambiguity that CAV can retrogradely transduce projection neurons non-specifically in any presynaptic region, as well as neurons near the injection site through their dendrites and somata, which express low but significant levels of CAR (Bru et al., 2010; Zussy et al., 2016; Dopeso-Reyes et al., 2019) and through their local axons (**Figure 1B**). To remove this ambiguity, a variety of conditional gene expression paradigms

have been developed, taking advantage of DNA recombinases (**Figures 1C–F**; Nagy, 2000). For instance, CAV viruses carrying the Cre recombinase gene can be injected into a target of interest, in addition to a second injection of AAV viruses carrying a target gene flanked by loxP sequences, injected into a potential presynaptic site (**Figure 1C**). Cre recognizes loxP and conditionally turns on (or off) the loxP-flanked target gene (Nagy, 2000). By combining CAV's retrograde capability with Cre-loxP conditional expression, this intersectional method (**Figure 1A**) labels specific neuronal projections (Senn et al., 2014; Penzo et al., 2015; Augur et al., 2016; Liu et al., 2016; de Git et al., 2018). This design was used to identify a corticofugal pathway from the VC to the brainstem and to ablate it exclusively (Liu et al., 2016), demonstrating the potential of CAV in projection pathway specific circuit analysis (Junyent and Kremer, 2015). The design in **Figure 1C** was ingeniously modified to express genes in an even more selective way (**Figure 1D**). In this new method, a second conditional expression system Flp–Frt (Flp, flippase recombinase; Frt, Flp recombinase target sequences) (Rodríguez et al., 2000) is added so that a Cre transgenic mouse line is used to restrict the expression of target genes in molecularly defined cell types, while Flp carried by CAV selects projection pathways. Therefore, both projection specificity and cell-type specificity are accomplished simultaneously with this clever design. This intersectional method was used in a few studies to lay out the projections of specific types of neurons (Schwarz et al., 2015; Chung et al., 2017; Kakava-Georgiadou et al., 2019). For example, Chung et al. (2017) examined the output pattern of GABAergic neurons in the preoptic area projecting to the TMN pathway.

The above intersectional strategy is not limited to the applications of mapping direct monosynaptic connections between two brain regions (a→b) (**Figures 1C,D**). Instead, it can also be applied to trace more complex neural circuits involving disynaptic connections (a→b→c), with the help of EnvA-pseudotyped, glycoprotein (G)-deleted rabies viruses (RVdG) (**Figures 1E,F**). Wild-type rabies viruses are capable of transsynaptic transport, which allows them to move from postsynaptic neurons, via synapses, to presynaptic neurons (Wall et al., 2010). The engineered RVdG, however, loses this capability unless the target postsynaptic neurons (the so-called starter cells) express both avian sarcoma leukosis virus receptor (TVA) and G (Wall et al., 2010). TVA receptor is required for EnvA-pseudotyped rabies to enter starter cells, and G protein is necessary for rabies's transsynaptic capability (Wall et al., 2010). The expression of those two proteins in starter cells complements RVdG and allows it to infect the starter cell's presynaptic neurons (Wall et al., 2010). Making use of this elegant design, the disynaptic tracing outlined in **Figures 1E,F** occurs in two steps: (1) the intersectional method detailed previously, which uses CAV-Cre to selectively express TVA and G protein in starter cells, defining the output projections (b→d); (2) the retrograde transsynaptic transport of RVdG determines the input innervation of starter cells (a→b). These disynaptic tracing methods have been used to determine the pattern of inputs received by individual noradrenaline populations in LC defined by their output target and cell type (Schwarz et al., 2015). This study benefited greatly from CAV's large size and low diffusion rate, which confines CAV-Cre within the size of small brain regions of interest (Schwarz et al., 2015). In sum, CAV is most widely used to carry recombinases or recombinase-dependent constructs (**Table 1**), making it a powerful retrograde vector to investigate both monosynaptic and disynaptic connections within a neural circuit.

Even though most of our examples of CAV and intersectional method applications concerned circuit anatomy, the same intersectional approaches can be easily tweaked for functional analyses or molecular profiling. For instance, a variety of effector molecules have been conditionally expressed for either chemogenetics (Boender et al., 2014; Augur et al., 2016; Alcaraz et al., 2018; Fernandez et al., 2018; Ramanathan et al., 2018; Kakava-Georgiadou et al., 2019), optogenetic (Eliava et al., 2016; Li et al., 2016), projection-specific genetic ablations

TABLE 2 | Summary of cell type or projection-specific CAV tropism.

System	Circuit	Comparison	References
Glutamatergic	BLA → mPFC	CAV: bias medial BLA cells HSV: bias lateral BLA cells Retro-beads: no bias	Senn et al., 2014
	(contra. ACC, ORBvl, VISal, RSP) → ACC	CAV: bias L5 cells Retro-AAV: bias L2/3 cells Rabies: both L5 and L2/3 cells	Chatterjee et al., 2018
	Cortices → BPN	CAV: low efficiency rAAV2-retro: high efficiency Fluro-Gold: high efficiency	Tervo et al., 2016
	OFC → VS	CAV: low efficiency CAV + AAV-CAR: high efficiency	Li et al., 2018
	BLA → mPFC	CAV: low efficiency CAV + AAV-CAR: high efficiency	Kakava-Georgiadou et al., 2019
Dopaminergic	(VTA, DNC) → DLS	CAV + AAV-CAR: high efficiency rAAV2-retro: low efficiency	
	VTA → NAc	CAV = CAV + AAV-CAR: high efficiency rAAV2-retro: low efficiency	

(Wu et al., 2012; Liu et al., 2016), optical calcium imaging (Otis et al., 2017, 2019), and molecular profiling (Ekstrand et al., 2014). Furthermore, the ability of CAV to seamlessly deliver and selectively express effectors can be paired with classical techniques, such as slice or *in vivo* electrophysiology (Eliava et al., 2016; Li et al., 2016), and a variety of behavior paradigms (Liu et al., 2016; Kakava-Georgiadou et al., 2019). Pairing these techniques with CAV and intersectional methods enables a wide range of combinations, allowing substantial versatility and creativity in experimental designs. It should be noted that, regardless of the vector used, long-term overexpression of Cre recombinase can be toxic (Silver and Livingston, 2001; Braz et al., 2002; Whitsett and Perl, 2006; Gong et al., 2007; Harno et al., 2013; Janbandhu et al., 2014; Lam et al., 2019), and therefore, precautions are needed when Cre is used in functional assays.

CAV LIMITATIONS AND FUTURE DIRECTIONS

In spite of the great success of CAV in the above studies, one should be cautious of the limitations of this tool and aware of the caveats when interpreting experimental results. For instance, there is evidence that CAV transduction biases some types of neurons or pathways (**Table 2**), likely due to varying CAR expression level in different types of neurons (Kremer, 2004; Grove and Marsh, 2011). For example, when examining the projection from basolateral Amy (BLA) to mPFC, Senn et al. (2014) found that CAV and herpes simplex virus 1 retrogradely labeled largely non-overlapping subpopulations of BLA neurons when injected into the mPFC area, indicating that CAV transduced only a part of this projection population. In addition, the strong tropisms of CAV for particular cell types over others was also observed in corticocortical projections. In particular, CAV injected in the ACC of mice preferentially transduced neurons in layer 5 of the primary VC; in contrast, other retrograde viruses, such as engineered rabies and rAAV2-retro, injected in the same cortical area transduced neurons across multiple layers of the primary VC (Chatterjee et al., 2018). Therefore, when using CAV to map unknown connectivity, one must be cautious when drawing conclusions about negative results, as a lack of evidence for connectivity could be alternatively explained by CAV tropism.

A second limitation of CAV is its efficacy of retrograde transduction. While sufficient to drive gene expression for both anatomical and functional experiments (**Table 1**), CAV viruses are not quite comparable in infectivity and retrograde transport to other retrograde viruses such as rAAV2-retro and rabies virus (Aschauer et al., 2013; Tervo et al., 2016; Chatterjee et al., 2018; **Table 2**). For example, in the corticopontine circuit, rAAV2-retro viruses injected into the basal pontine nuclei transduced 22 times more layer 5 projection neurons in the cortex than the CAV viruses (Tervo et al., 2016). As such, a more efficient CAV virus with little tropism would be a great improvement, since it could facilitate the detection of sparse projections and increase the strength of functional manipulations, facilitating the detection of subtle physiological or behavioral effects.

To improve the efficiency of CAV or even overcome its tropism against some neuronal types, an elegant receptor complementation strategy was recently developed, focusing on CAR, a key receptor molecule for the retrograde capability of the CAV (Li et al., 2018). In this method, the CAR receptor was virally expressed in candidate projection neurons, which in turn facilitated the retrograde transduction of those targeted neurons by CAV carrying Cre recombinase (Li et al., 2018). This strategy increased the efficacy of CAV retrograde transport in the BLA-to-mPFC pathway, where CAV has limited infectivity in control animals (Li et al., 2018). This strategy is also potentially useful to circumvent the tropism of other retrograde viruses, providing CAR/CAV combination a significant advantage over rAAV2-retro and rabies (Li et al., 2018). For example, rAAV2-retro viruses showed marginal retrograde transduction of dopaminergic neurons in the VTA and SNc (VTA/SNc) that project to dorsolateral striatum (DLS) (Tervo et al., 2016). By virally expressing the CAR receptor in VTA/SNc, the number of dopaminergic neurons that were retrogradely infected by the CAV injected into the DLS was approximately nine times larger than when rAAV2-retro was used. Nevertheless, the applicability and limitations of this receptor complementation strategy in other cell types and pathways need to be explored and validated (Kakava-Georgiadou et al., 2019).

CONCLUSION

In summary, the unique characteristics of CAV make it an intriguing choice for neuroscientists. CAV vectors complement the toolbox of retrograde viruses, which can be used to reveal the connectivity and physiology of neural circuits. In particular, due to low toxicity, minimal immunogenicity, and stable gene expression, CAV is ideal for long-term functional analyses of brain circuits. Moreover, the capability of combining CAV with conditional expression and transsynaptic tracing makes it a promising tool to study circuits in cell- and/or projection-type specific manners. Finally, the success of the CAR receptor complementation strategy provides a method to circumvent the limitations of CAV, opening a new era for circuit analysis. Needless to say, CAV will continue to facilitate the long-standing quest to ultimately understand the biological substrates and logics of brain functions.

AUTHOR CONTRIBUTIONS

Both authors contributed to the writing and figure design.

FUNDING

Work in the authors' laboratory was supported by the Canadian Foundation of Innovation and Ontario Research Fund (CFI/ORF project no. 37597), NSERC (RGPIN-2019-06479), Research and Scholarly Activity Fund, and Connaught New Researcher Awards.

REFERENCES

Ährlund-Richter, S., Xuan, Y., van Lunteren, J. A., Kim, H., Ortiz, C., Dorocic, I. P., et al. (2019). A whole-brain atlas of monosynaptic input targeting four different cell types in the medial prefrontal cortex of the mouse. *Nat. Neurosci.* 22, 657–668. doi: 10.1038/s41593-019-0354-y

Alcaraz, F., Fresno, V., Marchand, A. R., Kremer, E. J., Coutureau, E., and Wolff, M. (2018). Thalamocortical and corticothalamic pathways differentially contribute to goal-directed behaviors in the rat. *eLife* 7:e32517.

Alhadeff, A. L., Holland, R. A., Zheng, H., Rinaman, L., Grill, H. J., and De Jonghe, B. C. (2017). Excitatory hindbrain–forebrain communication is required for cisplatin-induced anorexia and weight loss. *J. Neurosci.* 37, 362–370. doi: 10.1523/jneurosci.2714-16.2016

Andreoli, M., Marketkar, T., and Dimitrov, E. (2017). Contribution of amygdala CRF neurons to chronic pain. *Exp. Neurol.* 298, 1–12. doi: 10.1016/j.expneurol.2017.08.010

Aschauer, D. F., Kreuz, S., and Rumpel, S. (2013). Analysis of transduction efficiency, tropism and axonal transport of AAV serotypes 1, 2, 5, 6, 8 and 9 in the mouse brain. *PLoS One* 8:e76310. doi: 10.1371/journal.pone.0076310

Asokan, M. M., Williamson, R. S., Hancock, K. E., and Polley, D. B. (2018). Sensory overamplification in layer 5 auditory corticofugal projection neurons following cochlear nerve synaptic damage. *Nat. Commun.* 9:2468. doi: 10.1038/s41467-018-04852-y

Augur, I. F., Wyckoff, A. R., Aston-Jones, G., Kalivas, P. W., and Peters, J. (2016). Chemogenetic activation of an extinction neural circuit reduces cue-induced reinstatement of cocaine seeking. *J. Neurosci.* 36, 10174–10180. doi: 10.1523/jneurosci.0773-16.2016

Barik, A., Thompson, J. H., Seltzer, M., Ghitani, N., and Chesler, A. T. (2018). A brainstem-spinal circuit controlling nocifensive behavior. *Neuron* 100, 1491–1503.

Beier, K. T., Steinberg, E. E., DeLoach, K. E., Xie, S., Miyamichi, K., Schwarz, L., et al. (2015). Circuit architecture of VTA dopamine neurons revealed by systematic input-output mapping. *Cell* 162, 622–634. doi: 10.1016/j.cell.2015.07.015

Beyeler, A., Chang, C. J., Silvestre, M., Lévêque, C., Namburi, P., Wildes, C. P., et al. (2018). Organization of valence-encoding and projection-defined neurons in the basolateral amygdala. *Cell Rep.* 22, 905–918. doi: 10.1016/j.celrep.2017.12.097

Beyeler, A., Namburi, P., Glober, G. F., Simonnet, C., Calhoon, G. G., Conyers, G. F., et al. (2016). Divergent routing of positive and negative information from the amygdala during memory retrieval. *Neuron* 90, 348–361. doi: 10.1016/j.neuron.2016.03.004

Boender, A. J., de Jong, J. W., Boekhoudt, L., Luijendijk, M. C., van der Plasse, G., and Adan, R. A. (2014). Combined use of the canine adenovirus-2 and DREADD-technology to activate specific neural pathways *in vivo*. *PLoS One* 9:e95392. doi: 10.1371/journal.pone.0095392

Bohlen, M. O., El-Nahal, H. G., and Sommer, M. A. (2019). Transduction of craniofacial motoneurons following intramuscular injections of canine adenovirus type-2 (CAV-2) in rhesus macaques. *Front. Neuroanat.* 13:84. doi: 10.3389/fnana.2019.00084

Braz, J. M., Rico, B., and Basbaum, A. I. (2002). Transneuronal tracing of diverse CNS circuits by Cre-mediated induction of wheat germ agglutinin in transgenic mice. *Proc. Natl. Acad. Sci. U.S.A.* 99, 15148–15153. doi: 10.1073/pnas.222546999

Brito, C., Simão, D., Costa, I., Malpique, R., Pereira, C. I., Fernandes, P., et al. (2012). Generation and genetic modification of 3D cultures of human dopaminergic neurons derived from neural progenitor cells. *Methods* 56, 452–460. doi: 10.1016/j.ymeth.2012.03.005

Bru, T., Salinas, S., and Kremer, E. J. (2010). An update on canine adenovirus type 2 and its vectors. *Viruses* 2, 2134–2153. doi: 10.3390/v2092134

Campus, P., Covelo, I. R., Kim, Y., Parsegian, A., Kuhn, B., Lopez, S. A., et al. (2019). The paraventricular thalamus is a critical mediator of top-down control of cue-motivated behavior. *bioRxiv* [Preprint]. doi: 10.1101/637702

Carter, M. E., Soden, M. E., Zweifel, L. S., and Palmiter, R. D. (2013). Genetic identification of a neural circuit that suppresses appetite. *Nature* 503, 111–141.

Chartier, C., Degryse, E., Gantzer, M., Dieterle, A., Pavirani, A., and Mehtali, M. (1996). Efficient generation of recombinant adenovirus vectors by homologous recombination in *Escherichia coli*. *J. Virol.* 70, 4805–4810. doi: 10.1128/jvi.70.7.4805-4810.1996

Chatterjee, S., Sullivan, H. A., MacLennan, B. J., Xu, R., Hou, Y., Lavin, T. K., et al. (2018). Nontoxic, double-deletion-mutant rabies viral vectors for retrograde targeting of projection neurons. *Nat. Neurosci.* 21, 638–646. doi: 10.1038/s41593-018-0091-7

Chillon, M., and Kremer, E. J. (2001). Trafficking and propagation of canine adenovirus vectors lacking a known integrin-interacting motif. *Hum. Gen. Ther.* 12, 1815–1823. doi: 10.1089/104303401750476302

Chung, S., Weber, F., Zhong, P., Tan, C. L., Nguyen, T. N., Beier, K. T., et al. (2017). Identification of preoptic sleep neurons using retrograde labelling and gene profiling. *Nature* 545, 477–481. doi: 10.1038/nature22350

Crick, F. C., and Koch, C. (2005). What is the function of the claustrum? *Philos. Trans. R. Soc. Lond. B Biol. Sci.* 360, 1271–1279. doi: 10.1098/rstb.2005.1661

de Git, K. C., van Tuijl, D. C., Luijendijk, M. C., Wolterink-Donselaar, I. G., Ghanem, A., Conzelmann, K. K., et al. (2018). Anatomical projections of the dorsomedial hypothalamus to the periaqueductal grey and their role in thermoregulation: a cautionary note. *Physiol. Rep.* 6:e13807. doi: 10.14814/phy2.13807

del Rio, D., Beucher, B., Lavigne, M., Wehbi, A., Gonzalez-Dopeso Reyes, I., Saggio, I., et al. (2019). CAV-2 vector development and gene transfer in the central and peripheral nervous systems. *Front. Mol. Neurosci.* 12:71. doi: 10.3389/fnmol.2019.00071

Diodato, A., De Brimont, M. R., Yim, Y. S., Derian, N., Perrin, S., Pouch, J., et al. (2016). Molecular signatures of neural connectivity in the olfactory cortex. *Nat. Commun.* 7:12238. doi: 10.1038/ncomms1223

Dopeso-Reyes, I. G., Junyent, F., Mestre-Francés, N., Whebi, A., Beucher, B., and Kremer, E. J. (2019). Identification of cerebellar afferent projections in a nonhuman primate using CAV-2 vectors. *bioRxiv* [Preprint]. doi: 10.1101/728709

Ekstrand, M. I., Nectow, A. R., Knight, Z. A., Latcha, K. N., Pomeranz, L. E., and Friedman, J. M. (2014). Molecular profiling of neurons based on connectivity. *Cell* 157, 1230–1242. doi: 10.1016/j.cell.2014.03.059

Eliava, M., Melchior, M., Knobloch-Bollmann, H. S., Wahis, J., da Silva Gouveia, M., et al. (2016). A new population of parvocellular oxytocin neurons controlling magnocellular neuron activity and inflammatory pain processing. *Neuron* 89, 1291–1304. doi: 10.1016/j.neuron.2016.01.041

Fadok, J. P., Darvas, M., Dickerson, T. M., and Palmiter, R. D. (2010). Long-term memory for pavlovian fear conditioning requires dopamine in the nucleus accumbens and basolateral amygdala. *PLoS One* 5:e12751. doi: 10.1371/journal.pone.0012751

Fernandes, P., Santiago, V. M., Rodrigues, A. F., Tomás, H., Kremer, E. J., Alves, P. M., et al. (2013). Impact of E1 and Cre on adenovirus vector amplification: developing MDCK CAV-2-E1 and E1-Cre transcomplementing cell lines. *PLoS One* 8:e60342. doi: 10.1371/journal.pone.0060342

Fernandez, S. P., Broussot, L., Marti, F., Contesse, T., Mouska, X., Soiza-Reilly, M., et al. (2018). Mesopontine cholinergic inputs to midbrain dopamine neurons drive stress-induced depressive-like behaviors. *Nat. Commun.* 9:4449. doi: 10.1038/s41467-018-0680

Gerhardt, G. A., and Palmer, M. R. (1987). Characterization of the techniques of pressure ejection and microiontophoresis using *in vivo* electrochemistry. *J. Neurosci. Methods* 22, 147–159. doi: 10.1016/0165-0270(87)90009-4

Gong, S., Doughty, M., Harbaugh, C. R., Cummins, A., Hatten, M. E., Heintz, N., et al. (2007). Targeting Cre recombinase to specific neuron populations with bacterial artificial chromosome constructs. *J. Neurosci.* 27, 9817–9823. doi: 10.1523/jneurosci.2707-07.2007

Grove, J., and Marsh, M. (2011). The cell biology of receptor-mediated virus entry. *J. Cell Biol.* 195, 1071–1082. doi: 10.1083/jcb.201108131

Han, W., Tellez, L. A., Perkins, M. H., Perez, I. O., Qu, T., Ferreira, J., et al. (2018). A neural circuit for gut-induced reward. *Cell* 175, 665–678.

Han, W., Tellez, L. A., Rangel, M. J. Jr., Motta, S. C., Zhang, X., Perez, I. O., et al. (2017). Integrated control of predatory hunting by the central nucleus of the amygdala. *Cell* 168, 311–324.

Harno, E., Cottrell, E. C., and White, A. (2013). Metabolic pitfalls of CNS Cre-based technology. *Cell Metab.* 18, 21–28. doi: 10.1016/j.cmet.2013.05.019

Hemmi, S., Geertsen, R., Mezzacasa, A., Peter, I., and Dummer, R. (1998). The presence of human coxsackievirus and adenovirus receptor is associated with

efficient adenovirus-mediated transgene expression in human melanoma cell cultures. *Hum. Gene Ther.* 9, 2363–2373. doi: 10.1089/hum.1998.9.16-2363

Herman, A. M., Ortiz-Guzman, J., Kochukov, M., Herman, I., Quast, K. B., Patel, J. M., et al. (2016). A cholinergic basal forebrain feeding circuit modulates appetite suppression. *Nature* 538, 253–256. doi: 10.1038/nature19789

Hirokawa, J., Vaughan, A., Masset, P., Ott, T., and Kepecs, A. (2019). Frontal cortex neuron types categorically encode single decision variables. *Nature* 576, 446–451. doi: 10.1038/s41586-019-1816-9

Hirschberg, S., Li, Y., Randall, A., Kremer, E. J., and Pickering, A. E. (2017). Functional dichotomy in spinal-vs prefrontal-projecting locus coeruleus modules splits descending noradrenergic analgesia from ascending aversion and anxiety in rats. *eLife* 6:e29808.

Hnasko, T. S., Perez, F. A., Scouras, A. D., Stoll, E. A., Gale, S. D., Luquet, S., et al. (2006). Cre recombinase-mediated restoration of nigrostriatal dopamine in dopamine-deficient mice reverses hypophagia and bradykinesia. *Proc. Natl. Acad. Sci. U.S.A.* 103, 8858–8863. doi: 10.1073/pnas.0603081103

Ibanes, S., and Kremer, E. J. (2013). Canine adenovirus type 2 vector generation via I-Sce1-mediated intracellular genome release. *PLoS One* 8:e71032. doi: 10.1371/journal.pone.0071

Janbandhu, V. C., Moik, D., and Fassler, R. (2014). Cre recombinase induces DNA damage and tetraploidy in the absence of loxP sites. *Cell Cycle* 13, 462–470. doi: 10.4161/cc.27271

Junyent, F., and Kremer, E. J. (2015). CAV-2—why a canine virus is a neurobiologist's best friend. *Curr. Opin. Pharmacol.* 24, 86–93. doi: 10.1016/j.coph.2015.08.004

Kakava-Georgiadou, N., Zwartkruis, M. M., Bullich-Vilarrubias, C., Luijendijk, M., Garner, K. M., van der Plasse, G., et al. (2019). An intersectional approach to target neural circuits with cell-and projection-type specificity: validation in the mesolimbic dopamine system. *Front. Mol. Neurosci.* 12:49. doi: 10.3389/fnmol.2019.00049

Karlin, S., and Brendel, V. (1988). Charge configurations in viral proteins. *Proc. Natl. Acad. Sci. U.S.A.* 85, 9396–9400. doi: 10.1073/pnas.85.24.9396

Kim, J., Hughes, E. G., Shetty, A. S., Arlotta, P., Goff, L. A., Bergles, D. E., et al. (2017). Changes in the excitability of neocortical neurons in a mouse model of amyotrophic lateral sclerosis are not specific to corticospinal neurons and are modulated by advancing disease. *J. Neurosci.* 37, 9037–9053. doi: 10.1523/jneurosci.0811-17.2017

Klonjkowski, B., Gilardi-Hebenstreit, P., Hadchouel, J., Randrianarison, V., Boutin, S., Yeh, P., et al. (1997). A recombinant E1-deleted canine adenoviral vector capable of transduction and expression of a transgene in human-derived cells and in vivo. *Hum. Gene Ther.* 8, 2103–2115. doi: 10.1089/hum.1997.8.17-2103

Kohl, J., Babayan, B. M., Rubinstein, N. D., Autry, A. E., Marin-Rodriguez, B., Kapoor, V., et al. (2018). Functional circuit architecture underlying parental behaviour. *Nature* 556, 326–331. doi: 10.1038/s41586-018-0027-0

Kremer, E. J. (2004). CAR chasing: canine adenovirus vectors – all bite and no bark? *J. Gene Med.* 6, 139–151.

Kremer, E. J., Boutin, S., Chillon, M., and Danos, O. (2000). Canine adenovirus vectors: an alternative for adenovirus-mediated gene transfer. *J. Virol.* 74, 505–512. doi: 10.1128/jvi.74.1.505-512.2000

Lam, P. T., Padula, S. L., Hoang, T. V., Poth, J. E., Liu, L., Liang, C., et al. (2019). Considerations for the use of Cre recombinase for conditional gene deletion in the mouse lens. *Hum. Genomics* 13:10. doi: 10.1186/s40246-019-0192-8

Lau, A. A., Hopwood, J. J., and Hemsley, K. M. (2019). Canine adenoviral vector-mediated gene transfer to the guinea pig brain. *Gene Rep.* 16:100432. doi: 10.1016/j.genrep.2019.100432

Lavi, K., Jacobson, G. A., Rosenblum, K., and Lüthi, A. (2018). Encoding of conditioned taste aversion in cortico-amygdala circuits. *Cell Rep.* 24, 278–283. doi: 10.1016/j.celrep.2018.06.053

Lecca, S., Meye, F. J., Trusel, M., Tchenio, A., Harris, J., Schwarz, M. K., et al. (2017). Aversive stimuli drive hypothalamus-to-habenula excitation to promote escape behavior. *eLife* 6:e30697. doi: 10.7554/eLife.30697

Lerner, T. N., Shilyansky, C., Davidson, T. J., Evans, K. E., Beier, K. T., Zalocusky, K. A., et al. (2015). Intact-brain analyses reveal distinct information carried by SNc dopamine subcircuits. *Cell* 162, 635–647. doi: 10.1016/j.cell.2015.07.014

Leroy, F., Brann, D. H., Meira, T., and Siegelbaum, S. A. (2017). Input-timing-dependent plasticity in the hippocampal CA2 region and its potential role in social memory. *Neuron* 95, 1089–1102.

Li, S. J., Vaughan, A., Sturgill, J. F., and Kepecs, A. (2018). A viral receptor complementation strategy to overcome CAV-2 tropism for efficient retrograde targeting of neurons. *Neuron* 98, 905–917.

Li, Y., Hickey, L., Perrins, R., Werlen, E., Patel, A. A., Hirschberg, S., et al. (2016). Retrograde optogenetic characterization of the pontospinal module of the locus coeruleus with a canine adenoviral vector. *Brain Res.* 1641, 274–290. doi: 10.1016/j.brainres.2016.02.023

Liu, B. H., Huberman, A. D., and Scanziani, M. (2016). Cortico-fugal output from visual cortex promotes plasticity of innate motor behaviour. *Nature* 538, 383–387. doi: 10.1038/nature19818

Liu, Y., Kelly, M. A., Sexton, T. J., and Neumaier, J. F. (2015). 5-HT1B autoreceptors differentially modulate the expression of conditioned fear in a circuit-specific manner. *Neuroscience* 298, 436–447. doi: 10.1016/j.neuroscience.2015.04.032

Luo, R., Uematsu, A., Weitemier, A., Aquili, L., Koivumaa, J., McHugh, T. J., et al. (2018). A dopaminergic switch for fear to safety transitions. *Nat. Commun.* 9:2483. doi: 10.1038/s41467-018-04784-7

Mestre-Francés, N., Serratrice, N., Gennetier, A., Devau, G., Cobo, S., Trouche, S. G., et al. (2018). Exogenous LRRK2G2019S induces parkinsonian-like pathology in a nonhuman primate. *JCI Insight* 3:e98202.

Miller, O. H., Bruns, A., Ammar, I. B., Mueggler, T., and Hall, B. J. (2017). Synaptic regulation of a thalamocortical circuit controls depression-related behavior. *Cell Rep.* 20, 1867–1880. doi: 10.1016/j.celrep.2017.08.002

Mo, C., and Sherman, S. M. (2019). A sensorimotor pathway via higher-order thalamus. *J. Neurosci.* 39, 692–704. doi: 10.1523/jneurosci.1467-18.2018

Murugan, M., Jang, H. J., Park, M., Miller, E. M., Cox, J., Taliaferro, J. P., et al. (2017). Combined social and spatial coding in a descending projection from the prefrontal cortex. *Cell* 171, 1663–1677.

Nagy, A. (2000). Cre recombinase: the universal reagent for genome tailoring. *Genesis* 26, 99–109. doi: 10.1002/(sici)1526-968x(200002)26:2<99::aid-gene1>3.0.co;2-b

Namburi, P., Beyeler, A., Yorozu, S., Calhoon, G. G., Halbert, S. A., Wichmann, R., et al. (2015). A circuit mechanism for differentiating positive and negative associations. *Nature* 520, 675–678. doi: 10.1038/nature14366

Otis, J. M., Namboodiri, V. M., Matan, A. M., Voets, E. S., Mohorn, E. P., Kosyk, O., et al. (2017). Prefrontal cortex output circuits guide reward seeking through divergent cue encoding. *Nature* 543, 103–107. doi: 10.1038/nature21376

Otis, J. M., Zhu, M., Namboodiri, V. M., Cook, C. A., Kosyk, O., Matan, A. M., et al. (2019). Paraventricular thalamus projection neurons integrate cortical and hypothalamic signals for Cue-reward processing. *Neuron* 103, 423–431.

Parfitt, G. M., Nguyen, R., Bang, J. Y., Aqrabawi, A. J., Tran, M. M., Seo, D. K., et al. (2017). Bidirectional control of anxiety-related behaviors in mice: role of inputs arising from the ventral hippocampus to the lateral septum and medial prefrontal cortex. *Neuropsychopharmacology* 42, 1715–1728. doi: 10.1038/npp.2017.56

Penzo, M. A., Robert, V., Tucciarone, J., De Bundel, D., Wang, M., Van Aelst, L., et al. (2015). The paraventricular thalamus controls a central amygdala fear circuit. *Nature* 519, 455–459. doi: 10.1038/nature13978

Perreau, M., and Kremer, E. J. (2005). Frequency, proliferation, and activation of human memory T cells induced by a nonhuman adenovirus. *J. Virol.* 79, 14595–14605. doi: 10.1128/jvi.79.23.14595-14605.2005

Persson, A., Fan, X., Widegren, B., and Englund, E. (2006). Cell type-and region-dependent coxsackie adenovirus receptor expression in the central nervous system. *J. Neurooncol.* 78, 1–6. doi: 10.1007/s11060-005-9055-3

Piersanti, S., Astrologo, L., Licursi, V., Costa, R., Roncaglia, E., Gennetier, A., et al. (2013). Differentiated neuroprogenitor cells incubated with human or canine adenovirus, or lentiviral vectors have distinct transcriptome profiles. *PLoS One* 8:e69808. doi: 10.1371/journal.pone.0069808

Ponvert, N. D., and Jaramillo, S. (2019). Auditory thalamostriatal and corticostriatal pathways convey complementary information about sound features. *J. Neurosci.* 39, 271–280. doi: 10.1523/jneurosci.1188-18.2018

Rajasethupathy, P., Sankaran, S., Marshel, J. H., Kim, C. K., Ferenczi, E., Lee, S. Y., et al. (2015). Projections from neocortex mediate top-down control of memory retrieval. *Nature* 526, 653–659. doi: 10.1038/nature15389

Ramanathan, K. R., Jin, J., Giustino, T. F., Payne, M. R., and Maren, S. (2018). Prefrontal projections to the thalamic nucleus reuniens mediate fear extinction. *Nat. Commun.* 9:4527. doi: 10.1038/s41467-018-06970-z

Reynolds, L. M., Pokinko, M., Torres-Berrío, A., Cuesta, S., Lambert, L. C., Pellitero, E. D. C., et al. (2018). DCC receptors drive prefrontal cortex

maturation by determining dopamine axon targeting in adolescence. *Biol. Psychiatry* 83, 181–192. doi: 10.1016/j.biopsych.2017.06.009

Robinson, S., Rainwater, A. J., Hnasko, T. S., and Palmiter, R. D. (2007). Viral restoration of dopamine signaling to the dorsal striatum restores instrumental conditioning to dopamine-deficient mice. *Psychopharmacology* 191, 567–578. doi: 10.1007/s00213-006-0579-9

Rodríguez, C. I., Buchholz, F., Galloway, J., Sequerra, R., Kasper, J., Ayala, R., et al. (2000). High-efficiency deleteter mice show that FLPe is an alternative to Cre-loxP. *Nat. Genet.* 25, 139–140. doi: 10.1038/75973

Roth, B. (2016). DREADDs for neuroscientists. *Neuron* 89, 683–694. doi: 10.1016/j.neuron.2016.01.040

Ruder, L., Takeoka, A., and Arber, S. (2016). Long-distance descending spinal neurons ensure quadrupedal locomotor stability. *Neuron* 92, 1063–1078. doi: 10.1016/j.neuron.2016.10.032

Salay, L. D., Ishiko, N., and Huberman, A. D. (2018). A midline thalamic circuit determines reactions to visual threat. *Nature* 557, 183–189. doi: 10.1038/s41586-018-0078-2

Salinas, S., Bilsland, L. G., Henaff, D., Weston, A. E., Keriel, A., Schiavo, G., et al. (2009). CAR-associated vesicular transport of an adenovirus in motor neuron axons. *PLoS Pathog.* 5:e1000442. doi: 10.1371/journal.ppat.1000442

Schwarz, L. A., Miyamichi, K., Gao, X. J., Beier, K. T., Weissbourd, B., DeLoach, K. E., et al. (2015). Viral-genetic tracing of the input–output organization of a central noradrenaline circuit. *Nature* 524, 88–92. doi: 10.1038/nature14600

Senn, V., Wolff, S. B., Herry, C., Grenier, F., Ehrlich, I., Gründemann, J., et al. (2014). Long-range connectivity defines behavioral specificity of amygdala neurons. *Neuron* 81, 428–437. doi: 10.1016/j.neuron.2013.11.006

Silver, D. P., and Livingston, D. M. (2001). Self-excising retroviral vectors encoding the Cre recombinase overcome Cre-mediated cellular toxicity. *Mol. Cell* 8, 233–243. doi: 10.1016/s1097-2765(01)00295-7

Simão, D., Pinto, C., Fernandes, P., Peddie, C. J., Piersanti, S., Collinson, L. M., et al. (2016). Evaluation of helper-dependent canine adenovirus vectors in a 3D human CNS model. *Gene Ther.* 23, 86–94. doi: 10.1038/gt.2015.75

Sotak, B. N., Hnasko, T. S., Robinson, S., Kremer, E. J., and Palmiter, R. D. (2005). Dysregulation of dopamine signaling in the dorsal striatum inhibits feeding. *Brain Res.* 1061, 88–96. doi: 10.1016/j.brainres.2005.08.053

Soudais, C., Boutin, S., and Kremer, E. J. (2001). Characterization of cis-acting sequences involved in canine adenovirus packaging. *Mol. Ther.* 3, 631–640. doi: 10.1006/mthe.2001.0263

Soudais, C., Skander, N., and Kremer, E. J. (2004). Long-term in vivo transduction of neurons throughout the rat CNS using novel helper-dependent CAV-2 vectors. *FASEB J.* 18, 391–393. doi: 10.1096/fj.03-0438fje

Tervo, D. G. R., Hwang, B. Y., Viswanathan, S., Gaj, T., Lavzin, M., Ritola, K. D., et al. (2016). A designer AAV variant permits efficient retrograde access to projection neurons. *Neuron* 92, 372–382. doi: 10.1016/j.neuron.2016.09.021

Thompson, K. R., and Towne, C. (2018). "A hitchhiker's guide to the selection of viral vectors for optogenetic studies," in *Optogenetics: A Roadmap*, ed. A. Stroh, (New York, NY: Humana Press), 1–23. doi: 10.1007/978-1-4939-7417-7_1

Uematsu, A., Tan, B. Z., Ycu, E. A., Cuevas, J. S., Koivumaa, J., Junyent, F., et al. (2017). Modular organization of the brainstem noradrenaline system coordinates opposing learning states. *Nat. Neurosci.* 20, 1602–1611. doi: 10.1038/nn.4642

Vander Weele, C. M., Siciliano, C. A., Matthews, G. A., Namburi, P., Izadmehr, E. M., Espinel, I. C., et al. (2018). Dopamine enhances signal-to-noise ratio in cortical-brainstem encoding of aversive stimuli. *Nature* 563, 397–401. doi: 10.1038/s41586-018-0682-1

Vogel, E., Krabbe, S., Gründemann, J., Cusulin, J. I. W., and Lüthi, A. (2016). Projection-specific dynamic regulation of inhibition in amygdala micro-circuits. *Neuron* 91, 644–651. doi: 10.1016/j.neuron.2016.06.036

Wagner, M. J., Kim, T. H., Kadmon, J., Nguyen, N. D., Ganguli, S., Schnitzer, M. J., et al. (2019). Shared cortex-cerebellum dynamics in the execution and learning of a motor task. *Cell* 177, 669–682.

Wall, N. R., Wickersham, I. R., Cetin, A., De La Parra, M., and Callaway, E. M. (2010). Monosynaptic circuit tracing in vivo through Cre-dependent targeting and complementation of modified rabies virus. *Proc. Natl. Acad. Sci. U.S.A.* 107, 21848–21853. doi: 10.1073/pnas.1011756107

Whitsett, J. A., and Perl, A. K. T. (2006). Conditional control of gene expression in the respiratory epithelium: a cautionary note. *Am. J. Respir. Cell. Mol. Biol.* 34, 519–520. doi: 10.1165/rcmb.f310

Williamson, R. S., and Polley, D. B. (2019). Parallel pathways for sound processing and functional connectivity among layer 5 and 6 auditory corticofugal neurons. *eLife* 8:e42974.

Wu, Q., Clark, M. S., and Palmiter, R. D. (2012). Deciphering a neuronal circuit that mediates appetite. *Nature* 483, 594–597. doi: 10.1038/nature10899

Xu, C., Krabbe, S., Gründemann, J., Botta, P., Fadok, J. P., Osakada, F., et al. (2016). Distinct hippocampal pathways mediate dissociable roles of context in memory retrieval. *Cell* 167, 961–972.

Yackle, K., Schwarz, L. A., Kam, K., Sorokin, J. M., Huguenard, J. R., Feldman, J. L., et al. (2017). Breathing control center neurons that promote arousal in mice. *Science* 355, 1411–1415. doi: 10.1126/science.aai7984

Zingg, B., Chou, X. L., Zhang, Z. G., Mesik, L., Liang, F., Tao, H. W., et al. (2017). AAV-mediated anterograde transsynaptic tagging: mapping corticocollicular input-defined neural pathways for defense behaviors. *Neuron* 93, 33–47. doi: 10.1016/j.neuron.2016.11.045

Zussy, C., Loustalot, F., Junyent, F., Gardoni, F., Bories, C., Valero, J., et al. (2016). Coxsackievirus adenovirus receptor loss impairs adult neurogenesis, synapse content, and hippocampus plasticity. *J. Neurosci.* 36, 9558–9571. doi: 10.1523/jneurosci.0132-16.2016

Conflict of Interest: The authors declare that the research was conducted in the absence of any commercial or financial relationships that could be construed as a potential conflict of interest.

frontiers in Molecular Neuroscience

ORIGINAL RESEARCH
published: 25 March 2020
doi: 10.3389/fnmol.2020.00049

CAV-2-Mediated GFP and LRRK2^{G2019S} Expression in the *Macaca fascicularis* Brain

Carla di Caudo[1,2†], *Ivan Martínez-Valbuena*[1,2,3†], *Iñaki-Carril Mundiñano*[1], *Aurelie Gennetier*[4], *Maria Hernandez*[1,3], *Mar Carmona-Abellan*[1,2], *Irene Marcilla Garcia*[1], *Eric J. Kremer*[4‡] *and Rosario Luquin*[1,2,3*‡]

[1]*Division of Neuroscience, Center for Applied Medical Research (CIMA), Universidad de Navarra, Pamplona, Spain,* [2]*Department of Neurology, Clinica Universidad de Navarra, Pamplona, Spain,* [3]*Instituto de Investigación Sanitaria de Navarra (IDISNA), Pamplona, Spain,* [4]*Institut de Génétique Moléculaire de Montpellier, Université de Montpellier, CNRS, Montpellier, France*

Parkinson's disease is characterized by motor and nonmotor symptoms that gradually appear as a consequence of the selective loss of dopaminergic neurons in the *substantia nigra pars compacta*. Currently, no treatment can slow Parkinson's disease progression. Inasmuch, there is a need to develop animal models that can be used to understand the pathophysiological mechanisms underlying dopaminergic neuron death. The initial goal of this study was to determine if canine adenovirus type 2 (CAV-2) vectors are effective gene transfer tools in the monkey brain. A second objective was to explore the possibility of developing a large nonhuman primate that expresses one of the most common genetic mutations causing Parkinson's disease. Our studies demonstrate the neuronal tropism, retrograde transport, biodistribution, and efficacy of CAV-2 vectors expressing GFP and leucine-rich repeat kinase 2 (LRRK2^{G2019S}) in the *Macaca fascicularis* brain. Our data also suggest that following optimization CAV-2-mediated LRRK2^{G2019S} expression could help us model the neurodegenerative processes of this genetic subtype of Parkinson's disease in monkeys.

Keywords: ***M. fascicularis, CAV-2, viral vectors, GFP, LRRK2, Parkinson's disease, nonhuman primate, CNS***

OPEN ACCESS

Edited by:
Serena Carra,
University of Modena and Reggio Emilia, Italy

Reviewed by:
Martin Levesque,
Laval University, Canada
Rosario Moratalla,
Spanish National Research Council, Spain

****Correspondence:***
Rosario Luquin
rluquin@unav.es

†These authors have contributed equally to this work

‡These authors share senior authorship

Received: *15 May 2019*
Accepted: *09 March 2020*
Published: *25 March 2020*

Citation:
di Caudo C, Martínez-Valbuena I, Mundiñano I-C, Gennetier A, Hernandez M, Carmona-Abellan M, Marcilla Garcia I, Kremer EJ and Luquin R (2020) CAV-2-Mediated GFP and LRRK2^{G2019S} Expression in the Macaca fascicularis Brain. Front. Mol. Neurosci. 13:49. doi: 10.3389/fnmol.2020.00049

INTRODUCTION

Parkinson's disease is a complex neurodegenerative disorder clinically characterized by a triad of motor symptoms, including tremor, rigidity, and bradykinesia (Poewe et al., 2017). Approximately 9 million individuals are directly affected by Parkinson's disease, making it the second most prevalent neurodegenerative disease among the elderly. The etiology and pathogenic mechanisms of Parkinson's disease remain poorly understood with only a small proportion having an identifiable monogenic cause (with an overall prevalence lower than 5%; Poewe et al., 2017). Among the genetic causes, autosomal dominant mutations in PARK8, the gene coding for leucine-rich repeat kinase 2 (LRRK2), are the most common cause of familial Parkinson's disease (Paisán-Ruíz et al., 2004; Zimprich et al., 2004). LRRK2 is a 285 kDa multifunctional protein that contains several predicted domains including a serine/threonine kinase domain, a GTPase domain and putative protein-protein interaction domains (Gloeckner et al., 2006; Smith et al., 2006; Guo et al., 2007; Ito et al., 2007; Li et al., 2007). LRRK2 is expressed in brain areas receiving dopaminergic innervation, such as the striatum, hippocampus, cortex, and cerebellum, while lower levels have

been reported in neurons of the *substantia nigra* (SN) and ventral tegmental area (Taymans and Baekelandt, 2014). In neurons, LRRK2 plays a role in neurogenesis, axonal outgrowth, mitochondrial function, autophagy, and synaptic function (Shin et al., 2008; Matta et al., 2012; Wang et al., 2012; MacLeod et al., 2013; Sepulveda et al., 2013; Godena et al., 2014; Law et al., 2014; Sweet et al., 2015). At least six mutations in LRRK2 are pathogenic. A glycine to serine change at amino acid 2019 (LRRK2^{G2019S}) accounts for ∼7% of familial cases and ∼2% of sporadic, late-onset, cases (Gasser et al., 2011). LRRK2^{G2019S} is thought to have modestly increased kinase activity, which, by an unknown mechanism, induces neuronal and non-neuronal cell loss (Mortiboys et al., 2015).

Several LRRK2^{G2019S} rodent models have been generated with the goal of better understanding the molecular pathogenesis of Parkinson's disease. These models include knock-out (KO; Andres-Mateos et al., 2009; Lin et al., 2009; Tong et al., 2010, 2012; Hinkle et al., 2012; Ness et al., 2013) or knock-in (KI; Tong et al., 2009; Yue et al., 2015), bacterial artificial chromosome (BAC)-mediated transgenesis (Li et al., 2009, 2010; Melrose et al., 2010; Winner et al., 2011; Bichler et al., 2013; Lee et al., 2015; Sweet et al., 2015), non-BAC transgenics (Chen et al., 2012; Chou et al., 2014; Walker et al., 2014), and those with temporally-controlled or inducible LRRK2 expression (Lin et al., 2009; Lee et al., 2010; Dusonchet et al., 2011; Zhou et al., 2011; Walker et al., 2014; Tsika et al., 2015). The data from LRRK2 KO mice suggest that LRRK2 plays little, if any, role in the development or maintenance of murine dopaminergic neurons (Li et al., 2010; Melrose et al., 2010). In addition, KI LRRK2^{G2019S} mice have minimal reduction in dopamine (DA) release, axonal pathology, and/or evidence of neurodegeneration (Li et al., 2010; Melrose et al., 2010). The reasons why rodents do not exhibit substantial pathology are still uncertain, but not unusual—many rodent models poorly recapitulate human neurodegenerative diseases. In the case of BAC and KI mice, LRRK2 is expressed during development and therefore compensatory mechanisms may prevent the loss of DA neurons (Dawson et al., 2010) and the appearance of motor symptoms. Thus, alternative models are needed to reproduce the progressive degeneration of nigral neurons associated with the LRRK2^{G2019S}.

A handful of studies using vector-mediated delivery of LRRK2^{G2019S} to the rodent brain reported a modest loss of dopaminergic cells without changes in motor performance (Lee et al., 2010; Dusonchet et al., 2011). These studies used herpes simplex virus (HSV) or human adenovirus 5 (HAdV-C5) vectors, but did not target SN neurons and/or allow long-term transgene expression (Dai et al., 1995; Silva et al., 2010; Lentz et al., 2012). For gene transfer to neurons in the CNS, canine adenovirus type 2 (CAV-2) vectors are particularly interesting: in rodents, dogs, and prosimians, the vectors preferentially transduce neurons and are efficiently transported from the injection site to efferent regions (Soudais et al., 2001; Cubizolle et al., 2013; Junyent and Kremer, 2015; Mestre-Francés et al., 2018). Helper-dependent (HD) CAV-2 vectors, which are devoid of all viral coding sequences, also lead to long-term expression in the CNS (del Rio et al., 2019). In the case of LRRK2 expression, the ∼8 kb cDNA is challenging to express from some viral vectors. Of note though, HD CAV-2 vectors are an ideal option because they can harbor an expression cassette as large as 30 kb (Soudais et al., 2004). We previously showed that injections of HD-LRRK2^{G2019S}, an HD CAV-2 vector containing a leucine-rich repeat kinase 2^{G2019S} expression cassette, in the striatum of the gray mouse lemur (*Microcebus murinus*) induces Parkinson's disease-like histological lesions and motor symptoms (Mestre-Francés et al., 2018; Lasbleiz et al., 2019). As a prelude to the development of a monkey with Parkinson's disease, CAV-2 vector efficacy studies in large brains need to be documented. Here, our study using CAV-2 vectors expressing GFP and LRRK2^{G2019S} demonstrate the neuronal tropism, retrograde transport, efficient biodistribution, and efficacy following injections in monkey striatum and the SN.

MATERIALS AND METHODS

Animals

Experimental protocols were carried out under a project license according to the European Communities Council Directive of 24/11/1986 (86/609/EEC) regarding the care and use of animals for experimental procedures and under the guidance of the Ethics Committee for Animal Experimentation of the University of Navarra. Twenty, 4–5-year-old, male, 3–5 kg, *M. fascicularis* were included in the study. Animals were housed in a facility under standard conditions of air exchange (16 l/min), humidity (50%), and light/night cycles, and were fed fresh fruit and commercial pellets, with free access to water.

CAV-2 Vectors

CAV-GFP (Kremer et al., 2000), HD-GFP (Soudais et al., 2004), and HD-LRRK2^{G2019S} (Mestre-Francés et al., 2018) have been previously described. CAV-GFP is a replication-defective E1-deleted vector harboring a cytomegalovirus early promoter (CMV), GFP, SV40 polyA cassette. HD-GFP is a HD CAV-2 vector expressing GFP. HD-LRRK2^{G2019S} contains a Rous sarcoma virus (RSV) promoter, a codon-optimized LRRK2^{G2019S} cDNA, followed by an internal ribosomal entry site (IRES), GFP, and an SV40 polyA. This cassette was initially cloned into pGut3 and then inserted into a pEJK25 *via* homologous recombination to create pHD-LRRK2^{G2019S}. HD-LRRK2^{G2019S} was amplified and purified similar to that used for HD-GFP with minor modifications (Cubizolle et al., 2013). The HD-GFP stock used during this study was 1.3×10^{12} pp/ml with an infectious particle to a physical particle ratio of 1:10. The HD-LRRK2^{G2019S} stocks used during this study were $3–7 \times 10^{11}$ pp/ml with an infectious particle to a physical particle ratio of ∼1:25.

Injections

Four monkeys received CAV-GFP injections and were killed 1 month postinjection to assess safety and biodistribution of the CAV-2 in the brain: two of these four monkeys received an injection in the left putamen, and the other two monkeys received bilateral injections in the SN. In one of the latter monkeys, the injections missed the target and therefore was not included in the analyses. Eight monkeys received injections of HD-LRRK2^{G2019S}: four of the eight monkeys received an injection into the left

putamen and were killed as planned 6 months postinjection; and the remaining four monkeys received injections in the SN. One monkey in the latter cohort died due to intracranial hemorrhage at 15 days postinjection. Also, four monkeys received injections of HD-GFP into the left SN. One monkey died due to heart failure. The six remaining monkeys were killed 12 months postinjection. As the neuropathological changes observed 6 months postinjection in the monkeys injected in the putamen with the HD-LRRK2^{G2019S} were sparse, a different timepoint of 12 months postinjection was used for those monkeys that received a nigral injection, to try to induce more robust neuropathological changes. A cohort of four non-injected (intact) animals were used as a control for histological analyses.

Surgery

Stereotaxic surgery was performed according to the coordinates for stereotaxic injections based upon MRI guidance and ventriculography. Before surgery, a brain MRI was performed in each animal under light sedation with an intramuscular injection of ketamine (10 mg/kg) and midazolam (0.5 mg/kg) and. Initial coordinates for injection sites were ascertained using the Osirix Medical Image Software (version 3.9.1). On the day of surgery, the monkeys were anesthetized by intramuscular injections of ketamine and midazolam at the same doses above mentioned. Supplementary doses were given during surgery if necessary. The animals were placed in the stereotaxic frame and the vector delivery was performed following the convection-enhanced delivery (CED) method using an infusion pump (KDS200, LabNet Biotecnica, Madrid, Spain) at a rate of 1 μl/min the first 10 μl, 1.5 μl/min until 20 μl and 2 μl/min until 30 μl. CAV-GFP and HD-LRRK2^{G201S} were injected in 60 μl [1×10^{10} physical particles (pp)] of the corresponding vector divided in two 30 μl injections in left putamen (target 1: $X = 10$, $Y = +1$, $Z = +1$ and target 2: $X = 12$, $Y = 4$, $Z = +3$). A volume of 10 μl with 1×10^{10} pp of the corresponding vector was injected in each SN in CAV-GFP and left SN in HD-LRRK2^{G2019S} and HD-GFP groups (target: $X = 4$, $Y = -8$, $Z = -4$). These volumes were used based on the relative size of the structure being targeted and the advice and collective results from the Bankiewicz lab (UCSF). Coordinates were derived from Martin and Bowden (1996).

PET Scans With ^{11}C- DTBZ and ^{18}F-FDG Ligands

Positron emission tomography (PET) with ^{11}C-(+)-α-dihydro-tetrabenazine (DTBZ; used to quantify the nigrostriatal terminal density) and with ^{18}F-deoxyglucose (FDG; to evaluate the glucose metabolism) were performed as previously described (Blesa et al., 2010).

Transcardiac Perfusion and Tissue Preparation

After an overdose of a mixture of ketamine and midazolam, animals were transcardially perfused with 0.01 M PBS/4% paraformaldehyde (PFA, Sigma–Aldrich, St. Louis, MO, USA). Brains were immediately removed, blocked using a monkey brain matrix (ASI Instruments, Warren, MI, USA) and post-fixed for 2 days in 4% PFA/PBS. The brains were then cryoprotected in a 30% sucrose (Sigma–Aldrich, St. Louis, MO, USA) solution in 0.01 M PBS until processing. Brains were sliced into 40-μm-thick coronal sections along the rostral axis with a freezing microtome (SM 2000R, Leica, Germany) and collected in 0.125 M PBS containing 2% dimethylsulphoxide (Sigma–Aldrich, St. Louis, MO, USA), 20% glycerine (Panreac, Barcelona, Spain) and 0.05% sodium azide (Sigma–Aldrich, St. Louis, MO, USA) and were stored at −20°C until ulterior analysis.

DNA Extraction and qPCR

Total DNA was extracted from fifteen 40-μm-thick PFA-fixed sections from the putamen, motor cortex and the SN of each animal with the QIAamp DNA FFPE Kit (Qiagen, Gaithersburg, MD, USA) and according to manufacturer's protocol (without the deparaffinization step). Right and left hemispheres were analyzed separately. DNA integrity was confirmed by electrophoresis, and its concentration and purity assessed spectrophotometrically. CAV-2 vector genomes were then quantified by PCR (qPCR) using the inverted terminal repeats (ITR) sequences. To detect the amplification products, qPCR was performed on these DNAs with Power SYBR® Green (Applied Biosystems, Foster City, CA, USA) and specific primers using an ABI Prism 7300 sequence detector (Applied Biosystems, Foster City, CA, USA). The primer sequences used for qPCR were forward: AGGACAAAGAGGTGTGGCTTA; reverse: GAACTCGCCCTGTCGTAAAA. The samples were run in triplicate. Data were normalized against the GAPDH sequence amplified using the primers GAPDH forward: CCACCCAGAAGACTGTGGAT; GADPH reverse: TTCAGCTCAGGGATGACCTT. Reference curves were established by determining cycle threshold (Ct) values for the amplification of serial dilutions of the CAV-2 genome.

Histology

Immunohistochemistry (IHC) and immunofluorescence (IF) staining were performed on free-floating sections (see **Table 1** for primary antibodies and **Table 2** for secondary antibodies). Tissue sections were washed in bi-distilled water and 0.01 M PBS to remove the cryoprotectant solution and incubated in PBS with 0.02% hydrogen peroxide (H_2O_2; Merck Millipore, Darmstadt, Germany) for endogenous peroxidase inhibition. After that, they were blocked in 5% normal serum (goat or donkey in the function of the secondary antibody used) with 0.2% Triton X-100 (Sigma–Aldrich, St. Louis, MO, USA) for 60 min and then incubated overnight in the same solution containing a primary antibody. After being rinsed in 0.01 M PBS, tissue sections were incubated in 0.01 M PBS with 5% normal serum and containing the corresponding secondary antibody. The type of antibody, the time of incubation and subsequent steps were dependent on IHC or IF technique performed. In the IHC, the sections were incubated at room temperature with the corresponding biotin secondary antibody for 30 min and after, the sections were rinsed with the vector avidin-biotin complex (1:200 Vectastain ABC kit, Vector Laboratories, Burlingame, CA, USA) for 30 min. Staining for peroxidase was performed with the DAB substrate kit (Vector Laboratories, Burlingame, CA,

TABLE 1 | Primary antibodies used in the study.

Antigen	Host	Source, catalog	Working concentration/ Incubation period (h)	Normal localization
GFP	Rabbit polyclonal	Molecular Probes, A11122 RRID:AB_221569	1:1,000/16	Recognizes the CAV-GFP/ HD-GFP transduced areas
MTCO2	Mouse monoclonal	Abcam, AB3298 RRID:AB_303683	1:500/24	Recognizes mitochondria
NeuN	Mouse monoclonal	Millipore, MAB377 RRID:AB_2298772	1:1,000/24	Neurons
PHF-1	Rabbit polyclonal	Calbiochem, 577815	1:500/24	Recognizes the phospho-Tau epitope ($^{Ser396/Ser404}$)
Tyrosine Hydroxylase (TH)	Mouse monoclonal	Millipore, MAB5280 RRID:AB_2201526	1:1,000/16	Dopaminergic neurons
TH	Rabbit polyclonal	Millipore, AB152 RRID:AB_390204	1:1,000/16	Dopaminergic neurons
VMAT2	Rabbit polyclonal	Novus Biologicals, NBP1-69750 RRID:AB_11035444	1:500/16	Monoaminergic neurons

TABLE 2 | Secondary antibodies used in the study.

Antigen	Host	Source, catalog	Working concentration/Incubation period (h)
Anti-mouse Alexa 546	Goat	Molecular Probes, A11003 RRID:AB_141370	1:500/2
Anti-mouse Alexa 568	Donkey	Molecular Probes, A10037 RRID:AB_2534013	1:500/2
Anti-mouse Alexa 488	Goat	Molecular Probes, A11029 RRID:AB_138404	1:500/2
Anti-mouse Alexa 488	Donkey	Molecular Probes, A21202 RRID:AB_141607	1:500/2
Anti-rabbit Alexa 555	Donkey	Molecular Probes, A31572 RRID:AB_162543	1:500/2
Anti-rabbit Alexa 568	Goat	Molecular Probes, A11011 RRID:AB_143157	1:500/2
Anti-rabbit Alexa 488	Goat	Molecular Probes, A11034 RRID:AB_2576217	1:500/2
Biotin anti-mouse	Goat	Dako, E0433012 RRID:AB_2687905	1:200/0.5
Biotin anti-rabbit	Goat	Dako, E0432 RRID:AB_2313609	1:200/0.5

USA). Finally, the sections were rinsed in double-distilled water and 0.01 M PBS, mounted on gelatin-coated slides and air-dried. The next day, almost all the sections were Nissl counterstained and coverslipped using DPX (VWR, Radnor, PE, USA). In the IF, the corresponding secondary antibody was incubated for 2 h in 0.01 M PBS containing normal donkey/goat serum (1:20). Finally, some sections were counterstained with a nucleic acid stain (TO-PRO-3 iodide, Molecular Probes, Waltham, MA, USA) and coverslipped with mounting medium (Immu-mount, Thermo-Shandon).

Cell Counting and Volume Measurement

The total number of TH^+ and $VMAT2^+$ neurons in the SN were quantified according to the optical fractionator principle (Olympus CAST system, Denmark). Cells in every 14th section were quantified. To determine the area transduced following CAV-GFP injection in the putamen, 40-μm-thick coronal sections were generated and anti-GFP IHC and Nissl counterstaining was performed. Every 12th section, from +7 to −8 (according to the Martin and Bowden atlas) was used. The striatal volume (caudate + putamen) and the volume of GFP-immunoreactivity were quantified according to the Cavalieri principle using CAST software. The transduced area in SN in the animals of the CAV-GFP group was determined using stereology in consecutive serial coronal sections of SN stained using anti-TH and anti-GFP IHC.

Densitometry of pTau Immunoreactivity

Samples were viewed and digitalized with an Olympus BX-51 microscope equipped with an Olympus DP-70 camera using the CAST grid software package (Olympus, Denmark). The images were analyzed using ImageJ software, converted to an 8-bit (binary) format and the background (20 pixels) subtracted. Consequently, the perimeter of each layer was outlined manually for each image excluding any unwanted immune stained structures (i.e., capillary). Then, the same threshold limits were defined for each image and the percentage of immune-reactive area was determined. The images were obtained from different brain regions and different magnification according to the protein in the study. IHC was performed using the same incubation times. The same investigator performed all quantifications with masked sections.

Statistical Analyses

The histological findings (volume, stereology, and densitometry) were analyzed by parametric tests by comparing intact and animals injected with HD-$LRRK2^{G2019S}$ in the putamen, whereas the comparisons between SN-injected HD-GFP/$LRRK2^{G2019S}$ animals were performed with non-parametric analysis. Finally, comparisons between different groups were performed using the Kruskal–Wallis test followed by the Mann–Whitney test (2–2). The results are expressed as a mean ± standard error of the mean (SEM).

RESULTS

CAV-2 Preferentially Infects Neurons and Is Transported to Efferent Regions

Targeting the putamen in the monkey brain is straightforward and allows one to rapidly determine the efficacy of vector transduction and retrograde transport, due to its multiple and well-characterized connections. We, therefore, injected CAV-GFP, a replication-defective CAV-2 vector harboring a GFP expression cassette, in the *M. fascicularis* left putamen. GFP was observed within cell bodies and projections with neuron-like morphology (**Figures 1A–G**). The GFP signal in the putamen and caudate (**Figure 1A**) corresponds to a volume of 540 mm^3 (∼47% of total striatum (1,140 mm^3), with an approximative ratio between injected volume and transduced volume of 1:9. We also detected GFP expression in the soma of cells located in the injected and contralateral motor cortex, claustrum, parafascicularis, centromedian thalamus nuclei, and in the SN,

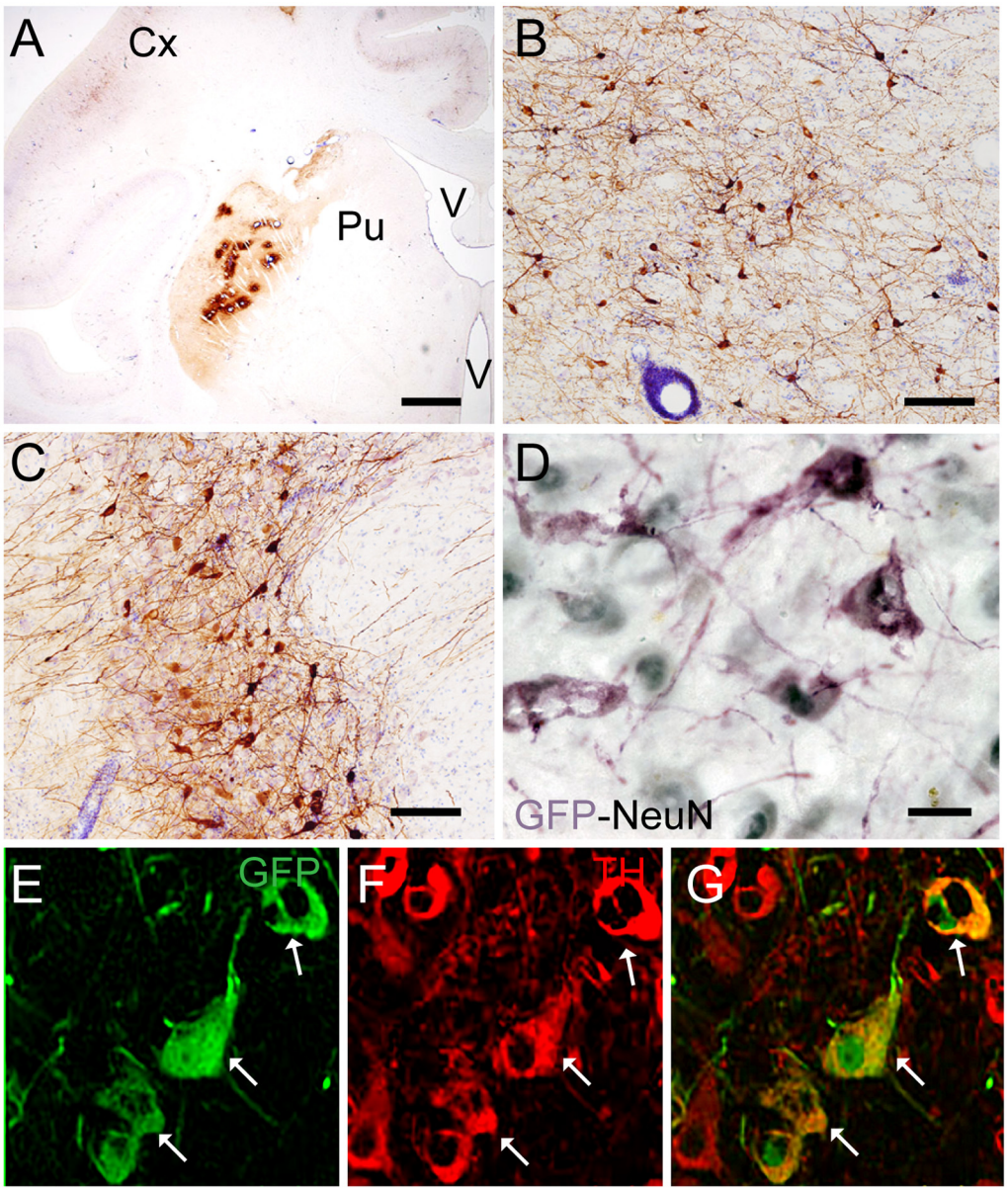

FIGURE 1 | Coronal sections of animals injected with canine adenovirus type (CAV)-GFP in the left putamen. **(A)** Low magnification of immunohistochemistry (IHC) against GFP and Nissl counterstained of the injected putamen; **(B)** higher magnification of IHC against GFP and Nissl counterstained of the injected thalamus; **(C)** IHC against GFP and Nissl counterstained of the substantia nigra (SN) of the injected hemisphere; **(D)** IHC against GFP (pink) and NeuN (black) in the SN of the injected hemisphere; and in the contralateral SN **(E)** immunofluorescence (IF) against GFP (green; **F**) IF against TH (red; **G**) merge of **(E,F)**. White arrows denoted TH^+/GFP^+ cells. Scale bars: **(A)** 1 mm; **(B,C)** 100 μm; **(D)** 10 μm; **(E)** 5 μm.

where the majority were NeuN$^+$ (**Figure 1D**). We also quantified the efficacy of retrograde transport from the putamen to the SN. In this pilot assay, ∼5% of the ∼1,20,000 TH$^+$ cells neurons in the ipsilateral SN were GFP$^+$. Of note, we also found a handful of GFP$^+$/TH$^+$ cells in the contralateral SN (**Figures 1E–G**). Together, these data demonstrate CAV-2 vector infection at the site of injection, the retrograde transport from the putamen to efferent regions, and that the monkey SN sends DA projection to the striatum in each hemisphere.

Injections of HD-LRRK2G2019S in the Putamen

We then explored the injection of HD-LRRK2^{G2019S} (Mestre-Francés et al., 2018) in the *Macaca fascicularis* brain. Because dopaminergic neurons in the SN are lost in Parkinson's disease patients, our null hypothesis was that one may need to target these neurons to induce disease-like features. Notably, striatal injection of CAV-2 vectors leads to a transduction efficacy of ∼70% of the dopaminergic neurons in the SN of the gray mouse lemur (Mestre-Francés et al., 2018). While the injection of CAV-GFP in the monkey putamen suggested that technical improvements would be needed to reach this level, a non-cell autonomous effect of LRRK2^{G2019S} activity might impact the putamen and/or SN (di Domenico et al., 2019). We, therefore, injected four monkeys in the left putamen with HD-LRRK2^{G2019S}. Of note, in the gray mouse lemur, we found no adverse physiological, histological, or biological effects from a control vector (HD-GFP) injections. Nonetheless, because a cohort of monkeys injected with HD-GFP was not performed at this stage, the below results are only suggestive.

To determine if LRRK2^{G2019S} activity could influence nigrostriatal termini density or DA uptake in the striatum, we measured ^{11}C-DTBZ and ^{18}F-FDG levels by PET. Compared to pre-injection levels, we found a decrease in DTBZ uptake throughout the injected striatum at 15 days postinjection, which remained stable during the 6-months follow-up (**Figure 2A**). When the anterior and posterior striatum were analyzed separately, we found that DTBZ uptake was reduced during the first month in the anterior putamen (**Figure 2B**), and a progressive reduction in the posterior putamen (**Figure 2C**). DTBZ uptake in the caudate was relatively stable (**Figure 2D**). FDG-PET scans at 0.5, 3, and 6 months postinjection showed bilateral hypermetabolism in the ventral striatum, thalamus and midbrain at 6 months (**Figures 2E–G**). Quantification suggested that the ipsilateral pre-frontal gyro, bilateral superior frontal gyro, and bilateral thalamus displayed hypermetabolism 3 months postinjection. We also noted a trend towards a mild, bilateral, parieto-occipital hypometabolism (**Figure 2G**).

After the *in vivo* follow-up, the monkeys were killed, the brains fixed, and prepared for downstream assays. Initially, we found no difference in the number of TH$^+$ cells between the injected vs. the contralateral hemisphere (1,04,000 ± 24,000 vs. 1,14,000 ± 22,000, respectively), or in the number of VMAT$^+$ cells (1,14,000 ± 22,400 vs. 1,19,000 ± 14,000, respectively). In contrast to the contralateral hemisphere, some SN cells in the injected hemisphere presented with dystrophic neurites, and broken and swollen axons (**Figures 3A,B**). Also, the somas of some nigral neurons were fusiform and more mitochondrially-encoded cytochrome C oxidase II (MTCO2) immunoreactive (**Figures 3C,D**). The presence of pTau$^{Ser395/Ser404}$ in cortex regions is a common feature in LRRK2 model systems (MacLeod et al., 2006; Li et al., 2009; Melrose et al., 2010) and 79% of LRRK2 mutation carriers have been reported to have tau pathology (Poulopoulos et al., 2012). We, therefore, assayed for pTau$^{Ser395/Ser404}$ accumulation. We found increased IR in the white matter of the prefrontal, motor cortex and internal capsule of the injected vs. that from contralateral hemisphere and intact animals (**Figures 4A,B**). Finally, we used brain sections from the SN, putamen and motor cortex to isolate total DNA. Using qPCR targeting a conserved part of each vector sequence, we detected genomes in both hemispheres, with levels consistently higher in the injected hemisphere (**Table 3**).

Together, these data suggest but do not unequivocally demonstrate, that expression of LRRK2^{G2019S} induces some of the histopathological hallmarks present in patients with genetic Parkinson's disease. Although HD-CAV-2 vectors lead to long-term transgene expression *in vivo*, and that it is unlikely that capsid uptake still had an effect on neurons 6 months postinjection (Piersanti et al., 2015; Mestre-Francés et al., 2018; del Rio et al., 2019), further controls need to be performed to show that these phenotypes are not linked to the CAV-2 capsid.

CAV-GFP, HD-GFP, and HD-LRRK2G2019S Injections Into the SN

If a cell-autonomous effect of LRRK2^{G2019S} is responsible for the loss of SN neurons in Parkinson's disease, then gene transfer needs to be more efficient in these cells. Therefore, in the second set of pilot assays, we bilaterally injected CAV-GFP in the SN to test vector efficacy. GFP$^+$ neurons were detected in the SN, motor cortex, putamen, caudate, lateral hypothalamus, and the pedunculopontine nucleus bilaterally (**Figures 5A–G**). Of note, ∼72% of the TH$^+$ cells in SNs were GFP$^+$.

These data prompted us to compare HD-GFP (a HD CAV-2 vector expressing GFP) and HD-LRRK2^{G2019S} injections in the SN. The results from six monkeys (three received HD-LRRK2^{G2019S} and three received HD-GFP) injected in the left SN are shown. During the 6-month follow-up, we found no notable differences in DTBZ or FDG uptake in HD-LRRK2^{G2019S}-injected vs. the HD-GFP-injected animals, or between the injected and non-injected hemisphere (not shown). The monkeys were killed, and the brains were prepared for histology and stereology. While the number of VMAT2$^+$ cells was similar in all 12 SNs (i.e., three HD-GFP- and three HD-LRRK2^{G2019S}-injected hemispheres, and the six non-injected hemispheres) there was a modest reduction in the number of TH$^+$ cells in the injected hemispheres (**Table 4**). We then compared pTau$^{Ser395/Ser404}$ IR in HD-LRRK2^{G2019S}- vs. HD-GFP-injected animals. While, we found no differences in pTau$^{Ser395/Ser404}$ IR in the internal capsule, there was a modest increase in the frontal and motor cortex of HD-LRRK2^{G2019S}-injected monkeys (**Figure 6**). Finally, we found vector genomes in both hemispheres and, as expected, higher levels in the injected hemispheres (**Table 5**).

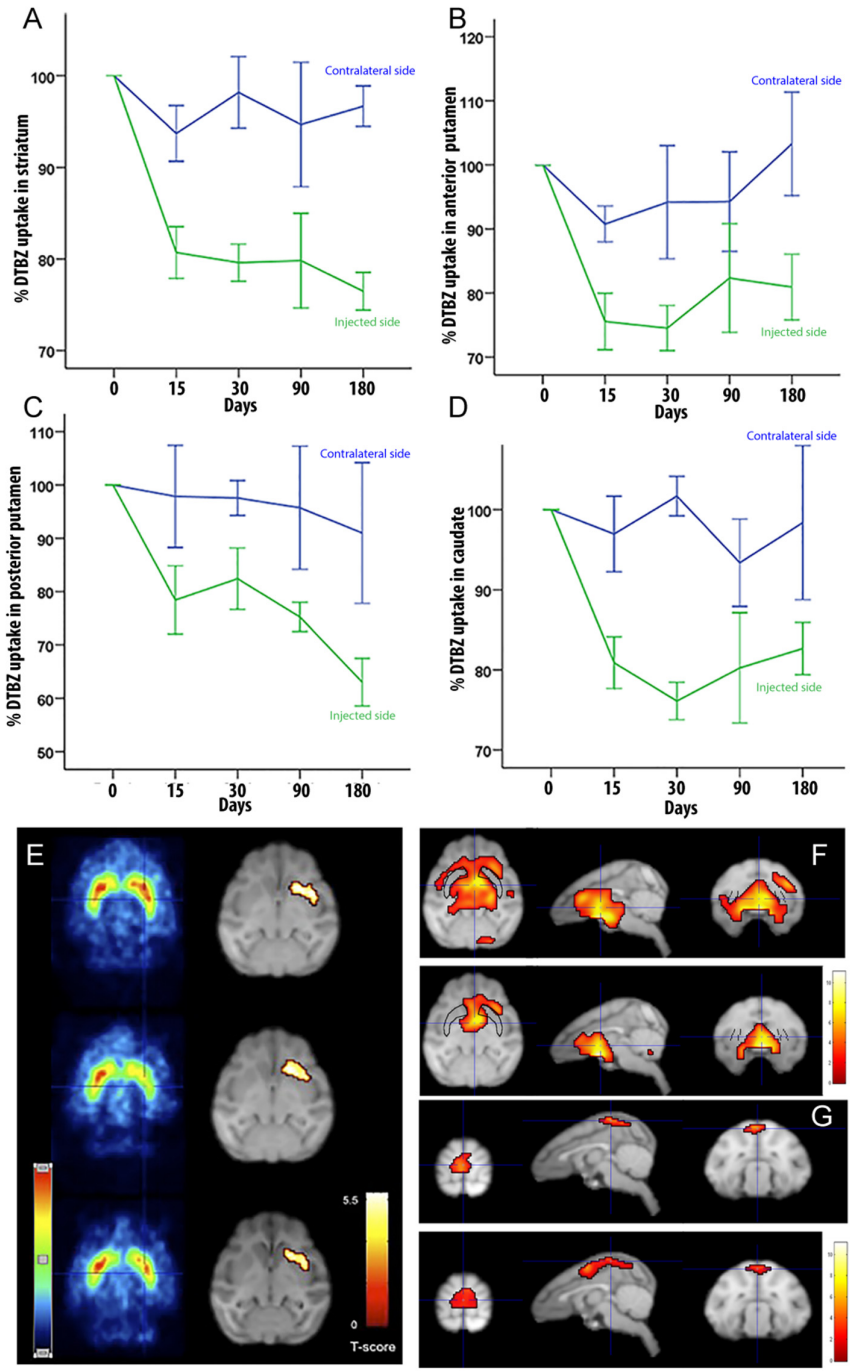

FIGURE 2 | Quantification of DTBZ and FDG uptake *via* PET scan following putamen injections of helper-dependent (HD)-LRRK2^{G2019S}. **(A)** Representative image of DTBZ-PET scan in the striatum; **(B)** anterior putamen; **(C)** posterior putamen; and **(D)** caudate. SPM analysis of the FDG PET scan showing **(E)** reduction in the hypermetabolic areas. SPM analyses suggested a change in dopaminergic uptake ($p \leq 0.001$) in the left striatum that remained stable at 0.5, 3, and 6 months after surgery right column; and **(F–G)** changes in the hypometabolic areas.

Together, these data suggest that following unilateral HD-LRRK2^{G2019S} injection into the SN, LRRK2^{G2019S} increased pTau$^{Ser395/Ser404}$ levels, but did not induce changes in nigrostriatal terminal density or glucose metabolism in the striatum, or the number of VMAT2^{+} cells in the SN.

DISCUSSION

Similar to the results found in other species (del Rio et al., 2019), we demonstrated here that CAV-2 preferentially infects neurons and is transported to efferent sites when injected into the

M. fascicularis brain parenchyma. These data are consistent with the neuronal expression of the coxsackievirus and adenovirus receptor (CAR) and its role in axonal transport in rodent neurons (Salinas et al., 2009; Loustalot et al., 2016; Zussy et al., 2016). While little is known concerning CAR in the *M. fascicularis* brain, CAR expression pattern (i.e., in which subtype/population of neurons and in which structure), as well as the monkey neuroanatomical connections, and brain size, likely influenced CAV-2 vector tropism and biodistribution efficacy.

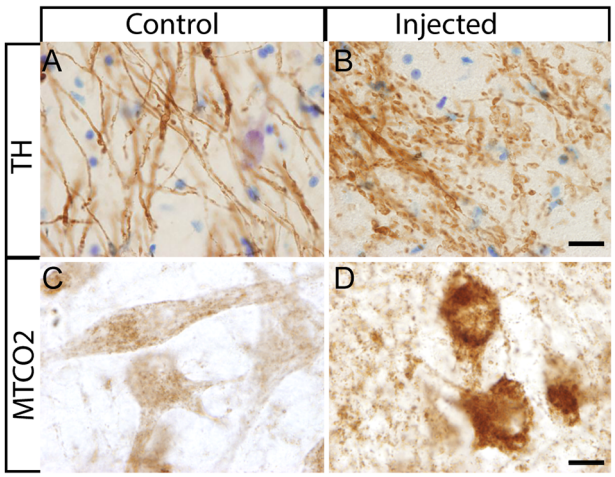

FIGURE 3 | Histological aspect of nigral neurons after the injection of HD-LRRK2^{G2019S} in the putamen. **(A,B)** IHC against TH and Nissl counterstained in the SN from an intact monkey and in the SN from a monkey injected in the putamen. Dystrophic neurites (broken and swollen axons) in the injected hemisphere. **(C,D)** IHC against mitochondrially-encoded cytochrome C oxidase II (MTCO2) in nigral neurons of an intact monkey and a representative image from an HD-LRRK2G2019S injected monkey. Scale bars = 20 μm.

The mean age of PD onset for LRRK2^{G2019S} mutation carriers is 57.5 years (Healy et al., 2008), which is similar to the age of onset of idiopathic PD, and suggest that age-related factors can also play a role in the genesis of symptoms in these patients. In our pilot assays, we used 4–5 years old monkeys, which may have precluded the rapid inception of functional and/or histological LRRK2^{G2019S}-associated disease phenotype. Of note, we also used the relatively weak RSV promoter to drive LRRK^{G2019S} expression to better mimic physiological levels, and therefore disease progression. While injections in the putamen led to a lower efficacy of SN infection, they appeared to induce greater impact concerning perturbed striatal metabolic activity and histological factors. Whether these data reflect a greater pathological role for LRRK2^{G2019S} activity in the neurons in the putamen vs. those in the SN, or that the neurodegenerative process could begin in the nigrostriatal projections (Burke and O'Malley, 2013) needs more analyses. However, if this is the case, bilateral putamen injections in aged monkeys will likely allow more robust disease inception. Consistent with this reasoning, the modest reduction of DTBZ uptake in the contralateral putamen may be indicative of the impact of bilateral SN projections and compensatory effects. Interestingly, following HD-LRRK2^{G2019S} putamen injections the changes in DTBZ uptake resembles that seen patients (De La Fuente-Fernández et al., 2003; Ishibashi et al., 2014), and is in contrasts to that seen following MPTP intoxication (Snow et al., 2000; Blesa et al., 2010). While we did not compare DTBZ uptake to putamen injection of HD-GFP, our observations mirror the data from pre-symptomatic carriers of an LRRK2 mutation (Adams et al., 2005; Nandhagopal et al., 2008). The modest reduction in radiotracer uptake by the striatum could be indicative of the

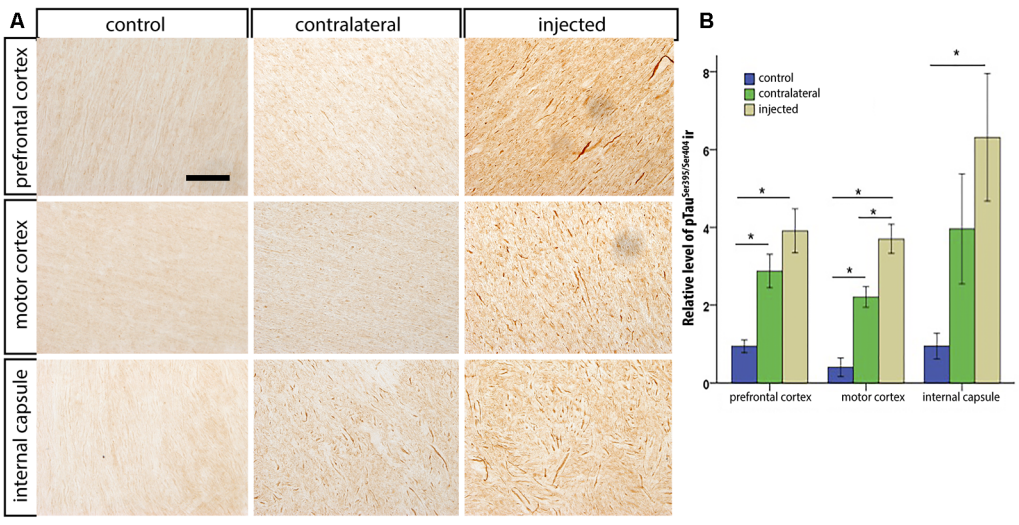

FIGURE 4 | pTau$^{Ser395/Ser404}$ immunoreactivity following HD-LRRK2^{G2019S} injections in the putamen: pTau$^{Ser395/Ser404}$ immunoreactivity in the internal capsule in **(A)** an intact animal (control), contralateral hemisphere, and injected hemisphere. Scale bar, 100 μm. **(B)** Quantification of pTau$^{Ser395/Ser404}$ immunoreactivity by optic densitometry. *$p \leq 0.05$ (student's *t*-test).

TABLE 3 | Vector genomes in the HD-LRRK2^{G2019S} putamen-injected cohort.

Left hemisphere (injected)			Right hemisphere		
SN	**putamen**	**cortex**	**SN**	**putamen**	**cortex**
7,070 (±2,320)	23,100 (± 8,960)	1,530 (± 270)	1,190 (± 390)	4,080 (± 325)	637 (± 90)

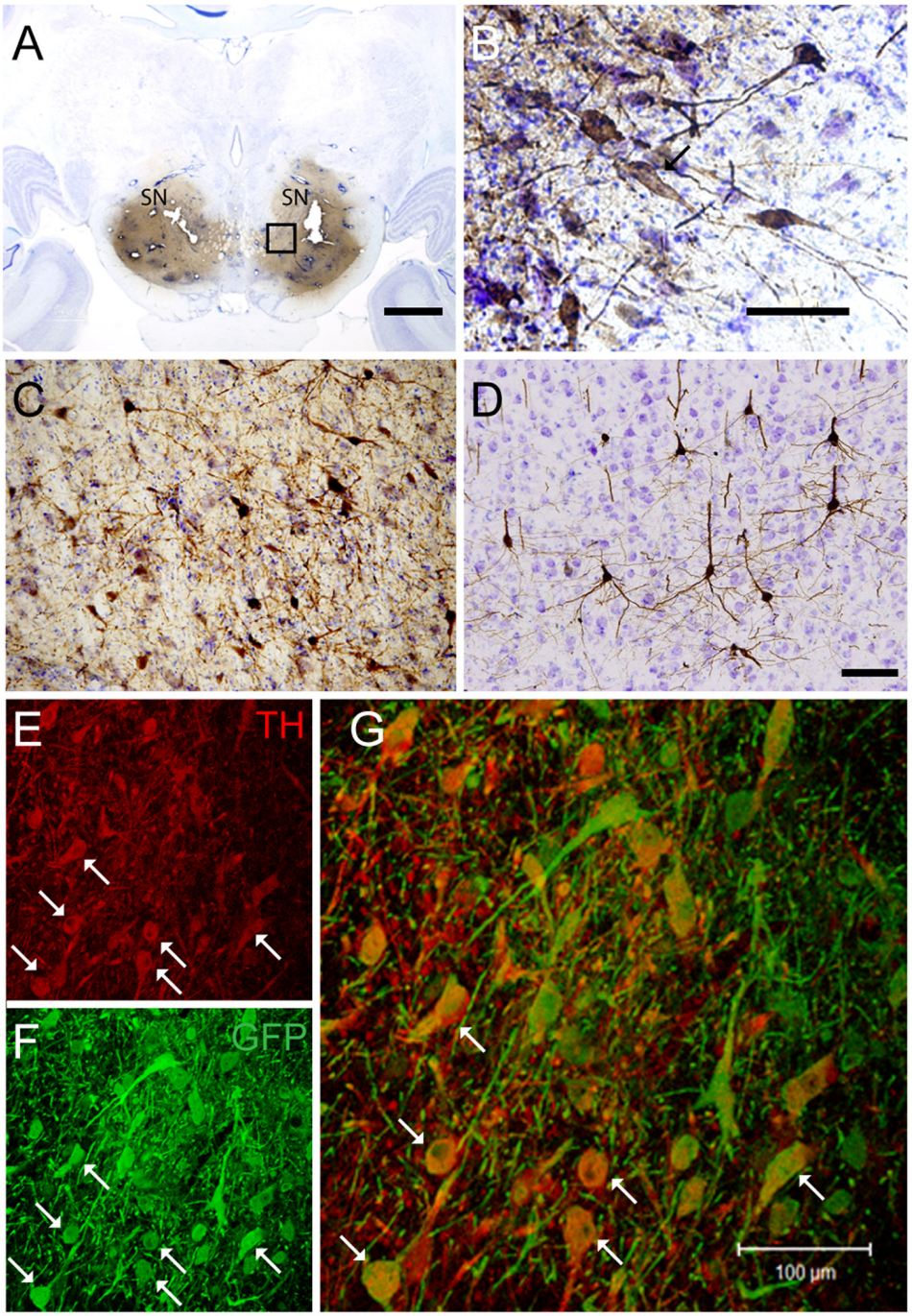

FIGURE 5 | CAV-GFP injection in macaque SN. Coronal sections of animals injected bilaterally in the SN. **(A)** Low magnification of IHC against GFP and Nissl counterstained of an injected SNs; **(B)** higher magnification of GFP expression and Nissl counterstaining in the SN; and **(C)** GFP-IR in the pedunculopontine tegmental nucleus; **(D)** GFP-IR in the motor cortex; **(E,F)** IF against GFP (green) and TH (red) in an SN **(G)** merge of **(E,F)**. White arrows denoted TH$^+$/GFP$^+$ cells. Scale bars **(A)** 5 mm; **(B–D)** 100 μm; **(E)** 20 μm.

TABLE 4 | TH^+ and $VMAT2^+$ cells in the SN.

Cohort	Side	TH^+ neurons mean (SD)	$VMAT2^+$ neurons mean (SD)	*p* TH/VMAT2*
HD-LRRK2^{G2019S}-SN	Right	1,24,000 (± 16,600)	86,300 (± 6,340)	0.08/0.03
	Left	1,04,000 (± 3,870)	87,300 (± 17,100)	0.03/0.03
HD-GFP -SN	Right	115,000 (± 10,200)	91,700 (± 17,400)	0.03/0.03
	Left	99,500 (± 2,500)	91,600 (± 27,800)	0.03/0.03

**U-Mann Whitney test.*

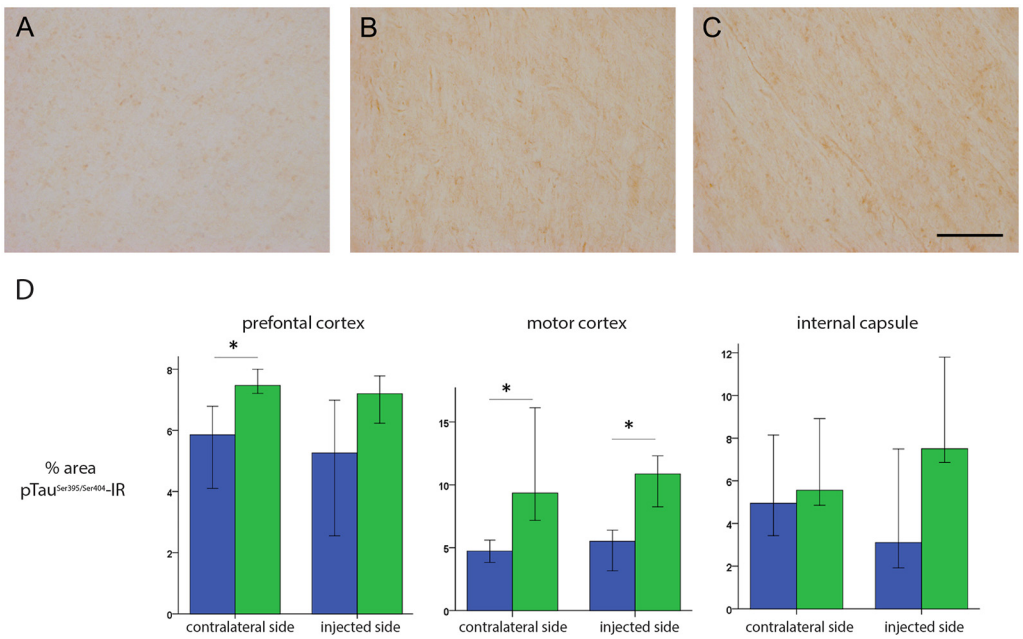

FIGURE 6 | pTau$^{Ser395/Ser404}$ IR following HD-GFP or HD-LRRK2^{G2019S} injection in the SN. Representative images of pTau$^{Ser395/Ser404}$ IR from the frontal cortex of **(A)** an intact animal; **(B)** the contralateral hemisphere and **(C)** the injected hemisphere. **(D)** Quantification of signal intensity from pTau$^{Ser395/Ser404}$ IR in the prefrontal cortex, motor cortex and internal capsule (n = 3 monkeys). Scale bar = 200 μm; $^*p \leq 0.05$.

TABLE 5 | Vector genomes in the SN-injected cohort.

	Left hemisphere			Right hemisphere		
	SN	putamen	cortex	SN	putamen	cortex
HD-GFP	80,000 (± 22,500)	2,550 (± 1,320)	186 (± 42)	7,450 (± 2,520)	49 (± 260)	65 (± 29)
HD-LRRK2^{G2019S}	2,20,000 (± 34,500)	1,270 (± 145)	434 (± 142)	2,840 (± 595)	552 (± 124)	76 (± 40)

preclinical phase of Parkinson's disease, which is estimated to be an annual reduction of 4.7% (Hilker et al., 2005). We do not know if the decrease in DTBZ uptake in these monkeys would have continued and led to the motor manifestations of Parkinson's disease.

Importantly, the morphological anomalies we found are similar to reports using other LRRK2 forms (Li et al., 2009; Ramonet et al., 2011), and were not found in the HD-GFP-injected animals. Interestingly, LRRK2^{G2019S} was able to increase the level of pTau$^{Ser395/Ser404}$ in fibers of brain regions that project into the putamen or SN. Tau binds tubulin to stabilize microtubules and promotes tubulin assembly into microtubules. The maintenance of cellular morphology and transport of molecules and organelles over long distances depends on microtubules stabilization by tau in neurons and altered tau function could block the transport of organelles, neurofilaments, and vesicles (Spires-Jones et al., 2009). Our results agree with those reported by Melrose et al. (2010) who described a similar increase in pTau$^{Ser395/Ser404}$ IR in white matter fibers in the thalamus, hypothalamus, striatum, and midbrain, as well as tracts in the pontine base and medulla of LRRK2^{G2019S} mice. Finally, 21–54% of LRRK2-associated Parkinson's disease patients do not show apparent Lewy bodies in the SN although they show loss of dopaminergic neurons in this area (Poulopoulos et al., 2012; Kalia et al., 2015). Also, higher grade tau pathology in cortical areas is a prominent feature of LRRK2-associated Parkinson's disease (Henderson et al., 2019).

In summary, our study demonstrates that CAV-2 vectors are powerful tools for gene transfer to the *M. fascicularis* brain and that, following optimization, CAV-2–mediated expression of LRRK2^{G2019S} may be used to induce a functional impairment of the nigrostriatal dopaminergic system inducing histological changes.

DATA AVAILABILITY STATEMENT

The datasets generated for this study are available on request to the corresponding author.

ETHICS STATEMENT

The animal study was reviewed and approved by Ethics Committee for Animal Experimentation of the University of Navarra.

AUTHOR CONTRIBUTIONS

RL and EK: study concept, design, and supervision. AG and EK: design and production of viral vectors. CC and I-CM: primates surgery. CC and IM: behavior test and data analyses. CC, IM, and MC-A: PET scan images acquisition and analysis. CC, I-CM, IM and MH: acquisition, analysis, and interpretation of histological data. IM-V: DNA extraction and PCR data analysis. CC: statistical analyses. IM-V and CC: initial draft of the manuscript. EK and RL: critical revision of the manuscript.

FUNDING

We thank the European Commission Seventh Framework Programme (FP7) CP (BrainCAV: FP7-HEALTH-2007-222992, EK and RL) and BrainVectors (FP7-HEALTH-2012-286071, EK); Government of Navarra (CTP-09-P8, RL); Foundation for Applied Medical Research (RL); Universidad de Navarra (RL); France Parkinson's (EK), Association pour la recherche sur la sclérose latérale amyotrophique (EK); Université de Montpellier (EK), La Fondation pour la Recherche Médicale (EK); and the LabEx EpiGenMed (EK). IM-V was supported by "Asociación de Amigos de la Universidad de Navarra."

ACKNOWLEDGMENTS

We thank the members of our laboratories for constructive comments throughout this study, in particular Iria G. Dopeso-Reyes. We thank K. Bankiewicz for advice and training in CED. We thank Thierry Gostan (Seranad) for help with statistical analyses, the MRI and RHEM platforms in Montpellier.

REFERENCES

Adams, J. R., van Netten, H., Schulzer, M., Mak, E., Mckenzie, J., Strongosky, A., et al. (2005). PET in LRRK2 mutations: comparison to sporadic Parkinson's disease and evidence for presymptomatic compensation. *Brain* 128, 2777–2785. doi: 10.1093/brain/awh607

Andres-Mateos, E., Mejias, R., Sasaki, M., Li, X., Lin, B. M., Biskup, S., et al. (2009). Unexpected lack of hypersensitivity in LRRK2 knock-out mice to MPTP (1-methyl-4-phenyl-1,2,3,6-tetrahydropyridine). *J. Neurosci.* 29, 15846–15850. doi: 10.1523/JNEUROSCI.4357-09.2009

Bichler, Z., Lim, H. C., Zeng, L., and Tan, E. K. (2013). Non-motor and motor features in LRRK2 transgenic mice. *PLoS One* 8:e70249. doi: 10.1371/journal.pone.0070249

Blesa, J., Juri, C., Collantes, M., Peñuelas, I., Prieto, E., Iglesias, E., et al. (2010). Progression of dopaminergic depletion in a model of MPTP-induced Parkinsonism in non-human primates. An ^{18}F-DOPA and ^{11}C-DTBZ PET study. *Neurobiol. Dis.* 38, 456–463. doi: 10.1016/j.nbd.2010.03.006

Burke, R. E., and O'Malley, K. (2013). Axon degeneration in Parkinson's disease. *Exp. Neurol.* 246, 72–83. doi: 10.1016/j.expneurol.2012.01.011

Chen, C.-Y., Weng, Y.-H., Chien, K.-Y., Lin, K.-J., Yeh, T.-H., Cheng, Y.-P., et al. (2012). (G2019S) LRRK2 activates MKK4-JNK pathway and causes degeneration of SN dopaminergic neurons in a transgenic mouse model of PD. *Cell Death Differ.* 19, 1623–1633. doi: 10.1038/cdd.2012.42

Chou, J. S., Chen, C. Y., Chen, Y. L., Weng, Y. H., Yeh, T. H., Lu, C. S., et al. (2014). (G2019S) LRRK2 causes early-phase dysfunction of SNpc dopaminergic neurons and impairment of corticostriatal long-term depression in the PD transgenic mouse. *Neurobiol. Dis.* 68, 190–199. doi: 10.1016/j.nbd.2014.04.021

Cubizolle, A., Serratrice, N., Skander, N., Colle, M.-A., Ibanes, S., Gennetier, A., et al. (2013). Corrective GUSB transfer to the canine mucopolysaccharidosis VII brain. *Mol. Ther.* 22, 762–773. doi: 10.1038/mt.2013.283

Dai, Y., Schwarz, E. M., Gu, D., Zhang, W. W., Sarvetnick, N., and Verma, I. M. (1995). Cellular and humoral immune responses to adenoviral vectors containing factor IX gene: tolerization of factor IX and vector antigens allows for long-term expression. *Proc. Natl. Acad. Sci. U S A* 92, 1401–1405. doi: 10.1073/pnas.92.5.1401

Dawson, T. M., Ko, H. S., and Dawson, V. L. (2010). Genetic animal models of Parkinson's disease. *Neuron* 66, 646–661. doi: 10.1016/j.neuron.2010.04.034

De La Fuente-Fernández, R., Lim, A. S., Sossi, V., Adam, M. J., Ruth, T. J., Calne, D. B., et al. (2003). Age and severity of nigrostriatal damage at onset of Parkinson's disease. *Synapse* 47, 152–158. doi: 10.1002/syn.10160

del Rio, D., Beucher, B., Lavigne, M., Wehbi, A., Gonzalez Dopeso-Reyes, I., Saggio, I., et al. (2019). CAV-2 vector development and gene transfer in the central and peripheral nervous systems. *Front. Mol. Neurosci.* 12:71. doi: 10.3389/fnmol.2019.00071

di Domenico, A., Carola, G., Calatayud, C., Pons-Espinal, M., Muñoz, J. P., Richaud-Patin, Y., et al. (2019). Patient-specific iPSC-derived astrocytes contribute to non-cell-autonomous neurodegeneration in Parkinson's disease. *Stem Cell Reports* 12, 213–229. doi: 10.1016/j.stemcr.2018.12.011

Dusonchet, J., Kochubey, O., Stafa, K., Young, S. M., Zufferey, R., Moore, D. J., et al. (2011). A rat model of progressive nigral neurodegeneration induced by the Parkinson's disease-associated G2019S mutation in LRRK2. *J. Neurosci.* 31, 907–912. doi: 10.1523/JNEUROSCI.5092-10.2011

Gasser, T., Hardy, J., and Mizuno, Y. (2011). Milestones in PD genetics. *Mov. Disord.* 26, 1042–1048. doi: 10.1002/mds.23637

Gloeckner, C. J., Kinkl, N., Schumacher, A., Braun, R. J., O'Neill, E., Meitinger, T., et al. (2006). The Parkinson disease causing LRRK2 mutation I2020T is associated with increased kinase activity. *Hum. Mol. Genet.* 15, 223–232. doi: 10.1093/hmg/ddi439

Godena, V. K., Brookes-Hocking, N., Moller, A., Shaw, G., Oswald, M., Sancho, R. M., et al. (2014). Increasing microtubule acetylation rescues axonal transport and locomotor deficits caused by LRRK2 Roc-COR domain mutations. *Nat. Commun.* 5:5245. doi: 10.1038/ncomms6245

Guo, L., Gandhi, P. N., Wang, W., Petersen, R. B., Wilson-Delfosse, A. L., and Chen, S. G. (2007). The Parkinson's disease-associated protein, leucine-rich repeat kinase 2 (LRRK2), is an authentic GTPase that stimulates kinase activity. *Exp. Cell Res.* 313, 3658–3670. doi: 10.1016/j.yexcr.2007.07.007

Healy, D. G., Falchi, M., O'Sullivan, S. S., Bonifati, V., Durr, A., Bressman, S., et al. (2008). Phenotype, genotype, and worldwide genetic penetrance of LRRK2-associated Parkinson's disease: a case-control study. *Lancet Neurol.* 7, 583–590. doi: 10.1016/S1474-4422(08)70117-0

Henderson, M. X., Sengupta, M., Trojanowski, J. Q., and Lee, V. M. Y. (2019). Alzheimer's disease tau is a prominent pathology in LRRK2 Parkinson's disease. *Acta Neuropathol. Commun.* 7:183. doi: 10.1186/s40478-019-0836-x

Hilker, R., Schweitzer, K., Coburger, S., Ghaemi, M., Weisenbach, S., Jacobs, A. H., et al. (2005). Nonlinear progression of Parkinson disease as determined by serial positron emission tomographic imaging of striatal fluorodopa F 18 activity. *Arch. Neurol.* 62, 378–382. doi: 10.1001/archneur.62.3.378

Hinkle, K. M., Yue, M., Behrouz, B., Dächsel, J. C., Lincoln, S. J., Bowles, E. E., et al. (2012). LRRK2 knockout mice have an intact dopaminergic system but display alterations in exploratory and motor co-ordination behaviors. *Mol. Neurodegener.* 7:25. doi: 10.1186/1750-1326-7-25

Ishibashi, K., Oda, K., Ishiwata, K., and Ishii, K. (2014). Comparison of dopamine transporter decline in a patient with Parkinson's disease and normal aging effect. *J. Neurol. Sci.* 339, 207–209. doi: 10.1016/j.jns.2014.01.015

Ito, G., Okai, T., Fujino, G., Takeda, K., Ichijo, H., Katada, T., et al. (2007). GTP binding is essential to the protein kinase activity of LRRK2, a causative gene product for familial Parkinson's disease. *Biochemistry* 46, 1380–1388. doi: 10.1021/bi061960m

Junyent, F., and Kremer, E. J. (2015). CAV-2—why a canine virus is a neurobiologist's best friend. *Curr. Opin. Pharmacol.* 24, 86–93. doi: 10.1016/j.coph.2015.08.004

Kalia, L. V., Lang, A. E., Hazrati, L. N., Fujioka, S., Wszolek, Z. K., Dickson, D. W., et al. (2015). Clinical correlations with lewy body pathology in LRRK2-related Parkinson disease. *JAMA Neurol.* 72, 100–105. doi: 10.1001/jamaneurol.2014.2704

Kremer, E. J., Boutin, S., Chillon, M., and Danos, O. (2000). Canine adenovirus vectors: an alternative for adenovirus-mediated gene transfer. *J. Virol.* 74, 505–512. doi: 10.1128/jvi.74.1.505-512.2000

Lasbleiz, C., Mestre-Francés, N., Devau, G., Luquin-Piudo, M., Tenenbaum, L., Kremer, E. J., et al. (2019). Combining gene transfer and nonhuman primates to better understand treat Parkinson's disease. *Front. Mol. Neurosci.* 12:10. doi: 10.3389/fnmol.2019.00010

Law, B. M. H., Spain, V. A., Leinster, V. H. L., Chia, R., Beilina, A., Cho, H. J., et al. (2014). A direct interaction between leucine-rich repeat kinase 2 and specific β-tubulin isoforms regulates tubulin acetylation. *J. Biol. Chem.* 289, 895–908. doi: 10.1074/jbc.M113.507913

Lee, H., Melrose, H. L., Yue, M., Pare, J.-F. F., Farrer, M. J., and Smith, Y. (2010). Lrrk2 localization in the primate basal ganglia and thalamus: a light and electron microscopic analysis in monkeys. *Exp. Neurol.* 224, 438–447. doi: 10.1016/j.expneurol.2010.05.004

Lee, J.-W., Tapias, V., Di Maio, R., Greenamyre, J. T., and Cannon, J. R. (2015). Behavioral, neurochemical, and pathologic alterations in bacterial artificial chromosome transgenic G2019S leucine-rich repeated kinase 2 rats. *Neurobiol. Aging* 36, 505–518. doi: 10.1016/j.neurobiolaging.2014.07.011

Lentz, T. B., Gray, S. J., and Samulski, R. J. (2012). Viral vectors for gene delivery to the central nervous system. *Neurobiol. Dis.* 48, 179–188. doi: 10.1016/j.nbd.2011.09.014

Li, Y., Liu, W., Oo, T. F., Wang, L., Tang, Y., Jackson-Lewis, V., et al. (2009). Mutant LRRK2(R1441G) BAC transgenic mice recapitulate cardinal features of Parkinson's disease. *Nat. Neurosci.* 12, 826–828. doi: 10.1038/nn.2349

Li, X., Patel, J. C., Wang, J., Avshalumov, M. V., Nicholson, C., Buxbaum, J. D., et al. (2010). Enhanced striatal dopamine transmission and motor performance with LRRK2 overexpression in mice is eliminated by familial Parkinson's disease mutation G2019S. *J. Neurosci.* 30, 1788–1797. doi: 10.1523/JNEUROSCI.5604-09.2010

Li, X., Tan, Y.-C., Poulose, S., Olanow, C. W., Huang, X.-Y., and Yue, Z. (2007). Leucine-rich repeat kinase 2 (LRRK2)/PARK8 possesses GTPase activity that is altered in familial Parkinson's disease R1441C/G mutants. *J. Neurochem.* 103, 238–247. doi: 10.1111/j.1471-4159.2007.04743.x

Lin, X., Parisiadou, L., Gu, X., Wang, L., Shim, H., Xie, C., et al. (2009). Leucine-rich repeat kinase 2 regulates the progression of neuropathology induced by Parkinson's disease-related mutantα-synuclein. *Neuron* 64, 807–827. doi: 10.1016/j.neuron.2009.11.006

Loustalot, F., Kremer, E. J., and Salinas, S. (2016). Membrane dynamics and signaling of the coxsackievirus and adenovirus receptor. *Int. Rev. Cell Mol. Biol.* 322, 331–362. doi: 10.1016/bs.ircmb.2015.10.006

MacLeod, D. A., Dowman, J., Hammond, R., Leete, T., Inoue, K., and Abeliovich, A. (2006). The familial Parkinsonism gene LRRK2 regulates neurite process morphology. *Neuron* 52, 587–593. doi: 10.1016/j.neuron.2006.10.008

MacLeod, D. A., Rhinn, H., Kuwahara, T., Zolin, A., Di Paolo, G., McCabe, B. D., et al. (2013). RAB7L1 interacts with LRRK2 to modify intraneuronal protein sorting and Parkinson's disease risk. *Neuron* 77, 425–439. doi: 10.1016/j.neuron.2012.11.033

Martin, R. F., and Bowden, D. M. (1996). A stereotaxic template atlas of the macaque brain for digital imaging and quantitative neuroanatomy. *NeuroImage* 4, 119–150. doi: 10.1006/nimg.1996.0036

Matta, S., Van Kolen, K., da Cunha, R., van den Bogaart, G., Mandemakers, W., Miskiewicz, K., et al. (2012). LRRK2 controls an EndoA phosphorylation cycle in synaptic endocytosis. *Neuron* 75, 1008–1021. doi: 10.1016/j.neuron.2012.08.022

Melrose, H. L., Dächsel, J. C., Behrouz, B., Lincoln, S. J., Yue, M., Hinkle, K. M., et al. (2010). Impaired dopaminergic neurotransmission and microtubule-associated protein tau alterations in human LRRK2 transgenic mice. *Neurobiol. Dis.* 40, 503–517. doi: 10.1016/j.nbd.2010.07.010

Mestre-Francés, N., Serratrice, N., Gennetier, A., Devau, G., Cobo, S., Trouche, S., et al. (2018). Exogenous LRRK2G2019S induces parkinsonian-like pathology in a nonhuman primate. *JCI Insight* 3:98202. doi: 10.1172/jci.insight.98202

Mortiboys, H., Furmston, R., Bronstad, G., Aasly, J., Elliott, C. J. H., and Bandmann, O. (2015). UDCA exerts beneficial effect on mitochondrial dysfunction in LRRK2G2019S carriers and *in vivo*. *Neurology* 85, 846–852. doi: 10.1212/wnl.0000000000001905

Nandhagopal, R., Mak, E., Schulzer, M., McKenzie, J., McCormick, S., Sossi, V., et al. (2008). Progression of dopaminergic dysfunction in a LRRK2 kindred: a multitracer PET study. *Neurology* 71, 1790–1795. doi: 10.1212/01.wnl.0000335973.66333.58

Ness, D., Ren, Z., Gardai, S., Sharpnack, D., Johnson, V. J., Brennan, R. J., et al. (2013). Leucine-rich repeat kinase 2 (LRRK2)-deficient rats exhibit renal tubule injury and perturbations in metabolic and immunological homeostasis. *PLoS One* 8:e66164. doi: 10.1371/journal.pone.0066164

Paisán-Ruíz, C., Jain, S., Evans, E. W., Gilks, W. P., Simón, J., van der Brug, M., et al. (2004). Cloning of the gene containing mutations that cause PARK8-linked Parkinson's disease. *Neuron* 44, 595–600. doi: 10.1016/j.neuron.2004.10.023

Piersanti, S., Burla, R., Licursi, V., Brito, C., La Torre, M., Alves, P. M., et al. (2015). Transcriptional response of human neurospheres to helper-dependent CAV-2 vectors involves the modulation of DNA damage response, microtubule and centromere gene groups. *PLoS One* 10:e0133607. doi: 10.1371/journal.pone.0133607

Poewe, W., Seppi, K., Tanner, C. M., Halliday, G. M., Brundin, P., Volkmann, J., et al. (2017). Parkinson disease. *Nat. Rev. Dis. Primers* 3:17013. doi: 10.1038/nrdp.2017.13

Poulopoulos, M., Levy, O. A., and Alcalay, R. N. (2012). The neuropathology of genetic Parkinson's disease. *Mov. Disord.* 27, 831–842. doi: 10.1002/mds.24962

Ramonet, D., Daher, J. P. L., Lin, B. M., Stafa, K., Kim, J., Banerjee, R., et al. (2011). Dopaminergic neuronal loss, reduced neurite complexity and autophagic abnormalities in transgenic mice expressing G2019S mutant LRRK2. *PLoS One* 6:e18568. doi: 10.1371/journal.pone.0018568

Salinas, S., Bilsland, L. G., Henaff, D., Weston, A. E., Keriel, A., Schiavo, G., et al. (2009). CAR-associated vesicular transport of an adenovirus in motor neuron axons. *PLoS Pathog.* 5:e1000442. doi: 10.1371/journal.ppat.1000442

Sepulveda, B., Mesias, R., Li, X., Yue, Z., and Benson, D. L. (2013). Short- and long-term effects of LRRK2 on axon and dendrite growth. *PLoS One* 8:e61986. doi: 10.1371/journal.pone.0061986

Shin, N., Jeong, H., Kwon, J., Heo, H. Y., Kwon, J. J., Yun, H. J., et al. (2008). LRRK2 regulates synaptic vesicle endocytosis. *Exp. Cell Res.* 314, 2055–2065. doi: 10.1016/j.yexcr.2008.02.015

Silva, A. C., Peixoto, C., Lucas, T., Küppers, C., Cruz, P. E., Alves, P. M., et al. (2010). Adenovirus vector production and purification. *Curr. Gene Ther.* 10, 437–455. doi: 10.2174/156652310793797694

Smith, W. W., Pei, Z., Jiang, H., Dawson, V. L., Dawson, T. M., and Ross, C. A. (2006). Kinase activity of mutant LRRK2 mediates neuronal toxicity. *Nat. Neurosci.* 9, 1231–1233. doi: 10.1038/nn1776

Snow, B. J., Vingerhoets, F. J., Langston, J. W., Tetrud, J. W., Sossi, V., and Calne, D. B. (2000). Pattern of dopaminergic loss in the striatum of

humans with MPTP induced parkinsonism. *J. Neurol. Neurosurg. Psychiatry* 68, 313–316. doi: 10.1136/jnnp.68.3.313

Soudais, C., Laplace-Builhe, C., Kissa, K., and Kremer, E. J. (2001). Preferential transduction of neurons by canine adenovirus vectors and their efficient retrograde transport *in vivo*. *FASEB J.* 15, 2283–2285. doi: 10.1096/fj.01-0321fje

Soudais, C., Skander, N., and Kremer, E. (2004). Long-term *in vivo* transduction of neurons throughout the rat CNS using novel helper-dependent CAV-2 vectors. *FASEB J.* 18, 391–393. doi: 10.1096/fj.03-0438fje

Spires-Jones, T. L., Stoothoff, W. H., de Calignon, A., Jones, P. B., and Hyman, B. T. (2009). Tau pathophysiology in neurodegeneration: a tangled issue. *Trends Neurosci.* 32, 150–159. doi: 10.1016/j.tins.2008.11.007

Sweet, E. S., Saunier-Rebori, B., Yue, Z., and Blitzer, R. D. (2015). The Parkinson's disease-associated mutation LRRK2–G2019S impairs synaptic plasticity in mouse hippocampus. *J. Neurosci.* 35, 11190–11195. doi: 10.1523/JNEUROSCI.0040-15.2015

Taymans, J.-M., and Baekelandt, V. (2014). Phosphatases of α-synuclein, LRRK2, and tau: important players in the phosphorylation-dependent pathology of Parkinsonism. *Front. Genet.* 5:382. doi: 10.3389/fgene.2014.00382

Tong, Y., Giaime, E., Yamaguchi, H., Ichimura, T., Liu, Y., Si, H., et al. (2012). Loss of leucine-rich repeat kinase 2 causes age-dependent bi-phasic alterations of the autophagy pathway. *Mol. Neurodegener.* 7:2. doi: 10.1186/1750-1326-7-2

Tong, Y., Pisani, A., Martella, G., Karouani, M., Yamaguchi, H., Pothos, E. N., et al. (2009). R1441C mutation in LRRK2 impairs dopaminergic neurotransmission in mice. *Proc. Natl. Acad. Sci. U S A* 106, 14622–14627. doi: 10.1073/pnas.0906334106

Tong, Y., Yamaguchi, H., Giaime, E., Boyle, S., Kopan, R., Kelleher, R. J. III., et al. (2010). Loss of leucine-rich repeat kinase 2 causes impairment of protein degradation pathways, accumulation of α-synuclein, and apoptotic cell death in aged mice. *Proc. Natl. Acad. Sci. U S A* 107, 9879–9884. doi: 10.1073/pnas.1004676107

Tsika, E., Nguyen, A. P. T., Dusonchet, J., Colin, P., Schneider, B. L., and Moore, D. J. (2015). Adenoviral-mediated expression of G2019S LRRK2 induces striatal pathology in a kinase-dependent manner in a rat model of Parkinson's disease. *Neurobiol. Dis.* 77, 49–61. doi: 10.1016/j.nbd.2015.02.019

Walker, M. D., Volta, M., Cataldi, S., Dinelle, K., Beccano-Kelly, D., Munsie, L., et al. (2014). Behavioral deficits and striatal DA signaling in LRRK2 p.G2019S transgenic rats: a multimodal investigation including PET neuroimaging. *J. Parkinsons Dis.* 4, 483–498. doi: 10.3233/jpd-140344

Wang, X., Yan, M. H., Fujioka, H., Liu, J., Wilson-Delfosse, A., Chen, S. G., et al. (2012). LRRK2 regulates mitochondrial dynamics and function through direct interaction with DLP1. *Hum. Mol. Genet.* 21, 1931–1944. doi: 10.1093/hmg/dds003

Winner, B., Melrose, H. L., Zhao, C., Hinkle, K. M., Yue, M., Kent, C., et al. (2011). Adult neurogenesis and neurite outgrowth are impaired in LRRK2 G2019S mice. *Neurobiol. Dis.* 41, 706–716. doi: 10.1016/j.nbd.2010.12.008

Yue, M., Hinkle, K., Davies, P., Trushina, E., Fiesel, F., Christenson, T., et al. (2015). Progressive dopaminergic alterations and mitochondrial abnormalities in LRRK2 G2019S knock in mice. *Neurobiol. Dis.* 78, 172–195. doi: 10.1016/j.nbd.2015.02.031

Zhou, H., Huang, C., Tong, J., Hong, W. C., Liu, Y. J., and Xia, X. G. (2011). Temporal expression of mutant LRRK2 in adult rats impairs dopamine reuptake. *Int. J. Biol. Sci.* 7, 753–761. doi: 10.7150/ijbs.7.753

Zimprich, A., Biskup, S., Leitner, P., Lichtner, P., Farrer, M., Lincoln, S., et al. (2004). Mutations in LRRK2 cause autosomal-dominant parkinsonism with pleomorphic pathology. *Neuron* 44, 601–607. doi: 10.1016/j.neuron.2004.11.005

Zussy, C., Loustalot, F., Junyent, F., Gardoni, F., Bories, C., Valero, J., et al. (2016). Coxsackievirus adenovirus receptor loss impairs adult neurogenesis, synapse content and hippocampus plasticity. *J. Neurosci.* 36, 9558–9571. doi: 10.1523/JNEUROSCI.0132-16.2016

Conflict of Interest: The authors declare that the research was conducted in the absence of any commercial or financial relationships that could be construed as a potential conflict of interest.

frontiers in Molecular Neuroscience

BRIEF RESEARCH REPORT
published: 15 May 2020
doi: 10.3389/fnmol.2020.00076

Targeted Transgene Expression in Cholinergic Interneurons in the Monkey Striatum Using Canine Adenovirus Serotype 2 Vectors

Anne-Caroline Martel[1†], Heba Elseedy[2,3†], Marina Lavigne[4], Jennyfer Scapula[2], Antoine Ghestem[2], Eric J. Kremer[4], Monique Esclapez[2†] and Paul Apicella[1†]*

[1]CNRS, Institut de Neurosciences de la Timone, Aix Marseille University, Marseille, France, [2]INSERM, Institut de Neurosciences des Systèmes, Aix Marseille University, Marseille, France, [3]Department of Zoology, Alexandria University, Alexandria, Egypt, [4]CNRS, Institut de Génétique Moléculaire de Montpellier, Montpellier, France

OPEN ACCESS

Edited by:
Jean-Marc Taymans, Institut National de la Santé et de la Recherche Médicale (INSERM), France

Reviewed by:
Jose L. Lanciego, University of Navarra, Spain
Andrew Steele, California State Polytechnic University, Pomona, United States
Gerry Coughlin, Caltech, United States, in collaboration with reviewer AS

***Correspondence:**
Paul Apicella
paul.apicella@univ-amu.fr

[†]These authors have contributed equally to this work

Received: 20 January 2020
Accepted: 17 April 2020
Published: 15 May 2020

Citation:
Martel A-C, Elseedy H, Lavigne M, Scapula J, Ghestem A, Kremer EJ, Esclapez M and Apicella P (2020) Targeted Transgene Expression in Cholinergic Interneurons in the Monkey Striatum Using Canine Adenovirus Serotype 2 Vectors. Front. Mol. Neurosci. 13:76. doi: 10.3389/fnmol.2020.00076

The striatum, the main input structure of the basal ganglia, is critical for action selection and adaptive motor control. To understand the neuronal mechanisms underlying these functions, an analysis of microcircuits that compose the striatum is necessary. Among these, cholinergic interneurons (ChIs) provide intrinsic striatal innervation whose dysfunction is implicated in neuropsychiatric diseases, such as Parkinson's disease and Tourette syndrome. The ability to experimentally manipulate the activity of ChIs is critical to gain insights into their contribution to the normal function of the striatum and the emergence of behavioral abnormalities in pathological states. In this study, we generated and tested CAV-pChAT-GFP, a replication-defective canine adenovirus type 2 (CAV-2) vector carrying the green fluorescent protein (GFP) sequence under the control of the human choline acetyltransferase (ChAT) promoter. We first tested the potential specificity of CAV-pChAT-GFP to label striatal ChIs in a rat before performing experiments on two macaque monkeys. In the vector-injected rat and monkey striatum, we found that GFP expression preferentially colocalized with ChAT-immunoreactivity throughout the striatum, including those from local circuit interneurons. CAV-2 vectors containing transgene driven by the ChAT promoter provide a powerful tool for investigating ChI contributions to circuit function and behavior in nonhuman primates.

Keywords: viral vector transduction, acetylcholine, microcircuit analysis, basal ganglia, nonhuman primate

INTRODUCTION

Numerous studies have suggested that the striatum, the main recipient of afferents to the basal ganglia, has a critical function in motor control and motivation. This structure mostly consists of GABAergic spiny projection neurons (SPNs) that target the output nuclei of the basal ganglia. The activity of SPNs is dependent upon excitatory inputs from the cortex and thalamus, under the control of dopaminergic and cholinergic modulation and different types of GABAergic interneurons (Silberberg and Bolam, 2015). The cholinergic innervation of the striatum mainly arises from cholinergic interneurons (ChIs)

scattered throughout the striatum. Although they make up a small fraction of striatal cells, ChIs exert a powerful influence on SPN activity (Calabresi et al., 2000; Pisani et al., 2007) and strongly modulate DA transmission in the striatum (Threlfell and Cragg, 2011). It has been suggested that the dysfunction of ChIs is relevant to the pathophysiology of basal ganglia. As an example, a reduction in the density of ChIs has been reported in brains from patients with Tourette syndrome (Kataoka et al., 2010), a neuropsychiatric disorder characterized by abnormal repetitive movements and altered behavioral flexibility. However, it remains unclear how these interneurons regulate the functioning of the striatal network underlying adaptive behavior. A major goal of research in this area is to develop animal models in which the activity of ChIs can be selectively modified to mimic behavioral impairments observed in human brain pathology.

The advent of tools for transgenics and genome manipulation has provided an opportunity to manipulate striatal microcircuits at an unprecedented level of accuracy. In this regard, there is a growing interest in the application of genetic tools to investigate the causal role of striatal ChIs in behavior. Transgenic rodents expressing Cre-recombinase in cholinergic neurons have allowed targeted approaches for specific manipulation of ChIs by opto- and chemogenetic approaches (Witten et al., 2010; Ztaou et al., 2016; Aoki et al., 2018). However, differences between rodent and primate brains limit the generality of insights into how striatal ChIs might contribute to adaptive behavior.

Among viral vector platforms, adeno-associated virus (AAV) and canine adenovirus type 2 (CAV-2) vectors are widely used in rodents and primates to express transgenes in neurons into various brain regions. Each platform has advantages and disadvantages. Due to the CAV-2 vector's capacity to harbor expression cassettes of 7–30 kb (Junyent and Kremer, 2015; vs. ∼4.7 kb for a typical AAV vector), and our downstream goals to use expression cassettes of greater than 5 kb, we opted for the latter.

In the present study, we developed a viral vector that uses an acetylcholine-specific promoter to selectively express a transgene in the ChI population of the primate striatum. Using CAV-pChAT-GFP, a canine adenovirus type 2 (CAV-2) vector carrying the green fluorescent protein (GFP) gene under the control of the human choline acetyltransferase promoter (pChAT), we report its ability to restrict GFP expression to striatal ChIs.

MATERIALS AND METHODS

Animals

All experimental procedures were approved by the Institutional Animal Care and Use Committee of INT (Permission Number: 14675-2018041009396760) and complied with the rules of the European Community Council Directive (2010/63/EU) for the care and use of laboratory animals. One adult male Long Evans rat (300 g) and two adult male macaques [one cynomolgus, *Macaca fascicularis*, (monkey P), 10.7 kg and one rhesus, *Macaca mulatta*, (monkey C), 11 kg] were used in this study. Monkeys C was chronically implanted with a head-fixation device and a recording chamber placed above the striatum. In this animal, injection coordinates were chosen based on electrophysiological mapping of the striatum we performed over several weeks before injections. Typically, the dorsal border of the striatum was identified by an increase of background noise and irregular spike activity after passing the cortex and underlying white matter. Striatal neurons (mostly output neurons or SPNs) were identified by their characteristic low-frequency discharge. These are different from neighboring structures, such as globus pallidus and adjacent fiber bundles (internal capsule and anterior commissure).

CAV-2 Vectors

CAV-pChAT-GFP and CAV-mCherry are E1/E3-deleted replication-defective vectors. The constructs used in this study are schematically shown in **Figure 1**. For CAV-pChAT-GFP, the cassette contains the 513 bp ChAT promoter, provided by Dr. W. Stauffer (University of Pittsburgh, PA, USA) and amplified with primers 5′-gaatgcaattgcgcgatttatt taaatcccgggag caggggtg-3′ and 5′-tcgcccttgctcaccatggcggccgc ggtggcgagcc aggcc-3′), upstream of the GFP open reading frame (ORF; amplified with primers 5′-ggcctggctcgccaccgcg gccgccatggtga gcaaggg-3′ and 5′-cagaggttgattgaattcttact tgtacagctcgtc-3′) from pEF-GFP; a gift from Connie Cepko (Addgene plasmid #11154), followed by the woodchuck hepatitis virus posttranscriptional regulatory element (WPRE), and polyadenylation sequences (amplified with primers 5′-gacgagctgtacaagtaagaattc aatcaacctctg and 5′-aggtacccgccgcgcgatttatttaaa taaggacagggaagggagc from the plasmid of Dr. W. Stauffer). The pChAT-GFP-polyA cassette was cloned in the E1 region of the CAV-2 vector by SLiCE and produced as described (Del Rio et al., 2019). CAV-mCherry contains the cytomegalovirus (CMV) early promoter, the mCherry ORF, and a polyA signal, cloned in the CAV-2 E3 region (**Figure 1**).

Surgery for Viral Vector Injections

The rat was anesthetized by an intraperitoneal injection of ketamine (100 mg/kg)/xylazine (10 mg/kg) solution and prepared for stereotaxic injections of the viral vectors. CAV-mCherry (10^9 pp/μl) and CAV-pChAT-GFP (10^9 pp/μl) were pressure-injected into the dorsal striatum of respectively the left and right hemispheres. Two injections (0.5 μl each for CAV-mCherry and 1 μl each for CAV-pChAT-GFP) were performed for each vector. After surgery, the skin was sutured, prophylactic antibiotics were injected (Baytril, 5 mg/kg i.m.), and the animal was replaced in its home cage for a survival period of 7 days.

Both monkeys received injections of CAV-2 vectors into the putamen (same constructs as those used in the rat). Monkey P had injections in both sides of the brain and monkey C on one side (i.e., the hemisphere where the recording chamber was placed). Under general anesthesia (sevoflurane 2%) and aseptic conditions, the head of monkey P was fixed in a stereotaxic frame and small holes were drilled into the skull at chosen coordinates above the striatum. After puncturing the dura, a 30-gauge needle connected to a 50 μl Hamilton syringe was slowly lowered through drilled holes to the target

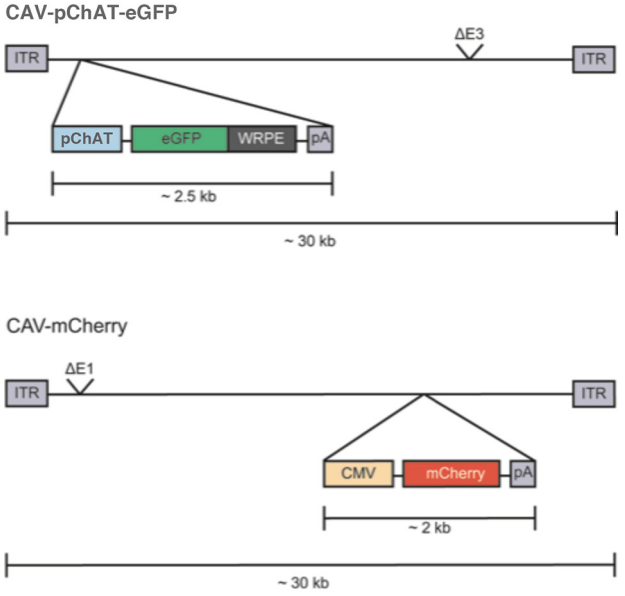

FIGURE 1 | Schematic representation of the CAV-2 construct. CAV-2 vector genomes (∼32 kbp) are flanked by an inverted terminal repeat (ITR) of ∼200 bp. "pChAT-eGFP-WRPE-pA" is the expression cassette that replaces the E1 region in the CAV-2 genome. "pChAT" is the promoter driving expression of choline acetylase gene, GFP is the optimized open reading frame (ORF) for green fluorescent protein (GFP) from jellyfish, WRPE is a sequence from a woodchuck hepatitis virus that increases mRNA stability and protein yield when placed 3′ to an ORF, and pA is the polyadenylation signal from human growth hormone gene (GH1). The CAV-2 E3 region is also deleted (ΔE3) to increase the packaging capacity.

depth. We injected a single volume of 50 μl of CAV-pChAT-GFP vector (2×10^9 pp/μl, 5 μl/min) delivered in one hemisphere and 20 μl of CAV-mCherry (2×10^9 pp/μl) delivered into 4 sites (5 μl per site, 2 μl/min) in the other hemisphere with tracks into the putamen at two rostrocaudal levels and two different depths per track. The distances between the injection sites were 7 mm along the rostrocaudal direction and 6 mm in depth. After each injection, the needle was left in place an additional 5 min to minimize reflux along the injection tract. When the injections were completed, the holes were filled with Spongel and the skin was sutured.

Monkey C was injected unilaterally into the putamen using a microdrive fixed on the chamber and we replaced the recording electrode with a 30-gauge needle connected to a 50 μl Hamilton syringe. The needle was positioned inside a metal guide tube designed to penetrate the dura. A total of 65 μl of the CAV-pChAT-GFP vector (2×10^9 pp/μl) was injected into the putamen at two rostrocaudally different levels: one single 50 μl injection (5 μl/min) and 15 μl divided in three 5 μl boluses (2 μl/min) along the same track. Also, 15 μl of CAV-mCherry (2×10^9 pp/μl) divided into three 5 μl injections (2 μl/min) separated by 2 mm along the same track were delivered at a more anterior level. After injections, the chamber was sealed with a cap. The two monkeys were monitored during recovery from anesthesia and then returned to their home cages for a survival period of 10 days.

Histology and Immunohistochemistry

Animals were deeply anesthetized with an overdose of pentobarbital and transcardially perfused with a solution of 4% paraformaldehyde (PFA) prepared in 0.12 M sodium phosphate buffer, pH 7.4 (PB). After perfusion, blocs of the brain containing the striatum were post-fixed and processed for sectioning (coronal sections 40 μm). One out of every ten sections was stained with cresyl violet to localize the injection sites within the striatum and to determine the general histological characteristics of the tissue throughout the rostrocaudal extent of the striatum.

Selected sections at the level of the striatum were processed for simultaneous immunohistofluorescence detection of GFP, mCherry, and ChAT according to a previously described protocol (Soussi et al., 2015). Sections were incubated overnight at RT in a solution containing the following primary antibodies: mouse anti-GFP (1:100, Invitrogen), rabbit anti-RFP (1:2,000) and goat anti-ChAT (1:100, Millipore). They were incubated for 2 h in the following secondary antibodies: Alexa488-conjugated donkey anti-rabbit IgG (1:200; Invitrogen), Cy5-conjugated donkey anti-goat (1:100; Jackson ImmunoResearch Laboratories, Inc., West Grove, PA, USA), and Cy3-conjugated donkey anti-mouse (1:100; Jackson ImmunoResearch Laboratories, Inc., West Grove, PA, USA). All sections were then mounted on super frost-coated slides (Menzel GmbH and Co KG, Germany) for rat or (HistoBond+ Supa Mega, Marienfeld, Germany) for monkey, dried overnight at RT and coverslipped with Fluoromount. The specimens were analyzed with a confocal microscope (Zeiss, LSM 510).

Quantification of Co-localizing GFP or mCherry and ChAT

Quantitative analysis of double-labeled neurons for ChAT and GFP or mCherry was conducted to evaluate the extent of GFP expression in cholinergic neurons in the striatum. This analysis was performed in the rat and monkey P injected with CAV-pChAT-GFP and CAV-mCherry. The numbers of single- and double-labeled neurons were determined in the striatum for each animal, from five sections (400 μm apart from each other) surrounding the injection sites previously localized on cresyl violet staining adjacent sections. For each section, an image of the entire striatal region was obtained from a single confocal slice with 20× objective and sequential acquisition of the different wavelength channels (LSM 510 Zen, Zeiss). The analysis was then performed with Neurolucida software (version 7, mbfBioscience) as followed: for each confocal image, all GFP-labeled neurons were identified on the green channels and examined for co-localization with ChAT in the blue channels and/or mCherry in the red one. Then, the relative percentages of double-labeled neurons for GFP and ChAT, and mCherry and ChAT, were determined. A total of 76 GFP-labeled and 20 mCherry-labeled neurons were counted in the rat. In monkey P, 86 GFP-labeled and 30 mCherry-labeled neurons were counted.

RESULTS

The Cholinergic Phenotype of Transduced Neurons After CAV-2 Injections in the Rat Striatum

Coronal sections of the rat brain injected with CAV-pChAT-GFP and CAV-mCherry into the striatum of the right and left hemispheres, respectively (**Figure 2A**), were processed for simultaneous detection of GFP, mCherry, and ChAT to determine the specificity of CAV-pChAT-GFP to label cholinergic neurons of the striatum, as compared to CAV-mCherry that potentially targets all neurons.

The right striatum injected with CAV-pChAT-GFP displayed many GFP-labeled neurons. These neurons were distributed at a distance of up to 600 μm surrounding the injection site. Qualitatively, it appeared that transduced cells were more rarely observed near the injection site (**Figure 2B** arrows). As shown in **Figures 2C,F,I**, these GFP-labeled neurons displayed a large cell body with bipolar (**Figure 2F**) or multipolar dendrites (**Figure 2I**). Labeled axonal processes and en passant boutons were also observed. These neurons exhibited the size and morphology characteristics of the "classical" giant neurons presumed to be ChIs (Bolam et al., 1984; Phelps et al., 1985). While a large majority of the GFP-expressing neurons were immunolabeled for ChAT (**Figures 2C–K**, arrows), some GFP-expressing neurons did not contain a detectable level of ChAT (**Figures 2C–E**, arrowheads). Quantitative analysis performed in five sections showed that 82% of the GFP-expressing neurons were ChAT immunolabeled.

In the left striatum, many mCherry-labeled cells were observed close to the injection site and within 600 μm (**Figure 2L**). mCherry was distributed throughout the cell body, dendrites (**Figures 2M,P,S** arrowheads) and axonal processes (**Figures 2P,S**). As illustrated in **Figures 2M–U**, most of these neurons expressing mCherry (red arrowhead) were not labeled for ChAT (blue arrows). Quantitative analysis performed from 5 sections showed that only 5% of the neurons expressing mCherry were ChAT immunolabeled. This encouraging proof-of-concept pilot assay in the rat striatum provided the impetus to test CAV-pChAT-GFP in the monkey brain.

The Cholinergic Phenotype of Transduced Neurons After CAV-2 Injections in the Macaque Striatum

We then injected CAV-pChAT-GFP and CAV-mCherry into the striatum of two macaques. In monkey C, the two viral vectors were injected in the same hemisphere. In this monkey, only the injection sites at the posterior levels (i.e., postcommissural putamen) were properly located in the striatum (**Figure 3A**). Sections processed at these levels for simultaneous detection of GFP, mCherry, and ChAT showed many ChAT-containing neurons distributed through the striatum (**Figure 3B**) as well as GFP-labeled and mCherry-labeled neurons in the striatum. Whereas almost all the GFP-expressing neurons were labeled for ChAT and mCherry (**Figures 3C–J** arrows), neurons expressing mCherry only were not labeled for ChAT (**Figures 3C–F** arrowhead). This reflects a strong but not exclusive bias toward cholinergic neurons in a co-injection procedure. Moreover, in monkey C, expression of GFP or mCherry was limited to cell bodies, no dendritic and axonal processes were observed. The absence of "Golgi-like" labeling of GFP or mCherry expressing neurons is in contrast to that found in the rat, and could reflect toxicity due to GFP, mCherry, and/or the dose of vector during the co-injections.

To address this possibility, monkey P received injections of CAV-pChAT-GFP and CAV-mCherry in the right and left hemispheres, respectively. As in the rat striatum, the right striatum contained neurons expressing GFP with a large cell body and several dendrites with multipolar or bipolar orientation (**Figures 3K,N,Q**). These morphological features are consistent with those of the giant neurons (DiFiglia, 1987; Yelnik et al., 1993) that correspond to ChIs in the primate striatum. Axonal processes and en passant boutons labeled for GFP were also observed (**Figures 3K,N**, arrowheads). A large majority of these GFP-expressing neurons were ChAT immunoreactive (**Figures 3K–P**, arrows, **3Q,R**). Quantitative analysis performed in monkey P on five brain sections showed that 86% of the GFP-expressing neurons were labeled for ChAT. In the striatum of the left hemisphere, neurons expressing mCherry were observed around the injection site. All these neurons displayed well-labeled cell body, dendritic and axonal processes (**Figure 3S**), and only 20% of these mCherry-labeled neurons co-expressed ChAT ($n = 5$ sections).

DISCUSSION

In the present experiment, we developed a cell-type-specific gene expression approach using a CAV-2 vector carrying a ChAT promoter to investigate the role of ChIs in nonhuman primates. The results of this pilot study indicate that CAV-2 vectors containing a human ChAT promoter can be a valuable tool to preferentially target transgene expression to the ChI population of the striatum in monkeys. This represents a promising outcome, particularly for primate models where genetic resources are underdeveloped.

CAV-2 Vectors for Delivering Genetic Material to the Primate Brain

Previous studies have shown that CAV-2 is an effective gene transfer tool in both rodents and primates (Junyent and Kremer, 2015; Mestre-Francés et al., 2018; Lasbleiz et al., 2019). CAV-2 vectors enter axon terminals at the site of injection and are transported along the axon back to the soma, where the transgene is expressed. To our knowledge, the present study is the first that investigated the transduction properties of CAV-2 under the control of a ChAT promoter. Consistent with specific GFP expression in ChIs, we found a substantial overlap between GFP- and ChAT–immunolabeled neurons in monkey striatum, indicating that transgene expression was largely restricted

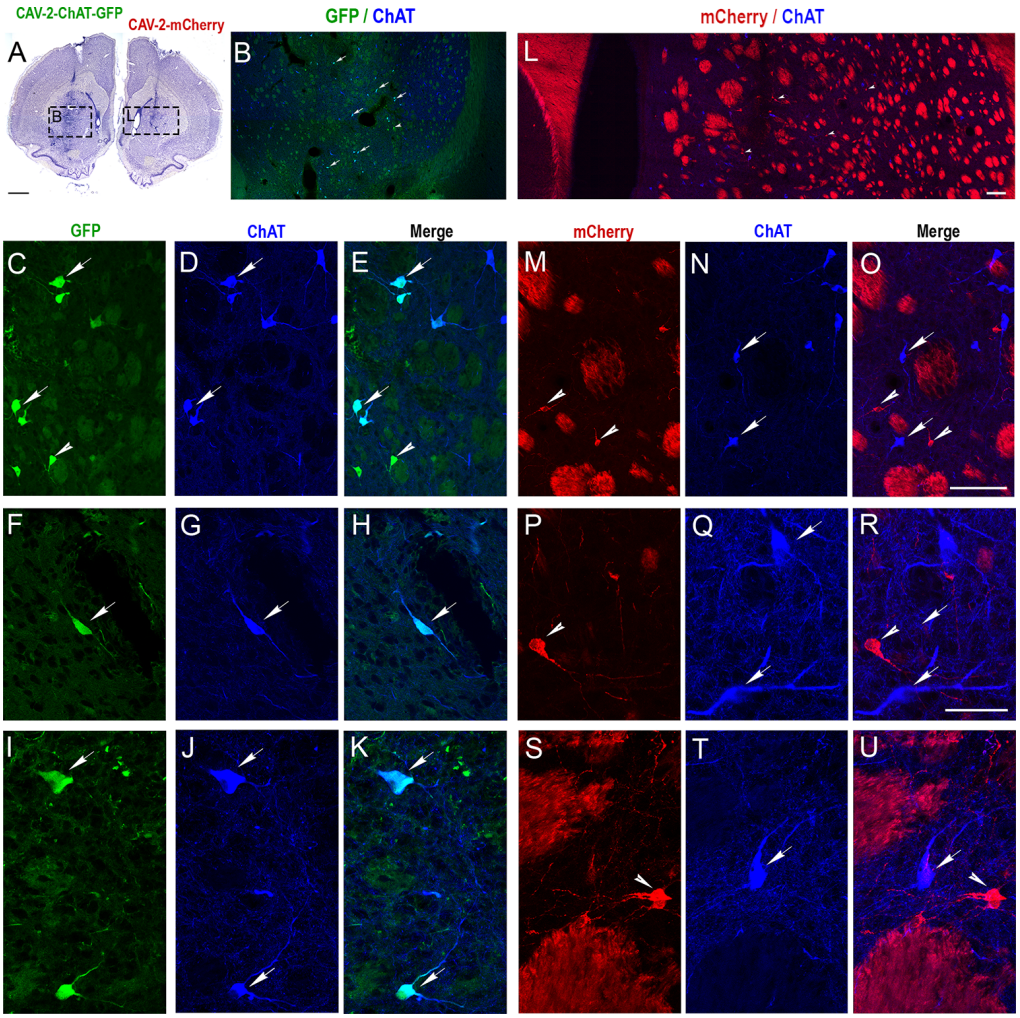

FIGURE 2 | Selective expression of GFP in cholinergic interneurons (ChIs) of the rat striatum with CAV-2 containing the human ChAT promoter (CAV-pChAT-GFP). **(A)** Coronal section of the rat brain stained with Cresyl violet showing the injection sites of CAV-pChAT-GFP and CAV-mCherry in the right and left striatum respectively. **(B–U)** Immunofluorescence labeling for simultaneous detection of ChAT (blue), GFP (green) and mCherry (red) in a coronal section. Images of the fluorophores obtained by sequential acquisition of separate wavelength channels from a single confocal slice. **(B,L)** Distributions of ChAT-containing neurons as well as GFP- (**B**, green) and mCherry- (**L**, red) expressing neurons within the right and left striatum. **(C–K)** Demonstrated that many cell bodies that were GFP+ (green, arrows) contained ChAT (blue arrows). A few GFP+ (green arrowhead) did not show a detectable level of ChAT. **(E)** Merge of **(C,D)**. **(H)** Merge of **(F,G)**. **(K)** Merge of **(I,J)**. **(M–U)** Demonstrated that most mCherry+ neurons (red, arrowheads) were not labeled for ChAT. These neurons were distributed among many ChAT-containing neurons (Blue, arrows). **(O)** Merge of **(M,N)**. **(R)** Merge of **(P,Q)**. **(U)** Merge of **(S,T)**. Scale bars: **(A)**, 500 μm; **(B–D,E,L,M–O)**, 100 μm; **(F–K,P–U)**, 50 μm.

to ChIs. These results demonstrate the utility of the CAV-2 vector for investigating the contributions of ChIs to striatal function and behavior, and they indicate that the ChAT promoter presently used can confer a degree of cell-type specificity to direct gene expression in the striatum of monkey.

Although the ChI system is a major contributor to the striatal cholinergic innervation, an extrinsic source of acetylcholine within the striatum also arises from the pedunculopontine and laterodorsal tegmental nuclei in the brainstem (Dautan et al., 2014). Considering that CAV-2 vectors enter axon terminals at the injection site and are transported along the axon back to the cell body, additional work will be needed to establish whether transgene expression under the control of the ChAT promoter is also present in midbrain nuclei.

Cell-Type Targeting With the Use of Promoters

The development of gene transfer strategies with viral vectors in nonhuman primates has grown rapidly in recent years (Galvan et al., 2017). However, targeting specific types of neurons with these tools remains challenging. There are very few reports in monkeys of viral vectors that drive gene expression exclusively in a targeted neuron type with the use of promoters. Notably, a tyrosine hydroxylase promoter has been used for targeting noradrenergic neurons of the locus

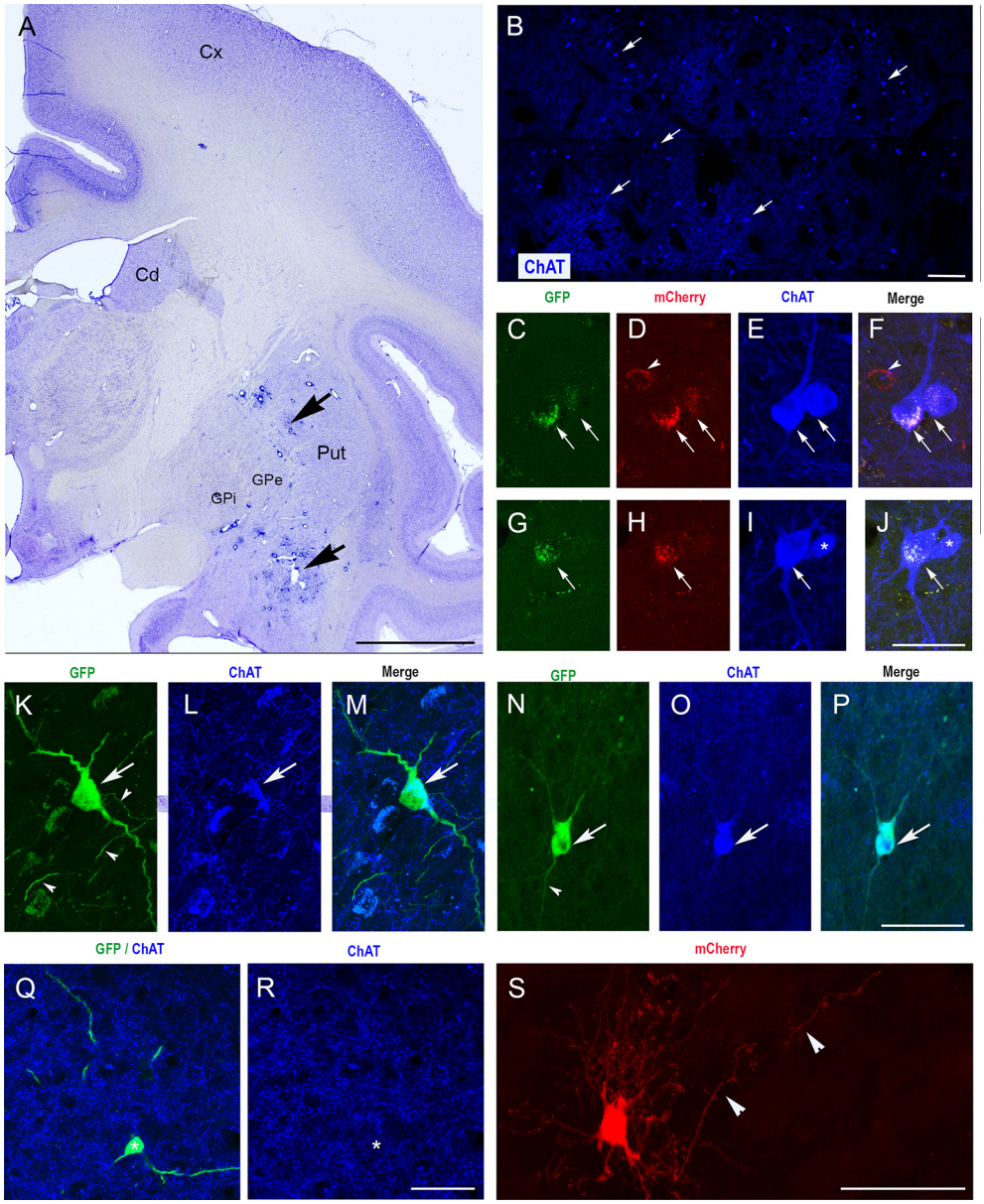

FIGURE 3 | Selective expression of GFP in ChIs of the monkey striatum with CAV-2 containing the human ChAT promoter (CAV-pChAT-GFP). **(A)** Coronal section of a macaque brain stained with Cresyl violet showing the injection sites of CAV-pChAT-GFP in the striatum. **(C–S)** Immunofluorescence labeling for simultaneous detection of, GFP (green), mCherry (red) and ChAT (blue) in an adjacent coronal section. Images of the fluorophores obtained by sequential acquisition of separate wavelength channels from a single confocal slice. **(B)** Distributions of ChAT-containing neurons within the striatum. **(C–J)** In monkey C in which both CAV-2 vectors were injected in the same hemisphere, GFP and mCherry expression were restricted to the cell bodies. Most of these neurons that were labeled for both GFP (green, arrows) and mCherry (red, arrows) contained ChAT (blue) whereas neurons expressing mCherry only (red, arrowheads) were not labeled for ChAT. **(K–S)** In Monkey P in which CAV-pChAT-GFP and CAV-mCherry were injected in the right and left striatum, respectively most neurons expressing GFP (**K,N,Q**, green) or mCherry **(S)** displayed well-labeled cell bodies as well as dendritic and axonal (arrowheads) processes. **(K–P)** Most neurons expressing GFP (green, arrows) contained ChAT (Blue, arrows). **(Q,R)** A few neurons expressing GFP did not show detectable levels of ChAT. **(F)** Merge of **(C–E)**. **(J)** Merge of **(G–I)**. **(M)** Merge of **(K,L)**. **(P)** Merge of **(N,O)**. Scale bars: **(A)**, 5 mm; **(B)**, 600 μm; **(C–S)** 50 μm.

coeruleus (Lerchner et al., 2014) and dopaminergic neurons of the substantia nigra in macaques (Stauffer et al., 2016). Also, El-Shamayleh et al. (2017) have successfully achieved targeted transduction on cerebellar neurons in macaques using a fragment of the Purkinje cell-specific L7 promoter. These results show that cell-type-specific promoters can be used in viral vectors for targeted manipulations of specific neuronal circuits in nonhuman primates. Our results indicate that striatal delivery of CAV-2 vectors carrying a ChAT promoter sequence can confer a sufficient degree of cell-type specificity to transduce ChIs in

monkey striatum. These data are comparable to the CAV-2-mediated preferential expression of a transgene in noradrenergic neurons using PRS, a catecholamine-selective synthetic promoter (Hwang et al., 2001; Li et al., 2016; Hirschberg et al., 2017).

Technical Considerations

To increase the applicability of this methodology, further improvements in vector delivery are needed. Although we found that CAV-2 vectors preferentially transduced ChIs around the site of injection, the extent of the spread of the 90 nm CAV-2 capsid needs to be optimized because the sparse population of ChIs is scattered across large volumes of the macaque striatum. Increasing the number of coordinates where the vector is delivered and the infusion volume with Convection Enhanced Delivery (Bankiewicz et al., 2000) could be used to increase the number of ChIs expressing the transgene. Accordingly, work is now in progress to maximize the spread of viral vector and transgene expression in large regions of the macaque striatum. Also, based on ChAT immunohistochemical detection, the 513 bp ChAT promoter did not confer exclusive cell-type specificity. Replication-defective CAV-2 vectors deleted in the E1 and E3 regions have a cloning capacity of ∼6 kbp, and therefore depending on the size of the transgene larger promoters/enhancer combinations could be readily incorporated. Finally, there is also uncertainty about the duration of transgene expression in longer-lasting experiments. While our work does not address long-term transgene expression in ChIs, helper-dependent CAV-2 (which have a 30 kb cloning capacity and are deleted in all CAV-2 coding regions) have led to long-term transgene expression in nonhuman primates (Mestre-Francés et al., 2018).

In conclusion, our pilot study demonstrates that the delivery of CAV-2 vectors containing a transgene driven by a ChAT promoter to the striatum results in preferential expression in ChIs in the macaque monkey. It, therefore, appears that our approach is efficient in enabling precise, targeted manipulation of a local circuit component in the striatal network of the primate. Given the complexity of the striatal circuitry, the manipulation of a single cell type that regulates striatal functions is an important step forward in mapping the local microcircuitry dysregulated in pathological conditions. The advent of molecular genetic techniques to label and manipulate specific populations of neurons opens up opportunities for linking ChI function and behavior. Our findings indicate promising capabilities of CAV-2 to enable analysis of specific microcircuits in the striatum when being combined with optogenetic or chemogenetic manipulation studies.

DATA AVAILABILITY STATEMENT

The datasets generated for this study are available on request to the corresponding author.

ETHICS STATEMENT

The animal study was reviewed and approved by Institutional Animal care and Use Committee of INT (Permission Number: 14675-2018041009396760).

AUTHOR CONTRIBUTIONS

ME, PA, and EK conceived and designed experiments. ML and EK produced the virus vectors. A-CM, HE, JS, AG, ME, and PA performed experiments. ME and A-CM analyzed data and made figures. PA, ME, and EK wrote the manuscript.

FUNDING

This work was supported by the Centre National de la Recherche Scientifique (PA), the Institut National de la Santé et de la Recherche Médicale (ME), Aix-Marseille University (PA, ME), University of Montpellier (EK), the Association France Parkinson (PA, EK), the Fondation pour la Recherche Médicale (EK), and the LabEx EpiGenMed (EK). A-CM was supported by a doctoral fellowship from the French Ministry of Education and Research, Fondation pour la Recherche Médicale, and Fondation des Treilles. HE was supported by a doctoral fellowship from Agence Universitaire Francophone and the Egyptian government. Partenariats Hubert Curien IMHOTEP (ME, HE).

ACKNOWLEDGMENTS

We thank L. Renaud and J.-A. Rathelot for help with surgery in monkeys. We thank the staff of the animal facilities (INT and CEFOS, AMU, Marseille), the imaging facility (INPHIM, AMU, Marseille), and the Plateforme de Vectorologie (BioCampus, CNRS Montpellier).

REFERENCES

Aoki, S., Liu, A. W., Akamine, Y., Zucca, A., Zucca, S., and Wickens, J. R. (2018). Cholinergic interneurons in the rat striatum modulate substitution of habits. *Eur. J. Neurosci.* 47, 1194–1205. doi: 10.1111/ejn.13820

Bankiewicz, K. S., Eberling, J. L., Kohutnicka, M., Jagust, W., Pivirotto, P., Bringas, J., et al. (2000). Convection-enhanced delivery of AAV vector in parkinsonian monkeys: *in vivo* detection of gene expression and restoration of dopaminergic function using pro-drug approach. *Exp. Neurol.* 164, 2–14. doi: 10.1006/exnr.2000.7408

Bolam, J. P., Wainer, B. H., and Smith, A. D. (1984). Characterization of cholinergic neurons in the rat neostriatum. A combination of choline acetyltransferase immunocytochemistry, Golgi-impregnation and electron-microscopy. *Neuroscience* 12, 71l–718. doi: 10.1016/0306-4522(84)90165-9

Calabresi, P., Centonze, D., Gubellini, P., Pisani, A., and Bernardi, G. (2000). Acetylcholine-mediated modulation of striatal function. *Trends Neurosci.* 23, 120–126. doi: 10.1016/s0166-2236(99)01501-5

Dautan, D., Huerta-Ocampo, I., Witten, I. B., Deisseroth, K., Bolam, J. P., Gerdjikov, T., et al. (2014). A major external source of cholinergic innervation of the striatum and nucleus accumbens originates in the brainstem. *J. Neurosci.* 34, 4509–4518. doi: 10.1523/JNEUROSCI.5071-13.2014

Del Rio, D., Beucher, B., Lavigne, M., Wehbi, A., Gonzalez Dopeso-Reyes, I., Saggio, I., et al. (2019). CAV-2 vector development and gene transfer in

the central and peripheral nervous systems. *Front. Mol. Neurosci.* 12:71. doi: 10.3389/fnmol.2019.00071

DiFiglia, M. (1987). Synaptic organization of cholinergic neurons in the monkey neostriatum. *J. Comp. Neurol.* 225, 245–258.doi: 10.1002/cne.902550208

El-Shamayleh, Y., Kojima, Y., Soetedjo, R., and Horwitz, G. D. (2017). Selective optogenetic control of Purkinje cells in monkey cerebellum. *Neuron* 95, 51–62. doi: 10.1016/j.neuron.2017.06.002

Galvan, A., Stauffer, W. R., Acker, L., El-Shamayleh, Y., Inoue, K. I., Ohayon, S., et al. (2017). Nonhuman primate optogenetics: recent advances and future directions. *J. Neurosci.* 37, 10894–10903. doi: 10.1523/JNEUROSCI.1839-17.2017

Hirschberg, S., Li, Y., Randall, A., Kremer, E. J., and Pickering, A. E. (2017). Functional dichotomy in spinal- vs prefrontal-projecting locus coeruleus modules splits descending noradrenergic analgesia from ascending aversion and anxiety in rats. *eLife* 136:e29808. doi: 10.7554/eLife.29808

Hwang, D. Y., Carlezon, W. A. Jr., Isacson, O., and Kim, K. S. (2001). A high-efficiency synthetic promoter that drives transgene expression selectively in noradrenergic neurons. *Hum. Gene Ther.* 12, 1731–1740. doi: 10.1089/104303401750476230

Junyent, F., and Kremer, E. J. (2015). CAV-2—why a canine virus is a neurobiologist's best friend. *Curr. Opin. Pharmacol.* 24, 86–93. doi: 10.1016/j.coph.2015.08.004

Kataoka, Y., Kalanithi, P. S., Grantz, H., Schwartz, M. L., Saper, C., Leckman, J. F., et al. (2010). Decreased number of parvalbumin and cholinergic interneurons in the striatum of individuals with Tourette syndrome. *J. Comp. Neurol.* 518, 277–291. doi: 10.1002/cne.22206

Lasbleiz, C., Mestre-Francés, N., Devau, G., Luquin, M., Tenenbaum, L., Kremer, E. J., et al. (2019). Combining gene transfer and nonhuman primates to better understand treat Parkinson's disease. *Front. Mol. Neurosci.* 12:10. doi: 10.3389/fnmol.2019.00010

Lerchner, W., Corgiat, B., Der Minassian, V., Saunders, R. C., and Richmond, B. J. (2014). Injection parameters and virus dependent choice of promoters to improve neuron targeting in the nonhuman primate brain. *Gene Ther.* 21, 233–241. doi: 10.1038/gt.2013.75

Li, Y., Hickey, L., Perrins, R., Werlen, E., Patel, A. A., Hirschberg, S., et al. (2016). Retrograde optogenetic characterization of the pontospinal module of the locus coeruleus with a canine adenoviral vector. *Brain Res.* 1641, 274–290. doi: 10.1016/j.brainres.2016.02.023

Mestre-Francés, N., Serratrice, N., Gennetier, A., Devau, G., Cobo, S., Trouche, S. G., et al. (2018). Exogenous LRRK2G2019S induces parkinsonian-like pathology in a nonhuman primate. *JCI Insight* 3:e98202. doi: 10.1172/jci.insight.98202

Phelps, P. E., Houser, C. R., and Vaughn, J. E. (1985). Immunocytochemical localization of choline acetyltransferase within the rat neostriatum: a correlated light and electron microscopic study of cholinergic neurons and synapses. *J. Comp. Neurol.* 238, 286–307. doi: 10.1002/cne.902380305

Pisani, A., Bernardi, G., Ding, J., and Surmeier, D. J. (2007). Re-emergence of striatal cholinergic interneurons in movement disorders. *Trends Neurosci.* 30, 545–553. doi: 10.1016/j.tins.2007.07.008

Silberberg, G., and Bolam, J. P. (2015). Local and afferent synaptic pathways in the striatal microcircuitry. *Curr. Opin. Neurobiol.* 33, 182–187. doi: 10.1016/j.conb.2015.05.002

Soussi, R., Boulland, J. L., Bassot, E., Bras, H., Coulon, P., Chaudhry, F. A., et al. (2015). Reorganization of supramammillary–hippocampal pathways in the rat pilocarpine model of temporal lobe epilepsy: evidence for axon terminal sprouting. *Brain Struct. Funct.* 220, 2449–2468. doi: 10.1007/s00429-014-0800-2

Stauffer, W. R., Lak, A., Yang, A., Borel, M., Paulsen, O., Boyden, E. S., et al. (2016). Dopamine neuron-specific optogenetic stimulation in rhesus macaques. *Cell* 166, 1564–1571. doi: 10.1016/j.cell.2016.08.024

Threlfell, S., and Cragg, S. J. (2011). Dopamine signaling in dorsal versus ventral striatum: the dynamic role of cholinergic interneurons. *Front. Syst. Neurosci.* 5:11. doi: 10.3389/fnsys.2011.00011

Witten, I. B., Lin, S. C., Brodsky, M., Prakash, R., Diester, I., Anikeeva, P., et al. (2010). Cholinergic interneurons control local circuit activity and cocaine conditioning. *Science* 330, 1677–1681. doi: 10.1126/science.1193771

Yelnik, J., Percheron, G., François, C., and Garnier, A. (1993). Cholinergic neurons of the rat and primate striatum are morphologically different. *Prog. Brain Res.* 99, 25–34. doi: 10.1016/s0079-6123(08)61336-9

Ztaou, S., Maurice, N., Camon, J., Guiraudie-Capraz, G., Kerkerian-Le Goff, L., Beurrier, C., et al. (2016). Involvement of striatal cholinergic interneurons and M1 and M4 muscarinic receptors in motor symptoms of Parkinson's disease. *J. Neurosci.* 36, 9161–9172. doi: 10.1523/JNEUROSCI.0873-16.2016

Conflict of Interest: The authors declare that the research was conducted in the absence of any commercial or financial relationships that could be construed as a potential conflict of interest.

frontiers in Neuroanatomy

ORIGINAL RESEARCH
published: 04 June 2020
doi: 10.3389/fnana.2020.00028

Location of the Cell Adhesion Molecule "Coxsackievirus and Adenovirus Receptor" in the Adult Mouse Brain

Amani Wehbi, Eric J. Kremer† and Iria G. Dopeso-Reyes†*

Institut de Génétique Moléculaire de Montpellier, CNRS, Université de Montpellier, Montpellier, France

The coxsackievirus and adenovirus receptor (CAR) is a single-pass transmembrane cell adhesion molecule (CAM). CAR is expressed in numerous mammalian tissues including the brain, heart, lung, and testes. In epithelial cells, CAR functions are typical of the quintessential roles of numerous CAMs. However, in the brain the multiple roles of CAR are poorly understood. To better understand the physiological role of CAR in the adult brain, characterizing its location is a primordial step to advance our knowledge of its functions. In addition, CAR is responsible for the attachment, internalization, and retrograde transport of canine adenovirus type 2 (CAV-2) vectors, which have found a niche in the mapping of neuronal circuits and gene transfer to treat and model neurodegenerative diseases. In this study, we used immunohistochemistry and immunofluorescence to document the global location of CAR in the healthy, young adult mouse brain. Globally, we found that CAR is expressed by maturing and mature neurons in the brain parenchyma and located on the soma and on projections. While CAR occasionally colocalizes with glial fibrillary acidic protein, this overlap was restricted to areas that are associated with adult neurogenesis.

Keywords: coxsackievirus and adenovirus receptor, adult neurogenesis, rostral migratory stream, hippocampus, extracellular matrix, synaptogenesis, cell adhesion molecules, canine adenovirus type 2 vector

OPEN ACCESS

Edited by:
Laurent Gautron, University of Texas Southwestern Medical Center, United States

Reviewed by:
Pierre-Yves Risold, University of Franche-Comté, France
Honglin Luo, The University of British Columbia, Canada

****Correspondence:***
Iria G. Dopeso-Reyes
iria.gonzalez-dopeso-reyes@igmm.cnrs.fr

†These authors share senior authorship

Received: *02 March 2020*
Accepted: *08 May 2020*
Published: *04 June 2020*

Citation:
Wehbi A, Kremer EJ and Dopeso-Reyes IG (2020) Location of the Cell Adhesion Molecule "Coxsackievirus and Adenovirus Receptor" in the Adult Mouse Brain. Front. Neuroanat. 14:28. doi: 10.3389/fnana.2020.00028

INTRODUCTION

Cell adhesion molecules (CAMs) are multifunctional proteins that, as the name suggests, also mediate interactions between cells or between cells and the extracellular matrix (ECM) (reviewed by Cavallaro and Dejana, 2011). While CAMs impact tissue structure, function, and cellular movement, they are also involved in cytoskeletal organization, contact inhibition, apoptosis, signaling, and transcriptional responses (reviewed by Gibson, 2001; Cavallaro and Dejana, 2011).

Abbreviations: Ac, anterior commissure; Alv, alveus; AON, anterior olfactory nucleus; AP, area postrema; Cc, corpus callosum; Cing, cingulum bundle; Cpd, cerebellar peduncle; Csc, superior colliculus commissure; Cx, cortex; Cx, pir piriform cortex; DCO, dorsal cochlear nucleus; DTN, dorsal tegmental nucleus; Em, external medullary lamina of the thalamus; EPL, external plexiform layer; F, fimbria; GL, glomerular layer; GL, granular cells layer hippocampus; GP, globus pallidum; GRL, granular cells layer of olfactory bulb; H, hilus; Hip, hipothalamus; Hipp, hippocampus; IO, inferior olive complex; IPN, interpeduncular nucleus; LOT, lateral olfactory tract; Ml, medial lemniscus; ML, molecular layer; Mtt, mammillothalamic tract; MV, medial vestibular nucleus; Opt, optical tract; PAG, periaqueductal gray; Po, polymorphic layer; RN, red nucleus; RphN, raphe nuclei; SC, superior colliculus; Scp, superior cerebellar peduncles; SLM, stratum lacunosum-moleculare; SLU, stratum lucidum; Sm, stria medullaris; SML, stratum molecular; SR, stratum radiatum; Str, striatum; Th, thalamus; V, ventricle.

Among the family of CAMs include a subset dubbed immunoglobulin superfamily (IgCAMs). In the central nervous system, some IgCAMs are indispensable for development and maintenance and several studies link their dysfunction with pathological conditions (reviewed Sakurai, 2017; Sytnyk et al., 2017).

The coxsackievirus and adenovirus receptor (CAR) belongs to the cortical thymocyte marker in *xenopus* CTX subfamily of IgCAMs (Chrétien et al., 1998; reviewed by Loustalot et al., 2016). As the name suggests, CAR was initially characterized for its role as an attachment molecule needed for binding and internalization of some coxsackievirus and adenoviruses (Bergelson et al., 1997, 1998; Carson et al., 1997; Tomko et al., 1997; Bergelson, 1999; Soudais et al., 2001). In contrast to most human adenovirus types, canine type 2 (CAdV-2 or CAV-2) appears to be dependent on CAR expression to infect cells and in particular neurons (Zussy et al., 2016; del Rio et al., 2019). CAR has the classical structure of IgCAMs: the extracellular domain (ECD) is composed of two Ig-like domains (D1 and D2) followed by a single-pass transmembrane domain (TM) and an intracellular domain (ICD) (Loustalot et al., 2016). In epithelial-like cells, the ECD and ICD of CAR interact with numerous intracellular and extracellular proteins (*ibid*). CAR is widely expressed in tight junction in the epithelial tissue in the adult mouse gastrointestinal tract, respiratory tract, kidney, and male reproductive system; it is also present in the liver, lymphatic system, skeletal muscle, and myocardial cells (Cohen et al., 2001; Shaw et al., 2004; Raschperger et al., 2006).

Like many prototypic CAMs, CAR engagement also induces signaling (Cavallaro and Dejana, 2011; Ortiz-Zapater et al., 2017). CAR overexpression leads to an increase in the phosphorylation/activation of GSK3β and Akt (Caruso et al., 2010). Moreover, CAR signaling influences E-cadherin levels and can increase MAPK activity (Farmer et al., 2009; Morton et al., 2013; Salinas et al., 2014). CAR engagement by viral proteins also activates the p44/p42 MAPK, JNK, and NF-κB pathways (Tamanini et al., 2006), suggesting that CAR is involved in pathways important for cellular homeostasis at the transcriptional level. The shedding of CAR's ECD, likely with cell-type variations, is mediated either by α-secretase and metalloprotease 10 (Houri et al., 2013), or by β-site amyloid precursor protein-cleaving enzyme (BACE1) (Zhou et al., 2012). Then, a γ-secretase complex releases the ICD that translocates to the nucleus (Houri et al., 2013).

Several studies have also documented the presence of CAR in the rodent brain. As CAR expression is temporally regulated, very high levels of protein and mRNA were readily detected during embryonic brain development (Honda et al., 2000; Hotta et al., 2003; Venkatraman et al., 2005; Chen et al., 2019). CAR is observed from early developmental stages all along the neural tube, and as the secondary brain vesicles emerge, CAR immunoreactivity was mainly observed in cells and fibers in the telencephalon and diencephalon (Hotta et al., 2003; Chen et al., 2019). While CAR levels decrease significantly after birth, it is still readily detected in the adult mammalian brain, particularly in the blood–brain barrier, ependymal cells, and new born neurons in the hippocampus and olfactory bulb (Honda et al., 2000; Hotta et al., 2003; Venkatraman et al., 2005; Raschperger et al., 2006; Zussy et al., 2016; Salinas et al., 2017). Moreover, the CAR ECD interacts with several molecules involved in neuronal homeostasis including Agrin, a proteoglycan involved in synaptogenesis in the adult brain, and heparin-binding domain 2, a fibronectin that promotes neurite extension (Patzke et al., 2010). The ICD interacts with zonula-occludens 1, podocin, and PSD-95 (Excoffon et al., 2004; Yan et al., 2015). Accumulating evidence suggests that CAR is important for the trafficking of some of these proteins in non-neuronal cells (Farmer et al., 2009; Morton et al., 2013; Salinas et al., 2014) and with proteins involved in vesicle exocytosis at presynaptic termini in neurons (Wrackmeyer et al., 2019).

Of note, the genetic ablation of CAR expression in the mouse brain affects adult neurogenesis, synaptic content and function, and behavior (Zussy et al., 2016). Moreover, CAR loss of function had a greater impact on spatial memory and long-term plasticity in female mice. In addition, when healthy mice were injected in the peritoneal cavity with lipopolysaccharides (LPS) from gram-negative bacterial membrane, CAR levels decreased notably in the dentate gyrus (DG) (*ibid*). Chronic CAR loss was also seen in the DG of a mouse model of Alzheimer's disease. These results link inflammation-induced posttranslational CAR loss in the hippocampus with changes in hippocampal plasticity and impaired cognition.

While numerous studies have focused on the role of CAR in the heart and epithelial tissues, there are only a handful of studies exploring its function in the brain. Detailing CAR's regional and subcellular location is a primordial step to lay a foundation to understand its function in the healthy brain. In addition to its physiological role, CAR is responsible for the binding, internalization, and trafficking of canine adenovirus type 2 (CAV-2) (Soudais et al., 2001; Salinas et al., 2009). Therefore, understanding in which cells and in which regions CAR is expressed will allow more targeted approaches of using CAV-2 vectors to study and manipulate neuronal networks, and its potential for gene therapy and modeling neurodegenerative diseases (Soudais et al., 2004; Cubizolle et al., 2014; Beier et al., 2015; Schwarz et al., 2015; Hirschberg et al., 2017; Mestre-Francés et al., 2018).

MATERIALS AND METHODS

Five C57BL/6J and five C57BL/6N male mice between 6 and 8 weeks old were used in this study. Animal handling was conducted in accordance with the European Council directive (2010/63/EU) as well as in agreement with the Society for Neuroscience Policy on the Use of Animals in Neuroscience Research. The experimental design was approved by the Ethical Committee for Animal Testing Comité régional Languedoc-Roussillon.

Because genetic and phenotypic differences exist between C57BL/6J and C57BL/6N mice (reviewed by Morris et al., 2010), we used both strains to preclude a report biased on one strain. Animals were anesthetized with an overdose of ketamine/xylazine and then perfused transcardially with a saline

solution (0.9% NaCl) followed by 50 ml of 4% paraformaldehyde prepared in phosphate buffer (PB), pH 7.4. The brains were removed and stored for 24 h in 4% paraformaldehyde. Afterward, the samples were washed in PB and cryopreserved in a solution containing 30% sucrose in PB. Finally, once the samples sank in the 30% sucrose solution they were frozen in Tissue Freezing Medium optimum cutting temperature (O.C.T.) (MicromMicrotech, TFM-5) and stored at −80°C. OCT blocks were cut in serial sagittal (1 brain each strain), horizontal (1 brain each strain), or coronal sections (3 brains each strain) (35 μm thick) using a cryostat and collected in a solution containing glycerol and ethylene glycol in PBS.

Immunohistochemistry

Free-floating sections were rinsed with Tris–buffered saline (TBS) pH 7.4 and then incubated in a blocking solution containing 1% of gelatin from cold fish water skin (Sigma G7041), 1% bovine serum albumin (BSA) and 0.05% Triton X-100 in TBS for 1 h; after that, sections were incubated overnight at 4°C with the appropriate primary antibody/antibodies diluted in the blocking solution. The following primary antibodies were used for immunofluorescence: (1) a goat anti-CXADR (CAR) (1:100, R&D systems, AF2654, RRID:AB_2245567, Lot VFT0119071); (2) a rabbit anti-glial fibrillary acidic protein (GFAP) (1:1000, DAKO, Z0334, RRID:AB_10013382); (3) a mouse anti-SOX2 (1:200, ABCAM, ab171380, RRID:AB_2732072); (4) a mouse anti-NeuN (1:500, ABCAM, ab104224, RRID:AB_10711040); (5) a rabbit anti-doublecortin (DCX) (1:500, ABCAM, ab18723, RRID:AB_732011); and (6) a chicken anti-nestin (1:1000, ABCAM, ab134017, RRID:AB_2753197).

Following the incubation with primary antibodies, sections were rinsed with TBS and incubated with the appropriated biotinylated or fluorescent secondary antibody/antibodies diluted in the blocking solution for 1 h. The following secondary antibodies were used in this study: biotinylated horse anti-goat antibody: (1:500, Vector, BA9500, RRID:AB_2336123); Alexa Fluor® 488 donkey anti-goat IgG (1:200, Molecular Probes A 11055, RRID:AB_2534102); Alexa Fluor® 555 donkey anti-rabbit IgG (1:200, Molecular Probes A 31572, RRID:AB_162543); Alexa Fluor® 647 donkey anti-mouse IgG (1:200, Molecular Probes A 31571, RRID:AB_162542); 4′,6-diamidino-2-phenylindole dihydrochloride (Sigma D8417); and Cy3 donkey anti-chicken IgG (1:200, Jackson ImmunoResearch, 703-165-155, RRID:AB_2340363.

The series incubated with biotinylated antibody were rinse in TBS and afterward with avidin–biotin complex (Vector Laboratories PK-6100, RRID:AB_2336819) for 1 h at room temperature. Once washed, the peroxidase reaction was visualized using 0.05% 3,3′-diaminobenzidine (Sigma, D5637) and 0.03% hydrogen peroxide.

Finally, sections were rinsed in TBS and mounted on SuperFrost Ultra Plus slides, dried at room temperature and counterstained using Harry's hematoxylin, dehydrated and coverslipped with Eukitt (Sigma, 03989), and kept at room temperature or dried at room temperature and coverslipped with DAKO fluorescence mounting medium (DAKO, S3023) and kept at 4°C.

To test the specificity of the secondary antibodies, we omitted the primary antibodies in some sections while maintaining the rest of the procedures. All the control sections exhibited a lack of positive staining.

Immunofluorescence signals were visualized using a Zeiss LSM880 Airyscan laser-scanning microscope. The colorimetric signals were visualized using a Zeiss Axioimager Z2 microscope and a Retiga Q-imaging color camera (1920 × 1460 interlines, 4.64 μm pixel size). Images were adjusted for brightness and contrast by using ImageJ. Picture setup was achieved with Adobe Illustrator CS6. Full resolution was maintained until the micrographs were cropped and assembled, at which time they were adjusted to a resolution of 300 dpi.

The brain regions were identified using a mouse brain atlas (Franklin and Paxinos, 1997).

RESULTS

To study CAR expression in the mouse brain, we used a polyclonal goat antibody against the N-terminal which we previously demonstrated to be CAR specific (Zussy et al., 2016). In this study, we compared *C57BL/6J* and *C57BL/6N* mice. We did not observe differences in the CAR expression, and therefore, the description of CAR location applies to both strains. CAR expression was mainly, but not exclusively, seen in the telencephalon and diencephalon (**Figures 1A,B**). CAR immunoreactivity was readily detected in the cortex, olfactory bulb, striatum, septum, amygdala, hippocampus, some areas of the thalamus and hypothalamus, superior colliculus, and the brainstem.

CAR Expression in the Telencephalon

In the telencephalon, the olfactory bulb and the accessory olfactory bulb contained the highest global level of CAR immunoreactivity. Using coronal, sagittal, and horizontal sections, we found CAR immunoreactivity in all the olfactory bulb layers, from the most inner layer to the outer layer (**Figure 1C**). CAR immunoreactivity was particularly intense in cells located in the rostral migratory stream (RMS) (**Figures 1C,D**): the cells had an elongated shape, and CAR was present in the soma and in the neurites. In the granular layer of the olfactory bulb, we observed CAR immunoreactivity in the neuropil and in some somas (**Figure 1E** arrows). A similar pattern was also observed in the mitral cells (**Figure 1F**) and plexiform layer (**Figure 1G**), where CAR was also present in the neuropil and in the soma of some mitral (arrows in **Figure 1F**) and periglomerular cells (arrows in **Figure 1G**).

The glomerulus in the olfactory bulb and the accessory olfactory bulb showed intense CAR immunoreactivity (white star in **Figures 1C,G**). CAR was also present in scattered fibers in the lateral olfactory tract (LOT) and with higher intensity in the layer I of the anterior olfactory nucleus (AON) (arrows in **Figure 1C**).

The pattern of CAR expression observed in the AON was also present in the olfactory tubercle and the rostral piriform cortex, where CAR immunoreactivity was present mainly in the

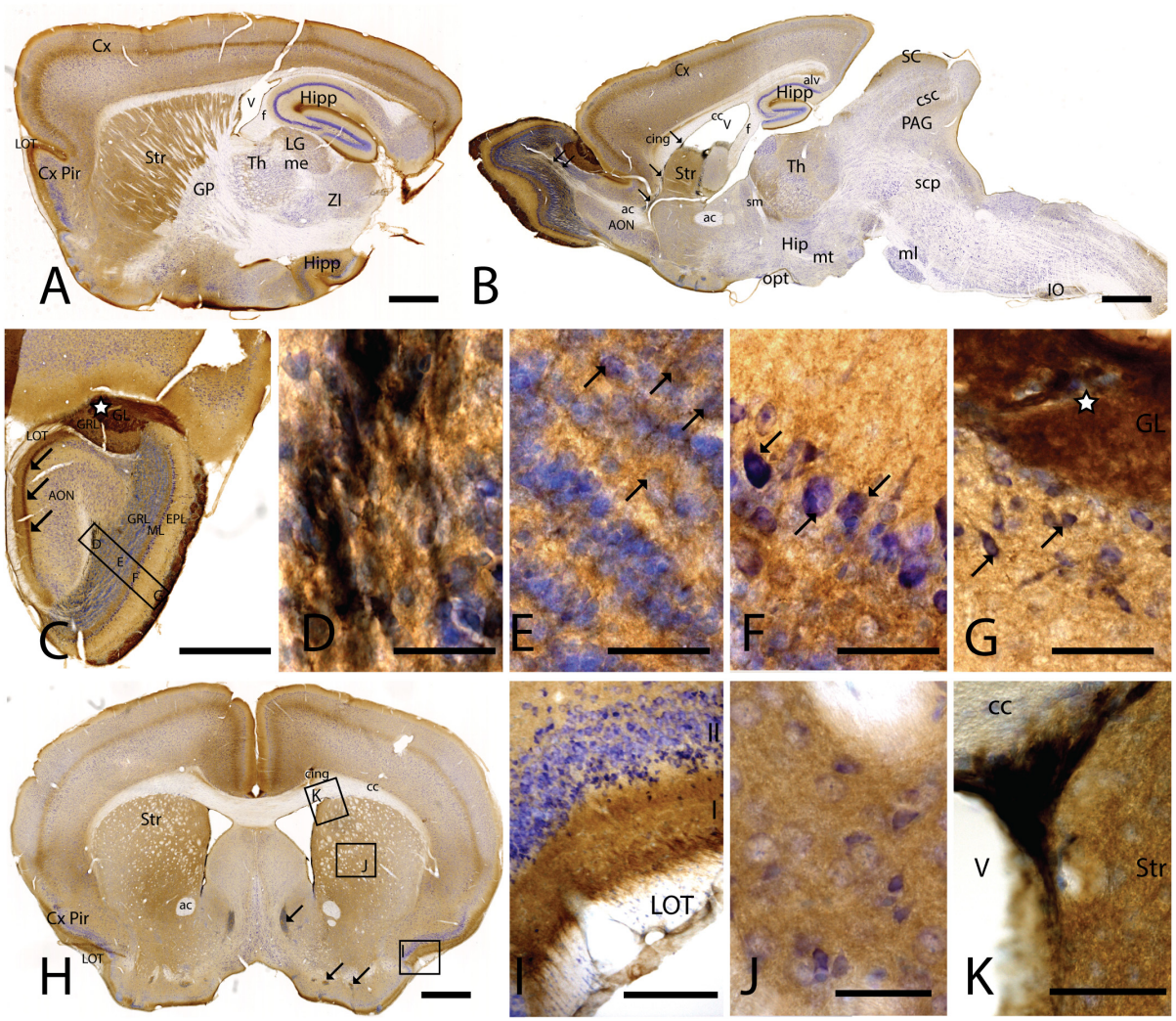

FIGURE 1 | CAR expression in mouse brain. CAR immunoreactivity in brown counterstained with Harry's hematoxylin in blue. **(A)** Sagittal lateral section of mouse brain. CAR is present in cortical areas—piriform cortex, isocortex, and hippocampus; and in non-laminated areas—striatum and thalamus. **(B)** Sagittal medial section of the mouse brain, where possible observe the presence of CAR mainly in the telencephalon and diencephalon, while the midbrain and rombencephalon showed CAR immunostaining only in specific regions. The cells of the RMS are indicated with arrows and also showed a high expression of CAR. **(C)** Coronal section of the olfactory bulb showing the presence of CAR in all the layers. It is noticeable the intense CAR immunolabeling present in layer I of the anterior olfactory nuclei are indicated with arrows. It is in the glomerulus of both the olfactory bulb and the accessory olfactory bulb where CAR staining is stronger (white star). **(D)** High magnification from **(C)** of the RMS. Due to the brown staining of CAR and the blue staining of the nuclei, in this photograph CAR expression is observed in black. CAR was located in the soma and in the neurites of the cells. **(E)** High magnification from **(C)** showing the granular cells layer. CAR was observed in some cellular somas (arrows) and also in the neuropil, which was detected as intense punctate. **(F)** High magnification of **(C)** showing the mitral cell layer. CAR is shown in the soma of some cells (arrows) and in the neuropil. **(G)** High magnification of **(C)** showing the external plexiform layer and the glomerulus of the olfactory bulb. The most streaking CAR expression was present in the glomerulus, where it was observed an intense extracellular labeling (white star), but it was also found in some cell soma of the periglomerular cells and in the neuropil of the external plexiform layer. **(H)** Coronal section of the telencephalon at the level of the striatum. Among other areas described before, CAR was observed along the cortical areas, the striatum, septum, Calleja islands, and subventricular zone. The arrows indicate the presence CAR immunolabeling in the Calleja islands. **(I)** High magnification of **(H)** showing a coronal section of the piriform cortex. The highest CAR expression is located in the layer I, while in the lateral olfactory bulb we can observe scattered CAR immunolabeled fibers, and layers II and III show staining in the neuropil. **(J)** High magnification of **(H)** showing the striatum. In this region, CAR was observed mainly in the neuropil. **(K)** High magnification of **(H)** where we can observe CAR expression in the dorso-lateral subventricular zone. The cells show an elongated shape and CAR was observed in the somas and neurites. Calibration bars: **(A,B)**: 1 mm, **(C)**: 100 c, **(D–G)**: 10 μm, **(H)**: 1 mm, **(I)**: 50 μm, **(J)**: 10 μm, **(K)**: 25 μm.

layer I (**Figures 1A,H,I**). The pyramidal layer of the piriform cortex and olfactory tubercle did not show significant CAR immunoreactivity. CAR immunoreactivity was also observed in the islands of Calleja (arrows in **Figure 1H**). In the striatum (**Figures 1A,B,H,J**), high CAR immunoreactivity was present in the neuropil but low or absent in the fiber tracts (**Figure 1J**). By contrast, the globus pallidus showed faint CAR immunostaining in the neuropil (**Figure 1A**).

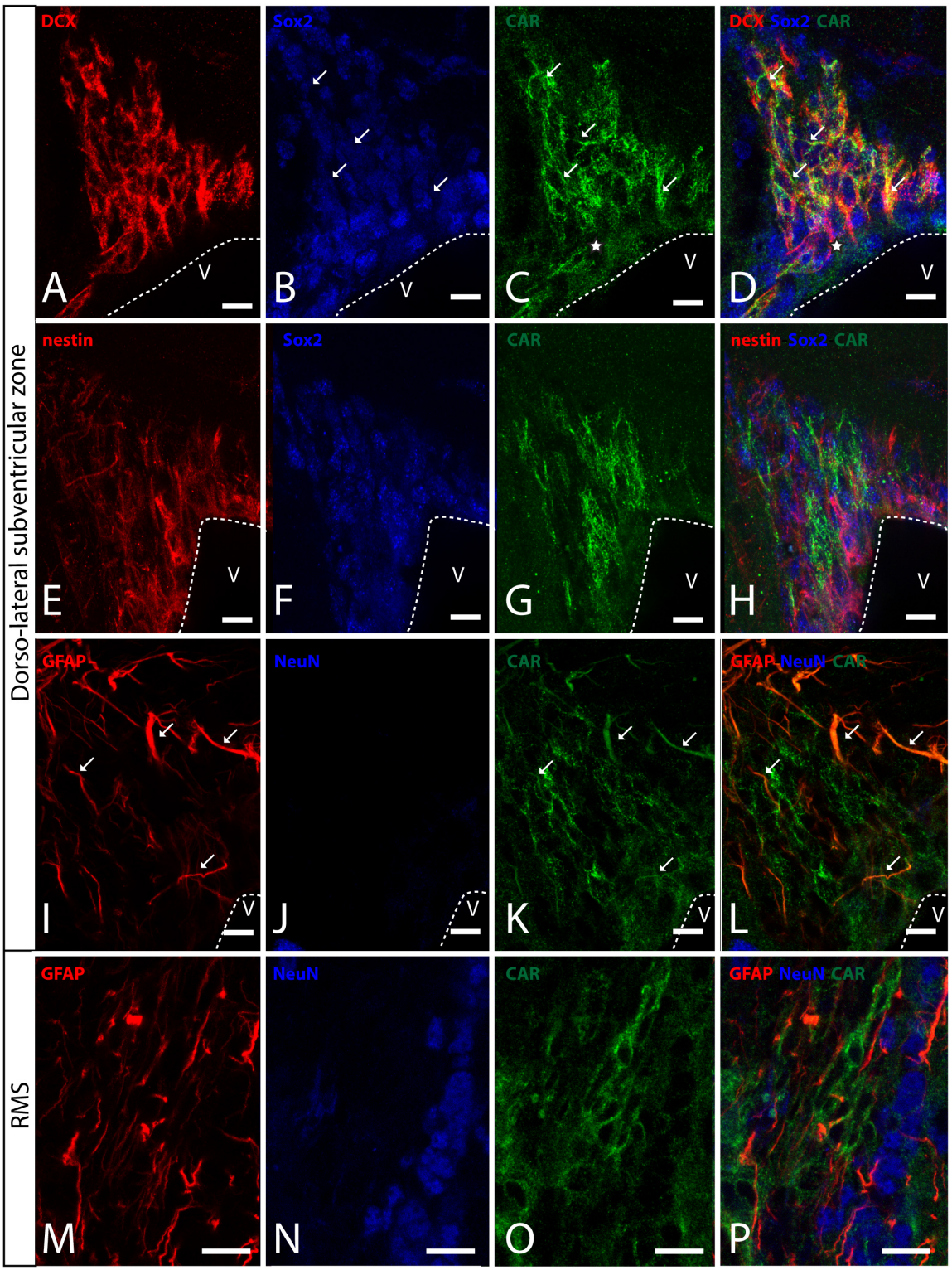

FIGURE 2 | CAR expression in the sub-ventricular zone and the rostral migratory stream. **(A–D)** Colocalization of CAR (green), DCX (red), and Sox2 (blue) in the SVZ. Both CAR and DCX are present in the same cells (white arrows) that also express low levels of Sox2 (Z-stack 10 μm). **(E–H)** Colocalization of CAR (green) and nestin (red) in the SVZ. Nestin and CAR colocalization in some cells but not in all. And both CAR and nestin colocalize in those cells with lower levels of Sox2 (blue) (Z-stack 10 μm). **(I–L)** Colocalization of CAR (green) and GFAP (red) in the SVZ. Also, there was no presence of NeuN (blue) in the CAR^{+} cells (Z-stack 10 μm). **(M–P)** Expression of CAR (green), GFAP (red), and NeuN (blue) in the RMS. On the contrary that we observed in the SVZ, in the RMS there was a lack of CAR expression in the GFAP-ir fibers. As in the SVZ, CAR-ir cells were not NeuN immunoreactive (Z-stack 10 μm). Calibration bars: **(A–P)**: 10 μm.

In horizontal and sagittal sections, we observed CAR along the RMS (arrows in **Figure 1B**) and in the subventricular zone (SVZ), clearly shown in the coronal section (**Figures 1H,K**). To identity the CAR^+ cells in the RMS and SVZ, we performed double and triple immunofluorescence labeling (**Figure 2**). In the SVZ, CAR (green **Figure 2**) colocalizes with markers for immature neurons DCX (**Figures 1A–D**) and SOX2 (**Figures 2A–D**). Of note, CAR was present mainly in the cells that showed low SOX2 immunoreactivity (arrows **Figures 1B–D**). This pattern was also the case for nestin positive cells in the SVZ (**Figures 2E–H**): higher CAR immunoreactivity in cells with lower levels of nestin immunoreactivity (**Figures 2E,G,H**). When we combined anti-CAR and anti-GFAP staining, we observed that the majority of GFAP-immunoreactive fibers (**Figures 2I–L**) in this area colocalized with CAR (white arrows in **Figures 2I,K,L**). However, not all the CAR-immunoreactive cells expressed GFAP (**Figures 2I,K,L**). Consistent with previous observations, CAR was not detected on the soma of NeuN-immunoreactive cells (mature neurons) (**Figures 2M–P**) in the areas surrounding the SVZ (**Figures 2J,L**).

This pattern of colocalization between CAR, DCX and nestin in the dorso-lateral SVZ was also observed in the ventro-medial SVZ and in the RMS (data not showed). However, in the RMS, GFAP (**Figures 2M–P**) and CAR (**Figures 2M–P**) were expressed in the same areas, but not in the same cells (**Figure 2P**). As described for the dorso-lateral SVZ, CAR did not colocalize with NeuN-Immunoreactive cells (**Figure 2P**).

As we analyzed more caudal regions, we observed CAR immunoreactivity in cortical areas (**Figures 3A,B**). In the hippocampus, CAR was present in all layers of the DG and the proper hippocampus (**Figure 3B**). In the subgranular zone (SGZ) of the DG, we found the biggest population of CAR-immunoreactive cell bodies (**Figures 3B,C**): CAR-immunoreactive cells showed intense immunoreactivity in the soma (arrowhead in **Figure 3C**) and in the apical (black arrows in **Figure 3C**) and basal projections (white arrows in **Figure 3C**). In the molecular layer of the DG, CAR was present in the neuropil and in several branched fibers, many of them clearly belonging to the CAR-immunoreactive cells present in the SGZ (arrows in **Figure 3D**). CAR expression was also observed in the hilus (**Figure 3E**), in thin fibers running across the plexiform layer (arrows in **Figure 3D**). It was also possible to observe CAR-immunoreactive thin fibers in the stratum lacunosum-moleculare of the CA3 region (arrows in **Figure 3F**). In addition, the stratum lacunosum-moleculare of CA1 showed intense CAR immunostaining in the neuropil, being more intense in the area near to the molecular layer of the DG (**Figures 3B,G**). Weaker CAR immunoreactivity was also observed in the neuropil of the stratum radiatum of the CA1 (**Figure 3G**) and in the soma of the pyramidal cells of the CA1 (**Figure 3H**).

As mentioned above, other cortical areas also showed CAR immunoreactivity. In the caudal region of the piriform cortex, CAR immunoreactivity was present in layer I, in the soma of scattered cells in layer II, and in fibers along the layer III (arrows in **Figure 3I**). In the isocortex, CAR was observed in the neuropil along all the cortical layers, being more intense in layer I (**Figure 3A**) and layer IV; in the latter, CAR was present in the neuropil and in the membrane of some cell bodies (arrows in **Figure 3J**).

Because CAR immunoreactivity was intense in the cells located in the SGZ, which is one place where adult neurogenesis occurs in the mouse brain, we performed double and triple immunolabeling to better identify these cells. By combining GFAP, NeuN, and CAR, we found that the majority of the CAR-immunoreactive soma do not colocalize with GFAP or NeuN (**Figures 4A–D**). However, there were a few fibers that were GFAP and CAR immunoreactive (white arrows in **Figures 4A,B,D**) and some cells expressing NeuN and CAR (yellow arrows in **Figures 4B–D**). Moreover, we found a handful of immunoreactive nestin and CAR fibers (yellow arrows **Figures 4E–H**). Similarly, co-immunolabeling with CAR and DCX showed overlapping immunoreactivity (yellow arrows in **Figures 4I–L**).

In general, the big fiber tracts in the mouse telencephalon were CAR negative. However, we found exceptions along the rostro-caudal axis (**Figures 1A,B**, **3A,B**, **5A–C**) as we observed CAR-immunoreactive fibers in the cingulum bundle, the corpus callosum (**Figure 3K**), external capsule (**Figures 1A,B**), and the amigdalar capsule (**Figures 5A–C**). We also observed scattered CAR-immunoreactive fibers in some regions of the anterior commissure, alveus and stria terminalis, but not in the stria medullaris, fornix, or internal capsule (**Figures 1A,B**, **5A–C**).

CAR Expression in the Diencephalon

As stated above, CAR immunoreactivity was also present in the thalamus and hypothalamus (**Figures 5**, **6**). The fiber tracts in the diencephalon showed a general lack of CAR immunostaining in the optical tract, external medullary lamina of the thalamus, medial lemniscus, mammillary tract or fasciculus retroflexus (**Figures 1A,B**, **5A–C**). However, we observed CAR-immunoreactive fibers in the diencephalon in the habenular commissure (**Figures 1A,B**).

In the thalamus, immunoreactivity was present in the neuropil of several nuclei including the nuclei of the anterior and lateral dorsal thalamus (**Figures 5A–F**), the lateral geniculate (**Figure 5E**) and reticular nuclei, the midline nuclei, and in some of the ventral nuclei (**Figure 5D**). In the habenula, CAR immunostaining appeared in what seemed to be fiber tracts running along the dorso-caudal axis (**Figure 5F**).

In the hypothalamus, CAR immunoreactivity was mainly present in the preoptic area and the rostral arcuate hypothalamic nucleus (arrows in **Figure 5G**), and along the ventricular zone of the mediobasal hypothalamus where immunoreactivity was strong in the ependymal cells lining the third ventricle and in fibers running from the ventricular wall toward the hypothalamic parenchyma (arrows in **Figures 5H,I**).

CAR immunoreactivity was also in the ependymal cells along the 3rd ventricle in the thalamus (**Figures 5A–C,J**), the lateral ventricles (**Figures 1A,B,H**), cerebral aqueduct, and 4th ventricle (data not shown). In the ependymal cells, CAR was present mainly in the plasma membrane (arrows in **Figure 5K**). CAR expression was also high in the choroid plexus along the rostro caudal axis (**Figure 5K**) and in the subcommissural organ (**Figure 5L**) where immunoreactivity

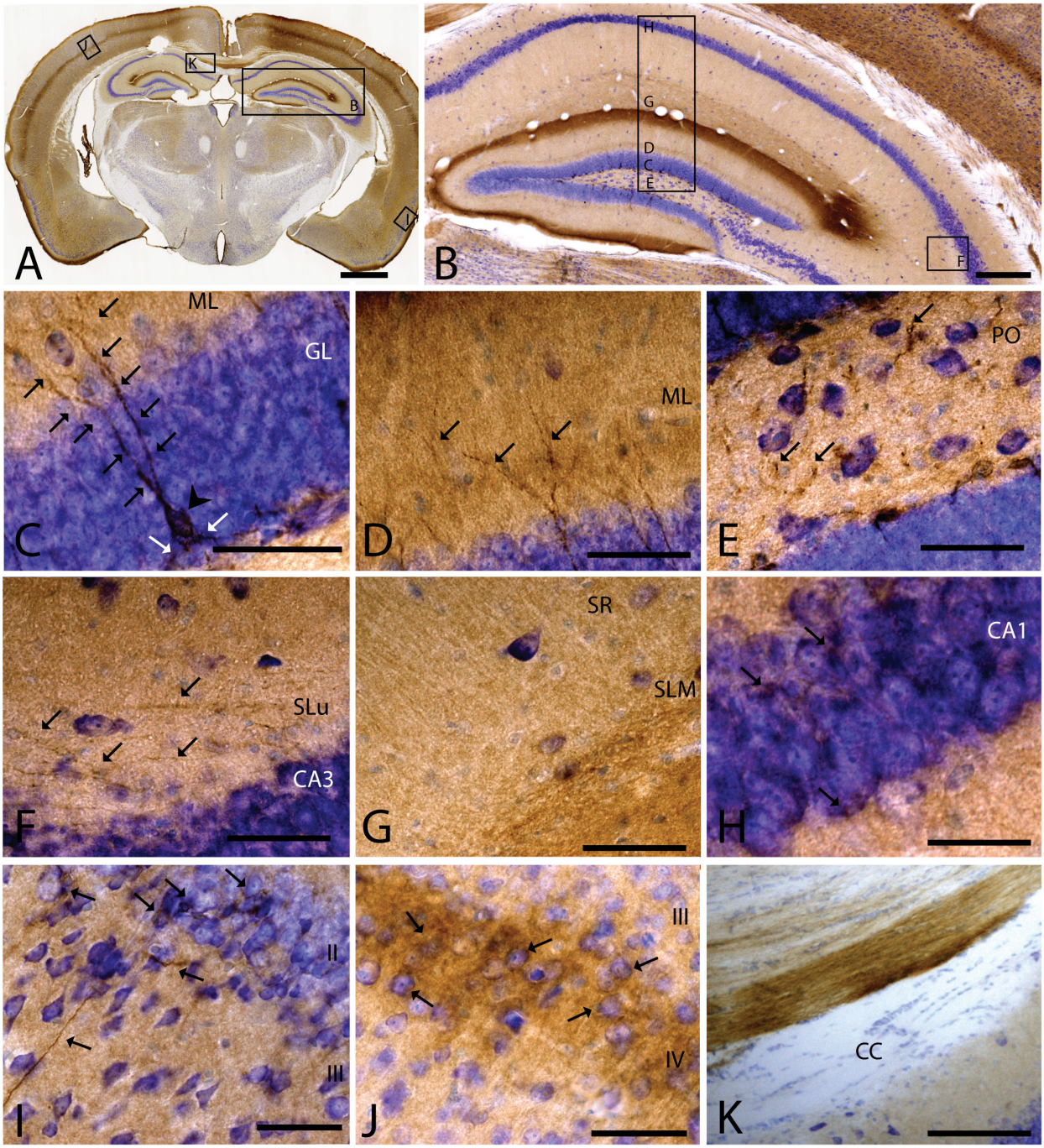

FIGURE 3 | CAR expression in the hippocampus, cortical areas, and corpus callosum. CAR immunoreactivity in brown counterstained with Harry's hematoxylin in blue. **(A)** Coronal section of mouse brain. CAR is present in cortical areas—piriform cortex, isocortex, and hippocampus; and in non-laminated areas—thalamus and hypothalamus. **(B)** High magnification of **(A)** showing the hippocampus. CAR is present in all layers of proper hippocampus and dentate gyrus. **(C)** Granular cell layer of the dentate gyrus high magnification of **(B)** showing the CAR-immunoreactive cells. The protein is present in the soma (arrow head) and in the apical and basal projections (arrows). **(D)** Molecular layer of the dentate gyrus, high magnification from **(B)**. In this layer, CAR is observed in the diffuse neuropil but also in the form of more intense dots in some the apical projection (arrows). **(E)** Presence of CAR^+ fibers (arrows) in the hilus, high magnification from **(E)**. **(F)** CAR^+ thin fibers in the stratum lucidus of CA3 (arrows), high magnification from **(B)**. **(G)** Detail of the stratum radiatum where CAR is present in the neuropil. **(H)** CAR expression in the CA1 pyramidal cell layer, high magnification from **(B)**. CAR is present in the cytoplasm of the cells (arrows). **(I)** CAR expression in the piriform cortex, which is present in thin fibers in layer III and cellular somas in layer II (arrows). **(J)** Layer IV of the isocortex showing the presence of CAR in the neuropil and in some cellular somas (arrows). **(K)** CAR-immunoreactive fibers in the medial portion of the corpus callosum. Calibration bars: **(A)**: 1 mm, **(B)**: 50 μm, **(D–K)**: 10 μm.

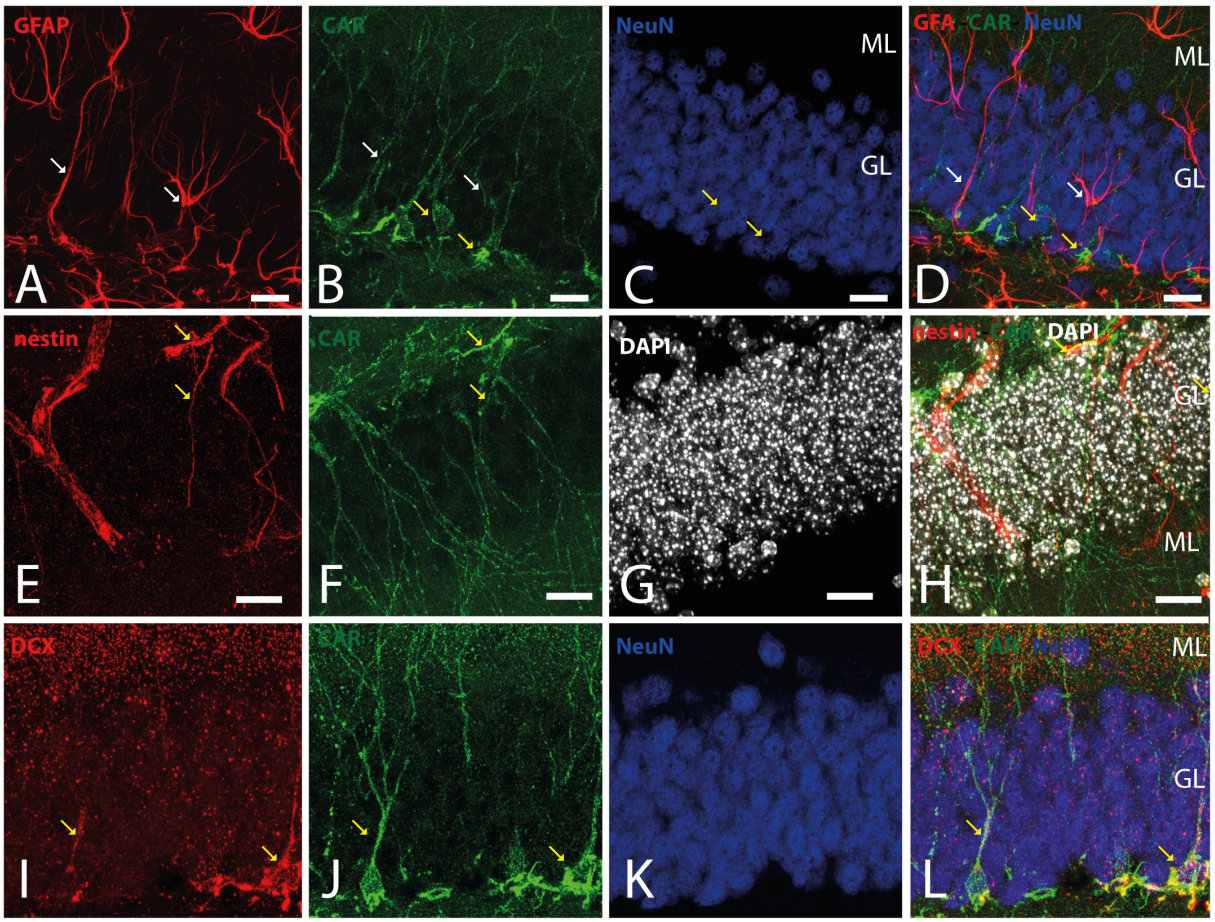

FIGURE 4 | CAR expression in the subgranular layer of the dentate gyrus. **(A–D)** Expression of CAR (green), GFAP (red), and NeuN (blue) in the SGZ of the dentate gyrus. There are some fibers GFAP$^+$ that also are CAR$^+$ (white arrows). Some CAR$^+$ cells are also expressing Neun (yellow arrows). **(E–H)** Colocalization of CAR (green), nestin (red), and DAPI (white) in the SGZ. Nestin and CAR colocalization in some cells (yellow arrows). **(I–L)** Colocalization of CAR (green), DCX (red), and DAPI (white) in the SGZ. Both CAR and DCX are present in the same cells (white arrows). Calibration bars: **(A–L)**: 10 μm.

was in the cytoplasmic membrane of ependymal cells (arrows in **Figure 5K**).

To identify the CAR-immunoreactive cells located in the mediobasal hypothalamus, we again perform double and triple immunolabeling (**Figure 6**). In the medial preoptic area, we found that CAR expression colocalizes with GFAP, but not with NeuN (**Figures 6A–D**). The white arrows in **Figures 6A–D** show CAR and GFAP-immunoreactive cells in this area. In the ventral area of mediobasal hypothalamus, the soma of the majority of the CAR-immunoreactive cells (**Figure 6**) lining the third ventricle did not colocalize with GFAP (**Figures 6E–H**), whereas some somas situated in the subventricular zone showed CAR-immunoreactive fibers running toward the hypothalamic parenchyma and those were also GFAP immunoreactive (white arrows in **Figures 6E–H**). In the arcuate nucleus, CAR-immunoreactive cells and fibers lining the ventricle were GFAP negative (white arrows in **Figures 6I–L**). However, in the same area in the parenchyma, a population of GFAP-immunoreactive cells were also CAR immunoreactive (yellow arrows in **Figures 6I–L**).

As expected in the dorsal area of mediobasal hypothalamus, we observed nestin-immunoreactive cells (**Figures 6M–P**) lining the 3rd ventricle as well as in fibers running toward the parenchyma. Although the CAR immunoreactivity had a similar distribution, these two proteins were mainly colocalized in the cells lining the ventricle and in some of the fibers in the parenchyma (white arrows in **Figures 6M–P**).

In the subcommissural organ, CAR and nestin immunoreactivity overlapped in some, but not all, cells (**Figures 6Q–T**).

CAR Expression in the Caudal Regions of the CNS

As noted above, CAR immunoreactivity was globally lower in the midbrain and rhombencephalon. In general, the fiber tracts in midbrain were CAR negative (**Figure 7**). We found CAR in the neuropil of the zonal layer of the superior colliculus (**Figures 7A,B**), all along the periaqueductal gray (**Figure 7A**), and in the ependymal cells of the cerebral

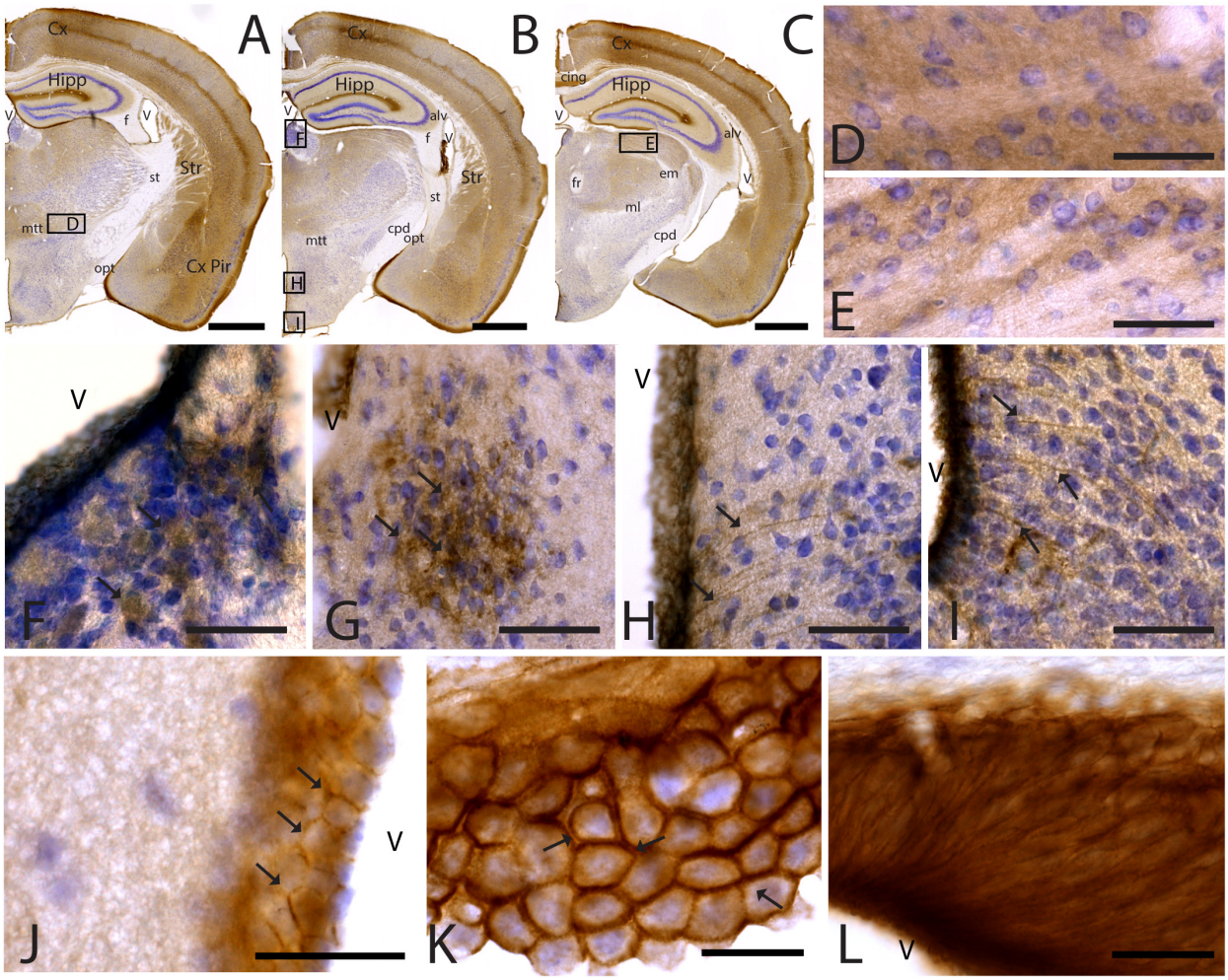

FIGURE 5 | CAR expression in the thalamus and hypothalamus. CAR immunoreactivity in brown counterstained with Harry's hematoxylin in blue. **(A–C)** Coronal section of mouse brain. CAR is present in the piriform cortex, isocortex, and hippocampus and in different nuclei of the thalamus and hypothalamus. **(D)** High magnification from **(A)**, ventral thalamus where CAR is present in the neuropil. **(E)** High magnification from **(C)** showing CAR immunoreactivity in the neuropil of the lateral geniculate nucleus. **(F)** CAR expression in the habenula, high magnification from **(B)**. **(G)** Detail of the preoptic area showing CAR expression (arrows). **(H)** Dorsal region of the medio basal hypothalamus showing the presence of CAR$^+$ cells lining the 3rd ventricle and fibers in the adjacent regions (arrows). **(I)** Ventral region of the mediobasal hypothalamus showing the presence of CAR$^+$ cells lining the 3rd ventricle and fibers in the adjacent regions. **(J)** CAR$^+$ cells lining the 3rd ventricle in the thalamus. CAR is present in the cellular membrane (arrows). **(K)** Presence of CAR in the choroid plexus; arrows are showing the presence of protein in the cellular membrane. **(L)** CAR immunoreactivity in the cells of the subcommissural organ. Calibration bars: **(A–C)**: 1 mm, **(D–L)**: 10 μm.

aqueduct. The substantia nigra showed a faint neuropil staining, mainly in the pars compacta. Caudally at the tegmentum, CAR immunoreactivity was found in the neuropil of the nuclei situated in the midline (**Figure 7C**), corresponding with the raphe formation (**Figures 7C,D**) and the tegmental reticular nucleus (**Figures 7C,E**). The nuclei of the lateral lemniscus showed a pattern of CAR immunoreactivity similar to that of the lateral geniculate nuclei.

In the rhombencephalon, notable CAR immunoreactivity was observed in the dorsal cochlear nucleus (**Figures 7F,G**), with an expression pattern similar to that of the habenula (arrows in **Figure 7G**). The nuclei situated in the medio-dorsal area of the rhombencephalon along the rostro-caudal axis showed faint CAR immunostaining in the neuropil, while in the locus coeruleus, inferior olive complex (**Figures 7H,I**), and in the area postrema, the labeling in the neuropil was more intense (**Figures 7J,L**). There was also CAR immunoreactivity in the neuropil of the dorsal motor nucleus of the vagus nerve and the hypoglossal nucleus.

In sagittal sections, we found a population of CAR-immunoreactive cells located in the caudal region of the 4th ventricle, area postrema, with the somas situated in the ventricular zone and the projections toward the parenchyma (**Figures 7J,L**). This pattern resembled that of in the hypothalamus (data not shown). The cerebellum showed

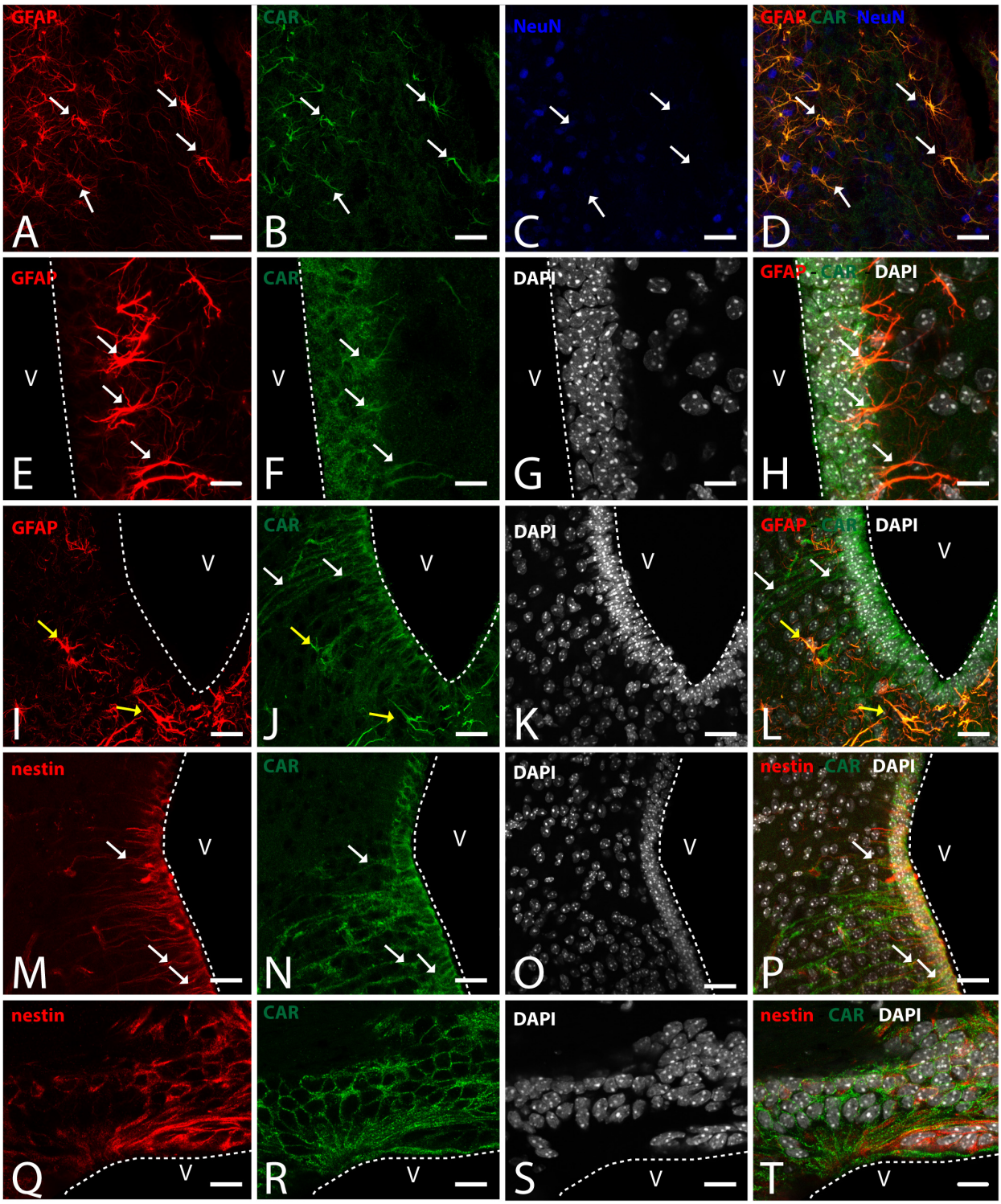

FIGURE 6 | CAR expression in the hypothalamus. **(A–D)** Expression of CAR (green), GFAP (red), and NeuN (blue) in the medial preoptic area. White arrows indicating the colocalization of CAR and GFAP. **(E–H)** Expression of CAR (green), GFAP (red), and DAPI (white) in the mediobasal hypothalamus. Cells expressing CAR and GFAP indicated with white arrows. **(I–L)** Expression of CAR (green), GFAP (red), and DAPI (white) in the arquate nucleus. CAR-immunoreactive cells lining the ventricle and CAR cells also expressing GFAP indicated with yellow arrows in the parenchyma. **(M–P)** Expression of CAR (green), nestin (red), and DAPI (white) in the mediobasal hypothalamus. White arrows indicating the colocalization of CAR and nestin. **(Q–T)** Expression of CAR (green), nestin (red), and DAPI (white) in the subcommissural organ. Calibration bars: **(A–T)**: 20 μm.

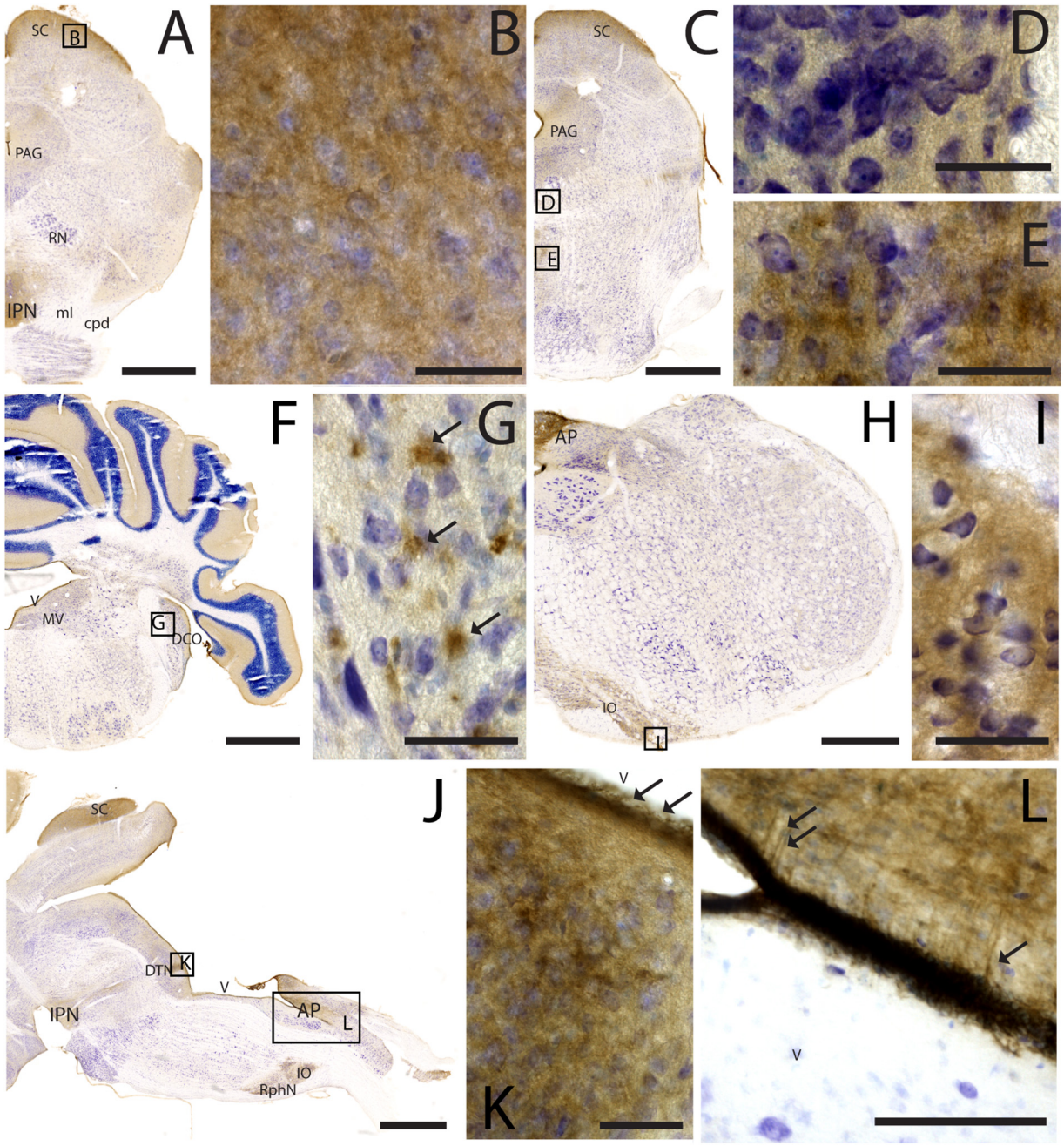

FIGURE 7 | CAR expression in the midbrain and brainstem. CAR immunoreactivity in brown counterstained with Harry's hematoxylin in blue. **(A)** Coronal section of mouse brain; CAR is present in the neuropil of the superior colliculus, the periaqueductal gray, and in the interpeduncular nucleus. **(B)** High magnification of **(A)** showing CAR immunostaining in the neuropil of the zonal layer in the superior colliculus. **(C)** Coronal section of mouse brain; CAR is present in the neuropil of the superior colliculus, the periaqueductal gray, and in the midline nuclei of raphe and reticular nuclei. **(D)** High magnification of **(C)** showing the presence of CAR in the neuropil of the midline raphe nuclei. **(E)** High magnification of **(C)** showing CAR immunoreactivity in the neuropil of the midline, corresponding to the tegmental reticular nucleus and raphe magnus. **(F)** Coronal section of mouse brain showing the presence of CAR immunostaining in the neuropil of the molecular layer of the cerebellar cortex, in the medial vestibular nucleus and dorsal cochlear nucleus. **(G)** High magnification of **(F)** showing the pattern of expression of CAR in the dorsal cochlear nucleus. **(H)** Coronal section of mouse brain showing CAR expression in the caudal rhombencephalon, in the area postrema, and inferior olive complex. **(I)** High magnification of **(H)** showing the presence of CAR immunostaining in the neuropil of the inferior olive complex. **(J)** Sagittal section of a mouse brain showing the presence of CAR immunolabeling in the superior colliculus, interpeduncular nucleus, in the dorsal tegmental nucleus, area postrema, inferior olive complex and raphe nuclei. **(K)** High magnification of **(J)** showing the presence of CAR in the neuropil of the dorsal tegmental nucleus and the ependymal cell lining the 4th ventricle (arrows). **(L)** Magnification of **(J)** showing the 4th ventricle and the area postrema. CAR is present in the neuropil and in the projections toward the parenchyma. Calibration bars: **(A–B)**: 1 mm; **(C–E)**: 5 μm; **(F)**: 1 mm; **(G)**: 5 μm; **(H)**: 1.5 mm; **(I)**: 5 μm; **(J)**: 1 mm; **(K)**: 5 μm; **(L)**: 15 μm.

a faint CAR immunostaining in the neuropil of the molecular layer (**Figure 7F**).

DISCUSSION

IgCAMs play a role in several processes during brain development and in the mature brain, which include dendritic spine development, neurite outgrowth, axon guidance and fasciculation, adult neurogenesis and synapse remodeling (reviewed by Gibson, 2001). This study characterized the expression of CAR throughout the adult mouse brain and will contribute to understanding its physiological role. Of note, the anti-CAR antibody used here (R&D systems, AF2654, RRID:AB_2245567, Lot VFT0119071) did not show immunoreactivity in brain sections from CAR-CNS knockout mice (see **Supplementary Figure 1**) (Zussy et al., 2016). We used C57BL/6J and C57BL/6N mice because previous studies have shown different pattern expression of several genes and proteins (Morris et al., 2010), metabolism and inflammatory response (Simon et al., 2013) and emotional responses to social stress (Hovatta et al., 2005; Bryant et al., 2008; Matsuo et al., 2010; Kulesskaya et al., 2011; Chen et al., 2019). In these mice, we found no striking differences in the intensity or pattern of CAR immunoreactivity.

While CAR levels decrease notably after birth, CAR is readily detected in cells, fibers, and in the neuropil of several brain areas in the adult brain. We observed CAR immunoreactivity in both cortical areas and nuclei all along the brain, with the olfactory bulb and the accessory olfactory bulb showing the highest immunoreactivity. Globally, we concluded that CAR is expressed primarily by maturing and mature neurons in the brain parenchyma. Of note, while CAR occasionally colocalizes with GFAP, it remained limited to the boundary of the 3rd ventricle, the SVZ (areas that are associated with adult neurogenesis) and specific populations located in the hypothalamus, an area that may generate new neurons in the adult mouse brain and is associated with hyperplasticity (Parkash and Kaur, 2007; Bolborea, 2011).

In the RMS, SVZ, and SGZ, we found CAR expression in accordance with previous studies (Hotta et al., 2003; Venkatraman et al., 2005; Zussy et al., 2016; Salinas et al., 2017; Chen et al., 2019; Wrackmeyer et al., 2019). The partial colocalization of CAR with GFAP, nestin and SOX2 in the SVZ demonstrates that CAR is express during adult neurogenesis, as was propose previously in the SGZ of the DG (Zussy et al., 2016).

In the SVZ, we found CAR in two different cell populations: in $SOX2^+$, $GFAP^+$ and $nestin^+$ cells, which is consistent with expression of CAR in stem cells and type B1 cells (Codega et al., 2014; Fuentealba et al., 2015; Llorens-Bobadilla et al., 2015), and DCX^+ cells, which correspond to type A or neuroblasts (reviewed by Ming and Song, 2011). The main difference between those two CAR-immunoreactive populations is the fact that the cells expressing SOX2, nestin, or GFAP in the SVZ only show a partial colocalization with CAR, while the DCX^+ cells showing a clear colocalization and also higher levels of CAR expression. These differences are clearer in the RMS where CAR^+/DCX^+ cells were readily detected, while CAR-immunoreactivity is absent in the $GFAP^+$ cells. In the RMS, the migrating neuroblasts are surrounded by glial cells that serve as a scaffold for the neuroblast migration (Lois and Alvarez-Buylla, 1994; Snapyan et al., 2009; Kaneko et al., 2010). The differences between the SVZ and the RMS could be due to two $GFAP^+$ cell populations, but this needs a more detailed study. In the SGZ, CAR also colocalizes with DCX, but in contrast to the SVZ, CAR was essentially absent in the $GFAP^+$ cells. These results agree with previous results showing the colocalization of CAR and PSA-CAM in this area (Salinas et al., 2017), suggesting that CAR plays a role at different stages of neuronal maturation and in different neurogenic areas. It is tempting to speculate that in the SGZ, CAR regulates network development and integration, whereas in the SVZ, it is involved in the migration of NPCs along the RMS and possibly also during differentiation and integration.

We show that CAR is present in an eclectic combination of regions in the adult mouse brain. In general, CAR is expressed in the neuropil of numerous adult brain regions. The cortex is present in all the layers but is more prominent in layers I and IV. PSA-NCAM is also in the cortical neuropil (Varea et al., 2005), which is involved in brain plasticity. Furthermore, in the thalamus and brainstem, CAR expression is similar to that of PSA-NCAM, where it is in the neuropil of several nuclei and characterized by structural plasticity and related to memory and learning (Mazzetti et al., 2007; Quartu et al., 2010).

Coxsackievirus and adenovirus receptor immunoreactivity in the preoptic area and hypothalamic median eminence-arcuate region had not been previously reported. The hypothalamic median eminence-arcuate region may be an additional site adult neurogenesis as a handful of studies suggested that α2 tanycytes may function as stem-like cells and that β tanycytes are lineage-restricted cells with limited proliferative potential (reviewed by Yoo and Blackshaw, 2018). In this area, CAR colocalizes with GFAP and nestin indicating that it is present in α1and α2 tanycytes. CAR was also present in the arcuate region in the cells lining the ventricle that were GFAP negative, and therefore possible β tanycytes. There are also other CAR-immunoreactive populations located in the preoptic area and the rostral arcuate hypothalamic nucleus that colocalize with GFAP. Previous studies have shown colocalization of PSA-NCAM and GFAP in tanycytes and in cells present in the parenchyma of the preoptic area and arcuate nucleus. Here, PSA-NCAM expression changes are related with a high capacity for neuroplastic changes in the adult rodent brain and the modulation of gonadotropin release induced by neuroendocrine signals (Parkash and Kaur, 2007; Bolborea, 2011). CAR's presence in these regions and in the $GFAP^+$ populations opens the door to study the changes in CAR expression induced by different neuroendocrine signals. Our previous results showed that under peripheral inflammatory conditions (peritoneal LPS injection), there is a posttranslational CAR loss that correlates with changes in hippocampal plasticity and neurogenesis (Zussy et al., 2016), which makes the preoptic area and the rostral arcuate hypothalamic nucleus candidates for further studies of the impact of inflammation on CAR levels. Moreover, the GFAP-immunoreactive population in

the hypothalamus has been studied in relation with reactive astrogliosis in the hypothalamus in response to diet in rodents; chronic low-grade inflammation in peripheral tissues due to a fat-rich diet induced hypothalamic inflammation, an increase of proinflammatory cytokines such as TNF and IL-1β and an increase in gliosis (reviewed by Seong et al., 2019). CAR levels in the hypothalamic median eminence-arcuate region could also be affected by a proinflammatory environment induced by disease or poor diet. It is also noteworthy that CXADR (the gene coding for CAR) contains an estrogen response element in its promoter (Lucas et al., 2003). Clearly, further studies are needed to characterize the role of CAR in this enigmatic region.

Consistent with previous studies, we found CAR in the epithelial cells of the adult choroid plexus and in the neuroepithelium surrounding the ventricles (Hotta et al., 2003; Chen et al., 2019), as well as in the aqueduct and in the subcommissural organ. In the epithelial cells, CAR was on the basolateral surface and low or absent on the apical surface, supporting the hypothesis that it may participate in the polarization of the neuronal stem cell niche favoring radial, asymmetric division of progenitors (reviewed by Hauwel et al., 2005). The choroid plexus and the subcommissural organ are secretory tissues responsible for producing the cerebrospinal fluid, as an interface between the blood and the CNS, and involved in the regulation of the adult neurogenesis. The choroid plexus is a port of entry for immune cells and thus a potential site for communication between the immune system and the CNS (reviewed by Lun et al., 2015). Recent studies have demonstrated that the choroid plexus expresses interferons which facilite the *trans*-epithelial passage of leukocytes (Peralta et al., 2017). CAR plays an active role in *trans*-epithelial passage in other epithelial monolayers, where it is phosphorylated in response to TNF (Morton et al., 2016). Therefore, in the choroid plexus CAR may play a similar role.

The study of connectivity and wiring in the brain is a challenge. Moreover, linking expression of proteins on projections and terminals to that of the soma needs specific tools. Traditionally, it was done using chemical tracer, molecules injected in the projection site and transported to the soma or in the other way around, helping us to identify the origin of the projections in specific areas. In recent years, viral vector has been used as tracers. CAV-2 vectors preferentially transduce neurons (Soudais et al., 2004; Cubizolle et al., 2014; Beier et al., 2015; Schwarz et al., 2015; Hirschberg et al., 2017; Mestre-Francés et al., 2018) and are widely used in brain studies. It is important to note that, to the best of our knowledge, CAV-2 depends on CAR to bind and be internalized in neurons. This CAR-tropic nature of CAV-2 is further supported by the lack of infection of cells in CAR CNS-KO mice (Zussy et al., 2016). Different *in vitro* assays have characterized the CAR-dependent mechanisms regulating CAV-2 entry and transport in primary rodent motor neurons (Salinas et al., 2009; Henaff et al., 2011; Simão et al., 2015), and how it occurs in pH neutral endosomes, which allows long-range transport in an environment that precludes conformational changes of the capsid and endosomal escape. Numerous studies have shown that CAV-2 vectors can target different subpopulations of neurons in the brain in rodents, dogs, and non-human primates (Soudais et al., 2004; Cubizolle et al., 2014; Beier et al., 2015; Schwarz et al., 2015; Hirschberg et al., 2017; Mestre-Francés et al., 2018). CAV-2 retrograde transport is also noteworthy: for example, from the striatum to the soma of dopaminergic neurons in the substantia nigra pars compacta, thalamic neurons, and cortical neurons (layer IV) of the ipsilateral and contralateral isocortex (Soudais et al., 2004; Hnasko et al., 2005; Kremer, 2005; Junyent and Kremer, 2015; del Rio et al., 2019). In addition to retrograde transport, infection of neurons at the site of injection is also robust. When a CAV-2 vector carrying GFP gene is injected in the striatum, one detects dense GFP signal in the soma of striatal neurons (Soudais et al., 2004; Cubizolle et al., 2014; Beier et al., 2015; Schwarz et al., 2015; Hirschberg et al., 2017; Mestre-Francés et al., 2018). Another example is the SOX2-positive cells lining the lateral ventricles that are infected by CAV-2 when it is injected into ventricles/cerebral spinal fluid (Salinas et al., 2017). Here is where the knowledge of CAR expression in the adult brain is an important factor to help in the study of the brain connectivity in healthy or pathological models. CAV-2 vectors are able to transduce different types of neurons, motor, sensory, parasympathetic, GABAergic, cholinergic, norepinephrine, and dopamine neurons (Hnasko et al., 2006; Salinas et al., 2009; Beier et al., 2015; Schwarz et al., 2015; Li et al., 2016; Uematsu et al., 2017), but the preference for neuronal subtypes is not fully characterized. The presence of CAR has been described in the presynaptic fraction of synaptosome preparations from adult mouse, prosimian, monkey, and human brains (Zussy et al., 2016; Mestre-Francés et al., 2018). *In vitro*, it is clear that CAV-2 can infect neurons by binding to CAR at axon terminals (Salinas et al., 2009, 2010); however, there is a lack of studies in relation with CAR distribution and density along the axons *in vivo* and its presence in the soma of different neuronal populations. The fact that CAV-2 vectors can efficiently enter a neuron via presynaptic termini does not, *a priori*, exclude other entry sites (Schwarz and Luo, 2015). However, anecdotal data suggest that if CAV-2 is taken up via axon *en passant*, it is not robust.

CONCLUSION

In conclusion, we generated a global description of CAR immunoreactivity in the male mouse brain. Our study is the basis for comparative studies with other mammals and to further explore the function of CAR in the neurogenic niches of the SVZ, SGZ, and in relation with plasticity in different areas of the brain in the healthy, diseased, or proinflammatory-challenged brain.

DATA AVAILABILITY STATEMENT

All datasets generated for this study are included in the article/**Supplementary Material**.

ETHICS STATEMENT

The animal study was reviewed and approved by the Comité Régional Languedoc-Roussillon.

AUTHOR CONTRIBUTIONS

ID-R and EK were responsible for the concept, design, supervision of the study, and contributed to the initial draft of the manuscript. AW and ID-R were responsible for the acquisition. ID-R was responsible of the analysis, and interpretation of histological data.

FUNDING

Funding for studies in the Kremer lab has been provided in part by the European Commission (FP7 BrainVector #222992, BrainVector #286071), EpiGenMed (ANR-10-LABX-12-01), La Fondation pour la Recherche Médicale, E-Rare (Grant# ANR-17-RAR3-0001-01), La Région Occitanie (ALDOCT 000411-2018001118), the ANR (GOAL: ANR-14-CE13-0014-03, NORAD: ANR-19-CE37-0008-01), and France Parkinson (FP-Kremer2015).

ACKNOWLEDGMENTS

We thank EKL members for constructive comments during the course of this study. We also thank Réseau d'Histologie Expérimentale de Montpellier, Montpellier Ressources Imagerie (ANR-10-INBS-04, "Investment for the Future"), and the Réseau des Animaleries de Montpellier.

SUPPLEMENTARY MATERIAL

The Supplementary Material for this article can be found online at: https://www.frontiersin.org/articles/10.3389/fnana.2020.00028/full#supplementary-material

REFERENCES

Beier, K., Steinberg, E., Deloach, K., Xie, S., Miyamichi, K., Schwarz, L., et al. (2015). Circuit architecture of VTA dopamine neurons revealed by systematic input-output mapping. *Cell* 162, 622–634. doi: 10.1016/j.cell.2015.07.015

Bergelson, J. M. (1999). Receptors mediating adenovirus attachment and internalization. *Biochem. Pharmacol.* 57, 975–979.

Bergelson, J. M., Cunningham, J. A., Droguett, G., Kurt-Jones, E. A., Krithivas, A., Hong, J. S., et al. (1997). Isolation of a common receptor for Coxsackie B viruses and Adenoviruses 2 and 5. *Science* 275, 1320–1323.

Bergelson, J. M., Krithivas, A., Celi, L., Droguett, G., Horwitz, M. S., Wickham, T., et al. (1998). The murine CAR homolog is a receptor for coxsackie B virus and adenoviruses. *J. Virol.* 72, 415–419.

Bolborea, M. (2011). Marie-pierre laran-chich, kamontip rasri, herbert hildebrandt, piyarat govitrapong, valérie simonneaux, paul pévet, stephan steinlechner, paul klosen, melatonin controls photoperiodic changes in tanycyte vimentin and neural cell adhesion molecule expression in the djungarian hamster (Phodopus sungorus). *Endocrinology* 152, 3871–3883. doi: 10.1210/en.2011-1039

Bryant, C. D., Zhang, N. N., Sokoloff, G., Fanselow, M. S., Ennes, H. S., Palmer, A. A., et al. (2008). Behavioral differences among C57BL/6 substrains: implications for transgenic and knockout studies. *J. Neurogenet.* 22, 315–331. doi: 10.1080/01677060802357388

Carson, S. D., Chapman, N. M., and Tracy, S. M. (1997). Purification of the putative coxsackievirus B receptor from HeLa cells. *Biochem. Biophys. Res. Commun.* 233, 325–328. doi: 10.1006/bbrc.1997.6449

Caruso, L., Yuen, S., Smith, J., Husain, M., and Opavsky, M. A. (2010). Cardiomyocyte-targeted overexpression of the coxsackie-adenovirus receptor causes a cardiomyopathy in association with b-catenin signaling. *J. Mol. Cell. Cardiol.* 48, 1194–1205. doi: 10.1016/j.yjmcc.2010.01.022

Cavallaro, U., and Dejana, E. (2011). Adhesion molecule signalling: not always a sticky business. *Nat. Rev. Mol. Cell Biol.* 12, 189–197. doi: 10.1038/nrm3068

Chen, M., Kato, T., and Kato, Y. (2019). Data on localization of coxsackievirus and adenovirus receptor (CAR) in the embryonic rat brain. *Data Brief.* 7:103726. doi: 10.1016/j.dib.2019.103726

Chrétien, I., Marcuz, A., Courtet, M., Katevuo, K., Vainio, O., Heath, J. K., et al. (1998). CTX, a Xenopus thymocyte receptor, defines a molecular family conserved throughout vertebrates. *Eur. J. Immunol.* 28, 4094–4104.

Codega, P., Silva-Vargas, V., Paul, A., Maldonado-Soto, A. R., DeLeo, A. M., Pastrana, E., et al. (2014). Prospective identification and purification of quiescent adult neural stem cells from their in vivo niche. *Neuron* 82, 545–559. doi: 10.1016/j.neuron.2014.02.039

Cohen, C. J., Shieh, J. T. C., Pickles, R. J., Okegawa, T., Hsieh, J.-T. T., and Bergelson, J. M. (2001). The coxsackievirus and adenovirus receptor is a transmembrane component of the tight junction. *Proc. Natl. Acad. Sci. U.S.A.* 98, 15191–15196. doi: 10.1073/pnas.261452898

Cubizolle, A., Serratrice, N., Skander, N., Colle, M. A., Ibanes, S., Gennetier, A., et al. (2014). Corrective GUSB transfer to the canine mucopolysaccharidosis VII brain. *Mol. Ther.* 22, 762–773. doi: 10.1038/mt.2013.283

del Rio, D., Beucher, B., Lavigne, M., Wehbi, A., Gonzalez Dopeso-Reyes, I., Saggio, I., et al. (2019). CAV-2 vector development and gene transfer in the central and peripheral nervous systems. *Front. Mol. Neurosci.* 12:71. doi: 10.3389/fnmol.2019.00071

Excoffon, K. J. D. A., Hruska-Hageman, A., Klotz, M., Traver, G. L., and Zabner, J. (2004). A role for the PDZ-binding domain of the coxsackie B virus and adenovirus receptor (CAR) in cell adhesion and growth. *J. Cell Sci.* 117, 4401–4409. doi: 10.1242/jcs.01300

Farmer, C., Morton, P. E., Snippe, M., Santis, G., and Parsons, M. (2009). Coxsackie adenovirus receptor (CAR) regulates integrin function through activation of p44/42 MAPK. *Exp. Cell Res.* 315, 2637–2647. doi: 10.1016/j.yexcr.2009.06.008

Franklin, K., and Paxinos, G. (1997). *The Mouse Brain in Stereotaxic Coordinates*. San Diego, CA: Academic Press.

Fuentealba, L. C., Rompani, S. B., Parraguez, J. I., Obernier, K., Romero, R., Cepko, C. L., et al. (2015). Embryonic origin of postnatal neural stem cells. *Cell* 161, 1644–1655. doi: 10.1016/j.cell.2015.05.041

Gibson, N. J. (2001). Cell adhesion molecules in context: CAM function depends on the neighborhood. *Cell Adh. Migr.* 5, 48–51.

Hauwel, M., Furon, E., and Gasque, P. (2005). Molecular and cellular insights into the coxsackie-adenovirus receptor: role in cellular interactions in the stem cell niche. *Brain Res. Brain Res. Rev.* 48, 265–272.

Henaff, D., Salinas, S., and Kremer, E. J. (2011). An adenovirus traffic update: from receptor engagement to the nuclear pore. *Fut. Microbiol.* 6, 179–192. doi: 10.2217/fmb.10.162

Hirschberg, S., Li, Y., Randall, A., Kremer, E. J., and Pickering, A. E. (2017). Functional dichotomy in spinal-vs prefrontal-projecting locus coeruleus modules splits descending noradrenergic analgesia from ascending aversion and anxiety in rats. *eLife* 6:29808. doi: 10.7554/eLife.29808.001

Hnasko, T. S., Perez, F. A., Scouras, A. D., Stoll, E. A., Gale, S. D., Luquet, S., et al. (2006). Cre recombinase-mediated restoration of nigrostriatal dopamine in dopamine-deficient mice reverses hypophagia and bradykinesia. *Proc. Natl. Acad. Sci. U.S.A.* 103, 8858–8863. doi: 10.1073/pnas.0603081103

Hnasko, T. S., Sotak, B. N., and Palmiter, R. D. (2005). Morphine reward in dopamine-deficient mice. *Nature* 438, 854–857.

Honda, T., Saitoh, H., Masuko, M., Katagiri-Abe, T., Tominaga, K., Kozakai, I., et al. (2000). The coxsackievirus-adenovirus receptor protein as a cell adhesion molecule in the developing mouse brain. *Brain Res. Mol. Brain Res.* 77, 19–28.

Hotta, Y., Honda, T., Naito, M., and Kuwano, R. (2003). Developmental distribution of coxsackie virus and adenovirus receptor localized in the nervous system. *Brain Res. Dev. Brain Res.* 143, 1–13.

Houri, N., Huang, K. C., and Nalbantoglu, J. (2013). The Coxsackievirus and Adenovirus Receptor (CAR) undergoes ectodomain shedding and regulated intramembrane proteolysis (RIP). *PLoS One* 8:e73296. doi: 10.1371/journal.pone.0073296

Hovatta, I., Tennant, R. S., Helton, R., Marr, R. A., Singer, O., Redwine, J. M., et al. (2005). Glyoxalase 1 and glutathione reductase 1 regulate anxiety in mice. *Nature* 438, 662–666.

Junyent, F., and Kremer, E. J. (2015). CAV-2–why a canine virus is a neurobiologist's best friend. *Curr. Opin. Pharmacol.* 24, 86–93. doi: 10.1016/j.coph.2015.08.004

Kaneko, N., Marín, O., Koike, M., Hirota, Y., Uchiyama, Y., Wu, J. Y., et al. (2010). New neurons clear the path of astrocytic processes for their rapid migration in the adult brain. *Neuron* 67, 213–223. doi: 10.1016/j.neuron.2010.06.018

Kremer, E. J. (2005). Gene transfer to the central nervous system: Current state of the art of the viral vectors. *Curr. Genomics* 6, 13–37. doi: 10.2174/1389202053202111

Kulesskaya, N., Rauvala, H., and Voikar, V. (2011). Evaluation of social and physical enrichment in modulation of behavioural phenotype in C57BL/6J female mice. *PLoS One* 6:e24755. doi: 10.1371/journal.pone.0024755

Li, Y., Hickey, L., Perrins, R., Werlen, E., Patel, A. A., Hirschberg, S., et al. (2016). Retrograde optogenetic characterization of the pontospinal module of the locus coeruleus with a canine adenoviral vector. *Brain Res.* 1641, 274–290. doi: 10.1016/j.brainres.2016.02.023

Llorens-Bobadilla, E., Zhao, S., Baser, A., Saiz-Castro, G., Zwadlo, K., and Martin-Villalba, A. (2015). Single-cell transcriptomics reveals a population of dormant neural stem cells that become activated upon brain injury. *Cell Stem Cell.* 17, 329–340. doi: 10.1016/j.stem.2015.07.002

Lois, C., and Alvarez-Buylla, A. (1994). Long-distance neuronal migration in the adult mammalian brain. *Science* 264, 1145–1148. doi: 10.1126/science.8178174

Loustalot, F., Kremer, E. J., and Salinas, S. (2016). Membrane dynamics and signaling of the coxsackievirus and adenovirus receptor. *Int. Rev. Cell Mol. Biol.* 322, 331–362. doi: 10.1016/bs.ircmb.2015.10.006

Lucas, A., Kremer, E. J., Hemmi, S., Luis, J., Vignon, F., and Lazennec, G. (2003). Comparative transductions of breast cancer cells by three DNA viruses. *Biochem. Biophys. Res. Commun.* 309, 1011–1016. doi: 10.1016/j.bbrc.2003.08.101

Lun, M. P., Monuki, E. S., and Lehtinen, M. K. (2015). Development and functions of the choroid plexus-cerebrospinal fluid system. *Nat Rev Neurosci.* 16, 445–457. doi: 10.1038/nrn3921

Matsuo, N., Takao, K., Nakanishi, K., Yamasaki, N., Tanda, K., and Miyakawa, T. (2010). Behavioral profiles of three C57BL/6 substrains. *Front Behav Neurosci.* 4:29.

Mazzetti, S., Ortino, B., Inverardi, F., Frassoni, C., and Amadeo, A. (2007). PSA-NCAM in the developing and mature thalamus. *Brain Res. Bull.* 71, 578–586.

Mestre-Francés, N., Serratrice, N., Gennetier, A., Devau, G., Cobo, S., Trouche, S., et al. (2018). Exogenous LRRK2G2019S induces parkinsonian-like pathology in a nonhuman primate. *JCI Insight* 3:e98202. doi: 10.1172/jci.insight.98202

Ming, G. L., and Song, H. (2011). Adult neurogenesis in the mammalian brain: significant answers and significant questions. *Neuron* 70, 687–702. doi: 10.1016/j.neuron.2011.05.001

Morris, J. A., Royall, J. J., Bertagnolli, D., Boe, A. F., Burnell, J. J., Byrnes, E. J., et al. (2010). Divergent and nonuniform gene expression patterns in mouse brain. *Proc. Natl. Acad. Sci. U.S.A.* 107, 19049–19054. doi: 10.1073/pnas.1003732107

Morton, P. E., Hicks, A., Nastos, T., Santis, G., and Parsons, M. (2013). CAR regulates epithelial cell junction stability through control of E-cadherin trafficking. *Sci. Rep.* 3:2889. doi: 10.1038/srep02889

Morton, P. E., Hicks, A., Ortiz-Zapater, E., Raghavan, S., Pike, R., Noble, A., et al. (2016). TNFα promotes CAR-dependent migration of leukocytes across epithelial monolayers. *Sci. Rep.* 6:26321. doi: 10.1038/srep26321

Ortiz-Zapater, E., Santis, G., and Parsons, M. (2017). CAR: A key regulator of adhesion and inflammation. *Int. J. Biochem. Cell Biol.* 89, 1–5. doi: 10.1016/j.biocel.2017.05.025

Parkash, J., and Kaur, G. (2007). Transcriptional regulation of PSA-NCAM mediated neuron-glial plasticity in the adult hypothalamus. *Neuron Glia Biol.* 3, 299–307. doi: 10.1017/S1740925X07000701

Patzke, C., Max, K. E., Behlke, J., Schreiber, J., Schmidt, H., Dorner, A. A., et al. (2010). The coxsackievirus-adenovirus receptor reveals complex homophilic and heterophilic interactions on neural cells. *J. Neurosci.* 30, 2897–2910. doi: 10.1523/JNEUROSCI.5725-09.2010

Peralta, R. J. M., Bussi, C., Gaviglio, E. A., Arroyo, D. S., Baez, N. S., Rodriguez-Galan, M. C., et al. (2017). Type I IFNs are required to promote central nervous system immune surveillance through the recruitment of inflammatory monocytes upon systemic inflammation. *Front. Immunol.* 8:1666. doi: 10.3389/fimmu.2017.01666

Quartu, M., Serra, M. P., Boi, M., Melis, T., Ambu, R., and Fiacco, M. D. (2010). Brain-derived neurotrophic factor (BDNF) and polysialylated-neural cell adhesion molecule (PSA-NCAM): codistribution in the human brainstem precerebellar nuclei from prenatal to adult age. *Brain Res.* 1363, 49–62. doi: 10.1016/j.brainres.2010.09.106

Raschperger, E., Thyberg, J., Pettersson, S., Philipson, L., Fuxe, J., and Pettersson, R. F. (2006). The coxsackie- and adenovirus receptor (CAR) is an in vivo marker for epithelial tight junctions, with a potential role in regulating permeability and tissue homeostasis. *Exp Cell Res.* 312, 1566–1580.

Sakurai, T. (2017). The role of cell adhesion molecules in brain wiring and neuropsychiatric disroders. *Mol. Cell Neurosci.* 81, 4–11. doi: 10.1016/j.mcn.2016.08.005

Salinas, S., Bilsland, L. G., Henaff, D., Weston, A. E., Keriel, A., Schiavo, G., et al. (2009). CAR-associated vesicular transport of an adenovirus in motor neuron axons. *PLoS Pathog.* 5:e1000442. doi: 10.1371/journal.ppat.1000442

Salinas, S., Junyent, F., Core, N., Cremer, H., and Kremer, E. J. (2017). What is CAR doing in the middle of the adult neurogenic road? *Neurogenesis* 4:e1304790. doi: 10.1080/23262133.2017.1304790

Salinas, S., Schiavo, G., and Kremer, E. J. (2010). A hitchhiker's guide to the nervous system: the complex journey of viruses and toxins. *Nat. Rev. Microbiol.* 8, 645–655. doi: 10.1038/nrmicro2395

Salinas, S., Zussy, C., Loustalot, F., Henaff, D., Menendez, G., Morton, P. E., et al. (2014). Disruption of the coxsackievirus and adenovirus receptor-homodimeric interaction triggers lipid microdomain-and dynamin-dependent endocytosis and lysosomal targeting. *J. Biol. Chem.* 289, 680–695. doi: 10.1074/jbc.M113.518365

Schwarz, L., Miyamichi, K., Gao, X. J., Beier, K. T., Weissbourd, B., DeLoach, K., et al. (2015). Viral-genetic tracing of the input–output organization of a central noradrenaline circuit. *Nature* 524, 88–92. doi: 10.1038/nature14600

Schwarz, L. A., and Luo, L. (2015). Organization of the locus coeruleus-norepinephrine system. *Curr. Biol.* 25, R1051–R1056. doi: 10.1016/j.cub.2015.09.039

Seong, J., Kang, J. Y., Sun, J. S., and Kim, K. W. (2019). Hypothalamic inflammation and obesity: a mechanistic review. *Arch. Pharm. Res.* 42, 383–392. doi: 10.1007/s12272-019-01138-9

Shaw, C. A., Holland, P. C., Sinnreich, M., Allen, C., Sollerbrant, K., Karpati, G., et al. (2004). Isoform-specific expression of the coxsackie and adenovirus receptor (CAR) in neuromuscular junction and cardiac intercalated discs. *BMC Cell Biol.* 5:42. doi: 10.1186/1471-2121-5-42

Simão, D., Pinto, C., Piersanti, S., Weston, A., Peddie, C. J., Bastos, A. E. P., et al. (2015). Modeling human neural functionality in vitro: three-dimensional culture for dopaminergic differentiation. *Tissue Eng. Part A* 21, 654–668. doi: 10.1089/ten.tea.2014.0079

Simon, M. M., Greenaway, S., White, J. K., Fuchs, H., Gailus-Durner, V., Wells, S., et al. (2013). A comparative phenotypic and genomic analysis of C57BL/6J and C57BL/6N mouse strains. *Genome Biol.* 14:R82. doi: 10.1186/gb-2013-14-7-r82

Snapyan, M., Lemasson, M., Brill, M. S., Blais, M., Massouh, M., Ninkovic, J., et al. (2009). Vasculature guides migrating neuronal precursors in the adult mammalian forebrain via brain-derived neurotrophic factor signaling. *J. Neurosci.* 29, 4172–4188. doi: 10.1523/JNEUROSCI.4956-08.2009

Soudais, C., Laplace-Builhe, C., Kissa, K., and Kremer, E. J. (2001). Preferential transduction of neurons by canine adenovirus vectors and their efficient retrograde transport in vivo. *FASEB J.* 15, 2283–2285. doi: 10.1096/fj.01-0321fje

Soudais, C., Skander, N., and Kremer, E. J. (2004). Long-term in vivo transduction of neurons throughout the rat CNS using novel helper-dependent CAV-2 vectors. *FASEB J.* 18, 391–393. doi: 10.1096/fj.03-0438fje

Sytnyk, V., Leshchyns'ka, I., and Schachner, M. (2017). Neural cell adhesion molecules of the immunoglobulin superfamily regulate synapse formation. Maintenance, and function. *Trends Neurosci.* 40, 295–308. doi: 10.1016/j.tins.2017.03.003

Tamanini, A., Nicolis, E., Bonizzato, A., Bezzerri, V., Melotti, P., Assael, B. M., et al. (2006). Interaction of adenovirus type 5 fiber with the coxsackievirus and adenovirus receptor activates inflammatory response in human respiratory cells. *J. Virol.* 80, 11241–11254.

Tomko, R. P., Xu, R., and Philipson, L. (1997). HCAR and MCAR: the human and mouse cellular receptors for subgroup C adenoviruses and group B coxsackieviruses. *Proc. Natl. Acad. Sci. U.S.A.* 94, 3352–3356. doi: 10.1073/pnas.94.7.3352

Uematsu, A., Tan, B., Ycu, E., Cuevas, J., Koivumaa, J., Junyent, F., et al. (2017). Modular organization of the brainstem noradrenaline system coordinates opposing learning states. *Nat. Neurosci.* 20, 1602–1611. doi: 10.1038/nn.4642

Varea, E., Nácher, J., Blasco-Ibáñez, J. M., Gómez-Climent, M. Á., Castillo-Gómez, E., Crespo, C., et al. (2005). PSA-NCAM expression in the rat medial prefrontal cortex. *Neuroscience* 136, 435–443. doi: 10.1016/j.neuroscience.2005.08.009

Venkatraman, G., Behrens, M., Pyrski, M., and Margolis, F. L. (2005). Expression of Coxsackie-Adenovirus receptor (CAR) in the developing mouse olfactory system. *J Neurocytol.* 34, 295–305.

Wrackmeyer, U., Kaldrack, J., Jüttner, R., Pannasch, U., Gimber, N., Freiberg, F., et al. (2019). The cell adhesion protein CAR is a negative regulator of synaptic transmission. *Sci. Rep.* 9:6768. doi: 10.1038/s41598-019-43150-5

Yan, R., Sharma, P., Kolawole, A. O., Martin, S. C., Readler, J. M., Kotha, P. L., et al. (2015). The PDZ3 domain of the cellular scaffolding protein MAGI-1 interacts with the Coxsackievirus and adenovirus receptor (CAR). *Int. J. Biochem. Cell Biol.* 61, 29–34. doi: 10.1016/j.biocel.2015.01.012

Yoo, S., and Blackshaw, S. (2018). Regulation and function of neurogenesis in the adult mammalian hypothalamus. *Prog. Neurobiol.* 170, 53–66. doi: 10.1016/j.pneurobio.2018.04.001

Zhou, L., Barao, S., Laga, M., Bockstael, K., Borgers, M., Gijsen, H., et al. (2012). The neural cell adhesion molecules L1 and CHL1 are cleaved by BACE1 protease in vivo. *J. Biol. Chem.* 287, 25927–25940. doi: 10.1074/jbc.M112.377465

Zussy, C., Loustalot, F., Junyent, F., Gardoni, F., Bories, C., Valero, J., et al. (2016). Coxsackievirus adenovirus receptor loss impairs adult neurogenesis, synapse content, and hippocampus plasticity. *J. Neurosci.* 36, 9558–9571. doi: 10.1523/JNEUROSCI.0132-16.2016

Conflict of Interest: The authors declare that the research was conducted in the absence of any commercial or financial relationships that could be construed as a potential conflict of interest.

frontiers in Molecular Neuroscience

BRIEF RESEARCH REPORT
published: 03 July 2020
doi: 10.3389/fnmol.2020.00121

Targeting Catecholaminergic Systems in Transgenic Rats With a CAV-2 Vector Harboring a Cre-Dependent DREADD Cassette

Juan-Carlos Cerpa[1,2], *Alain R. Marchand*[1,2], *Yoan Salafranque*[1,2], *Jean-Rémi Pape*[1,2], *Eric J. Kremer*[3] *and Etienne Coutureau*[1,2]*

[1]CNRS, Institut de Neurosciences Cognitives et Intégratives d'Aquitaine, Bordeaux, France, [2]Institut de Neurosciences Cognitives et Intégratives d'Aquitaine, Université de Bordeaux, Bordeaux, France, [3]Institut de Génétique Moléculaire de Montpellier, University of Montpellier, CNRS, Montpellier, France

Techniques that allow the manipulation of specific neural circuits have greatly increased in the past few years. DREADDs (Designer receptors exclusively activated by designer drugs) provide an elegant way to manipulate individual brain structures and/or neural circuits, including neuromodulatory pathways. Considerable efforts have been made to increase cell-type specificity of DREADD expression while decreasing possible limitations due to multiple viral vectors injections. In line with this, a retrograde canine adenovirus type 2 (CAV-2) vector carrying a Cre-dependent DREADD cassette has been recently developed. In combination with Cre-driver transgenic animals, the vector allows one to target neuromodulatory pathways with cell-type specificity. In the present study, we specifically targeted catecholaminergic pathways by injecting the vector in knock-in rat line containing Cre recombinase cassette under the control of the tyrosine hydroxylase promoter. We assessed the efficacy of infection of the nigrostriatal pathway and the catecholaminergic pathways ascending to the orbitofrontal cortex (OFC) and found cell-type-specific DREADD expression.

Keywords: DREADD, CAV-2, orbitofrontal cortex, striatum, dopamine, noradrenaline

OPEN ACCESS

Edited by:
Jean-Marc Taymans, Institut National de la Santé et de la Recherche Médicale (INSERM), France

Reviewed by:
Mitsuhiro Hashimoto, Fukushima Medical University, Japan
John J. Woodward, Medical University of South Carolina, United States

***Correspondence:**
Etienne Coutureau
etienne.coutureau@u-bordeaux.fr

Received: *22 November 2019*
Accepted: *10 June 2020*
Published: *03 July 2020*

Citation:
Cerpa J-C, Marchand AR, Salafranque Y, Pape J-R, Kremer EJ and Coutureau E (2020) Targeting Catecholaminergic Systems in Transgenic Rats With a CAV-2 Vector Harboring a Cre-Dependent DREADD Cassette. Front. Mol. Neurosci. 13:121. doi: 10.3389/fnmol.2020.00121

INTRODUCTION

Elucidation of neural circuits underlying complex animal behaviors depends on tools allowing control of neuronal activity. Designer receptors exclusively activated by designer drugs (DREADDs) technology (Roth, 2016) has been extensively used to transiently modulate activity within brain systems (Smith et al., 2016; Parkes et al., 2018). Intersectional approaches permit refined chemogenetic manipulation of specific circuits by targeting projections-defined neurons. Indeed, combining the injection of a canine adenovirus type 2 (CAV-2) vector carrying a Cre recombinase expression cassette, in the target region of a pathway, with the injection of Cre-dependent DREADDs, in the region of origin, provides a way to investigate the impact of activation (or inhibition) of specific pathways between brain areas (Alcaraz et al., 2018).

One of the main drawbacks of such a strategy is that it requires two vectors, which obviously increases the likelihood of injections misplacements and also raises the problem of the proportion of infected cells. To overcome these limitations, we report here a strategy that combines a single CAV-2 vector carrying a Cre-dependent DREADD cassette (CAV-hM4Di) and a Cre driver rat line. We assessed the efficacy of this method in the nigrostriatal dopaminergic pathway reaching the dorsolateral striatum (DLS), and the catecholaminergic pathways reaching the orbitofrontal cortex (OFC). We injected CAV-hM4Di in either the DLS or the OFC of TH-cre rats which express Cre-recombinase in dopaminergic and noradrenergic neurons. We show that this new CAV-2-based viral vector can specifically and effectively transduce catecholaminergic neurons with both projection and neuronal specificity.

MATERIALS AND METHODS

Animals and Housing Conditions

Animals were six male heterozygous TH-cre+ rats on a Long-Evans background [Long Evans-Tg(TH-cre)3.1Deis] as well as two male transgene-negative TH-cre$^-$ littermates, bred in our laboratory, and one male Long Evans rat (wild-type) obtained from Centre d'Elevage Janvier (France). Rats were aged 4 months at the time of the experiment and housed in pairs with *ad libitum* access to food and water. The facility was maintained at 21 ± 1°C with lights on from 08:00 to 20:00. Environmental enrichment was provided by orange-tinted polycarbonate tubing elements, following current French (Council directive 2013-118, February 1, 2013) and European (directive 2010-63, September 22, 2010, European Community) laws and policies regarding animal experiments.

Viral Vector

An E1/E3-deleted, replication-defective, CAV-2 vector carrying double-inverted flox sites flanking a hM4Di-mCherry fusion protein expression cassette (CAV-DIO-hM4Di-mCherry, concentration 1×10^{12} particles/ml) was obtained from Biocampus PVM, Montpellier, France. The vector will be hereafter mentioned as CAV-hM4Di.

Surgery

Rats were anesthetized with 5% isoflurane and placed in a stereotaxic frame with atraumatic ear bars (Kopf Instruments) in a flat skull position in which Bregma and Lambda are located at the same mediolateral and dorsoventral coordinates. Anesthesia was maintained with 1.5% isoflurane and complemented with a subcutaneous injection of analgesic ropivacaïne (a bolus of 0.1 ml at 2 mg/ml) at the incision locus. Intracerebral injections were made with a pump (UMP3-1 and Micro4 Controller, World Precision Instruments) *via* a 10 µl NanoFil syringe with a blunt, 34G needle. In the case of TH-Cre$^+$ rats, 1 µl of CAV-hM4Di was injected unilaterally at two sites of the OFC. Coordinates were: +4.2 anteroposterior (AP); ± 1.6 medio-lateral (ML); −5 dorso-ventral (DV) and +3.2 AP; ± 2.4 ML; −5.6 DV. For DLS, 1 µl of CAV-hM4Di was injected unilaterally at one site. Coordinates were: +0.7 AP; ± 3.6 ML; −5 DV. In the case of transgene-negative littermate TH-cre$^-$ and wild-type rats, 1 µl of CAV-hM4Di was injected unilaterally at one site of the OFC. Coordinates were +3.5 AP; +2.2 ML; −5.4 DV. All coordinates are given in millimeters from Bregma (Paxinos and Watson, 2014). The infusion was made at a rate of 200 nl/min and the pipette was left in place for an additional 5 min to allow diffusion of CAV-hM4Di. During recovery, rats were monitored and weighed daily. For an optimal migration and expression of the hM4Di-mCherry, we waited 4 weeks before perfusion.

Immunohistochemistry

Rats were rapidly and deeply anesthetized with an overdose of sodium pentobarbital (Exagon® Euthasol) and perfused transcardially with 60 ml of saline followed by 260 ml of 4% paraformaldehyde (4% PFA) in 0.1 M phosphate buffer (PB). Brains were removed and postfixed in the same 4% PFA solution overnight and then transferred to a 0.1 M PB solution. Subsequently, 40-µm-thick coronal sections were cut using a VT1200S Vibratome (Leica Microsystems). To form a series, every fourth section was collected into a cryoprotective solution and stored at −20°C. Fluorescent immunoreactivity was performed for mCherry and tyrosine hydroxylase (TH). Free-floating sections were first rinsed in 0.1 M PB saline (0.1 M PBS; 4 × 5 min) and then incubated in a blocking solution (0.1 M PBS, 0.3% Triton X-100, 3% of goat serum) for 1 h. Sections were then incubated with both primary antibodies rabbit anti-RFP (1/1,000 in blocking solution, PM005 MBL International Corporation) and monoclonal mouse anti-TH (1/2,500 in blocking solution, MAB318 Merck Millipore), for 48 h at 4°C on a shaker. After further rinses in 0.1 M PBS (4 × 5 min), sections were placed for 2 h in a bath containing both secondary antibodies TRITC goat anti-rabbit (1/200 in 0.1 M PBS, Jackson ImmunoResearch, code 111-025-003) and FITC goat anti-mouse (1/200 in 0.1 M PBS, Jackson ImmunoResearch, code 115-095-003) for 90 min on a shaker at room temperature. Following rinses in 0.1 M PBS (4 × 5 min), they were then incubated with Hoescht solution for counterstaining (1/5,000 in 0.1 M PBS, bisBenzimide H 33258, Sigma Aldrich, B2883) for 15 min on a shaker at room temperature. Finally, sections were rinsed with 0.1 M PBS, mounted in 0.05 M PB onto gelatin-coated slides, and coverslipped with Fluoromount G (SouthernBiotech, 0100-01). Sections were then imaged using an epifluorescence microscope (Olympus IX81) equipped with a camera (Orca ER, Hamamatsu) controlled by MicroManager Software (MM Studio).

For visible immunostaining, sections were rinsed in 0.1 M PBS containing 0.3% Triton X-100 (PBST; 4 × 5 min) and then incubated in PBST containing 1% hydrogen peroxide solution (H_2O_2) for 30 min. Further rinses were performed using PBST (4 × 5 min) before incubation in blocking solution for 1 h at room temperature. Then, sections were incubated in primary antibody rabbit anti-RFP (1/2,500 in blocking solution, PM005 MBL International Corporation) for 48 h at 4°C on a shaker. After further rinses in 0.1 M PBS (4 × 5 min), sections were placed for 2 h in a bath containing biotinylated goat anti-rabbit secondary antibody (1/1,000 in 0.1 M PBS, 111-065-003 Jackson ImmunoResearch) for 90 min at room temperature.

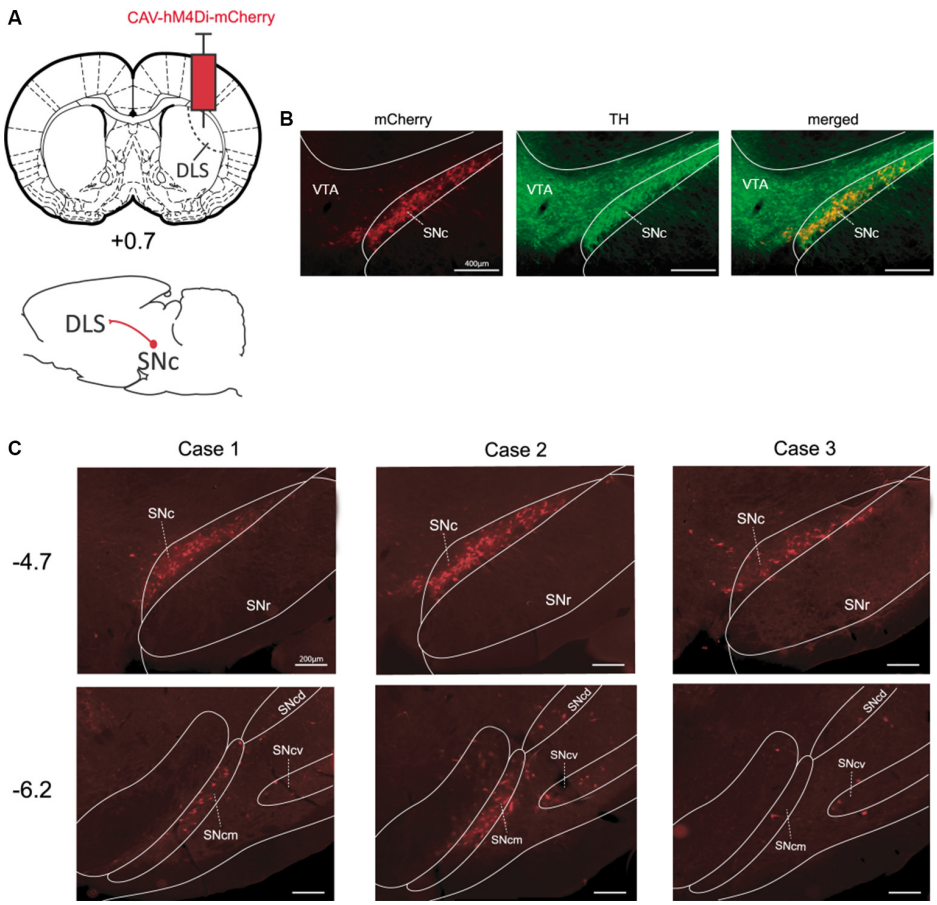

FIGURE 1 | Targeting the nigrostriatal pathway with CAV-hM4Di **(A)** Schematic illustration of viral vector injection into the dorsolateral striatum (DLS) to selectively infect nigrostriatal neurons. **(B)** Example of staining obtained in the SNc vs. the VTA for mCherry-positive and tyrosine hydroxylase (TH)-positive neurons [Case 2, anteroposterior (AP) −4.7 mm]. **(C)** The rostrocaudal extent of staining in SN for all pilot cases at coordinates AP −4.7 mm and AP −6.2 mm (from Bregma). DLS, dorsolateral striatum; SNc, substantia nigra pars compacta; SNcm, d, v: substantia nigra pars compacta, medial tier, dorsal tier, and ventral tier respectively; VTA, ventral tegmental area.

Following rinses in 0.1 M PBS (4 × 5 min), they were then incubated with avidin-biotin-peroxidase complex (1/200 in 0.1 M PBS, 32020 ThermoFisher Scientific) for 90 min at room temperature. The final staining was made with diaminobenzidine (DAB, 10 mg tablet, D5905 Sigma-Aldrich) dissolved in 50 ml of 0.05 M Tris buffer (0.05 M TB) and 30 µl H_2O_2. Sections were then rinsed in 0.05 M TB (2 × 5 min) and then 0.05 M PB (2 × 5 min). They were collected on gelatin-coated slides, dehydrated with xylene, mounted and coverslipped using Eukitt mounting medium. Sections were scanned using a Nanozoomer slide scanner (Hamamatsu Photonics) with a 20× lens and analyzed with the NDP.view 2 freeware (Hamamatsu Photonics).

RESULTS

Targeting the Dopaminergic Pathway Reaching the Dorsolateral Striatum

It has extensively been shown that the substantia nigra pars compacta (SNc) sends major projections to the dorsal striatum (Fallon and Moore, 1978). To selectively target this nigrostriatal pathway we injected CAV-hM4Di into the DLS of TH-cre$^+$ rats (**Figure 1A**). As expected, this manipulation resulted in a strong expression of hM4Di-mCherry mainly in cell bodies located unilaterally in the ipsilateral SNc, nevertheless, fluorescence can also be observed in axons originating from these cell bodies (**Figure 1B**). Moreover, the localization of these stained cell bodies corresponded to the localization of TH-positive cells as shown in **Figure 1B**, suggesting that neurons expressing hM4Di-mCherry are primarily dopaminergic cells. In these examples, we found that approximately 38% (417/1091) of TH-positive cells in the ipsilateral SNc expressed mCherry. The same Figure shows that dopaminergic cells in the ventral tegmental area (VTA), which do not target the DLS, did not express hM4Di-mCherry. Consistent with the latter, we did not observe labeled cells elsewhere in the brain. Interestingly, after a single injection into the DLS, the staining of cells covered a substantial distance along the rostrocaudal axis of the SNc (**Figure 1C**). Indeed, strong hM4Di-mCherry labeling of cells was found at AP −4.7 mm

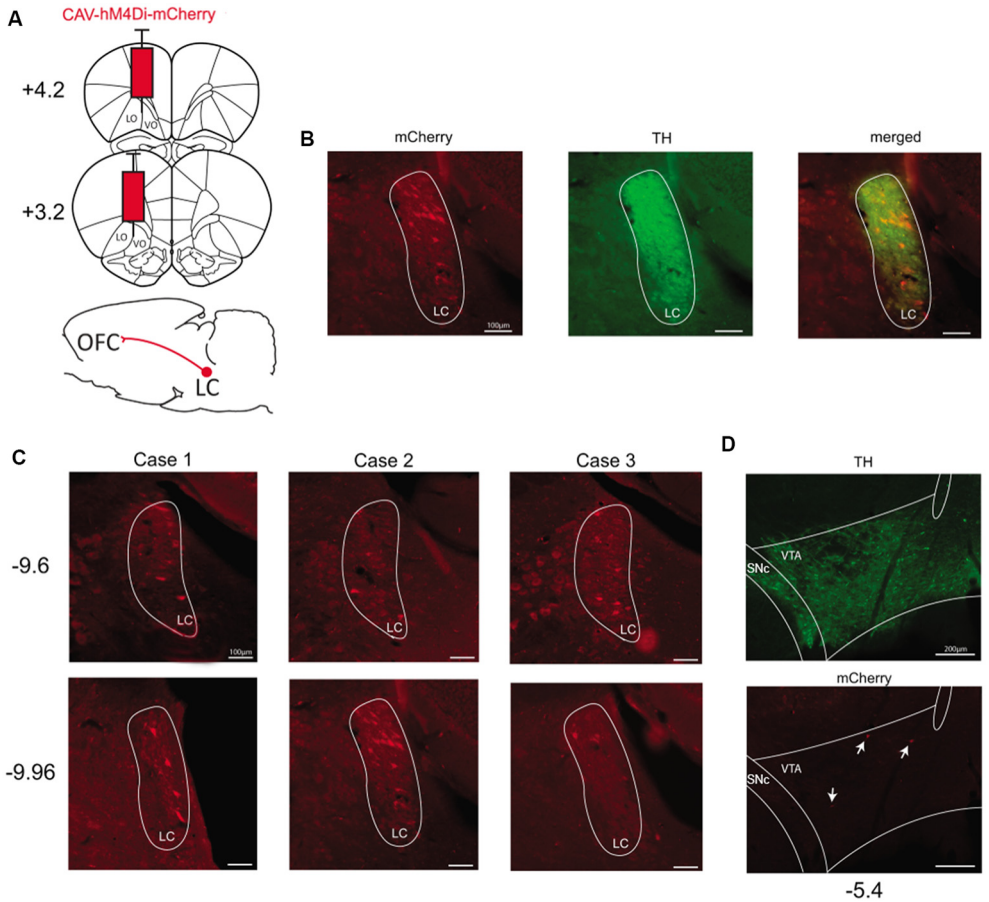

FIGURE 2 | Targeting the catecholaminergic pathway to the OFC. **(A)** Schematic illustration of viral vector injection into the OFC at two different coordinates taken from Bregma (AP +3.2 mm and AP +4.2 mm). **(B)** Example of staining obtained in the LC for mCherry-positive and TH-positive neurons (Case 2, AP −9.96 mm). **(C)** Staining obtained in LC for all pilot cases at two different anteroposterior coordinates taken from Bregma (AP −9.6 mm and AP −9.96 mm). **(D)** Example of staining obtained in the VTA for mCherry-positive and TH-positive neurons (AP −5.4 mm). OFC, orbitofrontal cortex; VO, ventral OFC; LO, lateral OFC; LC, locus coeruleus; VTA, ventral tegmental area.

(from Bregma) in all cases, and numerous hM4Di-mCherry positive cells were found even more posteriorly at AP −6.2 mm (from Bregma) in at two out of three cases.

Targeting Catecholaminergic Pathways Ascending Into the Orbitofrontal Cortex

To express hM4Di-mCherry in catecholaminergic pathways reaching the OFC, we injected CAV-hM4Di in the ventral and lateral portions of OFC (**Figure 2A**). We found substantial labeled neurons unilaterally in the ipsilateral locus coeruleus (LC). The localization of stained cells corresponded to TH-positive cells which are noradrenergic in the LC (**Figure 2B**). In all cases, we observed mCherry staining along the central portion of LC. Indeed, as observed in **Figure 2C**, stained cells were mostly located from AP −9.6 mm to −9.96 mm (from Bregma). However, regarding the dopaminergic pathway reaching the OFC, we found no staining or very few stained cells in the ipsilateral VTA (**Figure 2D**). Again, there was no evidence of labeled cells elsewhere in the brain, suggesting that the floxed hM4Di-mCherry cassette was inverted selectively in TH-positive and Cre-expressing cells.

Furthermore, we found no staining in LC after injection of CAV-hM4Di in the OFC of transgene-negative littermates TH-Cre- (one case reported in **Figure 3A**) or a wild-type animal (**Figure 3B**). Thus, in the absence of Cre-recombinase, no expression of DREADD is observable.

DISCUSSION

Our findings demonstrate that CAV-hM4Di can be used to express hM4Di-mCherry in different pathways using a single injection in a transgenic rat line. Indeed, injection of this vector in two different structures, specifically the DLS and the OFC, resulted in a reliable mCherry-reporter staining in catecholaminergic nuclei projecting to these structures.

Numerous studies have used DREADD technology to study the function of dopaminergic pathways using a combination of

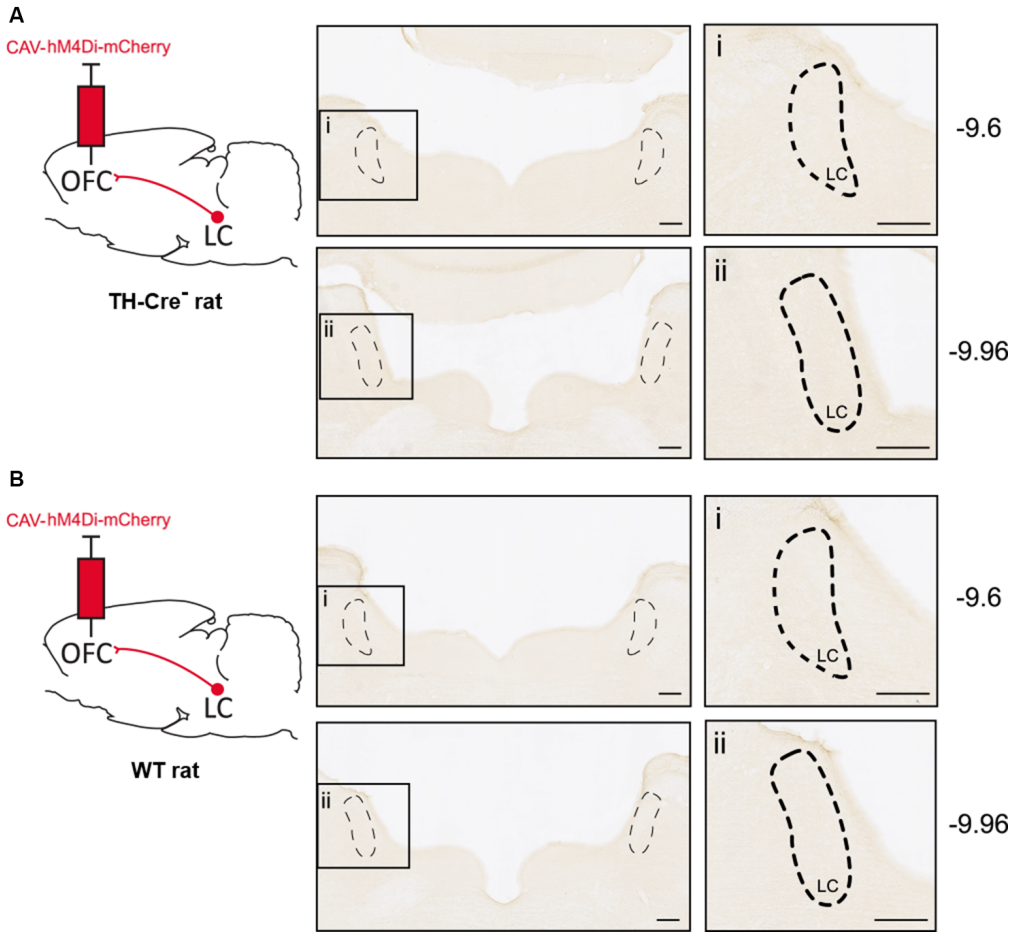

FIGURE 3 | Absence of CAV-hM4Di expression in animals lacking Cre-recombinase. **(A)** DAB immunostaining in LC after injection of CAV-hM4Di in the OFC of transgene-negative littermate TH-cre^{-} at two AP coordinates (AP −9.6 mm and AP −9.96 mm). **(B)** DAB immunostaining in LC with the same injection in wild-type rats.

viral vectors and transgenic rodent lines (Runegaard et al., 2019). Our report provides evidence to consider CAV-hM4Di as a new powerful tool to transiently inhibit the nigrostriatal dopaminergic pathway when used in combination with the TH-transgenic rodent line. Indeed, a single injection of CAV-hM4Di in DLS primarily resulted in strong staining at the level of the SNc along the rostrocaudal axis. Such staining is not surprising due to the strong connectivity between these two structures as previously described (Fallon and Moore, 1978). The neighboring VTA was not stained, confirming the anatomic specificity of the infection.

The pattern of expression we obtained in the nigrostriatal pathway looks very similar to both qualitatively and quantitatively to other reports reporting behavioral effects (Boekhoudt et al., 2016; Bouchet et al., 2018). The efficiency of expression in Bouchet et al. (2018) is not quantified. However, Boekhoudt et al. (2016), using a double-viral strategy to target the nigrostriatal pathway, have reported efficiency of 34.8% of SN (dopaminergic) neurons expressing the fluorescent reporter mCherry. In the three cases shown here, expression of mCherry was found in 38% of TH-positive neurons. Therefore, our strategy seems to be as effective as that of previous reports.

It is also important to note that a behavioral effect can be found with a very small proportion of neurons expressing the viral construct (∼3% in dlPFC of monkeys, Upright et al., 2018).

Recent studies have highlighted the involvement of noradrenergic pathways reaching different prefrontal areas to support distinct cognitive functions (Tervo et al., 2014; Cope et al., 2019). Therefore, simple methods allowing transient and specific modulation of these pathways are necessary to understand their functional specificity. In this study, we have provided an example of such a possibility by targeting the noradrenergic inputs into the OFC. The brainstem nucleus, LC, constitutes the major source of noradrenaline (NA) to the cortex (Loughlin et al., 1982) and sends projections to all prefrontal areas (Agster et al., 2013; Chandler et al., 2013; Cerpa et al., 2019). Accordingly, following CAV-hM4Di injection in the OFC, we found staining restricted to the LC. Furthermore, in all cases, labeled cells were mostly found in

the medial portion of the LC. This is in agreement with the topographic organization of LC efferent neurons showing that, along the rostrocaudal axis, neurons projecting to the neocortex are primarily located in the medial portion of LC (Loughlin et al., 1986).

In the present study, OFC injections only resulted in weak and rare staining in the VTA. Considering that the rodent OFC dopaminergic innervation exists (Chandler et al., 2013) but is only scarce (Descarries et al., 1987; Murphy and Deutch, 2018), it is difficult to conclude on the efficiency of the vector to infect this pathway. However, because the infection of neurons by CAV-2 vectors depends on CAR availability (Bru et al., 2010), one possibility is that mesocortical neurons reaching the OFC express few CAR molecules. Interestingly, recent studies have used a "CAR boost" strategy to enhance CAV-2 tropism in various pathways (Li et al., 2018). Such complementation could be used to promote CAV-hM4Di infection in pathways of interest.

The present report highlights the use of CAV-2 vector harboring a DREADD cassette with TH-Cre rats. However, it does not give an exhaustive presentation of other possibilities of single intracerebral injections. Indeed, while a similar study in TH-Cre mice is lacking, it is likely that CAV-hM4Di could be used in mice and in combination with other types of transgenic lines e.g Dbh-Cre mice, SERT-Cre mice. Moreover, CAV-2 vectors have the potential to include an expression cassette as large as 30 kb. Therefore, our proof-of-principle studies are a step towards using vectors with multiple expression cassettes. For example, one could imagine an excitatory DREADD, an inhibitory DREADD, and a drug inducible reporter gene cassette in the same vector. In addition, CAV-hM4Di could still be used in wild type animals with Cre provided by another viral vector (e.g AAV-cre vector) that infects neurons at the site of injection.

In control animals, lacking the Cre-recombinase, we found no evidence of recombination and expression of the hM4Di-mCherry indicating specific Cre-dependent expression. On the other hand, it has been argued that some non-specific expression could be observed with the use of floxed AAVs, as stated in this issue (Morceau et al., 2019). The present study suggests that the CAV-2 vector containing a floxed DREADD could be used to overcome this issue.

DATA AVAILABILITY STATEMENT

The raw data supporting the conclusions of this article will be made available by the authors, without undue reservation, to any qualified researcher.

ETHICS STATEMENT

The animal study was reviewed and approved by Bordeaux Ethics Committee (Université de Bordeaux).

AUTHOR CONTRIBUTIONS

J-CC, J-RP, YS, and EC performed research. J-CC, AM, EK, and EC wrote and edited the article.

FUNDING

This work was supported by the French National Research Agency (grant number ANR-14-CE13-0014 GOAL and grant number ANR-19-CE37-0008 NORAD to EC and EK) and by the Fondation pour la Recherche Médicale (FRM grant number ECO20160736024 to J-CC).

ACKNOWLEDGMENTS

We thank Gilles Courtand for technical assistance with image acquisition. Part of the microscopy was completed at the Bordeaux Imaging Center, a service unit of CNRS-INSERM and Bordeaux University, and a member of the national infrastructure, France BioImaging. We also thank Dr. Mathieu Wolff for his useful comments on an earlier version of the manuscript.

REFERENCES

Agster, K. L., Mejias-Aponte, C. A., Clark, B. D., and Waterhouse, B. D. (2013). Evidence for a regional specificity in the density and distribution of noradrenergic varicosities in rat cortex. *J. Comp. Neurol.* 521, 2195–2207. doi: 10.1002/cne.23270

Alcaraz, F., Fresno, V., Marchand, A. R., Kremer, E. J., Coutureau, E., and Wolff, M. (2018). Thalamocortical and corticothalamic pathways differentially contribute to goal-directed behaviors in the rat. *eLife* 7:e32517. doi: 10.7554/eLife.32517

Boekhoudt, L., Omrani, A., Luijendijk, M. C. M., Wolterink-Donselaar, I. G., Wijbrans, E. C., van der Plasse, G., et al. (2016). Chemogenetic activation of dopamine neurons in the ventral tegmental area, but not substantia nigra, induces hyperactivity in rats. *Eur. Neuropsychopharmacol.* 26, 1784–1793. doi: 10.1016/j.euroneuro.2016.09.003

Bouchet, C. A., Miner, M. A., Loetz, E. C., Rosberg, A. J., Hake, H. S., Farmer, C. E., et al. (2018). Activation of nigrostriatal dopamine neurons during fear extinction prevents the renewal of fear. *Neuropsychopharmacology* 43, 665–672. doi: 10.1038/npp.2017.235

Bru, T., Salinas, S., and Kremer, E. J. (2010). An update on canine adenovirus type 2 and its vectors. *Viruses* 2, 2134–2153. doi: 10.3390/v2092134

Cerpa, J. C., Marchand, A. R., and Coutureau, E. (2019). Distinct regional patterns in noradrenergic innervation of the rat prefrontal cortex. *J. Chem. Neuroanat.* 96, 102–109. doi: 10.1016/j.jchemneu.2019.01.002

Chandler, D. J., Lamperski, C. S., and Waterhouse, B. D. (2013). Identification and distribution of projections from monoaminergic and cholinergic nuclei to functionally differentiated subregions of prefrontal cortex. *Brain Res.* 1522, 38–58. doi: 10.1016/j.brainres.2013.04.057

Cope, Z. A., Vazey, E. M., Floresco, S. B., and Aston Jones, G. S. (2019). DREADD-mediated modulation of locus coeruleus inputs to mPFC improves strategy set-shifting. *Neurobiol. Learn. Mem.* 161, 1–11. doi: 10.1016/j.nlm.2019.02.009

Descarries, L., Lemay, B., Doucet, G., and Berger, B. (1987). Regional and laminar density of the dopamine innervation in adult rat cerebral cortex. *Neuroscience* 21, 807–824. doi: 10.1016/0306-4522(87)90038-8

Fallon, J. H., and Moore, R. Y. (1978). Catecholamine innervation of the basal forebrain. IV. Topography of the dopamine projection to the basal forebrain and neostriatum. *J. Comp. Neurol.* 180, 545–580. doi: 10.1002/cne.901800310

Li, S. J., Vaughan, A., Sturgill, J. F., and Kepecs, A. (2018). A viral receptor complementation strategy to overcome CAV-2 tropism for efficient retrograde targeting of neurons. *Neuron* 98, 905.e5–917.e5. doi: 10.1016/j.neuron.2018.05.028

Loughlin, S. E., Foote, S. L., and Fallon, J. H. (1982). Locus coeruleus projections to cortex: topography, morphology and collateralization. *Brain Res. Bull.* 9, 287–294. doi: 10.1016/0361-9230(82)90142-3

Loughlin, S. E., Foote, S. L., and Grzanna, R. (1986). Efferent projections of nucleus locus coeruleus: morphologic subpopulations have different efferent targets. *Neuroscience* 18, 307–319. doi: 10.1016/0306-4522(86)90156-9

Morceau, S., Piquet, R., Wolff, M., and Parkes, S. L. (2019). Targeting reciprocally connected brain regions through CAV-2 mediated interventions. *Front. Mol. Neurosci.* 12:303. doi: 10.3389/fnmol.2019.00303

Murphy, M. J. M., and Deutch, A. Y. (2018). Organization of afferents to the orbitofrontal cortex in the rat. *J. Comp. Neurol.* 526, 1498–1526. doi: 10.1002/cne.24424

Parkes, S. L., Ravassard, P. M., Cerpa, J. C., Wolff, M., Ferreira, G., and Coutureau, E. (2018). Insular and ventrolateral orbitofrontal cortices differentially contribute to goal-directed behavior in rodents. *Cereb. Cortex* 28, 2313–2325. doi: 10.1093/cercor/bhx132

Paxinos, G., and Watson, C. (eds). (2014). *The Rat Brain in Stereotaxic Coordinates* (7th Edn.). San Diego: Academic Press.

Roth, B. L. (2016). DREADDs for neuroscientists. *Neuron* 89, 683–694. doi: 10.1016/j.neuron.2016.01.040

Runegaard, A. H., Fitzpatrick, C. M., Woldbye, D. P. D., Andreasen, J. T., Sorensen, A. T., and Gether, U. (2019). Modulating dopamine signaling and behavior with chemogenetics: concepts, progress, and challenges. *Pharmacol. Rev.* 71, 123–156. doi: 10.1124/pr.117.013995

Smith, K. S., Bucci, D. J., Luikart, B. W., and Mahler, S. V. (2016). DREADDS: use and application in behavioral neuroscience. *Behav. Neurosci.* 130, 137–155. doi: 10.1037/bne0000135

Tervo, D. G. R., Proskurin, M., Manakov, M., Kabra, M., Vollmer, A., Branson, K., et al. (2014). Behavioral variability through stochastic choice and its gating by anterior cingulate cortex. *Cell* 159, 21–32. doi: 10.1016/j.cell.2014.08.037

Upright, N. A., Brookshire, S. W., Schnebelen, W., Damatac, C. G., Hof, P. R., Browning, P. G. F., et al. (2018). Behavioral effect of chemogenetic inhibition is directly related to receptor transduction levels in rhesus monkeys. *J. Neurosci.* 38, 7969–7975. doi: 10.1523/JNEUROSCI.1422-18.2018

Conflict of Interest: The authors declare that the research was conducted in the absence of any commercial or financial relationships that could be construed as a potential conflict of interest.

Advantages of publishing in Frontiers

OPEN ACCESS
Articles are free to read for greatest visibility and readership

FAST PUBLICATION
Around 90 days from submission to decision

HIGH QUALITY PEER-REVIEW
Rigorous, collaborative, and constructive peer-review

TRANSPARENT PEER-REVIEW
Editors and reviewers acknowledged by name on published articles

Frontiers
Avenue du Tribunal-Fédéral 34
1005 Lausanne | Switzerland

Visit us: www.frontiersin.org
Contact us: frontiersin.org/about/contact

REPRODUCIBILITY OF RESEARCH
Support open data and methods to enhance research reproducibility

DIGITAL PUBLISHING
Articles designed for optimal readership across devices

FOLLOW US
@frontiersin

IMPACT METRICS
Advanced article metrics track visibility across digital media

EXTENSIVE PROMOTION
Marketing and promotion of impactful research

LOOP RESEARCH NETWORK
Our network increases your article's readership